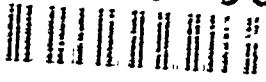


AD-A247 009



AEDSR-TR- 92 0120

FABRIC-STRESS-DEFORMATION RELATIONS

IN GRANULAR MATERIALS

FINAL TECHNICAL REPORT

October 1, 1986 to June 30, 1991

GRANT NO. AFOSR-87-0079

to

University of California, San Diego

by

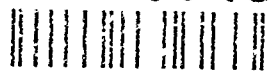
Air Force Office of Scientific Research

Principal Investigator: Dr. S. Nemat-Nasser

DTIC ELECTRIC MAR 4 1992

Vertical stamp: DTIC ELECTRIC MAR 4 1992, AFOSR (AFOSR), UNIVERSITY OF CALIFORNIA, SAN DIEGO, CA 92094

92-05481



92 3 02 166

REPORT DOCUMENTATION PAGE

Form Approved
OMB No. 0704-0188

Public reporting burden for this collection of information is estimated to average 1 hour per response, including the time for reviewing instructions, searching existing data sources, gathering and maintaining the data needed, and completing and reviewing the collection of information. Send comments regarding this burden estimate or any other aspect of this collection of information, including suggestions for reducing the burden to Washington Headquarters Services, Directorate for Information Operations and Reports, 1215 Jefferson Davis Highway, Suite 1204, Arlington, VA 22202-4302 and to the Office of Management and Budget, Paperwork Reduction Project (0704-0188), Washington, DC 20503.

1. AGENCY USE ONLY (Leave blank)	2. REPORT DATE 12/1/91	3. REPORT TYPE AND DATES COVERED Final Report 10/86 - 6/91
---	----------------------------------	--

4. TITLE AND SUBTITLE Fabric-Stress-Deformation Relations in Granular Materials	5. FUNDING NUMBERS Program Element No: 61102F Project Number: 2302 Task Number: C1
---	--

6. AUTHOR(S) S. Nemat-Nasser, et al	
---	--

7. PERFORMING ORGANIZATION NAME(S) AND ADDRESS(ES) University of California, San Diego 9500 Gilman Drive La Jolla, Ca 92093-0411	8. PERFORMING ORGANIZATION REPORT NUMBER
--	---

9. SPONSORING/MONITORING AGENCY NAME(S) AND ADDRESS(ES) AFOSR/NA Building 410 Bolling AFB D.C. 20332-6448	10. SPONSORING/MONITORING AGENCY REPORT NUMBER AFOSR-87-0079
---	--

11. SUPPLEMENTARY NOTES The view, opinions and/or findings contained in this report are those of the author(s) and should not be construed as an official Airforce Office position, policy, or decision, unless so designated by other documentation.

12a. DISTRIBUTION/AVAILABILITY STATEMENT Approved for public release; distribution unlimited.	12b. DISTRIBUTION CODE
---	-------------------------------

13. ABSTRACT (Maximum 200 words) The basic aims of this research program have been to study the mechanical properties and constitutive relations of granular materials that support the applied loads through interparticular frictional contacts, and to relate these to the granular fabric, both stress-induced and inherent. To this end a coordinated experimental and theoretical program was followed in order to identify: (1) effective parameters that measure the fabric of granular masses; (2) the difference between inherent and induced fabric, and the influence of each on the constitutive response of the material; (3) parameters which measure the evolution of fabric in the course of a given overall load or deformation history; (4) the relation between fabric and the overall stress and deformation, and (5) constitutive relations which directly involve fabric measures and the measure of their evolution, and hence, are based on the fundamental microstructural events which give rise to nonlinear material response.
--

14. SUBJECT TERMS Fabric Stress Deformation Granular Materials	15. NUMBER OF PAGES 206
	16. PRICE CODE

17. SECURITY CLASSIFICATION OF REPORT UNCLASSIFIED	18. SECURITY CLASSIFICATION OF THIS PAGE UNCLASSIFIED	19. SECURITY CLASSIFICATION OF ABSTRACT UNCLASSIFIED	20. LIMITATION OF ABSTRACT UL
--	---	--	---

19. ABSTRACT (Continued)

The experimental work included tests on large hollow cylindrical samples of granular materials (sands), where a true three-dimensional stress state could be produced in the sample and accurate measurements of forces and associated displacements were made. Parallel to this, a series of *model* experiments on two-dimensional photoelastic rods with oval cross section was also performed. By means of photoelastic procedures, the history of the evolution of the microstructure was recorded for simple shear loading paths. Using the existing image analysis facilities, the photoelastic pictures were analyzed, major microstructural features were identified, and were related to the overall stress and deformation histories, using stereological techniques, as well as by direct measurement of fabric parameters. The experimental studies were closely coordinated with the micromechanical modeling. (This report includes papers which publish the scientific findings of this research program)

FINAL SCIENTIFIC REPORT

for the period

October 1, 1986 to June 30, 1991

on

**FABRIC-STRESS-DEFORMATION RELATIONS
IN GRANULAR MATERIALS**

Grant No. AFOSR-87-0079

Dr. S. Nemat-Nasser, Principal Investigator

University of California, San Diego, La Jolla, California 92093

DTIC
COPY
INSPECTED
6

Accession For	
NTIS Grant	<input checked="" type="checkbox"/>
DTIC TAB	<input type="checkbox"/>
Unannounced	<input type="checkbox"/>
Justification	
By _____	
Distribution/ _____	
Availability Codes	
Dist	Avail and/or Special
A-1	

Table of Contents

	Page
Abstract	1
1. Research Accomplishments:	
1.1 Introduction	2
1.2 List of Publications Completed	4
1.3 Abstracts of Publications	5
1.4 Professional Personnel Associated with the Research Project; Degrees Awarded	9
1.5 Interactions (Coupling Activities)	10
2. Progress:	
<i>Papers Published:</i>	
Mehrabadi, M.M., S. Nemat-Nasser, H.M. Shodja and G. Subhash, "Some Basic Theoretical and Experimental Results on Micromechanics of Granular Flow",	Attachment 1
Nemat-Nasser, S., "Effect of Fabric on Liquefaction and Densification of Saturated Soil: Experiments and Theory,"	Attachment 2
Nemat-Nasser, S., "Anisotropy in Response and Failure Modes of Granular Materials,"	Attachment 3
Subhash, G., S. Nemat-Nasser, M.M. Mehrabadi and H.M. Shodja, "Experimental Investigation of Fabric-Stress Relations in Granular Materials"	Attachment 4

Table of Contents (continued)

Papers Submitted:

Mehrabadi, M.M., B. Loret and S. Nemat-Nasser, "Incremental Constitutive Relations for Granular Materials Based on Micromechanics,"	Attachment 5
Mehrabadi, M.M., B. Loret and S. Nemat-Nasser, "A Constitutive Model for Granular Materials Based on Micromechanics,"	Attachment 6
Nemat-Nasser, S. and B. Balendran, "Micromechanics of Flow and Failure Modes of Particulate Media Over a Wide Range of Strain Rates"	Attachment 7
Okada, N. and S. Nemat-Nasser, "Energy Dissipation in Inelastic Flow of Cohesionless Granular Media"	Attachment 8

ABSTRACT

The basic aims of this research program have been to study the mechanical properties and constitutive relations of granular materials that support the applied loads through interparticular frictional contacts, and to relate these to the granular fabric, both stress-induced and inherent. To this end a coordinated experimental and theoretical program was followed in order to identify:

1. Effective parameters that measure the fabric of granular masses.
2. The difference between inherent and induced fabric, and the influence of each on the constitutive response of the material
3. Parameters which measure the evolution of fabric in the course of a given overall load or deformation history
4. the relation between fabric and the overall stress and deformation
5. Constitutive relations which directly involve fabric measures and the measure of their evolution, and hence, are based on the fundamental microstructural events which give rise to nonlinear material response

The experimental work included tests on large hollow cylindrical samples of granular materials (sands), where a true three-dimensional stress state can be produced in the sample. Accurate measurements of forces and associated displacements were made in the unique state-of-the-art testing facilities of the Principal Investigator, at the University of California, San Diego (UCSD). Parallel to this, a series of *model* experiments on two-dimensional photoelastic rods with oval cross section was also performed. By means of photoelastic procedures, the history of the evolution of the microstructure was recorded for simple shear loading paths. Using the existing image analysis facilities, the photoelastic pictures were analyzed, major microstructural features were identified, and were related to the overall stress and deformation histories, using stereological techniques, as well as by direct measurement of fabric parameters. The experimental studies were closely coordinated with the micromechanical modeling. This report includes the scientific findings of this research program.

1.1 INTRODUCTION

A fundamental approach was followed in this program in order to develop physically-based constitutive relations for granular materials. The program included the following steps:

1. Micromechanical observations, in order to identify the major microscopic features that produce the overall nonlinear macroscopic response and associated failure modes;
2. Micromechanical modeling of the identified microscopic features on the basis of rigorous mechanics principles and systematic mathematical deduction of the macroscopic consequences of the model;
3. Systematic experiments on carefully prepared and reproducible samples, in order to test the validity of the model results, and hence, the model's basic assumptions;
4. Macroscopic constitutive models which encompass the experimentally verified micromechanical features; and
5. Systematic experiments to test the validity of the constitutive results and to quantify the constitutive parameters of the model.

Theoretical modeling at both the microscopic and macroscopic levels was pursued, guided by systematic experimental observation at both the microscale and macroscale, which provided vital information on the physics of the process.

The micromechanics of granular flow was studied in simple shear and in biaxial loading by using photoelastic, rod-like granules with circular *and* oval cross sections. Based on these observations, overall stress and deformation measures were calculated using fabric tensors which characterize the microstructure of the granular mass, and relations between the overall stress and various measures of the fabric have been carefully studied. These results have been summarized in Mehrabadi *et al.* (1988) and in Subhash *et al.* (1991). Of particular importance are two major findings which contradict some commonly held views. They are: (1) in general, a second-order tensor which represents approximately the distribution of contact normals is not coaxial with the stress tensor, although its principal directions follow those of the stress tensor in a determinable manner;

and (2) in general, the distribution of contact normals or unit branches cannot be adequately represented by a second-order tensor.

Furthermore, under this project, we have studied several alternative theories for quantifying the incremental measures of local (micro) deformation and forces, and related them to the relative sliding and rolling of granules, their frictional contact forces, and the statistical classes that encompass a set of granules associated with a particular orientation of either contact normals or unit branches. This study has produced a fundamental and definitive representation of incremental deformation measures and stress measures at the microlevel, based on subdividing contacts into classes with common contact normal orientations, and identifying each class as a micro-element; see Mehrabadi, Loret and Nemat-Nasser (1991).

In collaboration with Professors B. Loret of Grenoble, France, and M. Mehrabadi of Tulane University, a new approach has been developed, based on a general tensorial relation between local kinematical quantities and global ones, including the effect of overall stress and fabric. The basic framework for a general theory in two dimensions has thus been established. Based on it, and the Taylor averaging scheme, the overall rate-constitutive relations have been developed; Mehrabadi, Loret and Nemat-Nasser (1991).

Parallel with the theoretical work and micromechanical experimental validation, we have studied the effect of fabric (both inherent and induced) on the strength, and the liquefaction and densification potentials, of cohesionless granules. This experimental work involved both deformation-controlled and stress-controlled cyclic testing under complete computer-controlled conditions. It has resulted in several new observations which correct some (incorrect) commonly held views that were based on experimental results obtained by means of less advanced experimental techniques and facilities. In particular, we have found that preliquefaction *does not necessarily* result in a sample highly susceptible to reliquefaction: it may, in fact, strengthen the sample, depending on the *residual fabric*; Okada and Nemat-Nasser (1991).

In the course of the above-mentioned experimental study, we have obtained some interesting results which seem to suggest a unique relation between the pore pressure buildup and the associated energy input, at least for virgin samples in strain-controlled tests; Okada and Nemat-Nasser (1991). Attachment 6 contains these results. The strain amplitude ranges from 0.2 to 4.0%, in cyclic strain-controlled tests. They lead to a unique pore pressure-energy relationship. The effects of initial fabric were included by prestraining and/or preliquefying the samples. Based on micromechanics, a physically-

based model has been developed for this phenomenon, including the effects of fabric; see Attachment 6.

1.2 PUBLICATIONS COMPLETED UNDER GRANT AFOSR 87-0079

LIST OF PAPERS PUBLISHED

Mehrabadi, M.M., S. Nemat-Nasser, H.M. Shodja and G. Subhash, "Some Basic Theoretical and Experimental Results on Micromechanics of Granular Flow", *Micromechanics of Granular Materials*, M. Satake and J.T. Jenkins (eds), Elsevier (1988), 253-262.

Nemat-Nasser, S., "Effect of Fabric on Liquefaction and Densification of Saturated Soil: Experiments and Theory," *Micromechanics of Granular Materials*, M. Satake and J.T. Jenkins (eds), Elsevier (1988), 202-205.

Nemat-Nasser, S., "Anisotropy in Response and Failure Modes of Granular Materials," *Yielding, Damage and Failure of Anisotropic Solids (EGF5)*, Proceedings of the IUTAM/ICM Symposium, August (1987), Mechanical Engineering Publications, J.P. Boehler (ed.), London, (1990), 33-48.

Subhash, G., S. Nemat-Nasser, M.M. Mehrabadi and H.M. Shodja, "Experimental Investigation of Fabric-Stress Relations in Granular Materials", *Mechanics of Materials*, Vol. 11, No. 2 (1991), 87-106.

LIST OF PAPERS SUBMITTED

Mehrabadi, M.M., B. Lorent and S. Nemat-Nasser, "Incremental Constitutive Relations for Granular Materials Based on Micromechanics," *Proceedings of the Royal Society of London*, submitted 5/91

Mehrabadi, M.M., B. Lorent and S. Nemat-Nasser, "A Constitutive Model for Granular Materials Based on Micromechanics," presented at the Second US-Japan Seminar on Micromechanics of Granular Materials, Clarkson University, NY, August 5, 1991, submitted 9/91

Nemat-Nasser, S. and B. Balendran, "Micromechanics of Flow and Failure Modes of Particulate Media Over a Wide Range of Strain Rates", presented at the 2nd US-Japan Seminar on Micromechanics of Granular Materials, Clarkson Univ., NY, August 5, 1991.

Okada, N. and S. Nemat-Nasser, "Energy Dissipation in Inelastic Flow of Cohesionless Granular Media", *Geotechnique*, submitted 12/91

1.3 ABSTRACTS OF PUBLICATIONS

- 1.3.1 Mehrabadi, M.M., S. Nemat-Nasser, H.M. Shodja and G. Subhash, "Some Basic Theoretical and Experimental Results on Micromechanics of Granular Flow", *Micromechanics of Granular Materials*, M. Satake and J.T. Jenkins (eds), Elsevier (1988), 253-262.

In order to establish guidelines for modeling the macroscopic behavior of granular materials, an experimental study of the evolution of the microstructure of an assembly of granular materials under a uniform confining pressure and subjected to a pure shear was conducted. The granular material used in the study consisted of photoelastically sensitive rod-shaped particles of oval cross-sections. It was found that (i) the distribution of branches and contact normals are almost identical, (ii) the second-rank fabric tensor does not adequately describe the microstructure of highly anisotropic samples, (iii) the density of contacts whose normals lie along the major and minor principal stress axes, varies sharply initially and then approaches a constant value in the course of deformation, and (iv) the density of contacts with planes parallel to the maximum shear stress plane remains practically constant throughout the deformation.

- 1.3.2. Nemat-Nasser, S., "Effect of Fabric on Liquefaction and Densification of Saturated Soil: Experiments and Theory," *Micromechanics of Granular Materials*, M. Satake and J.T. Jenkins (eds), Elsevier (1988), 202-205.

It has been known that the inherent and induced anisotropy or fabric has considerable influence on the response and failure modes of granular masses. Some definitive recent experiments which clearly demonstrate this phenomenon in relation to the densification and liquefaction potential of saturated sands, are briefly reviewed, together with associated micromechanically based theoretical observations.

- 1.3.3. Nemat-Nasser, S., "Anisotropy in Response and Failure Modes of Granular Materials," *Yielding, Damage and Failure of Anisotropic Solids* (EGF5), Proceedings of the IUTAM/ICM Symposium, August (1987). Mechanical

This review addresses some recent experimental and theoretical studies of the mechanical properties of particulate media which support applied overall loads through individual contact resistance. We emphasize the inherent and induced fabric or anisotropy and its influence on the response and failure modes of this class of materials. The experimental studies include: (1) model experiments on photoelastic granular rods with circular and elliptical cross-sections, in biaxial as well as simple shear cyclic loading; and (2) dilatancy, liquefaction, and the overall stress-deformation relations studies on simple shearing apparatus and also on large hollow cylindrical samples of sand under complex, three-dimensional monotonic as well as cyclic stress paths. These experiments are designed in coordination with theoretical micromechanical models in order to bring out the major micromechanisms that are responsible for the observed highly path dependent behaviour of granular materials. The issues of inherent and induced anisotropy or fabric and their effects on the overall response of the material are of particular interest in these experiments. The theoretical studies emphasize recent micromechanically-based models of granular flow, which specifically seek to understand and quantify relevant measures of anisotropy or fabric, and the relation between fabric measures and the overall stress tensor.

- 1.3.4. Subhash, G., S. Nemat-Nasser, M.M. Mehrabadi and H.M. Shodja, "Experimental Investigation of Fabric-Stress Relations in Granular Materials", *Mechanics of Materials*, Vol. 11, No. 2 (1991), 87-106.

A brief summary of some relevant theoretical and experimental results on the microscopic aspects of the response of granular masses is presented. The results of a series of experiments involving simple shearing under a constant confining pressure, performed on photoelastic rod-like granules (plane strain) are reported. In these experiments, the components of various fabric tensors are measured, and their variations over one cycle of shearing are examined and compared. The orientations of the principal axes of all commonly used fabric tensors are observed to change sharply with the reversal of the shearing direction. It is also concluded that, in general, second-order fabric tensors are not adequate to accurately describe the distribution of fabric measures such as the distribution density function of unit contact normals or unit branches which are unit vectors along line segments connecting the centroids of adjacent contacting granules. This is particularly so when the response of the granular mass is highly anisotropic. Finally, the expression for the macroscopic stress in terms of the contact forces and other local quantities, is reviewed and its experimental verification is discussed.

- 1.3.5. Mehrabadi, M.M., B. Lorent and S. Nemat-Nasser, "Incremental Constitutive Relations for Granular Materials Based on Micromechanics," *Proceedings of the Royal Society of London*, submitted 5/91

Micromechanically-based constitutive relations for two-dimensional flow of granular materials are presented. First, the relations between the overall stresses and the relevant microscopic quantities, namely, the interparticle forces, the density

and orientation of contact unit normals, as well as the average size of the particles, are obtained. Then, the kinematics is examined, and the overall velocity gradient is related to measures characterizing the relative sliding and rotation of granules. A significant concept underlying all these developments is the notion of the *class* of contact unit normals with a continuously evolving distribution function, even though individual members of various classes may change discontinuously, as contacts are lost and new contacts are developed in the course of granular flow. Then, simple local constitutive relations are introduced for the rate of change of the contact forces, the evolution of the contact normals, the mechanism of local failure, and the density of contacts in a particular class. This leads to macroscopic rate constitutive equations through a Taylor averaging method. Due to the nonlinearity of the rate constitutive equations, the response is computed by an incremental procedure. As an illustration, the overall response of a two-dimensional assembly of disks subjected to an overall shearing deformation is determined. In addition, explicit results are presented for the evolution of fabric, contact forces, and the history of active and inactive classes of contacts. The stress-strain relations and the evolution of fabric and contact forces are in excellent qualitative agreement with the observed behavior of granular materials. In light of these results, the mechanisms of failure and inelastic deformation of dense, as well as loose granular, materials are discussed.

Although most features of the model could be readily generalized to three dimensions, for simplicity, the discussion is limited to planar deformation.

- 1.3.6. Mehrabadi, M.M., B. Lorez and S. Nemat-Nasser, "A Constitutive Model for Granular Materials Based on Micromechanics," presented at the Second US-Japan Seminar on Micromechanics of Granular Materials, Clarkson University, NY, August 5, 1991, submitted 9/91

A recently proposed constitutive model for two-dimensional flow of granular materials is briefly reviewed and some numerical results are presented in this paper. First, the concept of fabric and the relations between the overall stresses and the relevant microscopic quantities are reviewed. Then, the kinematics is briefly examined. A significant concept underlying all these developments is the notion of the *class* of contact unit normals with a continuously evolving distribution function, even though individual members of various classes may change discontinuously, as contacts are lost and new contacts are developed in the course of granular flow. Next, local and macroscopic constitutive relations are discussed and the evolution of the density of contacts in a particular class is considered. As an illustration, the overall response of a two-dimensional assembly of disks subjected to an overall shearing deformation is determined. The stress-strain relations and the evolution of fabric are in excellent qualitative agreement with the observed behavior of granular materials. In light of these results, the micromechanisms of failure and inelastic deformation of dense, as well as loose granular, materials are discussed.

- 1.3.7. Nemat-Nasser, S. and B. Balendran, "Micromechanics of Flow and Failure Modes of Particulate Media Over a Wide Range of Strain Rates", presented at the 2nd US-Japan Seminar on Micromechanics of Granular Materials, Clarkson Univ., NY, August 5, 1991.

A basic framework is proposed for the systematic micromechanically-based constitutive modeling of the flow of granular materials, over a broad range of strain rates, from quasi-static to high strain rates. Frictional effects, pressure sensitivity, and coupling between shearing and volumetric strain are included. Stress-induced anisotropy in elastic and inelastic instantaneous material response is incorporated. The model is flexible enough to account for both rate-independent and rate-dependent frictional sliding and rolling of the grains. For illustration, typical results for biaxial and simple shearing of granular materials with various void ratios are calculated in monotonic, as well as cyclic, loading, and they are shown to accurately correspond to actual observations.

1.3.8 Okada, N. and S. Nemat-Nasser, "Energy Dissipation in Inelastic Flow of Cohesionless Granular Media", *Geotechnique*, submitted 12/91

The results of a systematic study of energy dissipation in cohesionless granular media are presented. First, the relation between the excess pore water pressure, accumulated in a water-saturated granular mass, and the corresponding external work in cyclic loading is studied experimentally. Second, a micromechanical model of internal energy dissipation due to slip between contacting granules is introduced, and the results are compared with experimental measurements.

A series of undrained experiments is carried out using water-saturated large hollow cylindrical specimens. Most experiments are performed under displacement-controlled conditions. The imposed cyclic angular displacement which produces the applied shear strain, has a triangular time variation with constant strain rate over each quarter cycle. The specimens are subjected to two sequences of loading in order to simulate the reliquefaction phenomenon. External work per unit volume is calculated from the experimental results, and its correlation with the excess pore water pressure is examined. In the first loading, a unique nonlinear relation is observed to exist between the excess pore water pressure and the external work per unit volume. This relation is found to be independent of the shear strain amplitude. In the second loading, however, this relation is a function of strain amplitude. The cyclic shear strength is seen to have increased in the second loading, because of the strain history of the first loading.

External work supplied to cohesionless granular media is mainly consumed by the frictional slip between contacting granules. A micromechanical model is developed and validated by the experimental results. It is shown that the internal dissipation per unit volume in cohesionless granular media, can be expressed in terms of the time-history of the applied effective pressure and a single scalar parameter which depends on the density and strain amplitude. The model is further validated by torsion tests with random variation in the applied strain amplitude. The theoretical predications are in excellent agreement with the experimental results.

1.4 PROFESSIONAL PERSONNEL ASSOCIATED WITH THE RESEARCH EFFORT; DEGREES AWARDED (AFOSR SUPPORT)

Principal Investigator: S. Nemat-Nasser

Postdoctoral Research Associates and Research Engineers (Visiting):

Benjamin Loret (Professor, Domaine Universitaire, Institut de Mechanique de Grenoble, France), 5/86 - 12/86

Zong-Lian Qui (Associate Professor, Qinghua University, Beijing, China), 6/87 - 2/88

Staff Research Associates:

H.M. Shodja (Graduate Student, Department of Civil Engineering, Northwestern University, Evanston, IL), 11/86 - 9/87

Visiting Scholars:

Benjamin Loret (Professor, Domaine Universitaire, Institut de Mechanique de Grenoble, France)

Morteza M. Mehrabadi (Professor, Department of Mechanical Engineering, Tulane University, New Orleans, Louisiana)

Muneo Hori (Professor, Department of Civil Engineering, Tohoku University, Sendai, Japan)

Graduate Students:

Degree Awarded

A. Azhdari - Research Assistant, 7/90 - 4/91

B. Balendran - Research Assistant, 11/89 - 4/91

J. Y Chang - Research Assistant, 10/86 - 8/88

H. Deng - Research Assistant, 7/90 - 4/91

S. Ghatuparthi - Research Assistant, 7/87 - 9/89, 12/89 - 6/90

M.S., UCSD

M. Hori - Research Assistant, 10/86 - 12/86, 5/87 - 8/87

N. Okada - Research Assistant, 10/86 - 6/16/91

Engineering Aid (Undergraduate Students)

R. Sugimae, 8/87 - 10/89

B. Crafts, 6/89 - 8/89

1.5 INTERACTIONS (Coupling Activities)

A. PARTICIPATION OF PRINCIPAL INVESTIGATOR AT MEETINGS, PAPERS PRESENTED; LECTURES AT SEMINARS.

"Mechanics of Failure in Compression," Tohoku University, Sendai, Japan, June 27, 1986.

"Surface Instability," University of Southern California, May 8, 1987.

"Anisotropy in Response and Failure Modes of Granular Materials," IUTAM/ICM Symposium: Yielding, Damage and Failure of Anisotropic Solids, Villard-de-Lans, France, August 24-28, 1987.

"Constitutive Modeling Based on Micromechanics," ICES 88, Atlanta, GA, April 10-14, 1988.

"Compression-Induced Ductile Flow of Brittle Materials and Brittle Fracturing of Ductile Materials," Rensselaer Polytechnic Institute, New York, NY, May 12, 1988.

"Compression-Induced Ductile Flow of Brittle Materials and Brittle Fracturing of Ductile Materials," Alicia Golebewska Herrmann Memorial Lecture in Applied Mechanics, Stanford University, Stanford, CA, November 3, 1988.

"Compression-Induced Ductile Flow of Brittle Materials and Brittle Fracturing of Ductile Materials," Naval Research Laboratory, Washington, DC, December 16, 1988.

"Compression-Induced Ductile Flow of Brittle Materials and Brittle Fracturing of Ductile Materials," *Plenary Lecture*, ICF7 Conference on Fracture, Houston, TX, March 23-29, 1989.

"Compression-Induced Ductile Flow of Brittle Materials and Brittle Fracturing of Ductile Materials," MIT Applied Mechanics Seminar Series, Boston, MA, May 15, 1989.

"Compression-Induced Ductile Flow of Brittle Materials and Brittle Fracturing of Ductile Materials," Civil Engineering Seminar, Ohio State University, May 19, 1989.

"Compression-Induced Ductile Flow of Brittle Materials and Brittle Fracturing of Ductile Materials," Keynote Address, Twelfth Canadian Congress of Applied Mechanics -- CANCAM, May 28 - June 2, 1989, Ottawa, Ontario, Canada, May 28, 1989.

"Micromechanics of Deformation for Granular Materials," *Plenary Lecture*, ASME Winter Annual Meeting, San Francisco, CA, December 10-15, 1989, December 14, 1989.

"Paradoxes, Facts and Fiction in Material Failure under Compression," University of Utah, May 4, 1990.

"Paradoxes, Facts and Fiction in Material Failure under Compression," South Dakota School of Mines and Technology, Rapid City, SD, May 24, 1990.

"Paradoxes, Facts and Fiction in Material Failure under Compression," The Continuum Damage Mechanics Workshop at Sandia National Laboratories, Pleasanton, CA, June 12, 1990.

"Paradoxes, Facts and Fiction in Material Failure under Compression," The Department of Civil Engineering, Tohoku University, Sendai, Japan, September 25, 1990.

"Strain Localization in Granular Flow," *Invited Lecture*, The Japan Society of Civil Engineering Convention, Annual Meeting on Strain Localization and Bifurcation of Geomaterials, Niigata, Japan, September 29, 1990.

"Paradoxes, Facts and Fiction in Material Failure under Compression," Kyushu University, Fukuoka, Japan, October 3, 1990.

"Paradoxes, Facts and Fiction in Material Failure under Compression," Tulane University, New Orleans, LA, November 29, 1990.

"Micromechanics of Flow and Failure Modes of Particulate Media Over a Wide Range of Strain Rates", *Invited Lecture*, 2nd U.S. - Japan Seminar on Granular Materials, Potsdam NY, August 4 - 9, 1991.

B. CONSULTATIVE AND ADVISORY FUNCTIONS WITH OTHER AGENCIES, LABORATORIES AND UNIVERSITIES.

DARPA Panel Meeting, 10/89

Member of DARPA Panel on Material Modeling and Large Scale Computations

Society of Engineering Sciences (SES) Conference
Ann Arbor, Mich, 9/89

Member of SES
Organizer of "Computational Mechanics" and "Micromechanics of Damage and Failure" Sessions.

2nd U.S.- Japan Seminar On Micromechanics of Granular Materials, Clarkson University, Potsdam, NY, 8/91

Seminar Participant

Tulane University, Department of Mechanical Engineering,
New Orleans, LA

(to collaborate with Professor M. Mehrabadi)

Domaine Universitaire, Grenoble, France

(to collaborate with Professor B. Loret)

Tohoku-Gakuin University, Department of Civil Engineering
Tagajyo, Japan

(to collaborate with Professor M. Satake)

Tohoku University, Department of Civil Engineering,
Aoba, Sendai, Japan

(to collaborate with Professor Y. Kishino)

Hachinohe Institute of Technology, Department of
Civil Engineering, Hachinohe, Japan

(to collaborate with Professor Y. Tobita)

SOME BASIC THEORETICAL AND EXPERIMENTAL RESULTS ON MICROMECHANICS OF
GRANULAR FLOW

M. M. Mehrabadi,¹ S. Nemat-Nasser,² H. M. Shodja,³ G. Subhash²

¹Department of Mechanical Engineering, Tulane University,
New Orleans, Louisiana 70118

²Department of Applied Mechanics and Engineering Sciences, University of
California, San Diego, La Jolla, California 92093

³Department of Civil Engineering, The Technological Institute, Northwestern
University, Evanston, Illinois 60201

SUMMARY

In order to establish guidelines for modeling the macroscopic behavior of granular materials, an experimental study of the evolution of the microstructure of an assembly of granular materials under a uniform confining pressure and subjected to a pure shear was conducted. The granular material used in the study consisted of photoelastically sensitive rod-shaped particles of oval cross-sections. It was found that (i) the distribution of branches and contact normals are almost identical, (ii) the second rank fabric tensor does not adequately describe the microstructure of highly anisotropic samples, (iii) the density of contacts whose normals lie along the major and minor principal stress axes, varies sharply initially and then approaches a constant value in the course of deformation, and (iv) the density of contacts with planes parallel to the maximum shear stress plane remains practically constant throughout the deformation.

INTRODUCTION

A microscopic study of the evolution of the microstructure of an assembly of granular materials under a uniform confining pressure and, in addition, subjected to a pure shear is reported here. The granular material used in the study consisted of photoelastically sensitive rod-shaped particles of oval cross-sections.

The purpose of the experimental study, in general terms, was to establish guidelines for modeling the macroscopic behavior of granular materials. Specifically, the objective of this work was to investigate the correlation among certain microscopic fabric measures such as the distribution of contact normals, unit branches, etc., and to study the evolution of these quantities in the course of deformation.

Experiments on assemblies of photoelastic particles were pioneered by Dantu (ref. 1), Weber (ref. 2) and Wakabayashi (ref. 3), and later followed by several other

and Image Tool from Imaging Technology, a powerful program for obtaining histograms of several microscopic quantities was developed. After digitizing the photographs of the isochromatic fringe pattern obtained at each stage of loading, the program was employed to find the corresponding distributions of (i) contact normals, (ii) branches, and other related quantities.

REPRESENTATION OF DISTRIBUTION DENSITY FUNCTION

In works on crystallography, it is customary to represent the distribution density function of an orientation by spherical harmonic functions. Another alternative is the invariant formulation by Kanatani (ref. 17) which for two dimensions, is given by

$$E(n) = \frac{1}{2\pi} (1 + J_{ij}n_i n_j + J_{ijkl}n_i n_j n_k n_l + \dots) \quad (1)$$

where $E(n)$ is the distribution density function of the unit vector n , and where

$$J_{ij} = 4 \left[\langle n_i n_j \rangle - \frac{1}{2} \delta_{ij} \right], \quad (2)$$

$$J_{ijkl} = 16 \{ \langle n_i n_j n_k n_l \rangle - \delta_{ij} \langle n_k n_l \rangle + \frac{1}{8} \delta_{ij} \delta_{kl} \}. \quad (3)$$

The angular brackets denote averages taken over all orientations. The symmetric, traceless second-rank tensor J_{ij} is closely related to various fabric or anisotropy tensors (ref 18) previously introduced in the literature. The fourth-rank tensor J_{ijkl} is completely symmetric and traceless. The components of these two tensors can be represented, in two dimensions, in terms of four parameters, A, B, C and D, defined by

$$A = \langle \sin\theta \cos\theta \rangle, \quad C = \langle \cos^2\theta \rangle, \quad (4)$$

$$B = \langle \sin^2\theta \cos^2\theta \rangle, \quad D = \langle \cos^4\theta \rangle,$$

where θ is the orientation of n measured from the vertical. Note that the parameters A and C are related to the degree of concentration, J , and the preferred orientation, β , introduced by Konishi (ref 6),

$$J^2 = \frac{1}{8} J_{ij} J_{ij} = 4A^2 + (1-2C)^2, \quad (5)$$

that of the inclination of the principal axis of stress at or immediately after the peak stress.

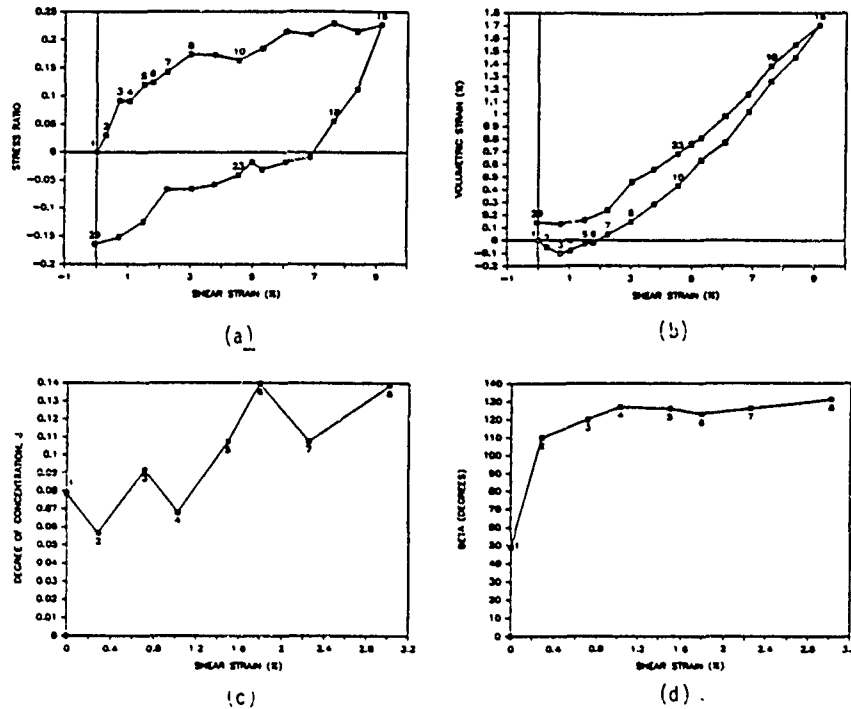


Fig. 1. Variation of (a) stress ratio, (b) volumetric strain, (c) degree of concentration, and (d) orientation of the major principal axis of the second-rank fabric tensor, J_{ij} , with shear strain.

The observed distribution of contact normals as well as its second and fourth order approximations (see Eqs. (7)) are shown in Fig. 2. Consistent with earlier observations, it is seen here also that some contacts with unit normals along the minor principal stress axis are lost while new contacts with unit normals along the major compressive principal stress axis are continually generated.

Clearly, the basic features of the actual distribution are well represented by the fourth-order approximation. In fact, it can be shown that the error in calculating $E(n)$ by excluding the fourth- and higher-order terms can be more than $\pm 30\%$ along the major and minor principal stress axes. Thus, for a highly anisotropic microstructure, the second-rank tensor J_{ij} does not appear to be adequate, and, for a more reasonable representation of the microstructure, one must, at least, retain the fourth-order term involving the fabric tensor J_{ijkl} .

the expression for $\Xi(n)$ (see Eqs. (7)), the sine terms (i.e., those involving the odd functions of θ) vary substantially in the course of shearing deformation, while the cosine terms (i.e., those that are even functions of θ) are practically constant throughout the deformation process.

The variation of A, B, C and D with the stress ratio is also found to be similar to the change of these parameters with the shear strain, shown in Fig. 3.

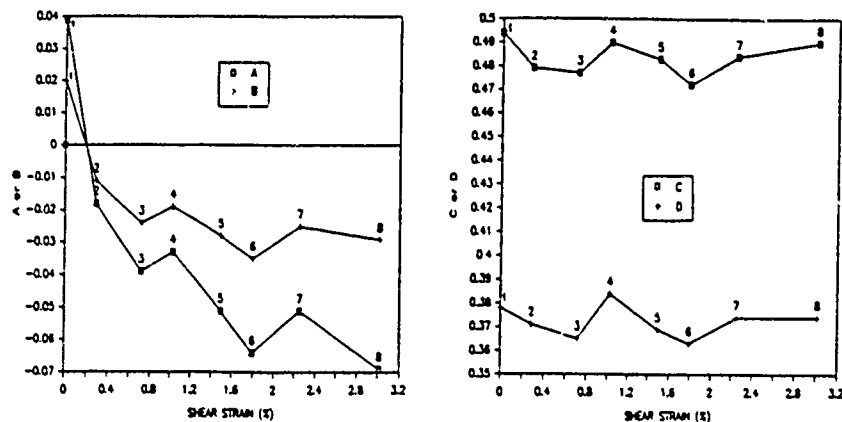


Fig. 3. Evolution of parameters A, B, C and D with shear strain.

As a corollary of the above observation, we can see that when the sine terms in the expression for $E(n)$ are zero, i.e., when

$$\sin 2n\theta = 0 \quad (n=1,2,\dots),$$

or when $\theta=0^\circ, 90^\circ, \dots$, then

$$\cos 2n\theta = (-1)^n,$$

and hence $E(0^\circ)$ and $E(90^\circ)$ are practically constant. Note that for $\theta=45^\circ, 135^\circ, \dots$, we have

$$\sin 2n\theta = (-1)^{n+1}, \quad \cos 2n\theta = 0$$

Therefore, $E(45^\circ)$ and $E(135^\circ)$, which are the distribution densities of contact normals along the major and minor principal stress axes, vary initially and then approach a constant value in the course of deformation: see Fig. 4.

REFERENCES

1. Dantu, P., "Etude mecanique d'un milieu pulverulent forme de spheres egales de compacite maxima." Proc. 5th Int'l Conf. Soil Mech. Found. Eng., 1, 1961, 61-70.
2. Weber, J. D., "Recherches concernant les contraintes intergranulaires dans les milieux pulverulents." Cahiers du Groupe Francais de Rheologie, 3, 1966, 161-170.
3. Wakabayashi, T., "Photoelastic Method for Determination of Stress in Powdered Mass." Proc. 7th Japan National Cong. for Appl. Mech., 1957, 153-163.
4. Oda, M. and Konishi, J., "Microscopic Deformation Mechanism of Granular Material in Simple Shear." Soils and Foundations, Vol. 14, No. 4, 1974, 25-38.
5. Konishi, J., "Microscopic Consideration on Deformation and Strength Behavior of Granular Material Like Sand." Faculty of Engineering Report, Shinshu University, 1978 (in Japanese).
6. Konishi, J., "Microscopic Model Studies on the Mechanical Behavior of Granular Materials." Proceedings of the U.S.-Japan Seminar on Continuum Mechanical and Statistical Approaches in the Mechanics of Granular Materials, eds., Cowin, S. C. and Satake, M., Gakujutsu Bunken Fukyukai, Tokyo, Japan, 1978, 27-45.
7. Ishizuka, M., Satake, M., and Niizeki, S., "Analysis of Deformation Mechanism of Granular Material in Simple Shear Using Photoelasticity." Proc. of the 35th Annual Meeting of the JSCE, Vol. III, 1980, 33-34 (in Japanese).
8. Biarez J. and Wicndteck, K., "La comparaison qualitative entre l'anisotropie mecanique et l'anisotropie de structure des milieux pulverulents." C. R. Acad. Sci., Vol. 256, 1217-1220.
9. Drescher, A. and de Josselin de Jong, G., "Photoelastic Verification of a Mechanical Model for the Flow of a Granular Material." J. Mech. Phys. Solids, Vol. 20, 1972, 337-351.
10. Drescher, A., "An Experimental Investigation of Flow Rules for Granular Materials Using Optically Sensitive Glass Particles." Geotechnique, Vol. 26, No. 4, 1976, 591-601.
11. Oda, M., Nemat-Nasser, S., and Konishi, J., "Stress-Induced Anisotropy in Granular Masses." Soils and Foundations, Vol. 25, No. 3, 1985, 85-97.
12. Allersma, H. G. B., "Photo-elastic Stress Analysis and Strains in Simple Shear." in Proc. of the IUTAM Conf. on Deformation and Failure of Granular Materials, eds., Vermeer, P. A., and Luger, H. J., Balkema, Rotterdam, 1982, 345-353.
13. Konishi, J., Oda, M., and Nemat-Nasser, S., "Induced Anisotropy in Assemblies of Oval Cross-Sectional Rods in Biaxial Compression." Mechanics of Granular Materials: New Models and Constitutive Relations, eds., Jenkins, J. T. and Satake, M., Elsevier, Amsterdam, 1983, 31-39.

EFFECT OF FABRIC ON LIQUEFACTION AND DENSIFICATION
OF SATURATED SOIL: EXPERIMENTS AND THEORY

S. Nemat-Nasser

Department of Applied Mechanics and Engineering Sciences, University of
California, San Diego, La Jolla, California 92093

SUMMARY

It has been known that the inherent and induced anisotropy or fabric has considerable influence on the response and failure modes of granular masses. Some definitive recent experiments which clearly demonstrate this phenomenon in relation to the densification and liquefaction potential of saturated sands, are briefly reviewed, together with associated micromechanically based theoretical observations.

INTRODUCTION

Cohesionless granular materials support the applied forces through contact friction. Therefore, the nature and distribution of the contacts are expected to have considerable influence on the overall mechanical response of the granular mass. The term "fabric" has been used to characterize this kind of microstructure. It relates to the distribution of the particles, their sizes and orientations, and, in particular, to the distribution of the contact normals and contact areas (which reflect the magnitude of the contact forces), as well as other geometrical entities. In this summary we shall not deal directly with the characterization of fabric, since the matter has been fully examined in other articles within this volume; see, e.g. the paper by Mehrabadi *et al.* (ref. 1). What is of concern here is to show how seemingly minute variations in a given loading history can change the fabric of the granular mass to such an extent that the load-bearing capacity of the sample is changed by orders of magnitude.

In particular, we shall examine the effect of pre-straining on the liquefaction potential of saturated sands, and point out the results of recent experiments by Nemat-Nasser and Tobita (ref. 2) and Nemat-Nasser and Takahashi (ref. 3), which clearly have brought into focus the effect of induced fabric on the potential to failure by liquefaction of undrained samples.

RESULTS AND DISCUSSION

It has been shown by Finn *et al.* (ref. 4) and confirmed by Ishihara *et*

a1. (ref. 5), and other investigators, that, once a saturated undrained sample of sand is liquefied in simple shearing, it will have essentially no resistance to reliquefaction in subsequent tests. These tests were all performed under a *load-controlled* condition, so that, with the confining pressure held fixed, the tests were terminated after liquefaction initiation, by reducing the shear stress to zero.

Faced with the above experimental facts, in the late seventies the present writer became very interested in this phenomenon, and sought to: (1) develop a micromechanical model which might clarify the phenomenon; and (2) seek to check the experimental results independently and in light of the micromechanics of the process. The work on the micromechanics of this phenomenon was reported in Nemat-Nasser (1980, ref. 6), and the experimental effort was done in collaboration with Dr. Tobita and Mr. Takahashi; see (ref. 2 and ref. 3).

Micromechanical Model:

The model considers two-dimensional shearing of a layer of a granular mass under uniform applied normal compressive stress, σ , and uniform shear stress, τ , which is viewed positive when clockwise. The macroscopic shear flow is the result of the microscopic motion (rolling and sliding) of grains relative to each other at active contact points. Fig. 1 shows this.

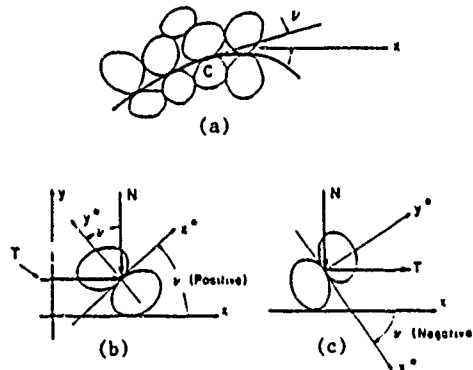


Figure 1

The angle ν is called the (micro) dilatancy angle. It varies from *active* contact to *active* contact, and when there is a very large number of such contacts, one may assume a continuous change and introduce a distribution-density function $p(\nu)$ in such a manner that $p(\nu_0) d\nu$ represents the volume fraction of active granules whose dilatancy angles are between ν_0 and $\nu_0 + d\nu$. ν is positive when it produces volume expansion. By considering the balance of forces transmitted across each active contact, and by equating

the rate of frictional dissipation at active contacts within a unit volume to the rate of the overall stress-work, Nemat-Nasser (ref. 6) obtains the following dilatancy equation:

$$\frac{1}{V} \frac{dV}{d\gamma} = \frac{1}{\cos \phi_\mu} \int_{\nu_0^-}^{\nu_0^+} p(\nu) \cos(\phi_\mu + \nu) \sin \nu d\nu \quad (1)$$

in which ϕ_μ = "grain-to-grain" friction angle; and the Mohr-Coulomb failure criterion is used to characterize the local (at the micro-level) flow process.

Nemat-Nasser (ref. 6) points out that upon shearing and under normal pressure, granules with negative dilatancy angles are activated first, leading to a distribution-density function, $p(\nu)$, which initially is biased toward negative dilatancy angles. Intuitively, this follows from the physical observation that the local normal force N hinders the motion of an active granule with positive dilatancy angle ν , whereas it assists when ν is negative (Figs. 1(b) and (c)). Hence, upon shearing under confinement, an initial densification is expected and is invariably observed.

As shearing proceeds, the distribution-density function $p(\nu)$ tends to become biased toward positive dilatancy angles, and this leads to subsequent dilation. During this stage, a greater number of active contacts has positive dilatancy angles, and this number increases with increasing shear strain amplitude, up to the strain corresponding to the peak stress. Now, if, after a microstate of this kind is attained, unloading begins, then some of the granules with suitably large dilatancy angles may actually start a downward motion under the action of the normal force N , which leads to some densification. However, it is reasonable to expect, and our experiments on photoelastic granules confirm (see ref. 7), that at zero shear stress there still exists a strong bias toward positive dilatancy angles for clockwise shearing. Now, upon load reversal (i.e., upon shearing in the counterclockwise direction), the previously positive dilatancy angles behave now as negative ones. Thus, a strong tendency toward densification would be expected during load reversal. Hence, prestraining to suitably large shear strain amplitudes in drained conditions should lead to immediate liquefaction when load reversal occurs under undrained conditions.

Experimental Results:

To test the liquefaction potential of a preliquefied sample in light of the micromechanical model, Nemat-Nasser and Tobita (ref. 2) compared the liquefaction potential of two similar samples which were liquefied by

cyclic shearing under constant confining pressure. The difference between the two tests was the state at which the initial liquefaction was terminated during the final cycle: (1) In one test the final cycle in the initial liquefaction was terminated at zero shear stress. (2) In the second, otherwise similar, sample, the final cycle was terminated at zero shear strain. It was found that, during reliquefaction, the first sample (which was stopped at zero shear stress) showed essentially no resistance to reliquefaction, whereas the second sample (which was stopped at zero shear strain) was essentially as resistant to liquefaction as a virgin sample. These and related results were reconfirmed in a series of carefully planned experiments by Nemat-Nasser and Takahashi (ref. 3).

Another related phenomenon is prestraining under drained conditions and its effect on the liquefaction potential of the saturated undrained sample. Guided by the micromechanical model, Nemat-Nasser and Tobita (ref. 2) showed that, if prestraining at a suitably large shear strain is terminated at zero shear stress, then the sample will have strong induced anisotropy and hence, in subsequent undrained cyclic shearing, will liquefy during the first cycle. On the other hand, if the prestraining is terminated at zero shear strain, the sample will be left with essentially no induced anisotropy, and will be at least as resistant to liquefaction as the corresponding virgin sample.

In an effort to further verify these facts and, in addition, to examine the influence of the sample preparation on the mechanical response of cohesionless sands in cyclic shearing, Nemat-Nasser and Takahashi (ref. 3) have made a series of strain-controlled tests on Monterey No. 0 sand samples. The same apparatus as the one used by Nemat-Nasser and Tobita (ref. 2) is employed, except that the horizontal shearing device is modified in such a manner as to control the horizontal stroke, and to measure the corresponding resulting horizontal force. Two sample preparation techniques are used: moist tamping and pluviating dry sand through air. The basic conclusions of these experimental results are as follows:

1. In cyclic simple shearing, the resistance to reliquefaction (undrained) or densification (drained) of a preliquefied sample actually increases, because of the concomitant densification, if the preliquefaction is terminated at zero residual shear strain, but this resistance becomes very small if the preliquefaction is terminated at zero residual shear stress.
2. The inherent anisotropy associated with sample preparation techniques affects both the densification and liquefaction potential of the sample.

3. Within each cycle of simple shearing, the induced anisotropy is essentially wiped out in the neighborhood of zero shear strain, and the anisotropy that exists at this state is basically due to the sample preparation techniques (i.e., it is the inherent anisotropy), provided that the sample is not very loose and the strain amplitude is not very large. (Note that the state of zero shear strain is essentially the same as that of the state of zero dilatancy which is, indeed, the basic underlying factor.)
4. For simple shearing, the distribution of the dilatancy angles characterizing the fabric may be related to the shear strain and, in this manner, the densification pattern may be estimated.

Since the simple shearing experiments are performed on small circular cylinders, the state of stress in the sample is quite complicated. In order to verify the validity of the results, a new series of tests has now been initiated at the author's laboratory. These tests are being performed on a large hollow cylindrical sample under carefully controlled conditions so as to ensure a uniform state of stress and deformation in the sample. The results of these experiments will be reported soon after they are completed.

ACKNOWLEDGMENTS

This work has been supported by Air Force Office of Scientific Research under Grant No. AFOSR-87-0079 to the University of California, San Diego.

REFERENCES

1. Mehrabadi, M. M., Nemat-Nasser, S., Shodja, H. M., and Subhash, G., "Some Basic Theoretical and Experimental Results on Micromechanics of Granular Flow."
2. Nemat-Nasser, S., and Tobita, Y., "Influence of Fabric on Liquefaction and Densification Potential of Cohesionless Sand," *Mechanics of Materials*, Vol. 1, 1982, pp. 43-62.
3. Nemat-Nasser, S., and Takahashi, K., "Liquefaction and Fabric of Sand," *Journal of Geotechnical Engineering Division*, ASCE, Vol. 110, No. 9, 1984, pp. 1291-1306.
4. Finn, W. D. L., Bransby, P. L., and Pickering, D. J., "Effects of Strain History on Liquefaction of Sand," *Journal of the Soil Mechanics and Foundations Division*, ASCE, Vol. 96, No. SM6, 1970, pp. 1917-1934.
5. Ishihara, K., Tatsuoka, F., and Yasuda, S., "Undrained Deformation and Liquefaction of Sand under Cyclic Stress," *Soils and Foundations*, Vol. 15, 1975, pp. 29-44.
6. Nemat-Nasser, S., "On Behavior of Granular Materials in Simple Shear," *Soils and Foundations*, Vol. 20, 1980, pp. 59-73.
7. Nemat-Nasser, S., Mehrabadi, M. M., Shodja, H., Subhash, G., "A Microscopic Study of the Granular Material Behavior in Pure Shear," in preparation.

Anisotropy in Response and Failure Modes of Granular Materials

REFERENCE Nemat-Nasser, S. *Anisotropy in response and failure modes of granular materials, Yielding, Damage, and Failure of Anisotropic Solids*. EGF5 (Edited by J. P. Boehler) 1990, Mechanical Engineering Publications, London, pp. 33-48.

ABSTRACT This review addresses some recent experimental and theoretical studies of the mechanical properties of particulate media which support applied overall loads through individual contact resistance. We emphasize the inherent and induced fabric or anisotropy and its influence on the response and failure modes of this class of materials. The experimental studies include: (1) model experiments on photoelastic granular rods with circular and elliptical cross-sections, in biaxial as well as simple shear cyclic loading; and (2) dilatancy, liquefaction, and the overall stress-deformation relations studied on simple shearing apparatus and also on large hollow cylindrical samples of sand under complex, three-dimensional monotonic as well as cyclic stress paths. These experiments are designed in coordination with theoretical micromechanical models in order to bring out the major micromechanisms that are responsible for the observed highly path-dependent behaviour of granular materials. The issues of inherent and induced anisotropy or fabric and their effects on the overall response of the material are of particular interest in these experiments. The theoretical studies emphasize recent micromechanically-based models of granular flow, which specifically seek to understand and quantify relevant measures of anisotropy or fabric, and the relation between fabric measures and the overall stress tensor.

Introduction

A fundamental understanding of the mechanical behaviour of granular masses which support the overall applied loads through contact friction is essential for many applications, from powder metallurgy, ceramic processing, and food processing, storage, and transportation, to the proper design of soil foundations to withstand earthquake-induced vibration. A dominant feature of materials of this kind is their strong anisotropic behaviour. Generally speaking, two types of anisotropy are identified. They are: (1) inherent anisotropy produced essentially by the process of deposition (natural or artificial); and (2) induced anisotropy, produced in the course of deformation in response to the overall applied loads. Both types of anisotropy can have a most profound influence on the response and failure modes of granular masses. Hence, attempts have been made to identify microstructural parameters which characterize these anisotropies, and relate these parameters to the overall measures of stress and the associated deformation.

The purpose of this article is to summarize some recent fundamental developments in the characterization of the mechanical properties of granular

* University of California, San Diego, Department of Applied Mechanics and Engineering Sciences, Mail Code R-011, La Jolla, CA 92093, USA

masses, emphasizing the effects of anisotropy or fabric on the overall mechanical response. No attempt will be made to provide a comprehensive review of the literature in the field, since the reader can easily obtain the relevant references by consulting, for example, the proceedings of the US–Japan seminars which are cited in references (6) and (14).

This paper is organized as follows. In the next section the relation between the overall stress tensor and the contact forces is developed, and the importance of fabric is discussed. Various measures of fabric are identified, and some major issues relating to the stress–fabric relation are examined in the light of recent experiments by the author and co-workers on biaxial deformation as well as on pure shearing of samples made of photoelastic rods of oval cross-section. The statistical description of the fabric and stress tensors is presented. In the third section the micromechanics of granular flow in cyclic simple shearing is examined in some detail, and the effects of fabric on the dilatancy (or densification) potential of the granular mass are demonstrated in terms of the failure modes of saturated cohesionless sands subjected to cyclic shearing under confining pressure. In particular, it is shown that the resistance to failure by liquefaction can be increased or reduced to almost zero by seemingly minute alterations in the fabric of the granular mass.

Representation of stress and fabric

General comments

Consider a collection of granules with overall volume V and overall surface S . Let self-equilibrating tractions \bar{T} be applied on the boundary surface S , producing contact forces at contacting granules. Assume that there are such a large number of granules contained in V that both a continuum and a statistical representation of the overall stress $\bar{\sigma}$ are permissible. Furthermore, assume that the granules are so stiff relative to the applied loads, that they may be regarded as essentially rigid. A fundamental problem is to relate the overall stress $\bar{\sigma}$ to the corresponding internal contact forces and the microstructure of the granular mass.

Let $\sigma(x)$ be a variable stress field in equilibrium with the applied traction \bar{T} , in the absence of any body forces. This stress field may vary discontinuously from granule to granule, but it is required to produce continuous tractions across the contact area of any two contacting granules. Using a fixed rectangular Cartesian coordinate system, with coordinate axes x_i , $i = 1, 2, 3$, we then have

$$\begin{aligned} \sigma_{ij,j} &= 0 \text{ in } V \\ \sigma_{ij}\nu_j &= \bar{T}_i \text{ on } S \end{aligned} \tag{1}$$

where ν is the exterior unit normal on S . The overall average stress is now

defined as the simple volume average of this self-equilibrating stress field

$$\bar{\sigma} \equiv \frac{1}{V} \int_V \sigma(\mathbf{x}) dV \quad (2)$$

Note that the continuity of the tractions across any two contacting granules, say, granules A and B, requires

$$[\sigma_{ij}]n_j = 0 \quad (3)$$

where \mathbf{n} is the unit normal on the contact area, which points from A to B, and the brackets indicate the 'jump' across the area, $[\sigma_{ij}] \equiv \sigma_{ij}^+ - \sigma_{ij}^-$, and where the superposed + and - denote the value of stress, respectively, in A and B at the contact point. Equation (3) simply implies that the contact force exerted by granule A, on its adjacent contacting granule B, is equal in magnitude but opposite in direction of the force exerted by B on A.

Overall stress

In the absence of any pore fluid or gas pressure, equation (2) may be written as

$$\bar{\sigma} = \frac{1}{V} \sum_{\alpha=1}^{M_G} \int_{V_\alpha} \sigma(\mathbf{x}) dV = \sum_{\alpha=1}^{M_G} c^\alpha \bar{\sigma}^\alpha \quad (4)$$

where c^α is the volume fraction of the α th granule, i.e., $c^\alpha = V_\alpha/V$, M_G is the total number of granules in volume V , and $\bar{\sigma}^\alpha$ is the average stress over the α th granule. In view of equations (1) and (3)

$$\int_V (x_j \sigma_{ik}),_k dV = \int_V \sigma_{ij} dV = \int_S x_j \bar{T}_i dS \quad (5)$$

and hence one has

$$\bar{\sigma}_{ij} = \frac{1}{V} \sum_{\alpha=1}^{M_S} x_j^\alpha F_i^\alpha \quad (6)$$

where M_S is the number of points on the *outer* boundary S at which concentrated forces \mathbf{F}^α are applied. It is important to note that this representation of stress does *not* involve the contact forces at the interior contacting granules. In (2.6) \mathbf{x}^α is the location on the *overall surface* S at point α , where the concentrated external force \mathbf{F}^α is applied. Hence, representation (6) does *not* involve the microstructure.

An alternative representation which does include the microstructure, has been given by Christoffersen *et al.* (1), using the principle of virtual work. In this approach, one considers virtual relative displacement Δ^α at a typical contact α , compatible with the virtual surface displacement \mathbf{u} . Then the virtual work yields

$$\sum_{\alpha=1}^M \Delta_i^\alpha f_i^\alpha = \int_S u_i \bar{T}_i dS \quad (7)$$

Choosing a virtual displacement field

$$u_i = \phi_{ij} x_j + a_i \quad (8)$$

with arbitrary constant ϕ_{ij} and a_i , we obtain

$$\bar{\sigma}_{ij} = \frac{1}{V} \sum_{\alpha=1}^M f_i^\alpha l_j^\alpha \equiv N \langle f_i l_j \rangle \quad (9)$$

where l_j^α is a vector which connects the centroids of the two granules which are in contact at α . The symmetry of the overall Cauchy stress then yields

$$\langle f_i l_j \rangle = \langle f_j l_i \rangle \quad (10)$$

In (9), $N = M/V$ is the number of contacts per unit volume, and

$$\langle \langle \dots \rangle \rangle \equiv \frac{1}{N} \sum_{\alpha=1}^N (\dots)_\alpha$$

We note that representation (9) can also be obtained if one considers average transactions transmitted across three mutually orthogonal planes. This approach was originally suggested by Weber (16) in examining the forces transmitted within a collection of glass rods with circular cross-section. Mehrabadi *et al.* (3) considered a similar approach and showed the relation between the statistical calculation of average transactions and the virtual work method; see their equations (27) and (29), p. 101.

Expression (9) may also be obtained by applying (5) to a single typical granule of, say, volume V_α and surface S_α , and then summing the results over all granules. Indeed, from (4) and (5), it follows that

$$\bar{\sigma}_{ij} = \frac{1}{V} \sum_{\alpha=1}^{M_G} \sum_{\beta=1}^{M_\alpha} (x_j^\beta - \bar{x}_j^\alpha) F_i^\beta \equiv N \langle f_i l_j \rangle$$

where M_α is the number of contacts of the α th granule, \bar{x}_j^α is the position of the centroid of this granule, and we have used the fact that the sum of all contact forces acting on the granule α must vanish.

Stress-fabric relation

There are a number of ways that the overall stress tensor can be related to certain measures of the microstructure or fabric of a granular mass. One alternative proposed by Nemat-Nasser and Mehrabadi (7) is to associate with a typical contact α a symmetric second-order tensor t_{ij}^α , such that

$$f_i^\alpha = a^\alpha t_{ij}^\alpha n_j^\alpha \quad (\alpha \text{ not summed}) \quad (11)$$

where a^α may be regarded a measure for the contact area. Then (9) can be written as

$$\bar{\sigma}_{ij} = \langle t_{ik} h_{kj} \rangle \quad (12)$$

where

$$h_{kj}^\alpha \equiv \varepsilon^\alpha n_k^\alpha m_j^\alpha, \quad \varepsilon^\alpha \equiv N a^\alpha l^\alpha, \quad l_j^\alpha = l^\alpha m_j^\alpha \quad (\alpha \text{ not summed}) \quad (13)$$

where \mathbf{m}^α is a unit vector in the direction of \mathbf{l}^α . The geometric quantity

$$H_{ij} = \langle h_{ij} \rangle \quad (14)$$

is a measure of the fabric of the granular mass. Other measures can be introduced, and some are briefly discussed later on in this section. If the granules are spherical (circular in two dimensions), then the unit vector \mathbf{m}^α coincides with the unit normal \mathbf{n}^α , and the fabric tensor \mathbf{H} becomes symmetric. Furthermore, the symmetry of the overall stress, equation (10), requires

$$\langle t_{ik} h_{kj} \rangle = \langle t_{jk} h_{ki} \rangle \quad (15)$$

If we now set

$$T_{ik} \equiv \langle t_{ik} \rangle \quad (16)$$

assume that t_{ik}^α and h_{kj}^α are uncorrelated, and that the tensor \mathbf{T} does not depend on any other tensor-valued quantities than \mathbf{H} , it follows from the symmetry condition (15) that the three symmetric second-order tensors $\bar{\boldsymbol{\sigma}}$, \mathbf{H} , and \mathbf{T} are coaxial, in the sense that they share the same principal directions. An immediate consequence of this then is the following stress–fabric relation:

$$\bar{\sigma}_{ij} = A_0 \delta_{ij} + A_1 H_{ij} + A_2 H_{ik} H_{kj} \quad (17)$$

where the coefficients A_0 , A_1 , and A_2 are functions of the basic invariants of \mathbf{H} .

Equation (17) is the simplest stress–fabric relation that emerges under the rather restrictive assumptions that: (1) granules are spherical (or circular); (2) the quantities \mathbf{t}^α and \mathbf{h}^α are uncorrelated, so that $\langle t_{ik} h_{kj} \rangle = \langle t_{ik} \rangle \langle h_{kj} \rangle$; (3) there are no other tensorial measures that are involved in expression $\bar{\boldsymbol{\sigma}} = T_{ik} H_{kj}$; and (4) the overall stress tensor is symmetric. Experiments on the biaxial deformation of photoelastic granules seem to support (17), although the granules involved were cylinders with oval cross-section; see Fig. 13 of Oda *et al.* (12). Expression (17), however, clearly shows that the ratio of the principal stresses in two-dimensional deformation cannot be proportional to the corresponding ratio of the principal values of the fabric tensor \mathbf{H} . Hence, equation (4) and the linear approximation of Fig. 13 of Oda *et al.* (11) (which were reported on the basis of triaxial compression tests on two Sōma sands by Oda (10)), cannot have general validity. Indeed, recent experiments on pure shearing of photoelastic granules have revealed that while the principal axes of the fabric tensor tend to follow the principal axes of the stress tensor, in general, *they do not*

coincide with the latter. The apparatus, constructed in the author's laboratory, is shown in Fig. 1(a) and sketched in Fig. 1(b). A typical example is given in Fig. 2(a). The corresponding stress-strain relations are displayed in Fig. 2(b). The apparatus produces a two-dimensional flow of the granules, which is very close to pure shearing under uniform confining pressure. The results of extensive experiments and their thorough analysis will be reported elsewhere. Suffice it to say here that, upon shearing, the principal directions associated with the distribution of contact normals immediately change toward the principal directions of the stress, but do not coincide with them. Indeed, the orientation of the principal directions of the stress and the distribution of the contact normals remain distinct and fixed, as the shearing continues monotonically in a fixed direction. On the other hand, if the fabric tensor is weighted by the intensity of the contact forces which can be represented by the magnitude of the corresponding contact area through the parameter ε^α in equation (13₂), then our tentative analysis seems to suggest that the corresponding fabric tensor and stress tensor have a tendency of becoming coaxial.

Fabric tensors

In the literature, a number of second- and higher-order fabric tensors have been introduced by different authors. These tensors are, by necessity, of even orders, and, in one way or another, seek to define the distribution of contact normals or unit branches. Some of these tensors are $\langle n_i n_j \rangle$, proposed by Satake (14); $N \hat{1} \langle m_i m_j \rangle$, proposed by Mehrabadi *et al.* (3); and the non-symmetric

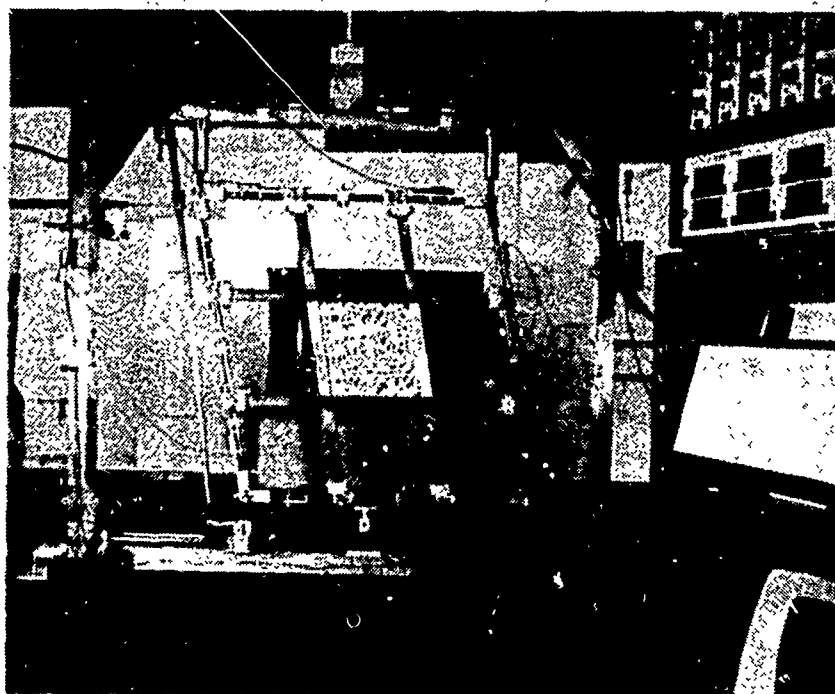
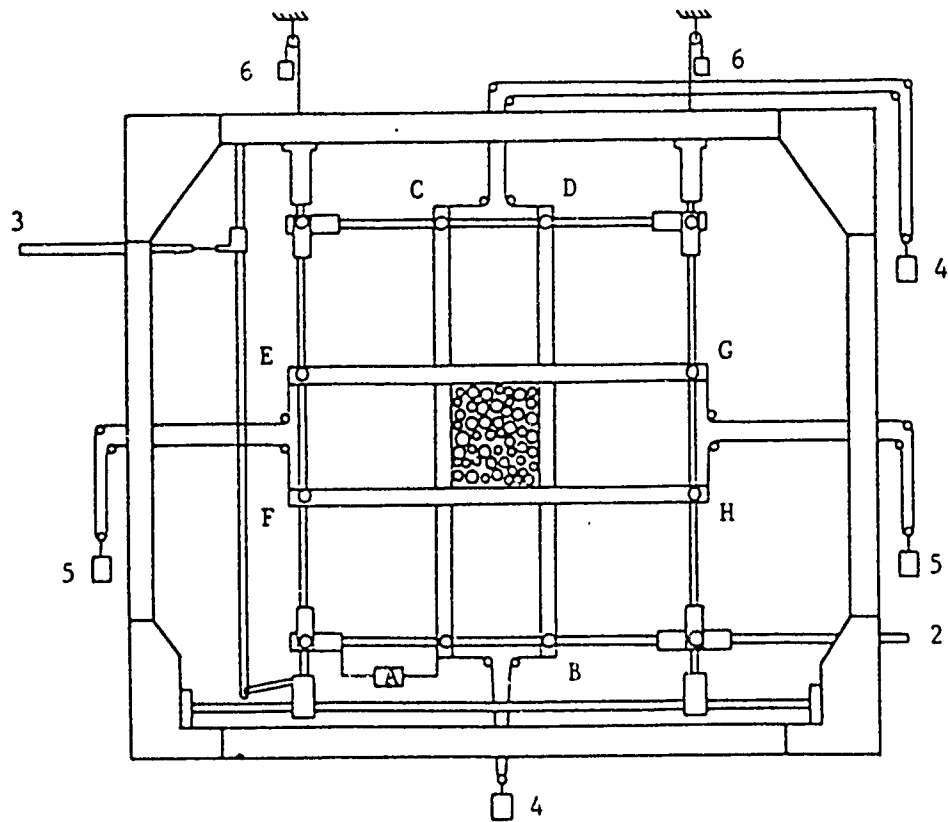


Fig 1(a) Equipment for simple shear deformation of photoelastic granules



1. loading frame
2. connection to load cell
3. LVDT
4. weights for lateral loading
5. weights for vertical loading
6. counterweights
7. linear potentiometer measuring displacement at A, B, C, D, E, F, G, and H

Fig 1(b) A schematic diagram of the simple shear apparatus (University of California, San Diego)

tensors $\langle n_i m_j \rangle$ and $\langle \epsilon n_i m_j \rangle$, proposed by Nemat-Nasser and Mehrabadi (6), who also considered $\langle \epsilon n_i n_j \rangle$ and $\langle \epsilon m_i m_j \rangle$. Higher-order fabric tensors also emerge in the micromechanical modelling of granular materials; for example, $\langle n_i n_j n_k n_l \rangle$ of Mehrabadi *et al.* (3), as well as $\langle n_i n_j m_k m_l \rangle$. It is clear that the information contained in higher-order tensors regarding the details of the distribution of contact normals or branches, will, in general, be lost, if only lower-order fabric tensors are employed; see Mehrabadi *et al.* (4).

If the fabric is characterized by the distribution of, say, the contact normals or the unit branches, then one introduces a distribution density function and seeks to quantify this directly. Representation of the distribution function in terms of spherical harmonics (in three dimensions) or Fourier series (in two dimensions) then naturally leads to various even-ordered tensors which can be

CONTACT NORMALS

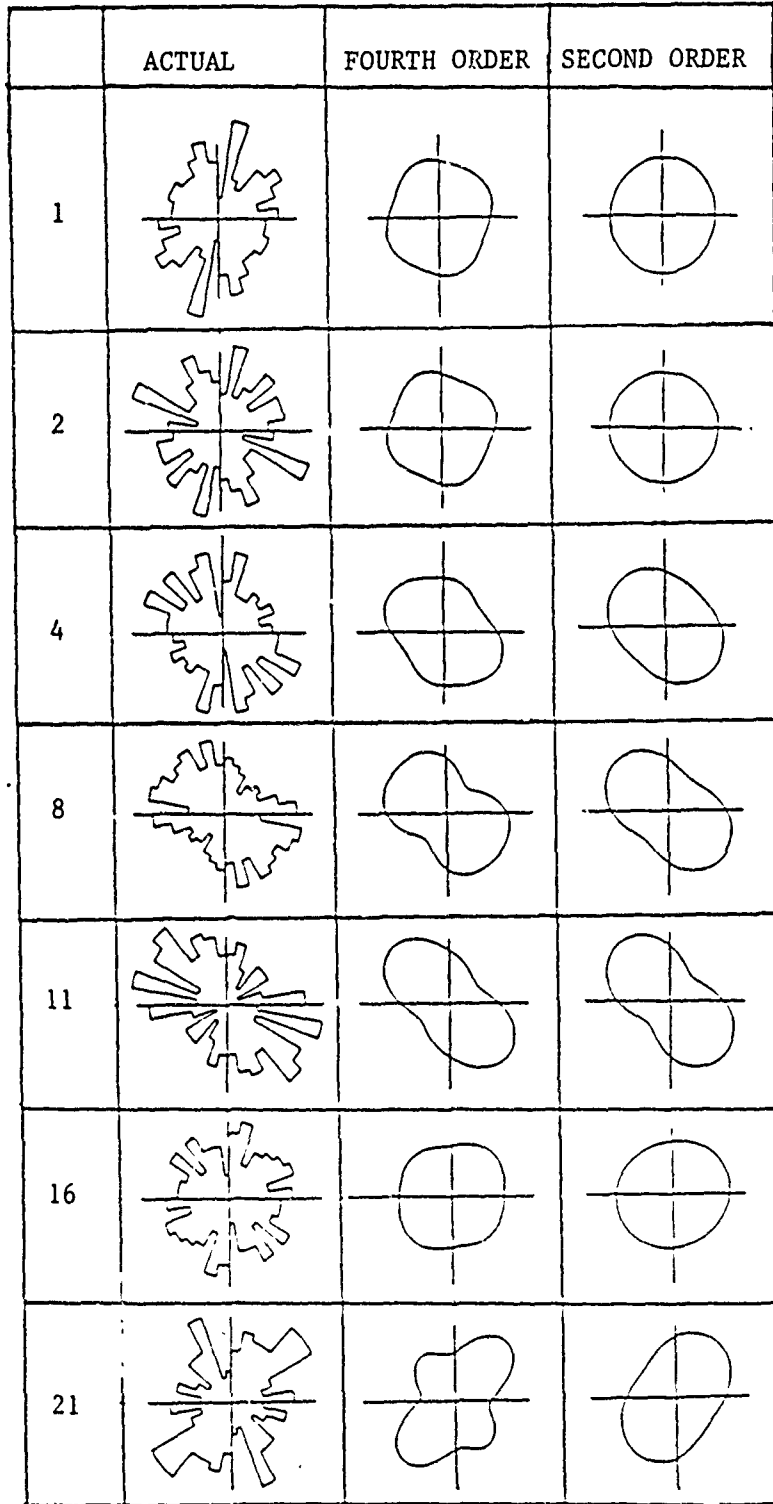


Fig 2(a) Distribution of contact normals at the seven stages of loading indicated in Fig. 2(b)

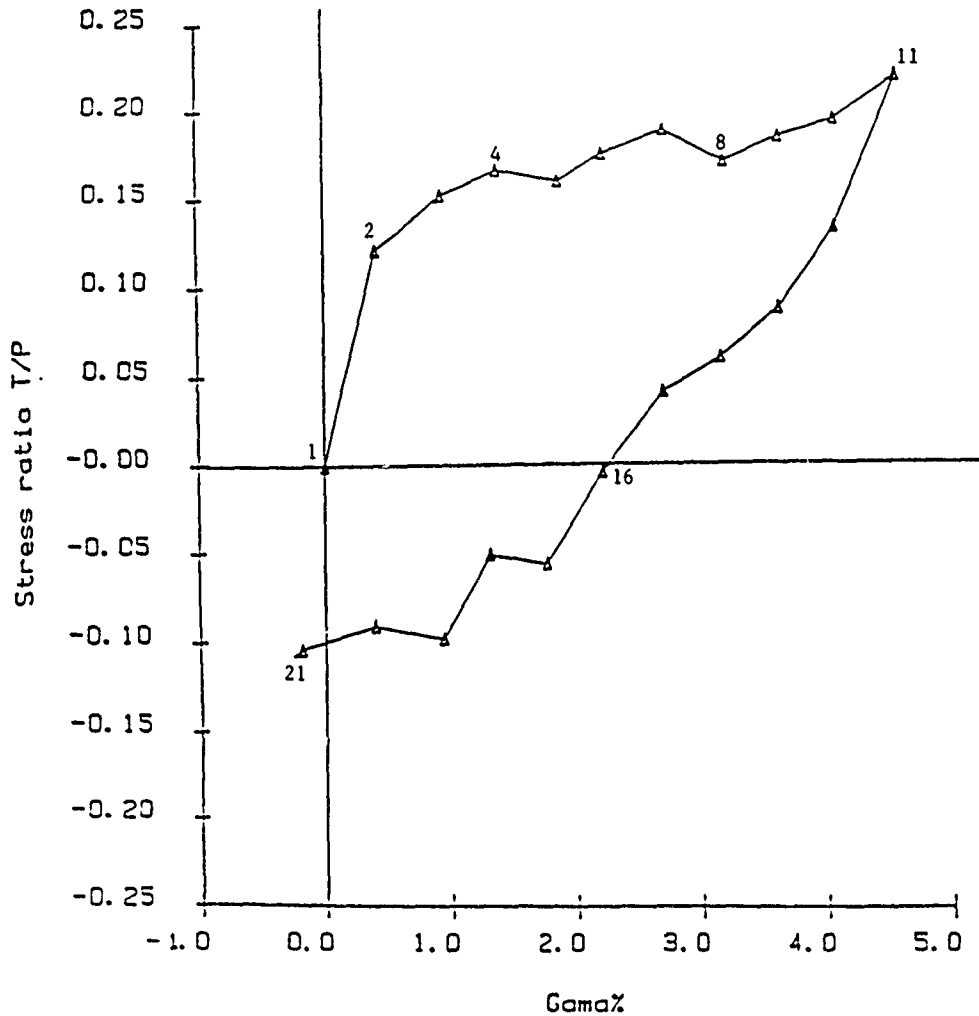


Fig 2(b) Variation of stress ratio with shear strain

used to characterize the fabric. A rather complete summary and a detailed discussion of the connections among various representations can be found in Kanatani (2); a brief review of some of the results is also given by Onat (13).

As an example, consider the distribution of contact normals, and let $E(\mathbf{n})$ be the density function for this distribution. Then

$$E(\mathbf{n}) = E(-\mathbf{n}), \quad \int_{\Omega} E(\mathbf{n}) d\Omega = 1 \quad (18)$$

where Ω is the unit sphere, and $E(\mathbf{n}) d\Omega$ is the number of contacts with the unit normal falling in the solid angle $d\Omega$, about the direction \mathbf{n} . Expanding $E(\mathbf{n})$ in spherical, or circular harmonics, one may write

$$E(\mathbf{n}) = A[1 + J_{ij}n_i n_j + J_{ijkl}n_i n_j n_k n_l + \dots] \quad (19)$$

where $A = 1/\pi$ in two dimensions, and $= 1/4\pi$ in three dimensions, and the tensors J are all deviatoric. They can easily be expressed in terms of various even-order moments of the distribution of the unit vectors \mathbf{n} . For example, if

these moments are denoted by M , and their deviatoric parts, by M' , one obtains

$$J_{i_1 \dots i_r} = \frac{2r+1}{2^r} \left(\frac{2r}{r} \right) M'_{i_1 \dots i_r} \quad (20)$$

where r is even.

Recent experiments by the author and co-workers on two-dimensional shearing of photoelastic granules have clearly shown that, in general, one must include at least the fourth-order fabric tensor, in order to capture both the inherent and the induced anisotropy of the granular material. This and related points are discussed elsewhere. In Fig. 3, however, we have shown a typical example with an actual distribution of contact normals and its second- and fourth-order approximations.

Fabric in simple shear

Simple shearing of granular materials can be attained in a large hollow circular cylindrical sample of relatively thin wall. (The special cell used in the author's laboratory has a 25 cm outside-, 20 cm inside-diameter, and is 25 cm high.) The shearing is produced by the torsion of the sample about its cylindrical axis. If we

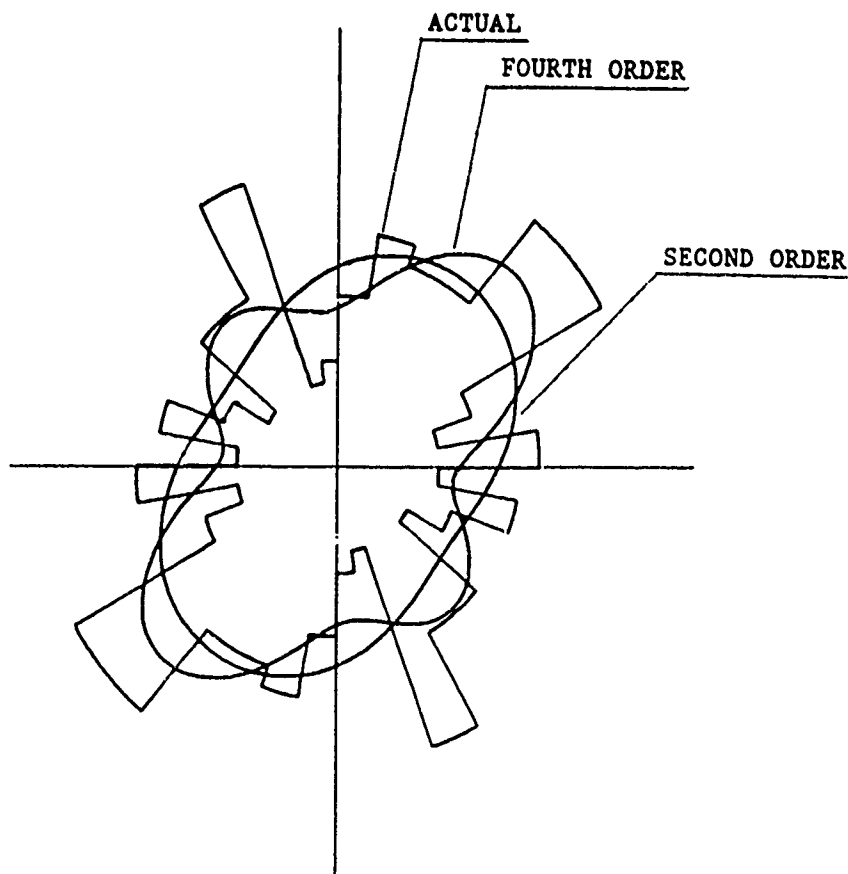


Fig. 3 Actual distribution of contact normals and its second- and fourth-order approximations

assume that during such shearing the wall thickness remains constant, then the volumetric change is associated with the change in the sample's height. In this case, a dilatancy theory for simple shearing developed by the author (5) can be applied to study the influence of fabric on the dilatancy and the liquefaction potential (saturated undrained samples) of the granular mass. While this theory has been experimentally verified using a small circular cylindrical sample 2 cm high and 7 cm in diameter, in cyclic horizontal shearing, the state of stress in such a test is very complex and clearly not simple shear; see Nemat-Nasser and Tobita (9) and Nemat-Nasser and Takahashi (8). In the following we shall give a very simple and straightforward derivation of the basic dilatancy equation and then discuss its consequences in relation to the simple cyclic shearing of saturated granular materials.

Dilatancy equation for simple shearing

Consider a column of granular material of height, h , measured along the y direction, and of unit area, being sheared in the x direction; Fig. 4(a). Assume that this shearing does not change the cross-sectional area of the column and therefore, volumetric changes occur due to the change in height. The volumetric strain rate, \dot{V}/V , then is

$$\dot{V}/V = \dot{h}/h \quad (21)$$

where the superimposed dot denotes time rate of change. While the overall shearing is in the x direction, the flow of the granules actually occurs over the wavy lines, such as SS, shown in Fig. 4(b). The motion of a typical granule, say, granule i , relative to its neighbouring granules, contributes to the overall volumetric expansion, if the dilatancy angle, ν_i , associated with this granule is positive. The dilatancy angle ν_i defines the direction of the motion of granule i , along SS, in relation to its neighboring granule. This motion occurs under the action of resultant forces T_i and N_i , which act on granule i ; see Fig. 4(c). Define the angle ϕ_i such that

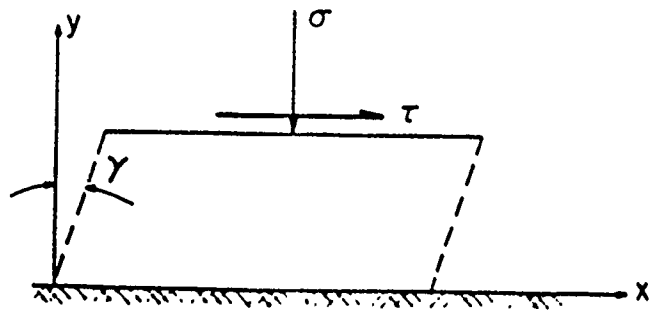
$$T_i = N_i \tan \phi_i \quad (22)$$

As a basic assumption, we regard the relative motion of granule i to be governed by the Mohr-Coulomb criterion, as sketched in Fig. 4(d). The mean force P_i (positive in compression) is then defined by the abscissa of the centre of the Mohr circle, as shown. In Fig. 4(c), x^* defines the direction of the relative motion of granule i . The resultant forces in the x^*, y^* coordinates then are

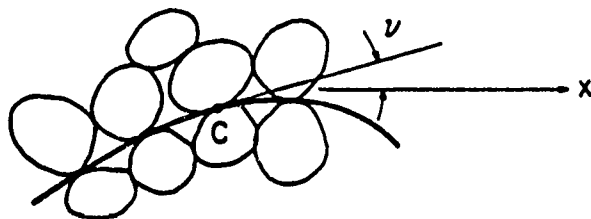
$$\begin{aligned} T_i^* &= T_i \cos \nu_i - N_i \sin \nu_i \\ N_i^* &= T_i \sin \nu_i + N_i \cos \nu_i \end{aligned} \quad (23)$$

As a second basic assumption, we introduce a constant friction angle ϕ_μ , and consider the friction law

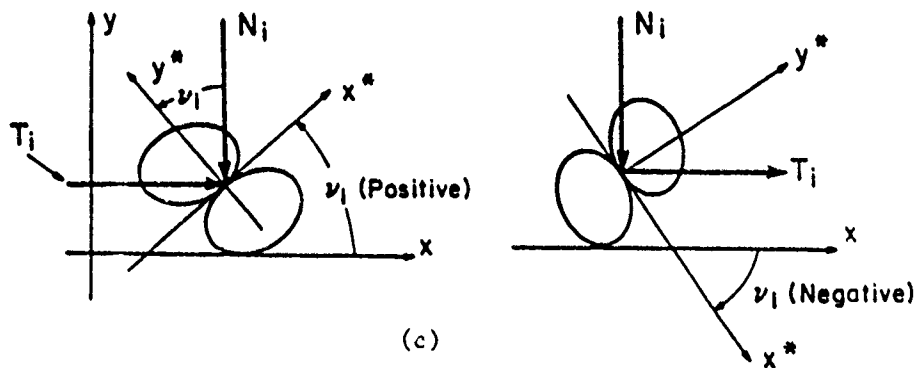
$$T_i^* = N_i^* \tan \phi_\mu \quad (24)$$



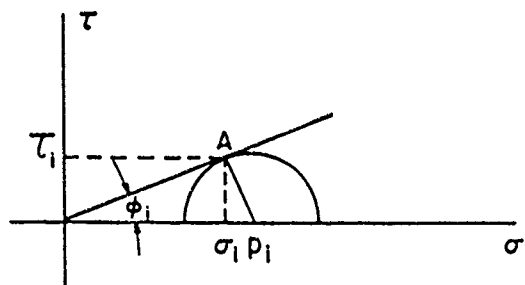
(a)



(b)



(c)



(d)

Fig. 4

to relate the tangential (positive in the direction of sliding) force T_i^* to the compressive (positive) force N_i^* when the granule i is active. From (22), (23), and (24) it follows that

$$\tan \phi_\mu = \tan (\phi_1 - \nu_i) \quad (25)$$

Hence, under compression, granules with negative dilatancy angles are the first to attain the critical sliding condition (25).

Consider now the rate of frictional work associated with the i th granule. Let \dot{l}_i^* be the rate of sliding of this granule in the x^* direction. The rate of frictional work then is

$$\dot{W}_f = T_i^* \dot{l}_i^* = \frac{T_i \sin \phi_\mu \dot{h}_i}{\sin (\phi_\mu - \nu_i) \sin \nu_i} \quad (26)$$

when $\dot{h} = \dot{l}_i^* \sin \nu_i$. The rate of frictional work must be balanced by the rate of stress work which consists of a part due to shearing, $T_i \dot{l}_i$, and a part due to volumetric expansion, $-P_i \dot{h}_i$. We hence have

$$T_i \dot{l}_i - P_i \dot{h}_i = T_i^* \dot{l}_i^*$$

from which it follows that

$$\dot{h}_i = \frac{\cos (\phi_\mu + \nu_i) \sin \nu_i}{\cos \phi_\mu} \dot{l}_i \quad (27)$$

note that \dot{l}_i is the slip-rate in the x direction.

Let p_i be the fraction of active granules with dilatancy angle ν_i

$$\sum_{i=1}^n p_i = 1 \quad (28)$$

where there are a total of n active dilatancy angles in a unit volume. The total rate of volumetric expansion then is

$$\frac{\dot{V}}{V} = \sum_{i=1}^n p_i \frac{\dot{h}_i}{h_i} = \sum_{i=1}^n p_i \frac{\cos (\phi_\mu + \nu_i) \sin \nu_i}{\cos \phi_\mu} \dot{\gamma}_i \quad (29)$$

where h_i is the length, measured in the y direction, associated with granule i , and $\dot{\gamma} \equiv \dot{l}_i/h_i$ is the rate of shearing contributed by the sliding of granule i .

We now make the third assumption (after Taylor (15)) that the local $\dot{\gamma}_i$ is the same as the global rate of shearing $\dot{\gamma}$, arriving at the dilatancy equation

$$\frac{1}{V} \frac{\dot{V}}{\dot{\gamma}} = \sum_{i=1}^n p_i \frac{\cos (\phi_\mu + \nu_i) \sin \nu_i}{\cos \phi_\mu} \quad (30)$$

When there are a very large number of granules, we introduce a density

function $p(\nu)$ for the distribution of the dilatancy angles, and replace (30) by

$$\frac{1}{V} \frac{\dot{V}}{\dot{\gamma}} = \int_{\nu^-}^{\nu^+} p(\nu) \frac{\cos(\phi_\mu + \nu) \sin \nu}{\cos \phi_\mu} d\nu \quad (31)$$

where $p(\nu) d\nu$ is the fraction of granules with dilatancy angle between ν and $\nu + d\nu$, and $\nu^- > -\pi/2$ and $\nu^+ < \pi/2$ define the range of the dilatancy angles.

A number of interesting observations emerge from equations (31) or (30), as follows:

- (1) Even if the distribution of the dilatancy angle, $p(\nu)$, may be initially symmetric with respect to $\nu = 0$, since ϕ_μ is positive, initial shearing under compression is always accompanied by an initial compaction. For example, if $p(\nu)$ is uniform for $|\nu| \leq \nu_0$, simple calculation immediately reveals this fact from equation (31).
- (2) Since $p(\nu)$ is the distribution function of the dilatancy angles at *active* granules, it is intuitively clear that, for an isotropically formed sample, this distribution tends to be biased toward negative dilatancy angles, under uniform confining pressures. This observation again suggests a greater tendency toward initial densification in shearing for an otherwise isotropic sample.
- (3) As the sample is monotonically sheared, the distribution function $p(\nu)$ tends to become more biased toward positive dilatancy angles, eventually leading to positive dilatancy. This is intuitively clear, since the granules tend to be engaged by the neighboring granules in a monotonic shearing, up to the peak stress. Furthermore, experimental observation on rod-shaped granules supports this.
- (4) Suppose a sample has been sheared monotonically, say, in the positive x direction, until a strong bias toward positive dilatancy angles has been developed. Upon reversal of the shearing, the distribution of the dilatancy angles will then be strongly biased toward the *negative* dilatancy angles, leading to a strong tendency toward densification. Hence, pre-shearing to large strain amplitudes (less than the strain associated with the peak stress) renders the sample strongly susceptible to densification (drained) or liquefaction (undrained) during load reversal.

The above observations have been systematically verified by the author and co-workers (Nemat-Nasser and Tobita (9) and Nemat-Nasser and Takahashi (8)) for a solid circular cylindrical sample of sand subjected to cyclic shearing. In particular, after a series of careful experiments, Nemat-Nasser and Takahashi (8) report the following conclusions, taken directly from p. 1305 of their paper.

- (1) In cyclic simple shearing, the resistance to re-liquefaction (undrained) or densification (drained) of a pre-liquefied sample actually increases, because of the concomitant densification, if the pre-liquefaction is termi-

nated at zero residual shear *strain*, but this resistance becomes very small, if the pre-liquefaction is terminated at zero residual shear *stress*.

- (2) The inherent anisotropy associated with sample preparation techniques affects both the densification and liquefaction potential of the sample.
- (3) Within each cycle of simple shearing, the *induced anisotropy is essentially wiped out in the neighbourhood* of zero shear *strain*, and the anisotropy that exists at this state is basically due to the sample preparation techniques (i.e., it is the *inherent anisotropy*), provided that the sample is not very loose and the strain amplitude is not very large.
- (4) For simple shearing, the distribution of the dilatancy angles characterizing the fabric may be related to the shear strain and, in this manner, the densification pattern may be estimated.

Since the state of deformation in the sample used to arrive at the above conclusions is very complex and is clearly not simple shearing, a new series of tests on large, hollow, circular, cylindrical samples has been initiated in the author's laboratory at the University of California at San Diego. Preliminary tests clearly support the basic conclusions listed above. However, in complex cyclic loading, where all three principal values of the deformation rate tensor may be non-zero, and hence there are, in general, three non-zero principal shear strains, some of the above notions will have to be generalized.

Acknowledgements

This work has been supported by the Air Force Office of Scientific Research under Grant No. AFOSR-87-0079 to the University of California, San Diego.

References

- (1) CHRISTOFFERSEN, J., MEHRABADI, M. M., and NEMAT-NASSER, S. (1981) A micromechanical description of granular material behavior, *J. Appl. Mech.*, **48**, 339-344.
- (2) KANATANI, K. (1984) Distribution of directional data and fabric tensors, *Int. J. Engng Sci.*, **22**, 149-164.
- (3) MEHRABADI, M. M., NEMAT-NASSER, S., and ODA, M. (1982) On statistical description of stress and fabric in granular materials, *Int. J. Numer. Analyt. Methods Geomech.*, **6**, 95-108.
- (4) MEHRABADI, M. M., NEMAT-NASSER, S., SHODJA, H. M., and SUBHASH, G. (1988) Some basic theoretical and experimental results on micromechanics of granular flow, *Proc. U.S.-Japan Seminar on the Mechanics of Granular Materials* (Edited by Jenkins, J. T. and Satake, M.), Elsevier, Amsterdam, pp. 253-262.
- (5) NEMAT-NASSER, S. (1980) On behavior of granular materials in simple shear, *Soils Foundations*, **20**, 59-73.
- (6) NEMAT-NASSER, S. and MEHRABADI, M. M. (1983) Stress and fabric in granular masses, in *Proc. US-Japan Seminar in the Mechanics of Granular Materials: New Models and Constitutive Relations* (Edited by Jenkins, J. J. and Satake, M.) Elsevier, Amsterdam, pp. 1-8.
- (7) NEMAT-NASSER, S. and MEHRABADI, M. M. (1984) Micromechanically based rate constitutive descriptions for granular materials, in *Proc. International Conference on Constitutive Laws for Engineering Materials: Theory and Application* (Edited by Desai, C. S. and Gallagher, R. H.), Wiley, New York.

- (8) NEMAT-NASSER, S. and TAKAHASHI, K. (1984) Liquefaction and fabric on sand. *J. Geotech. Engng.* **110**, 1291-1306.
- (9) NEMAT-NASSER, S. and TOBITA, Y. (1982) Influence of fabric on liquefaction and densification potential of cohesionless sand. *Mech. Mater.*, **1**, 43-62.
- (10) ODA, M. (1982) The mechanism of fabric changes during compressional deformation of sand. *Soils Foundations*, **12**, 1-18.
- (11) ODA, M., KONISHI, J., and NEMAT-NASSER, S. (1980) Some experimentally based fundamental results on the mechanical behavior of granular materials. *Geotechnique*, **30**, 479-495.
- (12) ODA, M., KONISHI, J., and NEMAT-NASSER, S. (1982) Experimental micromechanical evaluation of strength of granular materials: effects of particle rolling. *Mech. Mater.*, **1**, 269-283.
- (13) ONAT, E. T. (1984) Effective properties of elastic materials that contain penny shaped voids. *Int. J. Engng Sci.*, **22**, 1013-1021.
- (14) SATAKE, M. (1978) Constitution of mechanics of granular materials through the graph theory. in *Proc. US-Japan Seminar on Continuum-Mechanical and Statistical Approaches in the Mechanics of Granular Materials* (Edited by Cowin, S. C. and Satake, M.), Gakujutsu Bunken Fukyukai, Tokyo, pp. 47-62.
- (15) TAYLOR, G. I. (1938) Plastic strain in metals. *J. Inst. Metals*, **62**, 307-324.
- (16) WEBER, J. (1966) Recherches Concernant les Contraintes Intergranulaires dans les Milieux Pulverulents Application a la Rheologie de Ces Milieux. *Cahiers du Groupe Francois de Rheologie*, **3**, 161-170.

Experimental investigation of fabric-stress relations in granular materials

G. Subhash ^a, S. Nemat-Nasser ^a, M.M. Mehrabadi ^b and H.M. Shodja ^c

^a *Center of Excellence for Advanced Materials, Department of Applied Mechanics and Engineering Sciences, University of California, San Diego, CA 92093-0411, USA*

^b *Department of Mechanical Engineering, Tulane University, New Orleans, LA 70118, USA*

^c *Department of Civil Engineering, Northwestern University, Evanston, IL 60208-3109, USA*

Received 3 July 1990

A brief summary of some relevant theoretical and experimental results on the microscopic aspects of the response of granular masses is presented. The results of a series of experiments involving simple shearing under a constant confining pressure, performed on photoelastic rod-like granules (plane strain) are reported. In these experiments, the components of various fabric tensors are measured, and their variations over one cycle of shearing are examined and compared. The orientations of the principal axes of all commonly used fabric tensors are observed to change sharply with the reversal of the shearing direction. It is also concluded that, in general, second-order fabric tensors are not adequate to accurately describe the distribution of fabric measures such as the distribution density function of unit contact normals or unit branches which are unit vectors along line segments connecting the centroids of adjacent contacting granules. This is particularly so when the response of the granular mass is highly anisotropic. Finally, the expression for the macroscopic stress in terms of the contact forces and other local quantities, is reviewed and its experimental verification is discussed.

1. Introduction

A granular mass which consists of rigid cohesionless granules carries on the microscopic scale, the overall macroscopic stresses through forces transmitted across contact regions. It is essential to understand the micromechanics of the overall behavior of materials of this kind under various loading conditions. To this end, triaxial tests, biaxial compression, and shear tests have been performed on these materials (see, e.g., Parkin et al., 1968; Roscoe et al., 1967; Arthur and Menzies, 1972; Oda, 1972a, 1972b, 1978; Oda and Konishi, 1974a, 1974b; Ochiai, 1975; Nemat-Nasser, 1980; Oda et al., 1982; Konishi et al., 1983; Mehrabadi et al., 1988). In addition, theoretical models have been proposed in the literature in order to quantify from a fundamental point of view the experimental observations (Christoffersen et al., 1981; Oda, 1975; Konishi, 1978; Mehrabadi et al., 1982; Mehrabadi and Nemat-Nasser, 1983; Nemat-

Nasser, 1983, 1988). These models seek to include the essential ingredients of the underlying micro-mechanical features. They have led to the description of the overall stress, fabric, overall deformation rate, and the evolution of the corresponding rate constitutive relations in terms of various microquantities.

The present study is concerned with the micro-mechanical modelling of the behavior of granular materials, and with the understanding of their overall mechanical response under shearing in the presence of an overall confining pressure. The main objectives are (1) to measure the components of various fabric measures and compare them with each other, (2) to relate the overall stress and fabric measures and verify the results experimentally, (3) to observe how the orientations of the principal axes of each tensorial fabric measure change over a cycle of deformation, (4) to examine the representation of the corresponding distribution density functions and to establish the re-

quired accuracy in the order of their harmonic expansion, and finally (5) to study the relation between the macroscopic stress and the local quantities such as the contact forces.

To accomplish the above objectives, experiments have been performed on photoelastically sensitive rod-shaped particles of oval cross sections with different sizes. Microscopic quantities such as the orientations of unit contact normals and unit branches have been measured and their evolution during a cycle of shearing has been observed.

Results of these experiments show that fabric is closely related to stress. Though many fabric tensors have been proposed in the literature (Oda et al., 1982; Mehrabadi and Nemat-Nasser, 1983), our experimental results seem to suggest that the off-diagonal terms in all these tensors closely follow the overall stress-strain relation. It is also found that in the representation of the distribution density functions of contact normals and unit branches, the second-order terms alone are not adequate to capture accurately the involved anisotropy. Hence, the fourth-order terms must be included. The tensor, $(\langle m_i f_j \rangle + \langle m_j f_i \rangle)/2$, has been shown to be indeed proportional to the macroscopic stress. (Here, m_i are the components of the unit center-to-center vector of two contacting granules, called the branch, and f_j are the components of the force acting at the corresponding contact point; the symbol $\langle \dots \rangle$ denotes the unweighted volume average.) The diagonal terms, $\langle m_1 f_1 \rangle$ and $\langle m_2 f_2 \rangle$, remain constant, representing the constant confining pressure; the off-diagonal terms, $(\langle m_1 f_2 \rangle + \langle m_2 f_1 \rangle)/2$, follow the variation of the applied shear stress. This is also the case for the fabric tensors to be discussed later.

2. Material and apparatus

The granular materials tested are composed of cylindrical rods of oval cross sections. Three different sizes are used to obtain a dense packing; see Table 1. These granules have been cast using polyurethane rubber of photoelastic constant 82.5 mm/kg. The samples considered in the experi-

Table 1

Size	Max. dia. (mm)	Aspect ratio	Weight (g)
large	14.95	1.14	3.3
medium	9.7	1.1	1.5
small	6.4	1.1	0.7

ments were relatively dense with an initial void ratio of about 0.18. The average coordination number of the packing was around 1.27.

2.1. Experimental procedure

The equipment and the experimental procedure have been briefly described earlier by Mehrabadi et al. (1988).

The testing equipment consists of a rigid outer frame and an internal frame (Fig. 1) which can be deformed in shear while allowing for volumetric straining. On this internal frame, two horizontal and two vertical bars are mounted which could be moved in parallel on the internal frame. These are denoted by HB1, HB2, VB1, and VB2, respectively, in Fig. 2. The granules can be packed inside the frame formed by these bars. The confining pressure is applied on the sample by means of weights P . The bar HB1 is lifted up by springs to balance its weight. An additional weight W is applied on HB1 and HB2 to balance the weights of these bars and the granules, and the tension in the springs.

To assess the influence of the friction of the apparatus on the measured forces, an experiment was performed where the granules are replaced by equivalent weights, keeping the rest of the experimental conditions the same. The horizontal shear force is then applied to the frame and the frictional resistance of the frame is measured over one cycle.

A linear least-squares approximation is fitted through the points obtained from the friction test and these values are subtracted from the corresponding horizontal shear forces applied to the granules. Note that the friction test and the actual test on the granules are performed in the same direction and the same sequence over one cycle.

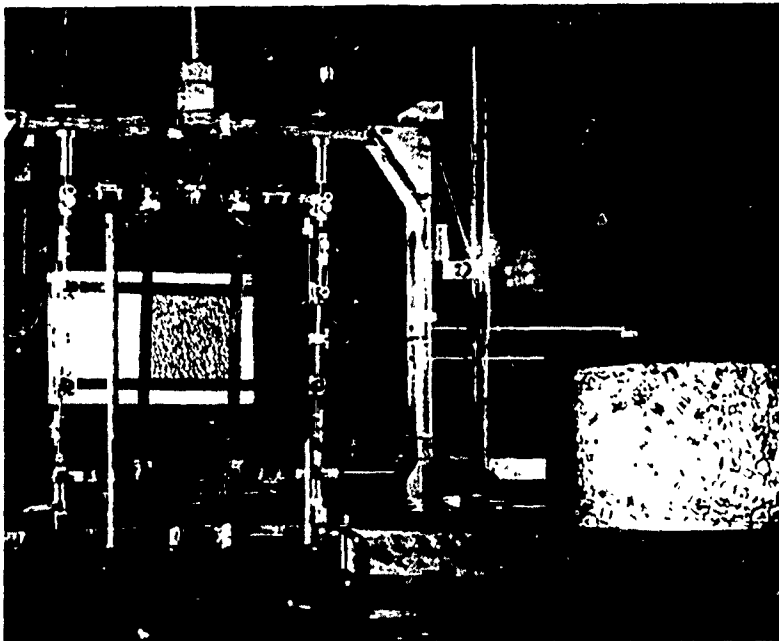


Fig. 1. Testing equipment.

The granules are packed in the internal frame of 20 cm by 20 cm, formed by bars HB1, HB1, VB1, and VB2. To minimize the effect of the boundaries, analyses are performed on granules within a central part which constitutes the sample, see Fig. 3. The granular mass is subjected to a

confining pressure of 1200 g and is sheared horizontally by incremental displacements. The applied load on the granules is measured by a load cell, Lc. The horizontal and vertical movements of the bars are measured by the transducers P1 to P8. The shear strain is recorded by an LVDT, Lv.

The loading frame is placed in the field of a circular polariscope consisting of a monochromatic light source, a polarizer, two quarter wave plates, and an analyzer. After the packing is com-

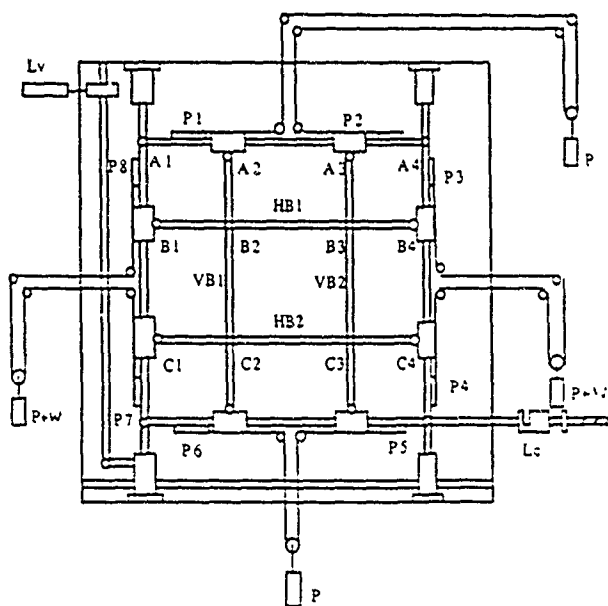


Fig. 2 Schematic of the experimental apparatus

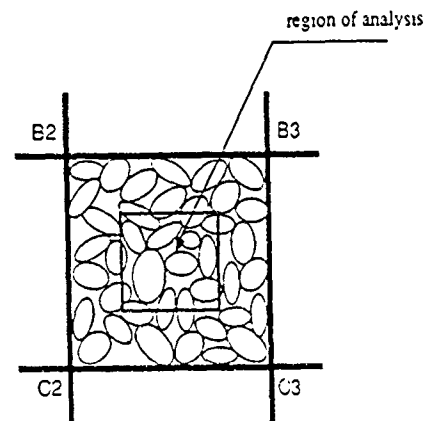


Fig. 3 Central region of the granular mass which constitutes the sample for analysis

plete, under a confining load, the shearing is applied incrementally. At each stage of loading, photographs of the isochromatic fringe pattern in the stressed assembly are taken. These photographs are later analyzed using a digital image analysis system consisting of a PC AT, a frame grabber (PC vision plus) from Imaging Technology Inc., a Vidicon camera (C1000) from Hamamatsu TV Co., and a Trinitron color video monitor from Sony. With the aid of software "Imlab" and "Im-tool" from Imaging Technology, a powerful program for obtaining several microscopic quantities was developed. With this program one can measure the number of fringes, length of major axes, orientation of contact normals and branches, and other needed parameters. One can also produce the actual, and the second- and fourth-order approximations of the distribution density functions of the unit contact normals, the unit branches, and their weighted averages which are given by the product of the particular unit vector and the number of fringes multiplied by the force per fringe factor. This factor is measured in a separate experiment to be 27 g/fringe for the granules used in this experiment. In this manner a wealth of microscopic measures is efficiently obtained. These results are then used to compute the tensorial components of various fabric measures which have been proposed earlier in the literature, and to check their relation to the overall stress and deformation measures.

To understand the response of the equipment under the loads applied to the granular mass, and, in particular, to establish whether simple or pure shearing is involved, a separate test is performed on the equipment under actual test conditions. A fixed reference point was chosen on the rigid frame, and the movement of the hinge points A1 to C4 is recorded over one cycle of deformation, see Fig. 2. The following conclusions are obtained:

- (1) there is no relative movement of points A1 to A4 throughout the entire cycle, and
- (2) points B1 to B4, and C1 to C4 do not undergo any appreciable motion in the vertical direction.

Therefore, it is concluded that the granular mass is subjected to simple shear rather than pure shear.

3. Fabric elements and their effect on overall properties of granular masses

Granular masses carry overall applied loads through contact friction. The description of the overall mechanical response of these materials requires description of the overall stress, fabric, deformation rate, their evolution, and the overall rate constitutive relations, in terms of various relevant microquantities. We will not address the question of constitutive relations here, since this is available elsewhere in the literature (see Nemat-Nasser and Mehrabadi, 1983).

Fabric refers to the spatial arrangement of particles and associated voids (Oda, 1978). This may include (1) orientation fabric, and (2) packing which is concerned with the mutual relation of individual particles.

The fabric measures are used to establish the anisotropy of a granular mass. Arthur and Menzies (1972), in their paper, state that Casagrande and Carrillo (1944) were probably the first to distinguish between two forms of anisotropy in soils, which they called the inherent and the induced anisotropies, suggesting that anisotropy may be present before the soil is strained or it may be induced by the straining process. They defined the inherent anisotropy as "a physical characteristic inherent in the material and entirely independent of the applied strains", and the induced anisotropy as "a physical characteristic which is exclusively due to the strain associated with an applied stress". Inherent anisotropy is produced essentially by the process of deposition (Arthur and Menzies, 1972; Oda, 1972a). This is because every particle tends to rest in the most stable position and preferred orientation, with respect to the gravitational or other relevant force. Induced anisotropy is produced in the course of deformation in response to overall applied loads. Both types of anisotropy can have a profound influence on the response and failure modes of granular masses. Arthur and Menzies (1972) concluded that any general formulation of stress-strain relations for noncohesive soils must account for the large influence of inherent anisotropy. Arthur et al. (1977), and Oda et al. (1985) studied induced anisotropy

in sand. A major difficulty in such a study is the controlled rotation of the principal stress during shear. In some tests, rotations have been imposed by cutting cohesive soil samples at chosen orientations from larger blocks of the soil (Bishop, 1966). In granular soils, Oda (1972b) made measurements of changes in particle packing at various stages of shearing with constant principal stress directions. Oda and Konishi (1974) observed the rotation of the principal stress directions in simple shear. Similar observations made under the present experimental work will be discussed later in this paper.

4. Stress and fabric in granular masses

Stress is a continuum concept. Many authors have defined stress in terms of average contact forces (see e.g., Christoffersen et al., 1981; Mehrabadi et al., 1982; Nemat-Nasser and Tobita, 1982; Oda et al., 1982). Nemat-Nasser (1988) has summarized some of these results within the framework of continuum mechanics. Consider a collection of granules with overall volume V and overall surface S , subjected to self-equilibrating tractions T applied on its boundary S . This produces contact forces at the contacting granules. If we assume a large number of granules in V , both continuum and statistical formulations of the overall stress are permissible. If $\sigma(x)$ is a variable stress field in equilibrium with the applied tractions T , and if body forces are zero, then we must have

$$\begin{aligned}\sigma_{i,j} &= 0 \quad \text{in } V, \\ \sigma_{i,j} \nu_j &= \bar{T}_i \quad \text{on } S,\end{aligned}\quad (4.1)$$

where ν is the exterior unit normal on S . The overall stress is the simple volume average of this self-equilibrating stress field,

$$\bar{\sigma} \equiv \frac{1}{V} \int_V \sigma(x) dV. \quad (4.2)$$

The stress field may vary discontinuously from granule to granule, but it must produce continu-

ous tractions across the contact area of any two contacting granules, say A and B. Therefore,

$$[\sigma_{i,j}] n_j = 0, \quad (4.3)$$

where n is the unit normal on the contact area, which points from A to B. The symbol $[\dots]$ indicates the "jump", i.e.,

$$[\sigma_{i,j}] \equiv \sigma_{i,j}^+ - \sigma_{i,j}^-, \quad (4.4)$$

which is the difference of stress in A and B at the contact point. In the absence of any pore fluid or gas pressure, (4.2) may be written as

$$\bar{\sigma} = \frac{1}{V} \sum_{\alpha=1}^{M_G} \int_{V_\alpha} \sigma(x) dV = \sum_{\alpha=1}^{M_G} c^\alpha \bar{\sigma}^\alpha, \quad (4.5)$$

where c^α is the volume fraction of the α th granule, i.e., $c^\alpha = V_\alpha/V$, M_G is the total number of granules in volume V , and $\bar{\sigma}^\alpha$ is the average stress within the α th granule. From (4.1) and (4.3), it follows that

$$\begin{aligned}\int_V (x_j \sigma_{ik})_{,k} dV &= \int_V \sigma_{i,j} dV = \int_S x_j \bar{T}_i dS = \bar{\sigma}_{i,j} \\ &= \frac{1}{V} \sum_{\alpha=1}^{M_s} x_j^\alpha F_i^\alpha,\end{aligned}\quad (4.6)$$

where M_s is the number of points on the outer boundary S at which concentrated forces F^α are applied. Since this representation does not involve the contact forces at the interior contacting granules, it does not involve the microstructure. Alternate representations which include the microstructure have, therefore, been proposed.

Christoffersen et al. (1981) showed that the overall stress may be defined in terms of the volume average of the tensor product of the contact forces and the associated branch vectors. They used the principle of virtual work to show that the overall average Cauchy stress, σ , in a representative sample of a granular mass can be written as

$$\sigma_{i,j} = \frac{1}{V} \int_V \sigma_{i,j} dv = N \langle l_i f_j \rangle, \quad (4.7)$$

where

$$\langle l_i f_j \rangle \equiv \frac{1}{N} \sum_{\alpha=1}^N l_i^\alpha f_j^\alpha. \quad (4.8)$$

Here, V is the volume of the sample, σ_{ij} is the variable stress in equilibrium with the applied loads, N is the number of contact points in the sample, f^α is the contact force at the typical contact α , and l^α is the corresponding branch, i.e. the center-to-center vector of two contacting granules.

Many fabric measures have been introduced in the literature. For spherical granules, Oda et al. (1982) proposed the fabric tensor

$$F_{ij} = N\hat{l}\langle n_i n_j \rangle, \quad (4.9)$$

and, for nonspherical granules, the tensor

$$F_{ij} = N\hat{l}\langle m_i m_j \rangle, \quad (4.10)$$

where \hat{l} is the average value of the branch lengths, and n_i and m_i are the components of a typical unit contact normal and a unit branch, respectively. Satake (1978) defined an "anisotropic tensor" by

$$\bar{J}_{ij} = \langle n_i n_j \rangle. \quad (4.11)$$

Another fabric measure considered by Nemat-Nasser and Mehrabadi (1983) is

$$H_{ij} = N\langle alm_i n_j \rangle, \quad (4.12)$$

where a is the contact area. We note that the choice of a particular fabric measure is a matter of convenience and its suitability is judged by comparison with experimental observation.

From our experimental data, many of the above tensors can be calculated. We have considered the tensor $\langle m_i f_j \rangle$, where f has been interpreted as the weighted fringe bias which is given by the product of the unit fringe bias and the number of fringes as measured on the digitized picture multiplied by the force per fringe. The average of the off-diagonal terms has been scaled so that its range is the same as that of the applied shear stress. The graph is then translated to match the stress at the extreme points, see Fig. 4. This does not change the shape of the curve, but determines a scale factor to relate the overall stress to the corresponding average quantities.

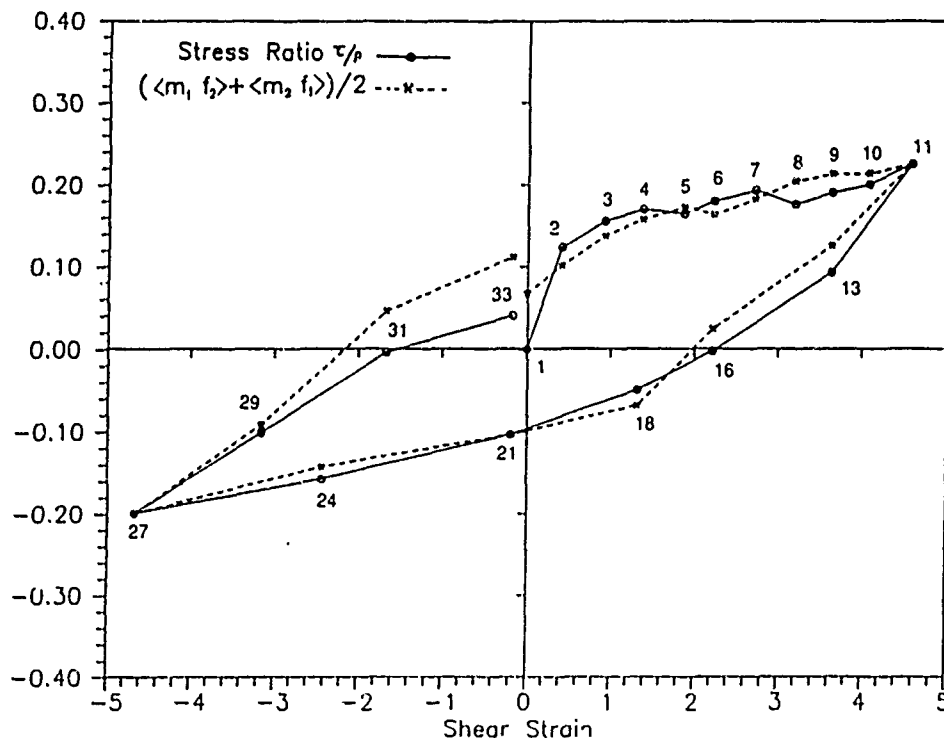


Fig. 4 Plot of stress ratio and the average of the off-diagonal terms of the tensor $\langle m_i f_j \rangle$ vs. shear strain. There is a very good agreement between the above two quantities.

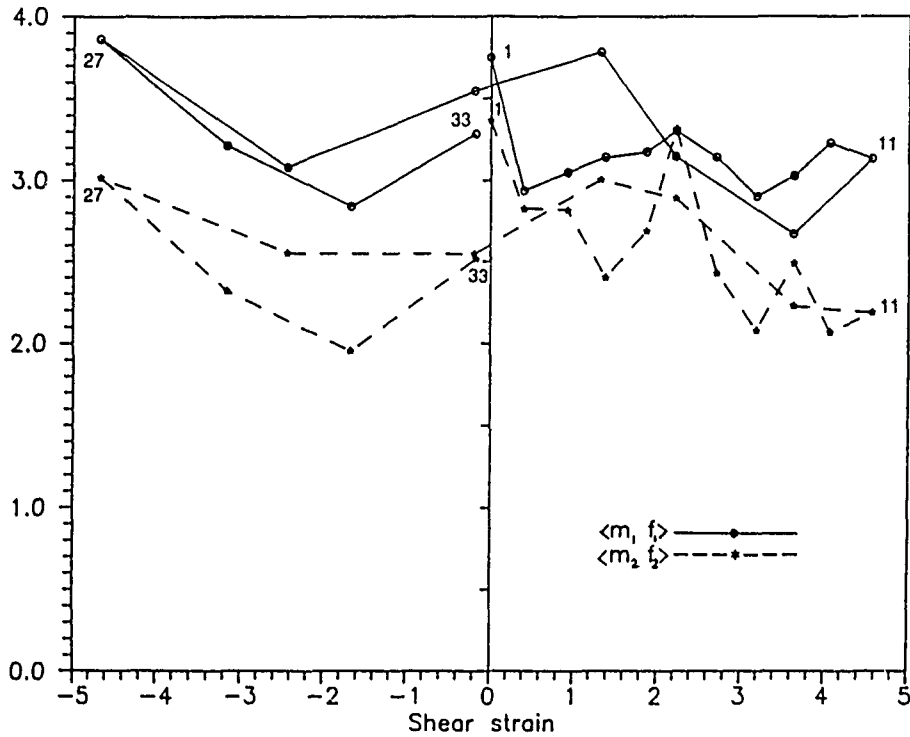


Fig. 5. The diagonal terms of the tensor $\langle m_i f_j \rangle$ remain almost constant throughout the deformation process.

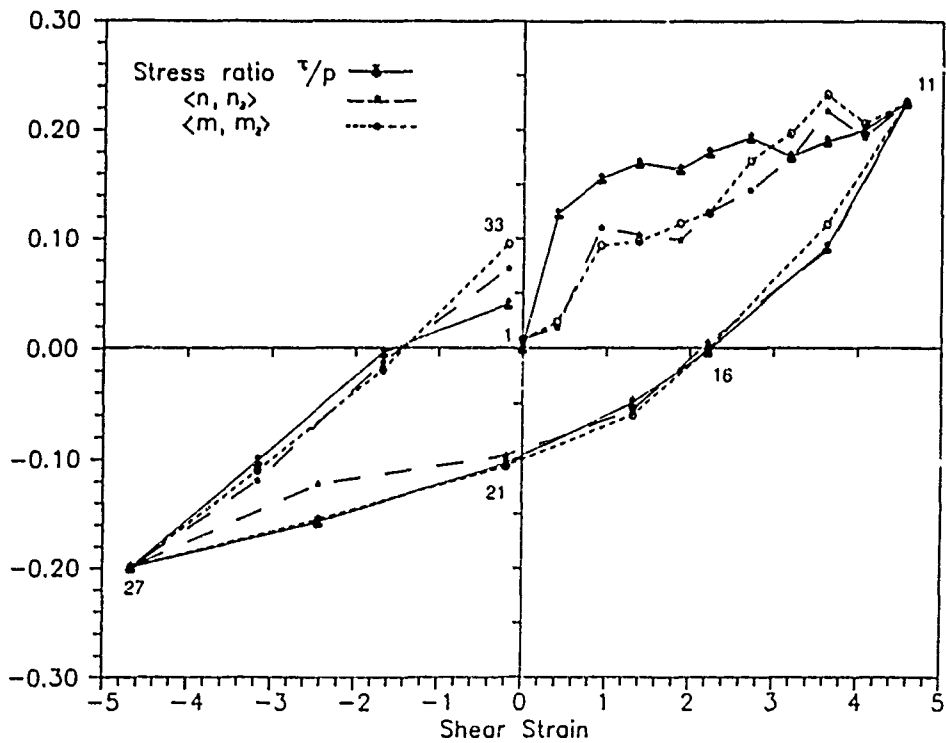


Fig. 6. The off-diagonal terms of the tensors $\langle n_i n_j \rangle$ and $\langle m_i m_j \rangle$ correspond well with the overall stress

The weighted fringe bias is not an exact representation of the contact force. It may however, be taken as a good measure of this force. The diagonal terms in the tensor $\langle m_i f_j \rangle$ remain almost constant, representing the constant confining pressure, see Fig. 5. The off-diagonal terms of the tensors $\langle m_i m_j \rangle$ and $\langle n_i n_j \rangle$, plotted in Fig. 6, have very good agreement with the overall stress ratio. Figure 7 is the plot of diagonal terms $\langle n_1 n_1 \rangle$ and $\langle m_1 m_1 \rangle$ vs. the shear strain. It is clearly apparent that these quantities remain almost constant throughout the deformation. (Note that $\langle n_2 n_2 \rangle$ and $\langle m_2 m_2 \rangle$ also remain almost constant because $\langle n_1 n_1 \rangle + \langle n_2 n_2 \rangle = 1$ and $\langle m_1 m_1 \rangle + \langle m_2 m_2 \rangle = 1$.) Thus, it can be concluded that the diagonal terms in each tensor are proportional to the confining pressure and the off-diagonal terms are proportional to the applied shear stress. Also, note that the corresponding components of the tensors associated with the branches and contact normals are almost identical.

5. Mechanism of strain hardening

A typical plot of stress ratio vs. shear strain is shown in Fig. 8. When a granular medium is strain hardening, its plastic deformation is accompanied by a stress increment. When the granular medium deforms under increasing stress ratios, rearrangement of particles occurs to withstand the increasing stress ratio. Therefore, contact normals tend to concentrate in the direction of the principal stress axis, as is clearly observed in the form of chains of heavily stressed particles. The average direction of these "chains" tends in the direction of the major principal stress axis. As a result of this concentration, a strong fabric anisotropy develops, see Oda (1974, 1978).

It is also observed that the principal stress axes of each tensor rotate with a change in the magnitude and direction of applied shear stress. This can be clearly observed from the rose diagrams of unit contact normals and unit branches, Figs. 9(a)

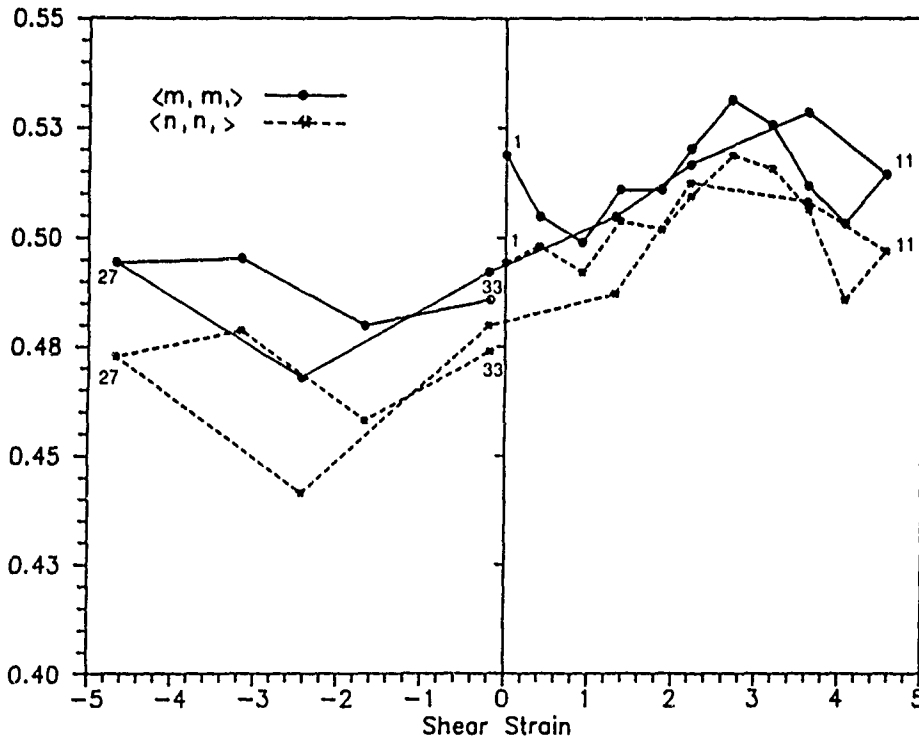


Fig 7 Plot of the diagonal terms of the tensors $\langle m_i m_i \rangle$ and $\langle n_i n_i \rangle$ which remain almost constant throughout the deformation process.

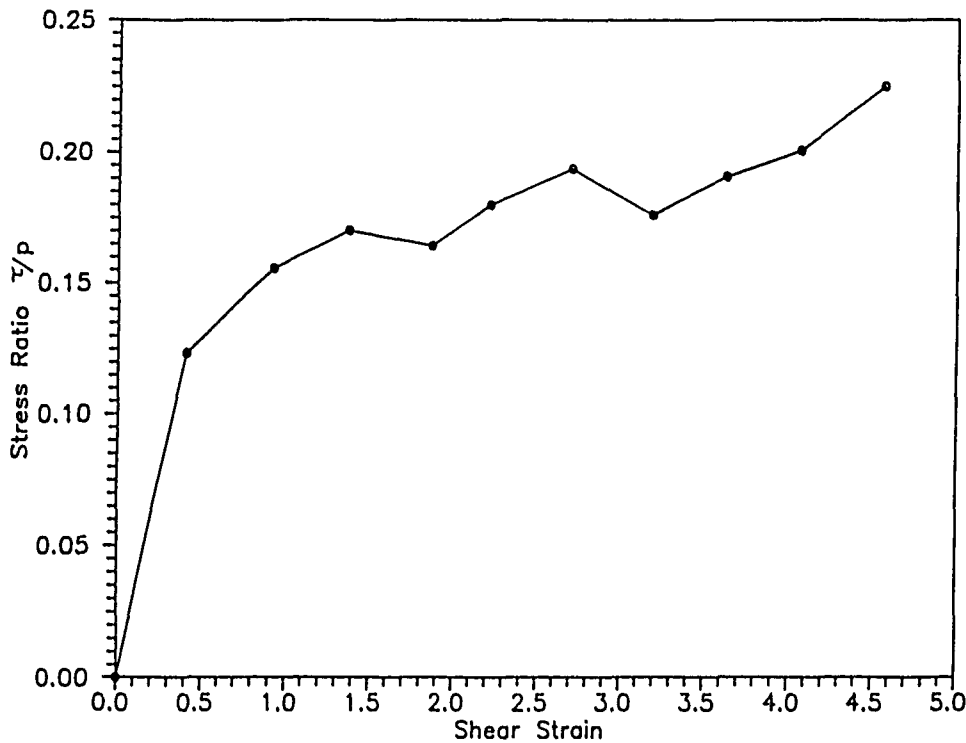


Fig. 8. Strain hardening behavior of granular materials can be clearly observed in the first quarter cycle of the experiment.

and 9(b). The distributions of both contact normals and branches and their evolutions are quite similar. The orientation of the major principal axis vs. the shear strain is plotted in Fig. 10 for tensors $\langle m, f_j \rangle$, $\langle m, m_j \rangle$, and $\langle n, n_j \rangle$. In all three cases, it is observed that the orientations of the corresponding principal axes change rapidly during the early stages of deformation, approach constant values in the range 130° – 140° , and remain constant thereafter. Once the direction of shearing is reversed, a rapid change by 90° in the orientations of the principal axes of the fabric occurs. Their orientations then remain constant until a further change in the direction of shearing occurs. This process repeats in each cycle.

6. Dilatancy

Granular materials exhibit volume changes when sheared under confining pressure. Figure 11 shows the relation between the shear and volumet-

ric strains. An initial densification is seen to be followed by dilation, typical of almost all granular materials.

The dilatancy equation proposed by Nemat-Nasser (1980) is,

$$\frac{\dot{V}}{V\dot{\gamma}} = \frac{1}{\cos \phi_\mu} \int_{\nu^-}^{\nu^+} p(\nu) \cos(\phi_\mu + \nu) \sin \nu \, d\nu, \quad (6.1)$$

where ν is the angle between the contact unit normal and the vertical axis, $p(\nu)$ is the distribution function for the angle of active contacts, $\nu^+ < \pi/2$ and $\nu^- > \pi/2$ define the range of variation of the dilatancy angles, and ϕ_μ is the angle of sliding friction.

In (6.1) it is assumed that the local $\dot{\gamma}_i$ is the same as the global rate of shearing $\dot{\gamma}$, where $\dot{\gamma}_i$ is the rate of shearing contributed by the sliding of granule i . Nemat-Nasser makes a number of interesting observations from (6.1), which explains the

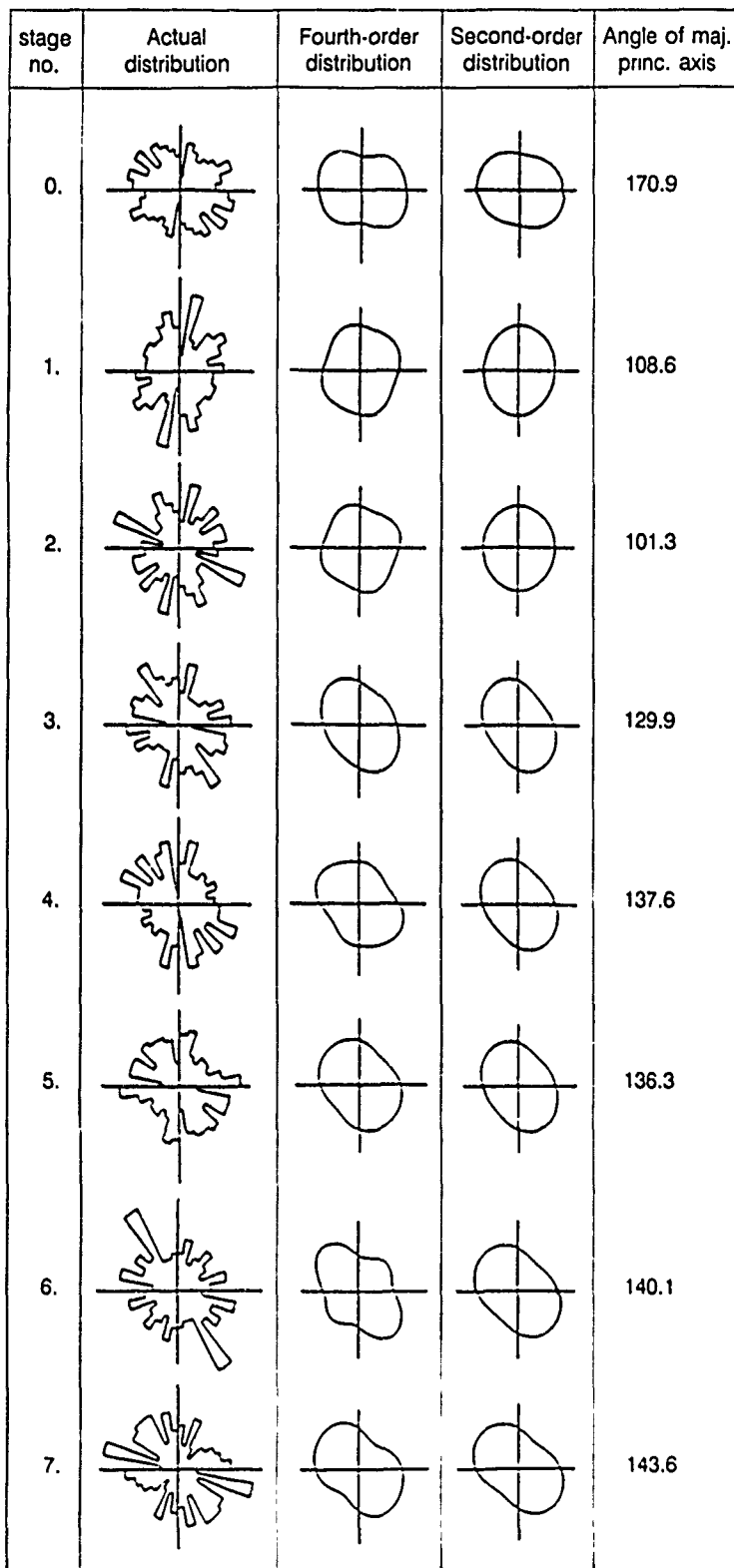


Fig 9a Rose diagrams of unit contact normals

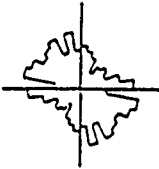
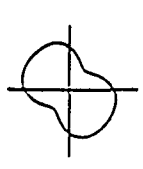
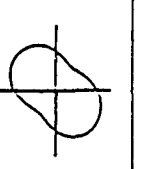
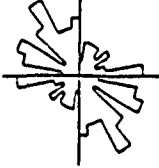
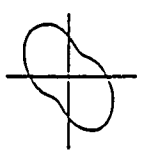
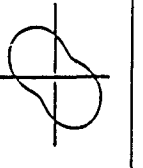
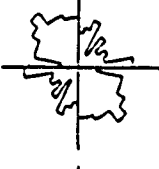
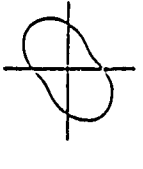
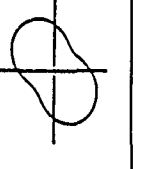
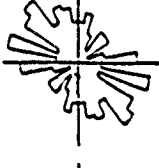
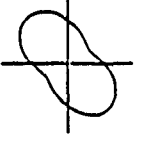
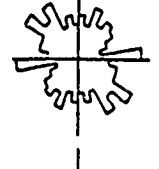
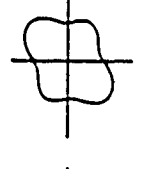
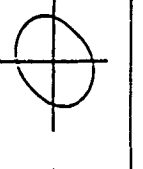
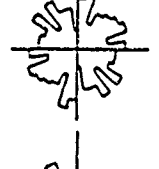
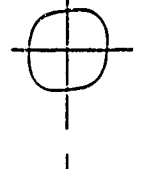
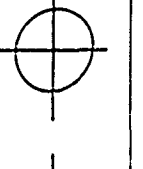
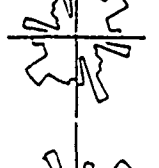
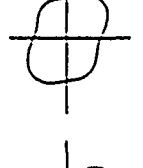
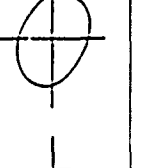
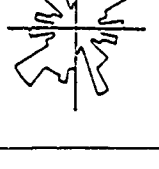
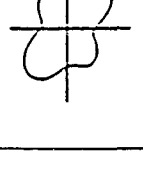
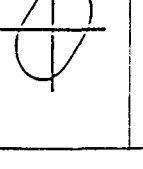
stage no.	Actual distribution	Fourth-order distribution	Second-order distribution	Angle of maj. princ. axis
8.				140.9
9.				136.9
10.				130.2
11.				143.1
13.				141.6
16.				69.5
18.				55.1
21.				55.1

Fig. 9a. (continued)

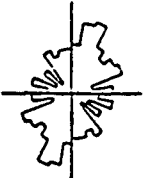
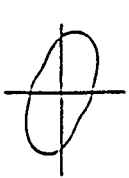
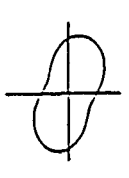
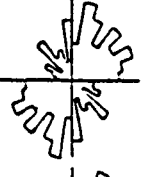
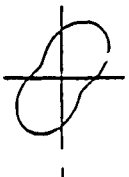
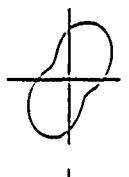
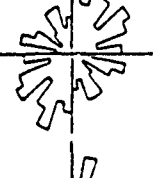
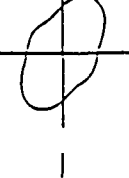
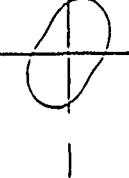
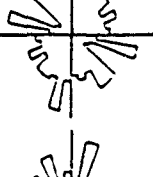
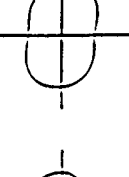
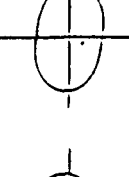
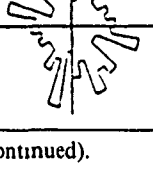
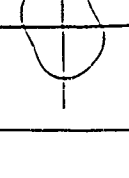
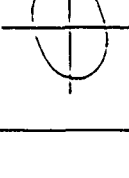
stage no.	Actual distribution	Fourth-order distribution	Second-order distribution	Angle of maj. princ. axis
24.				65.5
27.				52.3
29.				54.0
31.				80.72
33.				112.7

Fig. 9a. (continued).

dilatant behavior of granular materials. The observations are summarized below.

Under uniform confining pressure, the distribution density function of the dilatancy angles at active granules, $p(\nu)$, tends to be biased toward negative dilatancy angles, leading to initial densification in shearing. As the sample is monotonically sheared, the distribution function $p(\nu)$ tends to become biased toward positive dilatancy angles, eventually leading to positive dilatancy. Suppose a sample has been sheared monotonically, say, in the positive x -direction, until a strong bias toward

positive dilatancy angles has been developed. Upon reversal of shearing, the distribution of the dilatancy angles will then be strongly biased toward the negative dilatancy angles, leading to a strong tendency toward densification. Hence, pre-shearing to a large strain amplitude (less than the strain associated with the peak stress) renders the same strongly susceptible to densification (drained) or liquefaction (undrained) during load reversal. The above observations have been verified by Nemat-Nasser and Tobita (1982) and Nemat-Nasser and Takahashi (1984), for a cir-

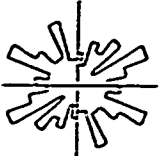
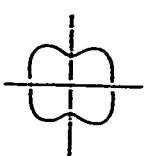
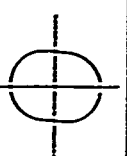
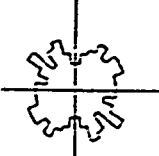
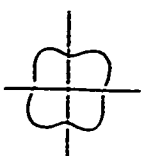
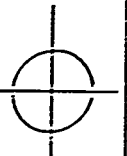
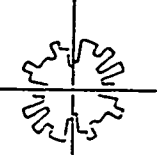
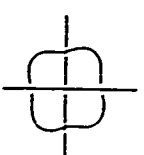
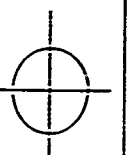
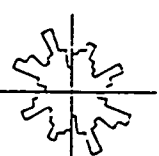
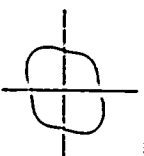
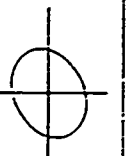
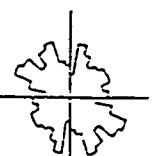
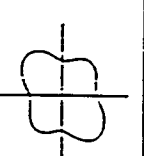
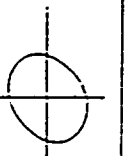
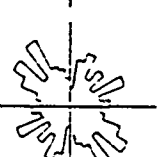
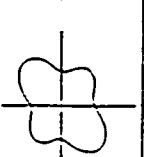
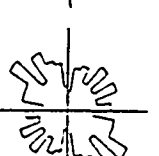
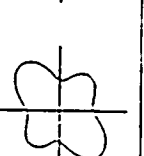
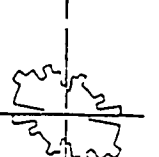
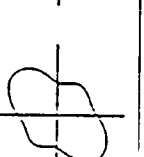
stage no.	Actual distribution	Fourth-order distribution	Second-order distribution	Angel of maj. princ. axis
0.				176.0
1.				167.55
2.				171.1
3.				133.96
4.				144.6
5.				142.8
6.				147.6
7.				148.0

Fig 9b Rose diagrams of unit branches

stage no.	Actual distribution	Fourth-order distribution	Second-order distribution	Angel of maj. princ. axis
8.				144.4
9.				138.7
10.				136.2
11.				139.6
13.				153.5
16.				71.2
18.				48.3
21.				41.16

Fig 9b (continued)

stage no.	Actual distribution	Fourth-order distribution	Second-order distribution	Angle of maj. princ. axis
24.				55.84
27.				43.4
29.				47.2
31.				67.11
33.				147.6

Fig. 9b. (continued).

cular cylindrical sample of sand subjected to cyclic shearing. The same is also verified in the present experiments on photoelastic rods.

7. Fabric tensors and representation of distribution density functions

Distribution of directional data is characterized by what is termed "fabric tensors". In our analysis, "direction" or "orientation" means "axis", and the direction is indicated by a unit vector n .

Several fabric tensors have been discussed in Section 4. These tensors are, by necessity, of even orders. They define the distribution of contact normals, n , or unit branches, m . Examples are

$\langle n_i n_j \rangle$ and $N \langle m_i m_j \rangle$ which are symmetric, and $\langle n_i m_j \rangle$ which is nonsymmetric. Higher order fabric tensors, like $\langle n_i n_j m_k m_l \rangle$ and $\langle n_i n_j n_k n_l \rangle$, may also be considered. The inclusion of higher order tensors provides more information regarding the details of the anisotropy involved in each distribution; Kanatani (1984).

Let $E(n)$ be a distribution density function of contact normals. Then

$$E(n) = E(-n) \quad \text{and} \quad \int_{\Omega} E(n) d\Omega = 1, \quad (7.1)$$

where Ω is the unit sphere, and $E(n) d\Omega$ is the number of data points falling in the solid angle

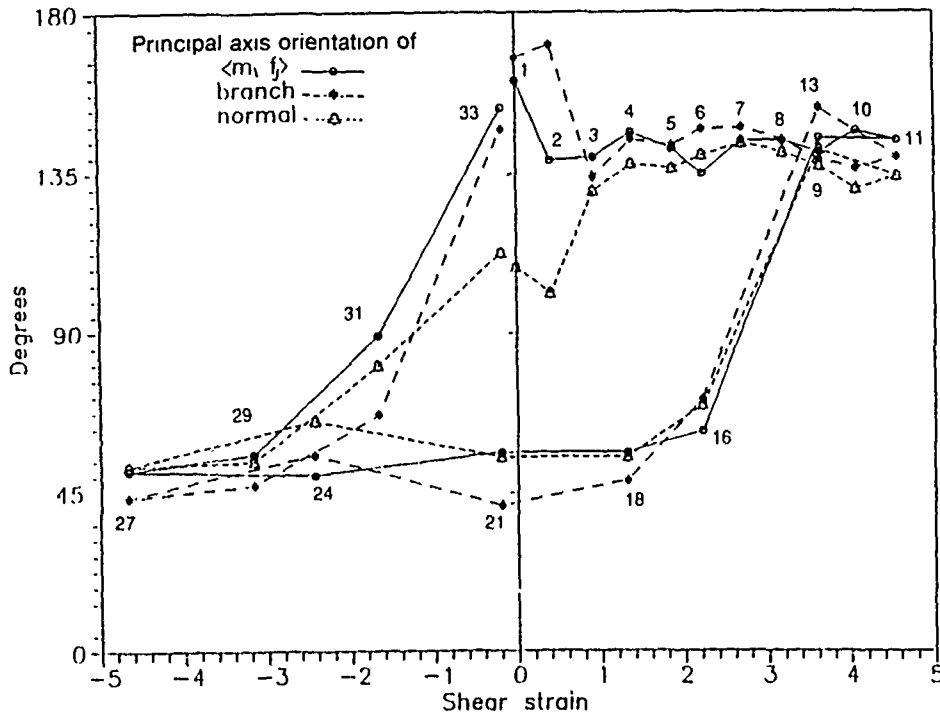


Fig. 10. Plot of orientations of the major principal axes of the tensors $\langle m_i f_j \rangle$, $\langle m_i m_j \rangle$, and $\langle n_i n_j \rangle$. The orientations of the principal axes change rapidly and reach a constant value between 130° and 140° , until further change in the direction of shearing occurs.

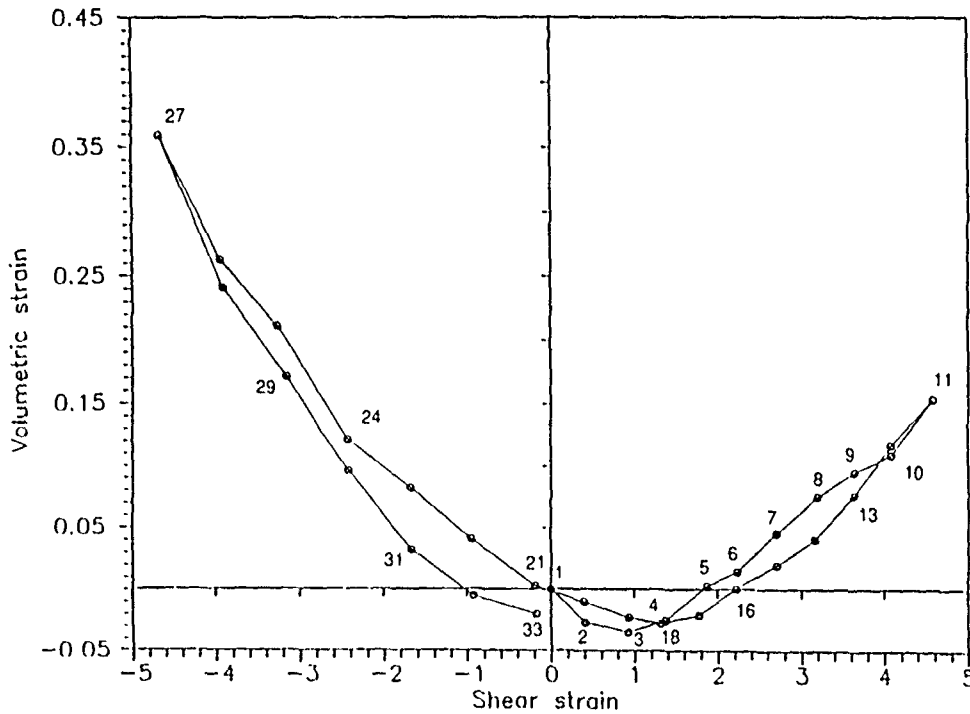


Fig. 11 Plot of volumetric strain vs shear strain in granular materials when subjected to shear under confining pressure

$d\Omega$, about the direction \mathbf{n} . Expanding $E(\mathbf{n})$ in spherical or circular harmonics, gives

$$E(\mathbf{n}) = A \left[1 + J_{ij} n_i n_j + J_{ijkl} n_i n_j n_k n_l + \dots \right], \quad (7.2)$$

where $A = 1/(2\pi)$ in two dimensions, and $1/(4\pi)$ in three dimensions. J_{ij} and J_{ijkl} are all deviatoric and are expressed in two dimensions as

$$J_{ij} = 4 \left[\langle n_i n_j \rangle - \frac{1}{2} \delta_{ij} \right],$$

$$J_{ijkl} = 16 \left[\langle n_i n_j n_k n_l \rangle - \delta_{(ij} \langle n_k n_l \rangle + \frac{1}{8} \delta_{(ijkl)} \right]. \quad (7.3)$$

The angular brackets denote averages taken over all orientations. J_{ij} and J_{ijkl} are symmetric and traceless. J_{ij} has been related to various fabric tensors in the literature.

The components of the above two tensors can be represented in two dimensions, in terms of the four parameters A , B , C , and D defined by

$$A = \langle \sin \theta \cos \theta \rangle, \quad B = \langle \sin \theta \cos^3 \theta \rangle, \quad (7.4)$$

$$C = \langle \cos^2 \theta \rangle, \quad D = \langle \cos^4 \theta \rangle,$$

where θ is the orientation of \mathbf{n} or \mathbf{m} , measured from the horizontal. The distribution density function in terms of these parameters now becomes

$$E^{(2)}(\mathbf{n}) = \frac{1}{2\pi} + \frac{1}{\pi} [2A \sin 2\theta + (2C - 1) \cos 2\theta],$$

$$E^{(4)}(\mathbf{n}) = \frac{1}{2\pi} + \frac{1}{\pi} [2A \sin 2\theta + (2C - 1) \cos 2\theta$$

$$+ (1 - 8C + 8D) \cos 4\theta$$

$$+ 4(2B - A) \sin 4\theta], \quad (7.5)$$

where the superscript on E indicates the order of terms included in the expansion of $E(\mathbf{n})$. Note that the parameters A and C are related to the degree of concentration, J , and the preferred orientation, β , introduced by Konishi (1978), where

$$J^2 = \frac{1}{8} J_{ij} J_{ij} = 4A^2 + (1 - 2C)^2, \quad (7.6)$$

and

$$\tan 2\beta = \frac{2J_{12}}{J_{11} - J_{22}} = \frac{2A}{1 - 2C}. \quad (7.7)$$

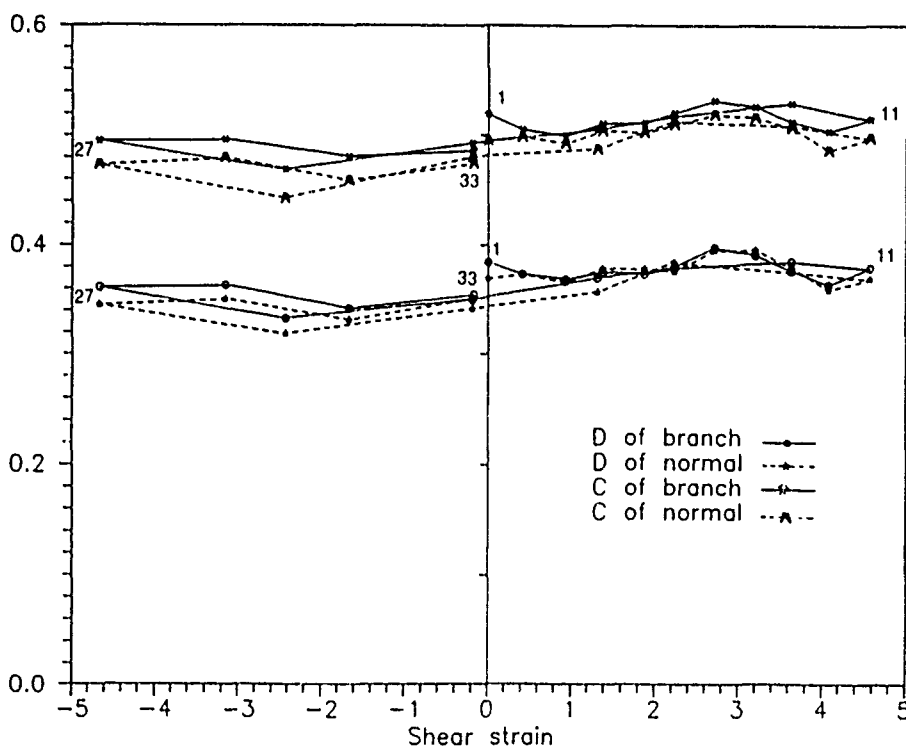


Fig 12 The parameters C and D , which are the diagonal terms in fabric tensors J_{ij} and J_{ijkl} , remain almost constant throughout the deformation process

Here, β is the same as the angle of the principal axis of tensor $\langle m_i m_j \rangle$ or $\langle n_i n_j \rangle$, which is plotted against shear strain in Fig. 10.

The parameters A , B , C , and D have been measured at each stage of the experiment. A and C represent the terms $\langle n_1 n_2 \rangle$, and $\langle n_1 n_1 \rangle$ or $\langle n_2 n_2 \rangle$ in the fabric tensor $\langle n_i n_j \rangle$, respectively (or the corresponding terms in $\langle m_i m_j \rangle$), as discussed before. The parameters C and D are the diagonal terms in the fabric tensors J_{ij} and J_{ijkl} , respectively, and from Fig. 12 they seem to remain almost constant throughout the deformation process, representing the constant confining pressure. The off-diagonal terms, for example A and B , behave similarly to the applied shear stress. The parameter A vs. the shear strain is already plotted for both unit normals and unit branches in Fig. 6, and B vs. shear strain is shown in Fig. 13. Also the parameters B and D behave similarly to A and C , respectively. Therefore, in the distribution density function, even terms like $\langle \cos^2 \theta \rangle$ and $\langle \cos^4 \theta \rangle$, or $\langle \sin^2 \theta \rangle$ and $\langle \sin^4 \theta \rangle$ relate to the applied confining pressure, and odd terms involving both sine and cosine, like A and B , relate to the overall applied shear stress. Note that the values

of A , B , C , and D , for unit branches as well as unit contact normals, are almost the same. Also, the distributions of the unit contact normals and the unit branches which are shown in Figs. 9(a) and 9(b), and the orientations of the principal axes which are shown in Fig. 10 for both the above tensors, are similar. So, for all practical purposes, the consideration of either one of them seems sufficient for the analysis of fabric. This was also observed in earlier experiments by Mehrabadi et al. (1988). Figures 9(a) and 9(b) show the actual, fourth-order and second-order, distributions of the contact normals and unit branches at various stages throughout the experiment. It is clear that the fourth-order approximation reveals the inherent anisotropy much more accurately than does the second-order approximation.

8. Conclusion

A summary of some theoretical and experimental developments on granular materials is pre-

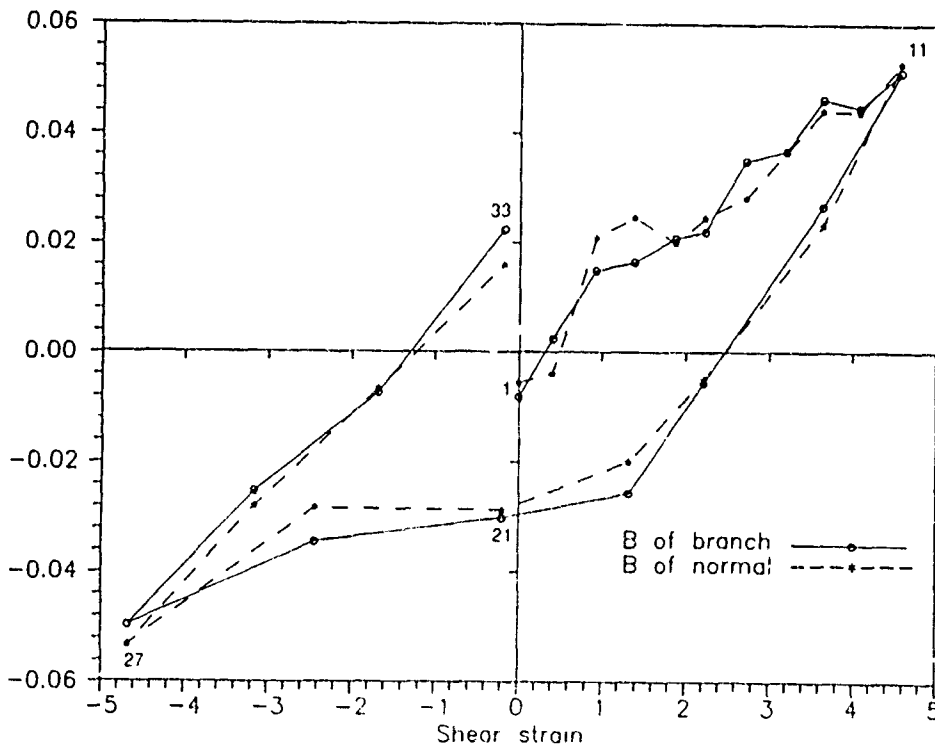


Fig. 13 The parameter B behaves similarly to the applied overall shear stress

sented. The results of a series of experiments performed on photoelastic granules in simple shearing under confining pressure, are discussed. The components of various fabric tensors proposed in the literature are measured experimentally. The tensor $\langle m, f_j \rangle$ is shown to be a good measure of the overall stress. The off-diagonal terms in the tensors $\langle m, f_j \rangle$, $\langle m, m_j \rangle$, and $\langle n, n_j \rangle$ have been found to represent the overall shear stress, as predicted by the theory, and the diagonal terms to represent the confining pressure which remains constant throughout the deformation process. The principal axes of all the above tensors rotate during cyclic shear. They rotate by 90° whenever a change in the direction of the applied shear occurs.

In the distribution density function, $E(\mathbf{n})$, of the unit contact normals, terms involving both sine and cosine follow the stress-strain relation closely, and terms involving sine or cosine alone remain constant throughout the deformation, representing the constant confining pressure. Also, it is important to include the fourth-order terms in the expansion of $E(\mathbf{n})$, in order to reveal the highly anisotropic nature inherent in the data.

Finally, since the distribution of contact normals and unit branch orientations, and other microscopic quantities associated with them are similar for both contact normals and unit branches, it may be concluded that any one of them can be taken as a good measure of the fabric.

Acknowledgments

This work has been supported in part by the Air Force Office of Scientific Research under Grant No. AFOSR-87-0079 and in part by the National Science Foundation under Grant No. MSM-85-15907 to the University of California, San Diego. The authors are thankful to Dr. Masoud Beizaie who digitized and analyzed the pictures. Acknowledgments are also due to Mr. John Schmidt of Northwestern University, who designed and constructed the experimental apparatus. The authors also thank Dr. Kishino who developed the early versions of the computer programs which were later modified. The work com-

pleted at Northwestern University was supported by the National Science Foundation under Grant No. CEE-83-13663 to Northwestern University.

References

- Arthur, J.R.F. and B.K. Menzies (1972), Inherent anisotropy in sand, *Geotechnique* 22, 115-129.
- Arthur, J.R.F., K.S. Chua and T. Dunstan (1977), Induced anisotropy in sand, *Geotechnique* 27, 13-30.
- Bishop, A.W. (1966), The strength of soils as engineering materials, *Geotechnique* 16, 91-130.
- Casagrande, A. and N. Carillo (1944), Shear failure of anisotropic materials, *Proceedings of Boston Society of Civil Engineers* 31, 74-87.
- Christoffersen, J., M.M. Mehrabadi and S. Nemat-Nasser (1981), A micromechanical description of granular material behavior, *J. Appl. Mech.* 48, 339-344.
- Kanatani, K. (1984), Distribution of directional data and fabric tensors, *Int. J. Eng. Sci.* 22 (2), 149-164.
- Konishi, J. (1978), Microscopic model studies on the mechanical behavior of granular materials, *Proceedings of U.S.-Japan Seminar on Continuum-Mechanics of Granular Materials*, 27-45.
- Konishi, J., M. Oda and S. Nemat-Nasser (1983), Induced anisotropy in oval cross-sectional rods in biaxial compression, in: J.T. Jenkins and M. Satake, eds., *Mechanics of Granular Materials: New Models and Constitutive Relations*, 31-39.
- Mehrabadi, M.M., S. Nemat-Nasser, H.M. Shodja and G. Subhash (1988), Some basic theoretical and experimental results on micromechanics of granular flow, in: J.T. Jenkins and M. Satake, eds., *Proceedings of U.S.-Japan Seminar on the Mechanics of Granular Materials*, 253-262.
- Mehrabadi, M.M., S. Nemat-Nasser and M. Oda (1982), On statistical description of stress and fabric in granular materials, *International Journal of Numerical and Analytical Methods in Geomechanics* 6, 95-108.
- Mehrabadi, M.M. and S. Nemat-Nasser (1983), Stress, dilatancy and fabric in granular materials, *Mech Mater* 2, 155-161.
- Nemat-Nasser, S. (1980), On behavior of granular materials in simple shear, *Soils and Foundations* 20, 59-73.
- Nemat-Nasser, S. (1983), Fabric and its influence on mechanical behavior of granular materials, *IUTAM Conference on Deformation and Failure of Granular Materials*, 37-42.
- Nemat-Nasser, S. (1989), Anisotropy in response and failure modes of granular materials, in: J.P. Boehler, ed., *Yielding, Damage and Failure of Anisotropic Elastic Solids*, (EGF5), Mechanical Engineering Publications, London.
- Nemat-Nasser S and M.M. Mehrabadi (1983), Micromechanically based rate constitutive description for granular materials, *Proceedings of International Conference on Constitutive Laws for Engineering Materials, Theory and Application*, Tucson, A.Z. Wiley, New York.

- Nemat-Nasser, S. and K. Takahashi (1984), Liquefaction and fabric of sand, *J. Geotechn. Eng.* 110, 1291-1306.
- Nemat-Nasser, S. and Y. Tobita (1982), Influence of fabric on liquefaction and densification potential of cohesionless sand, *Mech. Mater.* 1, 43-62.
- Ochiai, H. (1975), The Behavior of Sands in Direct Shear Tests, *J. JSSMFE* 15 (4), 93-100.
- Oda, M. (1972a), Initial fabrics and their relation to mechanical properties of granular material, *Soils and Foundations* 12 (1), 1-18.
- Oda, M. (1978), Significance of fabric in granular mechanics, *Proceedings of U.S.-Japan Seminar on Continuum-Mechanical and Statistical Approaches in the Mechanics of Granular Materials*, 7-26.
- Oda, M. (1972b), The mechanism of fabric changes during compressional deformation of sand, *Soils and Foundations* 12 (2), 1-18.
- Oda, M. (1975), On stress-dilatancy relation of sand in simple shear test, *Soils and Foundations* 15, 17-29.
- Oda, M. (1974), A mechanical and statistical model of granular material, *Soils and Foundations* 14 (1), 13-17.
- Oda, M. and J. Konishi (1974a), Rotation of principal stresses in granular material during simple shear, *Soils and Foundations* 14, 39-53.
- Oda, M. and J. Konishi (1974b), Microscopic deformation mechanism of granular material in simple shear, *Soils and Foundations* 14, 25-38.
- Oda, M., S. Nemat-Nasser and M.M. Mehrabadi (1982), A statistical study of fabric in a random assembly of spherical granules, *Int. J. Num. Anal. Methods Geomech.* 6, 77-94.
- Oda, M., S. Nemat-Nasser and J. Konishi (1985), Stress induced anisotropy in granular masses, *Soils and Foundations* 25, 85-97.
- Parkin, A.K., C.M. Gerrard and D.R. Willoughby (1968), Discussion on deformation of sand in shear, *J. Soil Mech. Foundations, Div. ASCE.* 94, 336-340.
- Roscoe, K.H., R.H. Bassett and E.R.L. Cole (1967), Principal axes observed during simple shear of sand, *Proceedings of Geotechnical Conference, Oslo*, 1, 231-237.
- Satake, M. (1978), Constitution of mechanics of granular materials through the graph theory, in: S.C. Cowin and M. Satake, eds., *U.S.-Japan Seminar on Continuum-Mechanics and Statistical Approaches in the Mechanics of Granular Materials*, 47-62.

Submitted for publication in August 1991

**INCREMENTAL CONSTITUTIVE RELATIONS FOR GRANULAR
MATERIALS BASED ON MICROMECHANICS**

by

M. M. Mehrabadi
Department of Mechanical
Engineering
Tulane University
New Orleans, LA 70118, U.S.A.

B. Loret
National Polytechnic Institute
of Grenoble
Institute of Mechanics
BP 53X 38041 Grenoble Cédex, FRANCE

and

S. Nemat-Nasser
Center of Excellence for Advanced Materials
Department of Applied Mechanics
and Engineering Sciences
University of California, San Diego
La Jolla, CA 92093, U.S.A.

ABSTRACT

Micromechanically-based constitutive relations for two-dimensional flow of granular materials are presented. First, the relations between the overall stresses and the relevant microscopic quantities, namely, the interparticle forces, the density and orientation of contact unit normals, as well as the average size of the particles, are obtained. Then, the kinematics is examined, and the overall velocity gradient is related to measures characterizing the relative sliding and rotation of granules. A significant concept underlying all these developments is the notion of the *class* of contact unit normals with a continuously evolving distribution function, even though individual members of various classes may change discontinuously, as contacts are lost and new contacts are developed in the course of granular flow. Then, simple local constitutive relations are introduced for the rate of change of the contact forces, the evolution of the contact normals, the mechanism of local failure, and the density of contacts in a particular class. This leads to macroscopic rate constitutive equations through a Taylor averaging method. Due to the nonlinearity of the rate constitutive equations, the response is computed by an incremental procedure. As an illustration, the overall response of a two-dimensional assembly of disks subjected to an overall shearing deformation is determined. In addition, explicit results are presented for the evolution of fabric, contact forces, and the history of active and inactive classes of contacts. The stress-strain relations and the evolution of fabric and contact forces are in excellent qualitative agreement with the observed behavior of granular materials. In light of these results, the mechanisms of failure and inelastic deformation of dense as well as loose granular materials are discussed.

Although most features of the model could be readily generalized to three dimensions, for simplicity, the discussion is limited to planar deformation.

1. INTRODUCTION

A fundamental issue of considerable scientific and technological importance in the mechanics of granular materials is the development of their overall macroscopic constitutive relations on the basis of simple and reasonable micromechanical assumptions. Many topics which either directly or indirectly bear on this fundamental issue, have been dealt with by many researchers over the past several decades, leading to considerable progress in this area, and better understanding of the major parameters involved.¹

A systematic approach to this problem inevitably would include considerations of: 1) a description of the overall macroscopic stresses in terms of contact forces, their distribution, and some relevant geometric measures of the microstructure; 2) a description of the overall measures of incremental deformation in terms of quantities that characterize micromechanisms of relative sliding or sliding and rolling of granules; 3) a description of the time rate of change of the overall stress measure in terms of the overall deformation-rate measures, based on simple models which characterize the corresponding rate of change in contact forces in terms of suitable local deformation-rate measures.

A stumbling block that seems to have hindered achieving all of the above-mentioned goals is the fact that, in the course of deformation, new contacts are constantly being generated as some of the existing contacts are being lost. This precludes analytic identification of the history of individual contacts, unless one approaches the problem numerically, using a large-scale computer program (see, e.g., Petrakis and Dobry, 1989). On the other hand, in the course of continuous deformation of a granular mass, one expects that suitable measures of the distribution of contacts can be employed, which characterize a certain *class* of contacts and, therefore, undergo continuous change. This is the viewpoint adopted in the present paper.

In this work the microstructure is identified with the "fabric" of the granular mass. There are

¹ For some recent contributions see the proceedings of the three U.S.-Japan Seminars (Cowin and Satake, 1978; Jenkins and Satake, 1983; Satake and Jenkins, 1988).

various tensorial measures that can be used for describing the fabric of a granular mass; see Nemat-Nasser and Mehrabadi (1983) for a discussion of some of these fabric measures. Here, following Oda (1972), the fabric is represented by the distribution of the unit contact normals. Accordingly, based on the observed evolution of fabric, we introduce local constitutive equations directly for the probability density function of the contact normals rather than for various fabric tensors which are defined by means of the distribution density function.

Based, in spirit, on our earlier work (Nemat-Nasser and Mehrabadi, 1984), we introduce simple constitutive models at the microlevel, which relate the change (or the rate of change) in the contact force associated with a given class of contacts to the corresponding micro-deformation increment (or rate) produced by the corresponding changes in the microstructure. Such an approach (which deals with classes of contacts rather than with individual contacts) bypasses the difficult issue of continuous loss of contacts and formation of new ones. As mentioned earlier, here the fabric is represented by the distribution of contact normals. Each orientation corresponds to a large number of contacts which, while individually may undergo abrupt changes, collectively evolve in a continuous manner during the course of the continuous flow of the representative granular sample. In this manner, one can, for example, identify an initial and a current orientation for a given class of contacts, while clearly the same identification may not, in general, be possible for an individual and specific contact.

After a discussion of the concept of stress in granular materials in Section 2, a description of the kinematics is presented in Section 3. At the local level, the description of kinematics corresponds to the double shearing model of Spencer (1964, 1982). The local constitutive assumptions for the time rate of change of contact forces, the local yield criterion, the time rate of change of the local nominal stress, and the evolution of the probability density function of contact normals are presented in Section 4. Macroscopic constitutive equations are found, in Section 5, by employing a Taylor averaging scheme.

Due to the nonlinearity of the rate constitutive equations, the response must be computed by an incremental procedure. Instead of using a scheme of subincrementation, we introduce another simpler

method based on the first-order approximation of the local yield function. This procedure is described in Section 6, where local and overall constitutive equations are written in incremental form.

Owing to the simplicity of the local rate constitutive equations introduced in Section 4, an analytical integration is possible and is carried out in Section 7, whereby explicit relations are derived, including those for the contact forces and contact normals. Using these relations, the overall nominal stress can be computed in two alternative ways which are described in Sections 6 and 7.

For boundary value problems on granular materials, with prescribed initial overall confining stresses, it is necessary to determine the initial equilibrium distribution of contact forces for each class of contacts. Hence, in Section 8, a relationship is developed between the local contact force corresponding to an individual class, and the overall confining stress and the initial fabric. Boundary conditions for the numerical examples are also considered in this section.

As an illustration, the response of a two-dimensional assembly of rigid cylindrical disks of circular cross section subjected to shearing deformation is determined in Section 9. Two numerical examples are presented, one of which simulates the response of dense and the other corresponds to the behavior of loose granular materials. The mechanism of strain hardening and failure followed by strain softening which is a characteristic response of densely packed samples of granular materials, and the inelastic deformation mechanism corresponding to the loosely packed samples are discussed in light of the model predictions of the evolution of fabric, contact forces, and the history of active and inactive contacts. In so far as the shearing deformation is concerned, the resulting stress-strain relations and the evolution of fabric, and the evolution of contact forces are in excellent qualitative agreement with the observed behavior of granular materials. However, the volumetric response of the model in cyclic shear is not realistic because the model predicts a net dilatancy rather than a net densification at the conclusion of a cycle of deformation. A further study of this point and the generalization of this model to three dimensions are left for future investigations.

2. DESCRIPTION OF STRESS AND ITS TIME RATE OF CHANGE

A granular mass is modeled as a continuum whose material points are endowed with the overall macroscopic characteristics of a typical sample which contains a representative set of granules. The typical sample must be large enough to be statistically representative of the properties of the granular material. The stress at a material point in the model continuum is then represented by the average stress in the typical sample of the granular mass.

An expression for the overall average stress tensor in the sample of the granular body, in terms of microscopic quantities such as contact forces and branches (which are vectors joining the centroids of adjacent contacting granules), can be obtained by applying the principle of virtual work. The following derivation is based on the work of Christoffersen, Mehrabadi, and Nemat-Nasser (1981).

Consider a representative sample of a granular mass which at time t has a volume V bounded by a surface S . The reference configuration of the sample has a volume V_0 and a surface S_0 . The sample is subjected on its boundary to a uniform traction T^0 measured per unit reference area. Choosing a fixed rectangular Cartesian coordinate system, denote the corresponding components of the local asymmetric nominal stress tensor by v_{ij} , and require that this nominal stress and its time rate of change remain in equilibrium with the applied tractions and their time rates of change, i.e., the spatially variable nominal stress and its rate are introduced in such a manner that the following equilibrium equations are satisfied at all times (body forces are absent and quasi-static problems are considered):¹

$$v_{ij}N_i^0 = T_j^0, \quad \dot{v}_{ij}N_i^0 = \dot{T}_j^0 \quad \text{on } S_0, \quad (2.1)$$

$$\frac{\partial v_{ij}}{\partial X_i} = \frac{\partial \dot{v}_{ij}}{\partial X_i} = 0 \quad \text{in } V_0, \quad (2.2)$$

where X is the position of a point of the granular mass in the reference configuration, N^0 is the normal to the boundary S_0 , and where a superimposed dot designates the time-rate of change. The introduction of the (variable) nominal stress and its rate in equilibrium with the prescribed boundary tractions and their rates is in agreement with similar concepts used in developing overall macroscopic properties of

¹ Here and throughout the paper, summation over the appropriate range of repeated indices is in force.

polycrystalline solids and composite materials in terms of their microscopic properties; Hill (1965, 1972). In this context, the overall average nominal stress and its time rate of change are simply given by the unweighted volume averages of the local quantities, i.e.,

$$N_{ij} = \frac{1}{V_0} \int_{V_0} v_{ij} dV_0, \quad (2.3)$$

and

$$\dot{N}_{ij} = \frac{1}{V_0} \int_{V_0} \dot{v}_{ij} dV_0. \quad (2.4)$$

Following the procedure outlined by Christoffersen *et al.* (1981), let f_i stand for the components of the contact force exerted by a typical granule on its neighboring granule over a contact point. At each contact point we identify one such contact force. We consider a spatially varying velocity field v_i which is kinematically admissible, and which produces at typical contact points relative *virtual* separations denoted by Δ_i . Then the virtual work principle requires

$$\begin{aligned} \sum_{\alpha=1}^{M_0} f_i^\alpha \Delta_i^\alpha &= \frac{1}{V_0} \int_{S_0} v_{ij} N_i^0 v_j dS_0, \\ &= \frac{1}{V_0} \int_{V_0} v_{ij} \frac{\partial v_j}{\partial X_i} dV_0, \end{aligned} \quad (2.5)$$

where M_0 is the number of contacts per unit volume in the reference configuration, and where the equilibrium equations (2.1)₁ and (2.2)₁ and the divergence theorem are used.

As pointed out in the introduction, in developing rate constitutive relations, we may deal with *classes of contacts* and the evolution of these classes, rather than with specific individual contacts which may be lost or generated in the course of deformations. This idea will be further discussed later on. Here, it suffices to comment that *we actually use the current configuration as the reference configuration*, which circumvents this problem.

Let the virtual velocity v_i be linear, so that the velocity gradient is constant, i.e.,

$$\frac{\partial v_i}{\partial X_j} = \phi_{ij}^0. \quad (2.6)$$

A compatible virtual relative separation velocity, Δ_{ij} , at a typical contact is then of the form

$$\Delta_i = \phi_y^0 \ell_j^0, \quad (2.7)$$

where ℓ^0 is the associated branch, i.e., the vector joining the centroids of two typical contacting granules; Christoffersen, Mehrabadi and Nemat-Nasser (1981). Note that there are two such branches associated with each contact point, ℓ^0 and $-\ell^0$. For each contact point we identify only one contact force, f_i , and one associated branch, ℓ^0 ; see Mehrabadi, Nemat-Nasser, and Oda (1982).

Substitution from (2.7) and (2.6) into (2.5) now yields

$$\left[\sum_{\alpha=1}^{M_0} f_i^\alpha \ell_j^{\rho\alpha} - \frac{1}{V_0} \int_{V_0} v_{j\alpha} dV_0 \right] \phi_y^0 = 0. \quad (2.8)$$

Since ϕ_y^0 is arbitrary, we obtain

$$\begin{aligned} N_{ij} &= \sum_{\alpha=1}^{M_0} \ell_i^{\rho\alpha} f_j^\alpha, \\ &= \sum_{\alpha=1}^{M_0} \ell^{\rho\alpha} m_i^{\rho\alpha} f_j^\alpha, \end{aligned} \quad (2.9)$$

where $\ell^{\rho\alpha}$ is the branch length, and $m_i^{\rho\alpha}$ is a unit vector referred to as the "unit branch".

Following Mehrabadi, Nemat-Nasser, and Oda (1982), the group of M_0 contacts per unit reference volume of granular mass is divided into, say Q classes, each with a common branch direction defined by the corresponding unit branch vector. If there are M_{0a} , ($a = 1, 2, \dots, Q$), contacts which belong to class a with common unit branch m^a , then

$$\sum_{a=1}^Q \frac{M_{0a}}{M_0} = 1. \quad (2.10)$$

Let α_a denote a typical contact in class a . In obtaining the average quantities in Eq. (2.9), one must first calculate the corresponding average over each class and then sum the results over all classes. Since, for a typical class a , there are M_{0a} contributing contacts,

$$N_{ij} = \sum_{a=1}^Q \left(\sum_{\alpha_a=1}^{M_{0a}} \ell_i^{\rho\alpha_a} f_j^{\alpha_a} \right) m_i^{\rho a}.$$

For the sake of simplicity, we assume that the contact forces $f_i^{\alpha_a}$ are not correlated with the branch

length, ℓ^{0a} . With this assumption, it follows that

$$N_{ij} = \sum_{a=1}^Q \frac{M_{0a}}{M_0} \varphi_{ij}^a \equiv \langle \varphi_{ij}^a \rangle_0, \quad (2.11)$$

where

$$\varphi_{ij}^a = M_0 \ell^{0a} m_i^{0a} f_j^a,$$

and where the angular brackets, $\langle \rangle$ denote averaging over all the classes. The subscript zero of the angular brackets is to indicate that the average is taken over the reference unit volume. A superposed hat in (2.11) designates averaging over the force-bearing contacts in a class. *Bearing in mind that the contact force and the branch length are average quantities over a class, and that these quantities and the unit branch vary from one class to another, to make the notation somewhat simpler, the superposed hats and the superscripts a will not be shown in the sequel.* For example (2.11), in the simplified notation, becomes

$$N_{ij} = \sum_{a=1}^Q \frac{M_{0a}}{M_0} v_{ij}^a \equiv \langle v_{ij}^a \rangle_0, \quad (2.12)$$

where

$$v_{ij}^a = M_0 \ell^0 m_i^0 f_j. \quad (2.13)$$

We now take the reference configuration to be the instantaneous current configuration, and obtain from (2.12) and (2.13)

$$\Sigma_{ij} = \langle \sigma_{ij} \rangle = \sum_{a=1}^Q \frac{M_a}{M} \sigma_{ij}^a, \quad (2.14)$$

where

$$\sigma_{ij}^a = M \ell m_i f_j, \quad (2.15)$$

and the angular brackets, $\langle \rangle$, denote averaging over all the classes in the current volume, $\Sigma_{ij} = \langle \sigma_{ij} \rangle$ is the average (overall) Cauchy stress, and M and M_a are, respectively, the total number of contacts per unit current volume and the number of contacts in class a per unit current volume

Note that although the average of σ_{ij} is the symmetric overall Cauchy stress, the local quantity σ_{ij} is not symmetric, in general.

When the number of classes, Q , is very large, we can introduce the distribution density function $E(m)$ to describe the angular distribution of unit branches. In this case (2.10) becomes

$$\int_{\Omega} E(m) d\Omega = 1, \quad (2.16)$$

where $E(m) = E(-m)$, and where $d\Omega$ is an elemental angle of the unit circle Ω . With (2.16), the average of any quantity $\varphi(m)$ is given by

$$\begin{aligned} \langle \varphi \rangle &\equiv \sum_{a=1}^Q \frac{M_a}{M} \varphi(m^a), \\ &= \int_{\Omega} E(m) \varphi(m) d\Omega. \end{aligned} \quad (2.17)$$

In particular,

$$N_{ij} \equiv \langle v_{ij} \rangle_0 = M_0 \langle \ell^0 m_i^0 f_j \rangle_0 = M_0 \int_{\Omega} E(m^0) \ell^0 m_i^0 f_j d\Omega, \quad (2.18)$$

and

$$\langle \sigma_{ij} \rangle = M \langle \ell m_i f_j \rangle = M \int_{\Omega} E(m) \ell m_i f_j d\Omega. \quad (2.19)$$

The macroscopic Cauchy stress, Σ_{ij} , is defined by the relations

$$\Sigma_{ij} = \frac{1}{\det \mathbf{G}} G_{ik} N_{kj}, \quad (2.20)$$

where \mathbf{G} , the average deformation gradient, is related to the local¹ deformation gradient, \mathbf{g} , by

$$\mathbf{G}_{ij} = \frac{1}{V_0} \int_{V_0} g_{ij} dV_0 \equiv \langle g_{ij} \rangle_0. \quad (2.21)$$

Hill (1984) has shown that under homogeneous macro-boundary conditions the average and macroscopic Cauchy stresses are equal, i.e.,

¹ The term "local" is used interchangeably with the term "class", so that \mathbf{g} , or more explicitly \mathbf{g}^a , defines the contribution of the typical class a to the overall deformation gradient.

$$\langle \sigma_{ij} \rangle = \frac{1}{V} \int_V \sigma_{ij} dV = \Sigma_{ij} . \quad (2.22)$$

Expressions similar to (2.19) for stress have been derived by many investigators beginning with Cauchy in 1822 (see Love, 1927, Note B) who derived an expression for stress in an anisotropic linearly elastic material on the basis of a molecular theory. Assuming that forces between the atoms are centric, Cauchy derived an expression of the form¹

$$\Sigma_{ij} = M \langle \ell f_{m_i} m_j \rangle . \quad (2.23)$$

Since the current configuration is used as the reference one, the nominal stress N_{ij} equals the Cauchy stress Σ_{ij} . The same, however, is not true for the corresponding rates. The advantage of working with the nominal stress of the form (2.10), is that one may employ a procedure similar to the one outlined above, and show that

$$\dot{N}_{ij} = \langle \dot{v}_{ij} \rangle_0 = M_0 \langle \ell^0 m_i^0 \dot{f}_j \rangle_0 . \quad (2.24)$$

When the current and the reference configurations are chosen to be coincident, Eq.(2.13) reduces to

$$\dot{N}_{ij} = M \langle \ell m_i \dot{f}_j \rangle . \quad (2.25)$$

This eliminates the need for a transport-type equation which, generally speaking, relates the time rate of change of the average of a quantity to the average of its time rate of change. The relation between the nominal stress rate and the Cauchy stress rate will be examined in Section 5 after the necessary kinematical quantities have been introduced.

¹ Cauchy's derivation of the form of the elasticity moduli on the basis of (2.23) yields only 15 independent moduli (rather than 21) for the least degree of symmetry (i.e., triclinic). The six "Cauchy relations" between the 21 elastic moduli are generally attributed to the centric force assumption. It is interesting to note that even when the tangential component of the force is non-zero and the stress is given by (2.14) and (2.15), under certain conditions, the six Cauchy relations cannot be avoided.

3. KINEMATICS

The flow of a granular mass which consists of rigid granules under the action of an overall applied load occurs through sliding and rolling of grains over each other. As pointed out earlier, in this process, some contacts are lost, and new contacts are continually developed. The overall deformation rate is the result of local relative motion of the grains over active contact points. The grains, however, are constrained by the neighboring grains during their relative motion, so that a compatible overall configuration is maintained. In the course of such flow, the microstructure or fabric changes; consequently contact forces and, hence, the overall stresses also change.

As mentioned before, in dealing with the evolution of the microstructure of a granular sample, it is more effective to consider a distribution of suitable measures of microstructure and its evolution in the course of deformation, rather than the changes of specific and individual local quantities. One such suitable measure of microstructure or fabric is the distribution of contact unit normals (Oda, 1972). Another, equally effective measure is the distribution of unit branches which are unit vectors in the direction of the branches. Both measures, or a combination of the two, have been discussed in the literature; see Nemat-Nasser and Mehrabadi (1983), and Mehrabadi *et al.* (1988). Here, we select to work with the distribution of contact normals, simply because it is easier to relate frictional sliding to this quantity. Also, for simplicity, we limit our discussion to circular disks in a plane or spherical granules for which the unit normals and the unit branches are of course, identical.

Hence, in what follows, the microstructure of a typical sample of a granular mass is characterized only by the distribution of contact unit normals. *Each orientation in this distribution corresponds to a class of contacts.* As the sample deforms, the distribution of unit normals changes and this change characterizes a corresponding change of the fabric or microstructure. The overall deformation is viewed as a suitable average of the local deformations associated with each class of contacts. Here, by "local deformation rate", we mean the deformation rate corresponding to a given class of contacts which includes contributions from a large number of specific individual contacts that are represented by a given orientation.

The local deformation rate associated with a given class of contacts comprises contributions from (i) *the relative motion of individual grains which leaves their associated orientation and, therefore, the microstructure of this class unchanged, and (ii) an accompanying part associated with the fabric change*

which renders the resulting velocity gradient for this class compatible and which induces a change in the contact force associated with the class. For example, if contacting granules undergo rigid rotation without sliding or rolling, the contact orientation and the contact force change, leading to a change in fabric. On the other hand, if contacting granules simply slide and roll in such a manner that the orientation of the contact normal is unchanged, no contribution to the change in fabric is made. In general, however, a compatible deformation is obtained only if both contributions are present. It should be noted that, for certain classes of contacts, this formulation allows nonzero velocity gradients solely due to fabric change, even when the granules are rigid.

Let l_{ij}^a , ($a = 1, \dots, Q$), denote the components of the velocity gradient associated with a typical class of contacts, a . Then

$$l_{ij}^a = l_{ij}^{*a} + l_{ij}^{**a}, \quad (a=1, \dots, Q), \quad (3.1)$$

where l_{ij}^{*a} is the velocity gradient corresponding to the fabric change, and l_{ij}^{**a} is the velocity gradient stemming from the relative sliding motion of the grains, which leaves the fabric unchanged. The part l_{ij}^{**a} in (3.1) is the counterpart of the slip-induced velocity gradient in single crystals, and the part l_{ij}^{*a} is the counterpart of that associated with the elastic lattice distortion. Note that, in a granular material which is modeled by rigid granules, no *elastic* deformation can be involved, it is the change in fabric that produces the change in the overall stress.

The part l_{ij}^{**a} is resolved into a symmetric and a skew-symmetric part, as

$$l_{ij}^{**a} = d_{ij}^{**a} + w_{ij}^{**a}, \quad (3.2)$$

where

$$d_{ij}^{**a} = \frac{1}{2}(l_{ij}^{**a} + l_{ji}^{**a}) \quad \text{and} \quad w_{ij}^{**a} = \frac{1}{2}(l_{ij}^{**a} - l_{ji}^{**a}), \quad (3.3)$$

are, respectively, the local inelastic deformation rate and spin; and where, *for ease in writing, the dependence on the class of contacts is not shown explicitly in (3.2)*. Similarly, the accommodating velocity gradient, l_{ij}^{*a} , associated with the fabric change, is decomposed as

$$l_{ij}^{*a} = d_{ij}^{*a} + w_{ij}^{*a}, \quad (3.4)$$

where

$$d_{ij}^* = \frac{1}{2}(l_{ij}^* + l_{ji}^*) \quad \text{and} \quad w_{ij}^* = \frac{1}{2}(l_{ij}^* - l_{ji}^*), \quad (3.5)$$

are the corresponding deformation rate and spin tensors.

The overall velocity gradient, deformation rate tensor, and spin tensor, are respectively defined by

$$L_{ij} = \langle l_{ij} \rangle, \quad (3.6)$$

and

$$D_{ij} = \frac{1}{2}(L_{ij} + L_{ji}) = \langle d_{ij} \rangle, \quad W_{ij} = \frac{1}{2}(L_{ij} - L_{ji}) = \langle w_{ij} \rangle, \quad (3.7)$$

where

$$d_{ij} = \frac{1}{2}(l_{ij} + l_{ji}) = d_{ij}^* + d_{ij}^{**}, \quad (3.8)$$

and where

$$w_{ij} = \frac{1}{2}(l_{ij} - l_{ji}) = w_{ij}^* + w_{ij}^{**}. \quad (3.9)$$

4. LOCAL CONSTITUTIVE EQUATIONS

The local constitutive assumption for the time rate of change of the contact force is considered in Section 4.1. The local yield criterion and the local inelastic part of the velocity gradient (i.e., I^{**}) associated with this yield condition are described in Sections 4.2 and 4.3, respectively. The rate of change of the local nominal stress is derived in Section 4.4, and the evolution of the probability density function of contact normals is considered in Section 4.5.

4.1. Time Rate of Change of Contact Force

To arrive at macroscopic constitutive relations for the nominal stress-rate given by Eq. (2.25), we proceed to relate the time rate of change of the contact force to the local kinematic measures. Following Nemat-Nasser and Mehrabadi (1984), the contact force is written, without loss in generality, in the form

$$f_i = \epsilon \tau_{ij} m_j, \quad (4.1)$$

where ϵ with the dimension of area is a parameter representing a measure of the total contact area and,

consequently, the number of contacts in a particular class a ; and where τ_{ij} are the components of a *local* stress associated with a class of contacts¹.

Recall that in the decomposition of the microscopic measure of the velocity gradient I , in the manner of Eq. (3.1), only the contribution I^* is responsible for the change of fabric and, therefore, the change in the magnitude and orientation of the corresponding contact force. Accordingly, it seems reasonable to write local constitutive relations for τ_{ij} , m_i , s_i (components of a unit vector normal to m and in the sliding direction), and $\dot{\epsilon}$, in terms of the rate of fabric change, quantified here by I^* . In particular, to keep the formulation as simple as possible, we set

$$\dot{m}_i - w_{ij}^* m_j = 0 \quad , \quad \dot{s}_i - w_{ij}^* s_j = 0 \quad , \quad (4.2)$$

$$\dot{\tau}_{ij} - w_{ik}^* \tau_{kj} + \tau_{ik} w_{kj}^* = \mathcal{Q}_{ijkl}^* d_{kl}^* \quad , \quad (4.3)$$

and choose for *illustration* an isotropic relation for \mathcal{Q}_{ijkl}^* ,

$$\mathcal{Q}_{ijkl}^* = \lambda^* \delta_{ij} \delta_{kl} + \mu^* (\delta_{ik} \delta_{jl} + \delta_{il} \delta_{jk}) \quad , \quad (4.4)$$

and set

$$\frac{\dot{\epsilon}}{\epsilon} = b d_{kk}^* \quad , \quad (4.5)$$

where λ^* , μ^* , and b are constants; and where δ_{ij} , are the components of the Kronecker delta. Assumption (4.2) defines the spin of a contact normal representing a typical class, and not the spin of individual contacts which form that class. It is consistent with earlier formulations of elasto-plastic theories for crystalline materials (Hill and Rice, 1972; Havner and Shalaby, 1977; Nemat-Nasser, Mehrabadi, and Iwakuma, 1981; Nemat-Nasser, 1983; and Nemat-Nasser and Mehrabadi, 1984), in which m_i , and s_i would define the crystal lattice. Here, since m_i and s_i characterize a class of contacts which define the corresponding local fabric, it is reasonable to require that the time rate of

¹ This local stress is related to the local nominal stress given by (2.13), and the local quantity σ_{ij} , defined by (2.15), as follows:

$$v_{ij} = M^0 \ell^0 \epsilon m_i^0 \tau_{jk} m_k \quad \text{and} \quad \sigma_{ij} = M \ell \epsilon m_i \tau_{jk} m_k \quad .$$

change of these quantities, measured with respect to an observer rotating with the fabric, vanishes.

Expressions (4.2-4) are based on the starting assumption that the time rate of change of the local stress and the parameter ϵ are affected by the rate of change of the fabric only.

It is convenient to resolve the contact force f into its components, $f^{(m)}$ along the contact normal and $f^{(s)}$ along the direction of sliding, i.e.,

$$f_i = f^{(m)} m_i + f^{(s)} s_i, \quad (4.6)$$

where, using (4.1),

$$f^{(m)} = \epsilon \tau_{ij} m_i m_j, \quad (4.7)$$

$$f^{(s)} = \epsilon \tau_{ij} s_i m_j.$$

Differentiating (4.7) with respect to time and employing (4.2-5), we obtain

$$\dot{f}^{(m)} = A_{ij}^{(m)} d_{ij}^* \quad , \quad \dot{f}^{(s)} = A_{ij}^{(s)} d_{ij}^*, \quad (4.8)$$

where

$$A_{ij}^{(m)} = b f^{(m)} \delta_{ij} + \epsilon (\lambda^* \delta_{ij} + 2\mu^* m_i m_j), \quad (4.9)$$

and

$$A_{ij}^{(s)} = b f^{(s)} \delta_{ij} + \epsilon \mu^* (m_i s_j + m_j s_i). \quad (4.10)$$

Upon use of (4.8), (4.9), (4.10), (3.4), and the definition of v_{ij} according to (2.13), the local nominal stress rate becomes

$$\dot{v}_{ij} = [M_0 \ell^0 m_i^0 (A_{kl}^{(m)} m_j + A_{kl}^{(s)} s_j) + \frac{1}{2} (v_{ik} \delta_{jl} - v_{il} \delta_{jk})] l_{ik}^*, \quad (4.11)$$

where, consistent with (2.24), we have written

$$\dot{v}_{ij} = M_0 \ell^0 m_i^0 \dot{f}_j. \quad (4.12)$$

Eliminating l^* in (4.11) using (3.1), we obtain

$$\dot{v}_{ij} = [M_0 \ell^0 m_i^0 (A_{kl}^{(m)} m_j + A_{kl}^{(s)} s_j) + \frac{1}{2} (v_{ik} \delta_{jl} - v_{il} \delta_{jk})] (l_{ik} - l_{ik}^*). \quad (4.13)$$

It should be emphasized that the isotropic relation (4.4) is used here for illustration only, and that, in general, one must use a relation which reflects the corresponding local conditions. However, since the contact force associated with a class is defined in terms of the yet unspecified tensor τ_{ij} , and since (4.3) relates the rate of change of this tensor to the rate of change of the local fabric, assumption (4.4) ought to be adequate.

In order to calculate I^{**} in terms of the local velocity gradient I , a local yield criterion is developed in the sequel.

4.2 The Local Yield Criterion

In the absence of cohesion, a simple model for the yielding mechanism is a Mohr-Coulomb-type condition written in terms of the normal and tangential components of the contact force associated with a given class. In addition to this, we require here that the normal contact force remains compressive, i.e., negative, if the granules associated with the corresponding class are to remain in contact. These conditions may easily be generalized to include an allowable tensile contact force due to cohesion or other phenomena. Hence, for no inelastic deformation to be present we must have

$$|f^{(s)}| + \mu f^{(m)} \leq 0, \quad f^{(m)} < 0, \quad (4.14)$$

where $| \cdot |$ stands for the absolute value of the quantity it encloses, and $\mu (> 0)$ is the coefficient of interparticle friction. Introducing a scalar parameter u which takes on values, -1, 0, and +1, the conditions represented by (4.14) can be deduced from the three yield functions

$$Y^{(u)} \equiv u f^{(s)} + \mu f^{(m)}, \quad (u = -1, 0, +1), \quad (4.15)$$

where the superscript (u) stands for (+), (0), or (-) corresponding to positive ($f^{(s)} > 0$), "null" ($f^{(m)} \leq 0$), or negative slip ($f^{(s)} < 0$), respectively. As shown in Figure (1), the plane of $f^{(m)}$, $f^{(s)}$ is divided into six regions by the three lines defined by the yield functions (4.15).

If the average contact force for a class falls in region E, there is no inelastic deformation. On the other hand, if the force falls within regions $S^{(+)}$ or $S^{(-)}$, the contacts in that particular class will be undergoing, in an average sense, an inelastic deformation consisting of either a single positive slip or a single negative slip, respectively. In the region designated by $DS^{(0)}$, the two yield functions $Y^{(0)}$ and $Y^{(+)}$ are both non-negative and the inelastic deformation will take place by double slip. Similarly in the

region designated by $DS^{(0)}$ the two yield conditions derived from $Y^{(0)}$ and $Y^{(0)}$ are violated and double slip is possible. Finally, since $f^{(0)}=0$ is outside the domain of $Y^{(0)}$ and $Y^{(0)}$, normal tensile contact forces will cause local inelastic volumetric deformation consisting of a single "null slip". Hence, the $f^{(0)}$ -axis is designated by $S^{(0)}$ in Figure 1.

The local inelastic velocity gradient, l_{ij}^{**} , corresponding to (but not "associated" with) the yield functions $Y^{(0)}$ for various regions in Figure (1) are as follows:

$$\begin{aligned}
 E: \quad & l_{ij}^{**} = 0, \\
 S^{(+)}: \quad & l_{ij}^{**} = \dot{\gamma}^{(+)}[+s_i m_j + \zeta^{(+)} m_i m_j], \\
 S^{(-)}: \quad & l_{ij}^{**} = \dot{\gamma}^{(-)}[-s_i m_j + \zeta^{(-)} m_i m_j], \\
 S^{(0)}: \quad & l_{ij}^{**} = \dot{\gamma}^{(0)} m_i m_j, \\
 DS^{(0,+)}: \quad & l_{ij}^{**} = \dot{\gamma}^{(+)}[+s_i m_j + \zeta^{(+)} m_i m_j] + \dot{\gamma}^{(0)} m_i m_j, \\
 DS^{(0,-)}: \quad & l_{ij}^{**} = \dot{\gamma}^{(-)}[-s_i m_j + \zeta^{(-)} m_i m_j] + \dot{\gamma}^{(0)} m_i m_j,
 \end{aligned} \tag{4.16}$$

where $\dot{\gamma}^{(u)}$, ($u = +, 0, -$) is the magnitude of the inelastic strain rate, and $\zeta^{(u)}$ is the coefficient of dilatancy. It can be shown (see, Anand, 1983) that the local inelastic velocity gradient in (4.16) are similar in form to the relations obtained for the velocity gradient in the double shearing model proposed by Spencer (1964, 1982) and later extended to dilatant materials by Mehrabadi and Cowin (1978, 1981).

The above relations can be written in compact form by making use of the scalar "u". For example, for single slip, $S^{(u)}$, we have

$$l_{ij}^{**} = \dot{\gamma}^{(u)}[u s_i m_j + \zeta^{(u)} m_i m_j] \quad (u = -1, 0, +1), \tag{4.17}$$

while for double slip, $DS^{(0,u)}$, we find

$$l_{ij}^{**} = \dot{\gamma}^{(u)}[u s_i m_j + \zeta^{(u)} m_i m_j] + \dot{\gamma}^{(0)} m_i m_j, \quad (u = -1, +1, u \neq 0). \tag{4.18}$$

Note that since $\zeta^{(0)}$ can be lumped with $\dot{\gamma}^{(0)}$, without any loss in generality, its value can be taken to be unity.

The local inelastic deformation rate and spin for the case of single slip, $S^{(u)}$, are found to be

$$d_{ij}^{**} = \dot{\gamma}^{(u)} p_{ij}^{(u)}, \quad w_{ij}^{**} = \dot{\gamma}^{(u)} r_{ij}^{(u)}, \quad (u = -1, 0, +1), \tag{4.19}$$

where

$$\begin{aligned}
p_{ij}^{(u)} &= \frac{k}{2}(s_i m_j + s_j m_i) + \zeta^{(u)} m_i m_j, \\
r_{ij}^{(u)} &= \frac{u}{2}(s_i m_j - s_j m_i),
\end{aligned}
\tag{4.20}$$

and where (3.3) and (4.17) have been employed. Notice that for $S^{(0)}$, the inelastic spin vanishes. Similarly for the case of double slip, $DS^{(0,u)}$, from (3.3) and (4.18), it follows that

$$d_{ij}^{**} = \dot{\gamma}^{(u)} p_{ij}^{(u)} + \dot{\gamma}^{(0)} p_{ij}^{(0)}, \quad w_{ij}^{**} = \dot{\gamma}^{(u)} r_{ij}^{(u)}, \quad (u = -1, +1, u \neq 0), \tag{4.21}$$

where $p_{ij}^{(u)}$, $p_{ij}^{(0)}$, and $r_{ij}^{(u)}$ are given by (4.20).

The magnitude of the inelastic strain rate $\dot{\gamma}^{(u)}$, appearing in the expressions for I^{**} , can now be calculated by employing the local yield condition described above. A derivation is given in the next section.

4.3. Calculation of $\dot{\gamma}^{(u)}$

In order to calculate $\dot{\gamma}^{(u)}$ in terms of the local deformation rate d_{ij} , the yield functions (4.15) are employed. The flow rules are:

$$\dot{\gamma}^{(u)} = 0 \quad \text{if} \quad Y^{(u)} < 0, \tag{4.22}_1$$

$$\dot{\gamma}^{(u)} = 0 \quad \text{if} \quad Y^{(u)} = 0 \quad \text{and} \quad \dot{Y}^{(u)} < 0, \tag{4.22}_2$$

$$\dot{\gamma}^{(u)} > 0 \quad \text{if} \quad Y^{(u)} = 0 \quad \text{and} \quad \dot{Y}^{(u)} \geq 0. \tag{4.22}_3$$

Various cases are considered below.

(a) Single Slip, $S^{(u)}$

The consistency relation is obtained from (4.15) and (4.22), as

$$\dot{Y}^{(u)} \equiv u f^{(s)} + \mu f^{(m)} = 0, \quad (u = -1, 0, +1). \tag{4.23}$$

Substituting for $f^{(s)}$ and $f^{(m)}$ from (4.8) into (4.23), we find

$$(u A_{ij}^{(s)} + \mu A_{ij}^{(m)}) d_{ij}^* = 0, \tag{4.24}$$

or using (3.8) and (4.19)₁,

$$(uA_{ij}^{(s)} + \mu A_{ij}^{(m)})(d_{ij} - \dot{\gamma}^{(u)} p_{ij}^{(u)}) = 0 . \quad (4.25)$$

The required expression for $\dot{\gamma}^{(u)}$ is obtained by solving (4.25), to arrive at

$$\dot{\gamma}^{(u)} = \kappa^{(u)}(uA_{ij}^{(s)} + \mu A_{ij}^{(m)})d_{ij} > 0 , \quad (4.26)$$

where $\kappa^{(u)} (> 0)$ satisfies the relation

$$\frac{1}{\kappa^{(u)}} = (uA_{ij}^{(s)} + \mu A_{ij}^{(m)})p_{ij}^{(u)} . \quad (4.27)$$

(b) *Double Slip, DS^(u)*

The two consistency relations are obtained from (4.15) and (4.22) as

$$\dot{\gamma}^{(u)} = u f^{(s)} + \mu f^{(m)} = 0 , \quad (u = -1, +1) , \quad (4.28)$$

$$\dot{\gamma}^{(0)} = f^{(m)} = 0 .$$

Hence, employing (4.8), (4.28) implies

$$A_{ij}^{(s)} d_{ij}^* = 0 , \quad A_{ij}^{(m)} d_{ij}^* = 0 , \quad (4.29)$$

or using (3.8) and (4.21),

$$\begin{aligned} A_{ij}^{(s)}(d_{ij} - \dot{\gamma}^{(u)} p_{ij}^{(u)} - \dot{\gamma}^{(0)} p_{ij}^{(0)}) &= 0 , \\ A_{ij}^{(m)}(d_{ij} - \dot{\gamma}^{(u)} p_{ij}^{(u)} - \dot{\gamma}^{(0)} p_{ij}^{(0)}) &= 0 . \end{aligned} \quad (4.30)$$

Solving the above equations for $\dot{\gamma}^{(u)}$ and $\dot{\gamma}^{(0)}$, we find

$$\dot{\gamma}^{(u)} = z_M^{(u)} d_M > 0 , \quad \dot{\gamma}^{(0)} = z_M^{(0)} d_M > 0 , \quad (u = -1, +1) , \quad (4.31)$$

where

$$\begin{aligned} z_M^{(u)} &= \eta^{(u)}(A_{ij}^{(s)} A_{kl}^{(m)} - A_{kl}^{(s)} A_{ij}^{(m)}) p_{ij}^{(0)} , \\ z_M^{(0)} &= \eta^{(u)}(A_{ij}^{(m)} A_{kl}^{(s)} - A_{kl}^{(m)} A_{ij}^{(s)}) p_{ij}^{(u)} , \end{aligned} \quad (u = -1, +1) , \quad (4.32)$$

and where

$$\frac{1}{\eta^{(u)}} = (A_{ij}^{(m)} A_{kl}^{(s)} - A_{kl}^{(m)} A_{ij}^{(s)}) p_{ij}^{(s)} p_{kl}^{(0)}, \quad (u = -1, +1). \quad (4.33)$$

4.4. Time Rate of Change of Local Nominal Stress

To find an expression for the time rate of change of the local nominal stress rate in terms of the local velocity gradient, we substitute for the local inelastic velocity gradient, I^{**} , from (4.17) or (4.18) into (4.13), making use of Eqs. (4.26) and (4.27), or (4.31) and (4.32). We find that

$$\dot{\nu}_{ij} = \kappa_{ijkl} l_{ik}, \quad (4.34)$$

where

$$\kappa_{ijkl} = \begin{cases} c_{ijkl} + H(\dot{\gamma}^{(u)}) c_{ijkl}^{(u)} & \text{for single slip, } S^{(u)}, \\ c_{ijkl} + H(\dot{\gamma}^{(u)}) c_{ijkl}^{(0,u)} & \text{for double slip, } DS^{(0,u)}. \end{cases} \quad (4.35)$$

Here $H(\dot{\gamma}^{(u)})$ is the Heaviside step-function, i.e.,

$$H(\dot{\gamma}^{(u)}) = \begin{cases} 0 & \text{for } \dot{\gamma}^{(u)} \leq 0 \\ 1 & \text{for } \dot{\gamma}^{(u)} > 0, \end{cases} \quad (4.36)$$

and

$$c_{ijkl} = M_0 \ell^0 m_i^0 (A_{kl}^{(m)} m_j + A_{kl}^{(s)} s_j) + \frac{1}{2} (v_{ik} \delta_{jl} - v_{il} \delta_{jk}), \quad (4.37)$$

$$c_{ijkl}^{(u)} = \kappa^{(u)} (u A_{kl}^{(s)} + \mu A_{kl}^{(m)}) [v_{ij} r_{pq}^{(u)} - M_0 \ell^0 m_i^0 (A_{pq}^{(m)} m_j + A_{pq}^{(s)} s_j) p_{pq}^{(u)}], \quad (4.38)$$

$$c_{ijkl}^{(0,u)} = \eta^{(u)} (A_{rs}^{(s)} A_{kl}^{(m)} - A_{kl}^{(s)} A_{rs}^{(m)}) [v_{ij} r_{pq}^{(u)} p_{rs}^{(0)} + M_0 \ell^0 m_i^0 (A_{pq}^{(m)} m_j + A_{pq}^{(s)} s_j) p_{pq}^{(u)} (p_{rs}^{(u)} - p_{rs}^{(0)})]. \quad (4.39)$$

Equations (4.34) with (4.35-39) and (4.9-10), are the desired constitutive relations at the local level.

4.5. Evolution of Distribution of Contact Normals

As seen from (4.35-4.39), the local moduli κ_{ij} depend in a complicated manner on the microstructure through the unit contact normal, m . An explicit calculation of the overall moduli (see Section 5) would be possible only when the distribution density functions $E(m)$ or M_a/M are known. Since the number of contacts in each class is strongly influenced by the magnitude of the contact force for that particular class as well as by the local volumetric change, we relate the density of contacts in each class to the magnitude of the corresponding contact force and the associated volumetric strain rate (see (4.5)) by

$$\frac{M_a}{M} = \frac{1}{\alpha} \epsilon^2 e^{\beta f}, \quad \alpha = \sum_{a=1}^Q \epsilon^2 e^{\beta f}, \quad (4.40)$$

where β is a macroscopic constant, and f is a nondimensional quantity related to the magnitude of the contact force for class a , i.e., f^a , as follows

$$f = \frac{M_c l^0 f}{-(1/2) \text{tr } \Sigma}. \quad (4.41)$$

Note that the superscript a is omitted in (4.41), as in all other equations starting with (2.12).

Employing (4.41), the average of any local quantity can be found in the manner of (2.17) after the values of the magnitude of the contact force and the parameter ϵ are calculated by integrating the rate equations (4.5) and (4.8). In quantitative crystallography, it is customary to expand the density function of the orientational data in a series of generalized spherical harmonics. In works on granular materials, it has also become customary in recent years to describe the distribution density in terms of "fabric tensors" of various ranks (Mehrabadi, Nemat-Nasser, Oda, 1982; Nemat-Nasser and Mehrabadi, 1983; Kanatani, 1984). Note that here, to characterize the fabric, we have made a constitutive assumption for the density distribution function itself, rather than for various approximations of it in the form of macroscopic "fabric tensors".

5. MACROSCOPIC CONSTITUTIVE EQUATIONS

To obtain the overall constitutive equations, we substitute for the local rate of nominal stress, \dot{v}_y , from (4.15) into (2.24), to arrive at the corresponding overall quantity,

$$\dot{N}_y = \langle \kappa_{ijk} l_k \rangle, \quad (5.1)$$

where the local moduli κ_{ijk} , i.e. those associated with a typical class, say a , are given by (4.35)-(4.39).

Next, we have to make assumptions concerning the dependence of the local velocity gradient l_y on the microstructure. In self-consistent theories for polycrystalline materials (Hill, 1965) and in earlier work on granular materials (Nemat-Nasser and Mehrabadi, 1984), a fourth-rank (concentration) tensor, A_{ijkl} , is introduced which depends on microstructure and which relates the local velocity gradient in a typical micro-element, e.g. a single crystal, to the macroscopic uniform velocity gradient (see Nemat-Nasser and Mehrabadi, 1984; and Iwakuma and Nemat-Nasser, 1984, for more details). This concentration tensor must then be calculated using an appropriate model. Iwakuma and Nemat-Nasser (1984) use a fully nonlinear self-consistent model proposed by Hill (1965, 1972), and actually calculate the corresponding concentration tensor for plane problems. It can, however, be shown that this type of self-consistent calculation breaks down when the density of voids or cracks is suitably large. For the granular materials, voids are connected through contact zones which may be viewed as cracks. Hence, the application of the self-consistent method is problematic, leading to unrealistic estimates of the overall instantaneous moduli. Here, to achieve our goal of developing the simplest micromechanical model that exhibits the basic features of granular material behavior, a Taylor-averaging method is adopted, i.e., it is assumed as a first approximation that the concentration tensor is the identity tensor, leading to

$$l_y = L_y. \quad (5.2)$$

Nemat-Nasser and Obata (1986) present a discussion and comparison between the Taylor averaging scheme and the self-consistent method for polycrystals. With assumption (5.2), (5.1) now reduces to

$$\dot{N}_y = \langle \kappa_{ijk} \rangle L_k \equiv \mathcal{F}_{ijk} L_k, \quad (5.3)$$

where \mathcal{F}_{ijk} are the overall moduli defined by

$$\mathcal{F}_{ijl} = \langle \kappa_{ijl} \rangle . \quad (5.4)$$

The relationship between the Jaumann rate of macroscopic stress, i.e.,

$$\dot{\Sigma}_{ij} = \dot{\Sigma}_{ij} - \bar{W}_{ik} \Sigma_{kj} + \Sigma_{ik} \bar{W}_{kj} , \quad (5.5)$$

and the rate of deformation, D_{ij} , is obtained by differentiating (2.20) and taking the initial and final configurations coincident. It is found that

$$\dot{\Sigma}_{ij} + D_{ik} \Sigma_{ij} = \dot{N}_{ij} + D_{ik} \Sigma_{kj} + \Sigma_{ik} \bar{W}_{kj} . \quad (5.6)$$

Substituting for \dot{N}_{ij} from (5.2) into (5.6), we obtain

$$\dot{\Sigma}_{ij} + D_{ik} \Sigma_{ij} = [\mathcal{F}_{ijl} + \frac{1}{2}(\delta_{il} \Sigma_{kj} + \delta_{ik} \Sigma_{lj} + \delta_{jk} \Sigma_{il} - \delta_{jl} \Sigma_{ik})] L_{ik} . \quad (5.7)$$

However, employing (5.4), (4.35), (4.37), (4.38), and (4.39), it follows that the quantity in brackets on the right-hand side of (5.7) is symmetric in the indices l and k , because

$$\mathcal{F}_{ijl} + \delta_{jk} \Sigma_{il} = \mathcal{F}_{ijl} + \delta_{jl} \Sigma_{ik} . \quad (5.8)$$

Using (5.8), (5.7) can be written as

$$\dot{\Sigma}_{ij} + D_{ik} \Sigma_{ij} = \frac{1}{2}(\mathcal{F}_{ijl} + \mathcal{F}_{ijl} + \delta_{il} \Sigma_{kj} + \delta_{ik} \Sigma_{lj}) D_{kl} . \quad (5.9)$$

Requiring the "continuing" symmetry of the Cauchy stress, we must also have

$$\mathcal{F}_{ijl} + \delta_{il} \Sigma_{kj} = \mathcal{F}_{jil} + \delta_{jl} \Sigma_{ik} . \quad (5.10)$$

Equations (5.9) subjected to the constraint (5.10), with the overall moduli defined by (5.4), (4.35), (4.37), (4.38), and (4.39) are the macroscopic constitutive relations of the model.

As mentioned before, in order to calculate an overall quantity from the corresponding local quantity, the expression for the probability density function of the contact normals, namely (4.40), is used in (2.17). In particular, the overall moduli are calculated from the following relation:

$$\mathcal{F}_{\text{WH}} = \sum_{a=1}^Q \frac{M_a}{M} \kappa_{\text{WH}} \quad (5.11)$$

where the index a denotes the corresponding class, and the summation is over all existing classes.

Finally, we assume an expression for the evolution of the coefficient, $M\ell$, which is required for calculating various stresses and stress-rates from expressions given in Section 2 (e.g., (2.15)). Recalling that M is the number of contacts per unit volume and that ℓ is the branch length, the quantity $M\ell$, with the dimension of $(\text{area})^{-1}$, is intimately related to the volumetric strain and strain rate represented by the quantities $\det G$, and $\text{tr} D$. The calculations presented in this paper are based on the following relation

$$M\ell = M_0 \ell^0 e^{n(\det G)\eta}, \quad (5.12)$$

where n is a negative constant, and where

$$\eta = \int_{t_0}^{t_F} \text{tr} D \, dt = (t_F - t_0) \text{tr} D(t^*), \quad (5.13)$$

where $t_0 \leq t^* \leq t_F$; for the numerical illustration given in Section 9, we have used $t^* = \frac{1}{2}(t_F + t_0)$. An equation resembling (5.12) has been introduced by Jagota, *et al.* (1988), for the evolution of the coordination number, in connection with the sintering and compaction of powder packings. The relation (5.12) follows from the assumption that the rate of change of $(M\ell)$ per its own unit is proportional to $(\det G)(\text{tr} D)$, i.e. $(M\ell)' / (M\ell) = n(\det G)(\text{tr} D)$. Upon integration over the time increment and using the value of $\det G$ at the start of time step (i.e., retaining only linear terms in $(t_F - t_0)$), we obtain (5.12) and (5.13).

6. CONSTITUTIVE RELATIONS IN INCREMENTAL FORM

Due to the nonlinearity of the local constitutive relations, the material response must be computed by an incremental procedure. In an incremental loading process, a part of the load increment may actually cause an elastic-plastic behavior while the remaining part may lead only to an elastic response. Instead of using a scheme of sub-incrementation, we introduce here another simpler method based on a first-order approximation of the local yield function.

Let the loading process be measured by the time-like parameter t which takes the values t_0 at the beginning of the increment under consideration and t_F at the end. Furthermore for any quantity x , $\Delta x = x(t_F) - x(t_0)$. Instead of seeking the time t^* for which the yield condition is satisfied, i.e., $Y^{(u)}(t^*) = 0$, we make the following approximation:

$$Y^{(u)}(t_F) \approx Y^{(u)}(t_0) + \dot{Y}^{(u)}(\xi) \Delta t, \quad t_0 \leq \xi \leq t_F, \quad (6.1)$$

or using (4.23), (4.8), and (4.19)¹, for single slip, $S^{(u)}$, ($u = -1, 0, +1$), we have

$$Y^{(u)}(t_F) \approx Y^{(u)}(t_0) + [uA_{ij}^{(s)} + \mu A_{ij}^{(m)}]_{t_0, t} [\Delta d_{ij} - \Delta \gamma^{(u)} p_{ij}^{(u)}]_{t_0, t}, \quad t_0 \leq \xi \leq t_F, \quad (6.2)$$

while for double slip, $DS^{(u)}$, ($u = -1, +1$), it follows from (4.28), (4.8), (3.8), and (4.21), that

$$Y^{(u)}(t_F) \approx Y^{(u)}(t_0) + [uA_{ij}^{(s)} + \mu A_{ij}^{(m)}]_{t_0, t} [\Delta d_{ij} - \Delta \gamma^{(u)} p_{ij}^{(u)} - \Delta \gamma^{(0)} p_{ij}^{(0)}]_{t_0, t}, \quad (6.3)$$

$$Y^{(0)}(t_F) \approx Y^{(0)}(t_0) + \mu [A_{ij}^{(m)}]_{t_0, t} [\Delta d_{ij} - \Delta \gamma^{(u)} p_{ij}^{(u)} - \Delta \gamma^{(0)} p_{ij}^{(0)}]_{t_0, t}.$$

In order to define the magnitudes of the inelastic strain increment $\Delta \gamma^{(u)}$ and $\Delta \gamma^{(0)}$, we proceed as follows. In a first step, the behavior is assumed to be elastic and for a given strain increment Δd_{ij} , the elastic response is computed. Let us denote by t_F^* the corresponding (fictitious) value of the time parameter t^* . It is important to make the distinction between the time-like parameters t and t^* (see the footnote on the next page). Then for single slip, $S^{(u)}$, the relations (4.22) and (4.26) will take the incremental form

$$\text{For } Y^{(u)}(t_F^*) \leq 0 \quad , \quad \Delta \gamma^{(u)} = 0 \quad , \quad (6.4)$$

$$\text{For } Y^{(u)}(t_F^*) \geq 0 \quad , \quad \Delta \gamma^{(u)} = \kappa^{(u)}(\xi) [Y^{(u)}(t_0) + (uA_{ij}^{(s)} + \mu A_{ij}^{(m)})_{i,\xi}] d_{ij} \quad ,$$

where, $\kappa^{(u)}$ is defined by (4.27). Similarly, for double slip, $DS^{(0,u)}$ ($u = -1, +1$), (4.28), (4.31), and (4.32) take the incremental form¹

$$\text{For } Y^{(u)}(t_F^*) \leq 0 \quad \text{and} \quad Y^{(0)}(t_F^*) \leq 0 \quad , \quad \begin{cases} \Delta \gamma^{(u)} = 0 \\ \Delta \gamma^{(0)} = 0 \end{cases} \quad , \quad (6.5)$$

$$\text{For } Y^{(u)}(t_F^*) \geq 0 \quad \text{and} \quad Y^{(0)}(t_F^*) \geq 0 \quad , \quad \begin{cases} \Delta \gamma^{(u)} = s^{(u)}(\xi) + z_H^{(u)}(\xi) \Delta d_H \\ \Delta \gamma^{(0)} = s^{(0)}(\xi) + z_H^{(0)}(\xi) \Delta d_H \end{cases} \quad ,$$

where

$$\begin{aligned} s^{(u)} &= u \eta^{(u)} [Y^{(0)}(t_0) (uA_{ij}^{(s)} + \mu A_{ij}^{(m)}) - Y^{(u)}(t_0) A_{ij}^{(m)}] p_{ij}^{(0)} \\ s^{(0)} &= -u \eta^{(u)} [Y^{(0)}(t_0) (uA_{ij}^{(s)} + \mu A_{ij}^{(m)}) - Y^{(u)}(t_0) A_{ij}^{(m)}] p_{ij}^{(u)} \end{aligned} \quad , \quad (u = -1, +1) \quad , \quad (6.6)$$

and where $z_H^{(u)}$ and $\eta^{(u)}$ are defined by (4.32) and (4.33), respectively.

Employing (6.4) or (6.5) and following the same procedure that led from (4.26) and (4.31) to (4.34), it is found that the incremental form of the stress-strain relation is of the form,

$$\Delta v_{ij} = \Delta v_{ij}^{(1)} + \Delta v_{ij}^{(2)} \quad , \quad (6.7)$$

where

$$\Delta v_{ij}^{(1)} = \kappa_{ijkl} \Delta I_{kl} \quad , \quad (6.8)$$

and where, for single slip, $S^{(u)}$, ($u = -1, 0, +1$),

¹ According to (6.2), $Y^{(u)}(t_F^*) \approx Y^{(u)}(t_0) + [uA_{ij}^{(s)} + \mu A_{ij}^{(m)}]_{i,\xi} \Delta d_{ij}$. Hence we assume $H(Y(t_F^*)) = H(\Delta \gamma)$.

$$\text{For } Y^{(u)}(t_F^*) \leq 0 \quad , \quad \Delta \gamma^{(u)} = 0 \quad , \quad (6.4)$$

$$\text{For } Y^{(u)}(t_F^*) \geq 0 \quad , \quad \Delta \gamma^{(u)} = \kappa^{(u)}(\xi) [Y^{(u)}(t_0) + (uA_y^{(s)} + \mu A_y^{(m)})_{t-\xi}] d_y \quad ,$$

where, $\kappa^{(u)}$ is defined by (4.27). Similarly, for double slip, $DS^{(0,u)}$ ($u = -1, +1$), (4.28), (4.31), and (4.32) take the incremental form¹

$$\begin{aligned} \text{For } Y^{(u)}(t_F^*) \leq 0 \quad \text{and} \quad Y^{(0)}(t_F^*) \leq 0 \quad , \quad & \begin{cases} \Delta \gamma^{(u)} = 0 \\ \Delta \gamma^{(0)} = 0 \end{cases} \quad , \\ \text{For } Y^{(u)}(t_F^*) \geq 0 \quad \text{and} \quad Y^{(0)}(t_F^*) \geq 0 \quad , \quad & \begin{cases} \Delta \gamma^{(u)} = s^{(u)}(\xi) + z_H^{(u)}(\xi) \Delta d_H \\ \Delta \gamma^{(0)} = s^{(0)}(\xi) + z_H^{(0)}(\xi) \Delta d_H \end{cases} \quad , \end{aligned} \quad (6.5)$$

where

$$\begin{aligned} s^{(u)} &= u\eta^{(u)} [Y^{(0)}(t_0)(uA_y^{(s)} + \mu A_y^{(m)}) - Y^{(u)}(t_0)A_y^{(m)}] p_y^{(0)} \quad , \\ s^{(0)} &= -u\eta^{(u)} [Y^{(0)}(t_0)(uA_y^{(s)} + \mu A_y^{(m)}) - Y^{(u)}(t_0)A_y^{(m)}] p_y^{(u)} \quad , \end{aligned} \quad (u = -1, +1) \quad , \quad (6.6)$$

and where $z_H^{(u)}$ and $\eta^{(u)}$ are defined by (4.32) and (4.33), respectively.

Employing (6.4) or (6.5) and following the same procedure that led from (4.26) and (4.31) to (4.34), it is found that the incremental form of the stress-strain relation is of the form,

$$\Delta v_y = \Delta v_y^{(1)} + \Delta v_y^{(2)} \quad , \quad (6.7)$$

where

$$\Delta v_y^{(1)} = \kappa_{yH} \Delta l_H \quad , \quad (6.8)$$

and where, for single slip, $S^{(u)}$, ($u = -1, 0, +1$),

¹ According to (6.2), $Y^{(u)}(t_F^*) \approx Y^{(u)}(t_0) + [uA_y^{(s)} + \mu A_y^{(m)}]_{t-\xi} \Delta d_y$. Hence we assume $H(Y(t_F^*)) = H(\Delta \gamma)$.

the present model in that the numerical evaluation of the overall response, in particular, the overall nominal stress, can be performed via two methods: In the first method, the overall nominal stress and the overall stiffness are directly computed, respectively, from (2.18) and (5.4), using the results of the integration presented in Section 7. In the second method, the nominal stress is computed from (6.12) which is obtained from rate constitutive relations through the incremental procedure described above and by using the overall moduli derived by the first method. Note that if the velocity gradient is given, then the material response is deduced without any need for computing the overall stiffness. On the other hand, if the boundary conditions are mixed or are expressed in terms of the stress-rates, then the overall stiffness must be computed.

7. ANALYTICAL INTEGRATION OVER A TIME INTERVAL

The local constitutive equations, (4.2), (4.5), and (4.8) are amenable to analytical integration over a small time interval $[t_0, t_F = t_0 + \Delta t]$, assuming that the velocity gradient, l , remains constant over the interval. The integration is performed in two steps, as described in Section 6. In the *first step*, the material is assumed to remain elastic under a total increment of loading $\Delta l = (t_F - t_0)l$. In the *second step*, the plastic deformation allowing for the yield condition to be satisfied is obtained. Hence, it is supposed that the yield criterion is satisfied in the second step, if it was not already satisfied at the end of the first step. Consistent with (3.1), the superposition of the two steps will correspond to $l' = l - l^{**}$.

7.1 The First Step of Integration

The integration of the evolution equations (4.2), (4.5), and (4.8) for m , ϵ , and f , respectively, are performed between the initial time t_0 and t_F^* . As mentioned earlier, the material is assumed to be elastic in this step. Details are given below.

(a) Integration of the evolution equations for m and s

Since in the first step the magnitude of the inelastic strain rate, $\dot{\gamma}$, is zero, Eqs. (4.2) can be written as

$$\dot{m}_i = w_{ij} m_j, \quad \dot{s}_i = w_{ij} s_j, \quad (7.1)$$

where (3.9)₂, (4.19)₂, and (4.21)₂ are used. The solution of the above equations can be written in terms

of an angle θ , defined by

$$\dot{\theta} \equiv -w_{12}^* = -w_{12} . \quad (7.2)$$

Integrating between t_0 and t_F^* ,

$$\theta^* - \theta_0 = - \int_{t_0}^{t_F^*} w_{12} dt = -w_{12}(t_F^* - t_0) = -\Delta w_{12} , \quad (7.3)$$

or

$$\theta^* = \theta_0 - \Delta w_{12} , \quad (7.4)$$

where $\theta^* = \theta(t_F^*)$ and $\theta_0 = \theta(t_0)$. Notice that at any time t_F^* , we have

$$m(t_F^*) = R(t_F^*, t_0) m(t_0) , \quad s(t_F^*) = R(t_F^*, t_0) s(t_0) , \quad (7.5)$$

where

$$R(t_F^*, t_0) = \begin{bmatrix} \cos(\theta^* - \theta_0) & -\sin(\theta^* - \theta_0) \\ \sin(\theta^* - \theta_0) & \cos(\theta^* - \theta_0) \end{bmatrix} .$$

Hence, since

$$\begin{aligned} m(t_0) &= \cos \theta_0 e_1 + \sin \theta_0 e_2 , \\ s(t_0) &= \sin \theta_0 e_1 - \cos \theta_0 e_2 , \end{aligned} \quad (7.6)$$

where e_1 and e_2 are unit vectors along the coordinate axes, it follows from (7.5) that at the end of the first step, the components of m and s are as follows:

$$\begin{aligned} m_1(t_F^*) &= \cos(\theta_0 - \Delta w_{12}) , & m_2(t_F^*) &= \sin(\theta_0 - \Delta w_{12}) , \\ s_1(t_F^*) &= m_2(t_F^*) , & s_2(t_F^*) &= -m_1(t_F^*) . \end{aligned} \quad (7.7)$$

(b) *Integration of the evolution equation for ϵ*

Again, since in the first step, $\dot{\gamma}$ is zero, Eq. (4.5) can be written as

$$\frac{\dot{\epsilon}}{\epsilon} = b \, d_{kk} . \quad (7.8)$$

Integrating this equation from t_0 to t_F^* , we have

$$\int_{t_0}^{t_F^*} \frac{d\epsilon}{\epsilon} = \int_{t_0}^{t_F^*} b \, (tr d) \, dt , \quad (7.9)$$

or

$$\ln \frac{\epsilon(t_F^*)}{\epsilon(t_0)} = b \, (tr d) \, (t_F^* - t_0) \equiv b \, (tr \Delta d) . \quad (7.10)$$

Hence, at the end of the first step of integration,

$$\epsilon(t_F^*) = \epsilon(t_0) e^{b(tr \Delta d)} . \quad (7.11)$$

(c) *Integration of the evolution equations for the contact force f*

The evolution equations for the contact force are given by (4.8-10). Substituting for $\epsilon(t)$ from (7.11) and for m and s from (7.7)₁ and (7.7)₃ into (4.9-10), using (7.4), it then follows from (4.8) that

$$\begin{aligned} f^{(m)} = & b \, (tr d) f^{(m)} + \epsilon(t_0) e^{b(tr d)(t-t_0)} [\lambda^* \, tr d + \\ & + 2\mu^* (d_{11} \cos^2 \theta + 2d_{12} \sin \theta \cos \theta + d_{22} \sin^2 \theta)] , \end{aligned} \quad (7.12)$$

and

$$\begin{aligned} f^{(s)} = & b \, (tr d) f^{(s)} + 2\mu^* \, \epsilon(t_0) e^{b(tr d)(t-t_0)} [d_{11} \sin \theta \cos \theta + \\ & + d_{12} (\sin^2 \theta - \cos^2 \theta) - d_{22} \sin \theta \cos \theta] , \end{aligned} \quad (7.13)$$

where, since $\dot{\gamma}$ is zero, $d^* = d$. Now let

$$A(t) = f^{(m)}(t) e^{-b \, tr d \, (t-t_0)} , \quad B(t) = f^{(s)}(t) e^{-b \, tr d \, (t-t_0)} , \quad (7.14)$$

then

$$\dot{A} = \epsilon(t_0) \{(\lambda^* + \mu^*) \text{tr} d + \mu^* [(d_{11} - d_{22}) \cos 2\theta + 2d_{12} \sin 2\theta]\} \quad (7.15)$$

$$\dot{B} = \epsilon(t_0) \mu^* [(d_{11} - d_{22}) \sin 2\theta - 2d_{12} \cos 2\theta] .$$

The above relations can be integrated by noting that all the quantities that appear in these equations remain constant over the interval except for θ which varies with time according to (see Eq. (7.3))

$$\theta(t) = \theta_0 - w_{12}(t - t_0) . \quad (7.16)$$

Proceeding with this integration (see Appendix A for details) and substituting for $A(t)$ and $B(t)$ into Eqs. (7.14), we find that when $w_{12} = 0$,

$$f^{(m)}(t_F^*) = e^{b \text{tr} \Delta d} \{ f^{(m)}(t_0) + \epsilon(t_0) [(\lambda^* \text{tr} \Delta d + 2\mu^* \Delta d_{ij} m_i(t_0) m_j(t_0))] \} , \quad (7.17)$$

$$f^{(s)}(t_F^*) = e^{b \text{tr} \Delta d} [f^{(s)}(t_0) + 2\mu^* \epsilon(t_0) \Delta d_{ij} m_i(t_0) s_j(t_0)] ,$$

and when $w_{12} \neq 0$,

$$f^{(m)}(t_F^*) = e^{b \text{tr} \Delta d} \{ f^{(m)}(t_0) + \epsilon(t_0) [(\lambda^* + \mu^*) \text{tr} \Delta d + \mu^* (a_1 a_3 + a_2 a_4)] \} , \quad (7.18)$$

$$f^{(s)}(t_F^*) = e^{b \text{tr} \Delta d} [f^{(s)}(t_0) + \mu^* \epsilon(t_0) (a_2 a_3 - a_1 a_4)] ,$$

where

$$a_1 = m_1(t_0) m_2(t_0) - m_1(t_F^*) m_2(t_F^*) ,$$

$$a_2 = m_1^2(t_F^*) - m_1^2(t_0) ,$$

$$a_3 = \frac{\Delta d_{11} - \Delta d_{22}}{\Delta w_{12}} , \quad (7.19)$$

$$a_4 = \frac{2\Delta d_{12}}{\Delta w_{12}} .$$

Equations (7.17) and (7.18) give the values of the normal and tangential components of the contact force at the intermediate time t_F^* , i.e., at the end of the first step of integration.

7.2 The Second Step of Integration

Integration of the evolution equations for m , s , ϵ , and f are performed between the intermediate time, t_F^* , and the final time t_F . Accordingly, in the second step, the yield condition is enforced if it was not already satisfied at time t_F^* .

(a) *Integration of the evolution equations for m and s*

Recalling the definition of angle θ , namely, (7.2)₁, we have

$$\dot{\theta} = -w_{12}^{\circ} = w_{12}^{**} . \quad (7.20)$$

The components of the local inelastic spin are given by Eq. (4.19)₂ for single-slip, $S^{(u)}$, and by Eq. (4.21)₂, for double-slip, $DS^{(u)}$. Employing these relations together with (4.20)₂, we have

$$w_{12}^{**} = \frac{u}{2} \dot{\gamma}^{(u)} , \quad (7.21)$$

where, $u = -1, 0, +1$ for single-slip, $S^{(u)}$; and where $u = -1, +1$ for double-slip, $DS^{(u)}$. Substituting from (7.21) into (7.20) and integrating between t_F^* and t_F ,

$$\theta_F = \theta^* + \frac{u}{2} \Delta \gamma , \quad (7.22)$$

where $\theta_F = \theta(t_F)$ and where, as in (7.4), $\theta^* \equiv \theta(t_F^*) = \theta_0 - \Delta w_{12}$. Following a procedure similar to that described earlier for step one, we find

$$\begin{aligned} m_1(t_F) &= \cos\left(\theta^* + \frac{u}{2} \Delta \gamma^{(u)}\right), & m_2(t_F) &= \sin\left(\theta^* + \frac{u}{2} \Delta \gamma^{(u)}\right) \\ s_1(t_F) &= m_2(t_F), & s_2(t_F) &= -m_1(t_F) . \end{aligned} \quad (7.23)$$

Given the magnitude of the local inelastic strain increment, $\Delta \gamma^{(u)}$, the final orientations of fabric vectors, m and s , can be calculated from the above relations. The values of $\Delta \gamma^{(u)}$ are calculated by imposing the appropriate yield criterion. This is done in Section (7.2d), after the evolution equations for the contact force are integrated in Section (7.2c).

(b) *Integration of the evolution equation for ϵ*

In the second step of integration the evolution equation for ϵ can be written as

$$\frac{\dot{\epsilon}}{\epsilon} = -b d_{kk}^{**}, \quad (7.24)$$

where the local inelastic rate of volume change, d_{kk}^{**} , must be calculated from (4.19)₁ for single-slip, $S^{(u)}$, and from (4.21)₁ for $DS^{(0,u)}$. Performing this calculation and integrating (7.24) from t_F^* to t_F , yields

$$\int_{t_F^*}^{t_F} \frac{d\epsilon}{\epsilon} = \begin{cases} \int_{t_F^*}^{t_F} -b \zeta^{(u)} \dot{\gamma}^{(u)} dt, & \text{for } S^{(u)}, \quad (u = -1, 0, +1), \\ \int_{t_F^*}^{t_F} -b(\zeta^{(u)} \dot{\gamma}^{(u)} + \zeta^{(0)} \dot{\gamma}^{(0)}) dt, & \text{for } DS^{(0,u)}, \quad (u = -1, +1), \end{cases} \quad (7.25)$$

or

$$\ln \frac{\epsilon(t_F)}{\epsilon(t_F^*)} = \begin{cases} -b \zeta^{(u)} \gamma^{(u)}(t_F - t_F^*) = -b \zeta^{(u)} \Delta \gamma^{(u)}, & \text{for } S^{(u)}, \\ -b(\zeta^{(u)} \gamma^{(u)} + \zeta^{(0)} \gamma^{(0)})(t_F - t_F^*) = -b(\zeta^{(u)} \Delta \gamma^{(u)} + \zeta^{(0)} \Delta \gamma^{(0)}), & \text{for } DS^{(0,u)}. \end{cases} \quad (7.26)$$

Hence, at the end of the first step of integration,

$$\epsilon(t_F) = \begin{cases} \epsilon(t_F^*) e^{-b \zeta^{(u)} \Delta \gamma^{(u)}} & , \quad \text{for } S^{(u)}, \quad (u = -1, 0, +1) \\ \epsilon(t_F^*) e^{-b(\zeta^{(u)} \Delta \gamma^{(u)} + \zeta^{(0)} \Delta \gamma^{(0)})} & , \quad \text{for } DS^{(0,u)}, \quad (u = -1, +1). \end{cases} \quad (7.27)$$

(c) *Integration of the evolution equations for the contact force f*

In the second step of integration, since $I^* \rightarrow -I^{**}$, the evolution equations for the contact force, i.e., equations (4.8), become

$$\begin{aligned} \dot{f}^{(m)} &= -b d_{kk}^{**} f^{(m)} - \epsilon (\lambda^* d_{kk}^{**} + 2\mu^* d_{ij}^{**} m_i m_j), \\ \dot{f}^{(s)} &= -b d_{kk}^{**} f^{(s)} - \epsilon (2\mu^* d_{ij}^{**} s_j m_i), \end{aligned} \quad (7.28)$$

where, (4.9) and (4.10) have been used in writing (7.28). Again the local inelastic strain rate, d_{ij}^{**} ,

must be calculated from (4.19)₁ for single slip, $S^{(u)}$, and from (4.21)₁ for $DS^{(0,u)}$. Performing this calculation and substituting the result into (7.28), we find that

$$\begin{aligned} f^{(m)} &= -C_1 f^{(m)} - C_2 e^{-C_1(t-t_F^*)}, \\ f^{(s)} &= -C_1 f^{(s)} - C_3 e^{-C_1(t-t_F^*)}, \end{aligned} \quad (7.29)$$

where (7.27) has been employed, and where

$$C_1 = \begin{cases} b \zeta^{(u)} \dot{\gamma}^{(u)}, & \text{for } S^{(u)}, \\ b(\zeta^{(u)} \dot{\gamma}^{(u)} + \zeta^{(0)} \dot{\gamma}^{(0)}), & \text{for } DS^{(0,u)}, \end{cases} \quad (7.30)$$

$$C_2 = \begin{cases} (\lambda^* + 2\mu^*) \varepsilon(t_F^*) \zeta^{(u)} \dot{\gamma}^{(u)}, & \text{for } S^{(u)}, \\ (\lambda^* + 2\mu^*) \varepsilon(t_F^*) (\zeta^{(u)} \dot{\gamma}^{(u)} + \zeta^{(0)} \dot{\gamma}^{(0)}), & \text{for } DS^{(0,u)}, \end{cases} \quad (7.31)$$

$$C_3 = \mu^* \varepsilon(t_F^*) u \dot{\gamma}^{(u)}, \quad \text{for } S^{(u)}, \text{ and for } DS^{(0,u)}, \quad (u = -1, 0, +1). \quad (7.32)$$

Integrating (7.29) between t_F^* and t_F , we find that

$$\begin{aligned} f^{(m)}(t_F) &= [f^{(m)}(t_F^*) - C_2 \Delta t] e^{-C_1 \Delta t}, \\ f^{(s)}(t_F) &= [f^{(s)}(t_F^*) - C_3 \Delta t] e^{-C_1 \Delta t}. \end{aligned} \quad (7.33)$$

Hence, for single slip, $S^{(u)}$, at the end of an increment we have,

$$\begin{aligned} f^{(m)}(t_F) &= [f^{(m)}(t_F^*) - (\lambda^* + 2\mu^*) \varepsilon(t_F^*) \zeta^{(u)} \Delta \gamma^{(u)}] e^{-b \zeta^{(u)} \Delta \gamma^{(u)}}, \\ f^{(s)}(t_F) &= [f^{(s)}(t_F^*) - \mu^* \varepsilon(t_F^*) u \Delta \gamma^{(u)}] e^{-b \zeta^{(u)} \Delta \gamma^{(u)}}, \end{aligned} \quad (7.34)$$

while, for double slip, $DS^{(0,u)}$, we find

$$f^{(n)}(t_F) = [f^{(n)}(t_F^0) - (\lambda^* + 2\mu^*)\epsilon(t_F^0)(\zeta^{(n)}\Delta\gamma^{(n)} + \zeta^{(0)}\Delta\gamma^{(0)})]e^{-\beta(\zeta^{(n)}\Delta\gamma^{(n)} + \zeta^{(0)}\Delta\gamma^{(0)})}, \quad (7.35)$$

$$f^{(0)}(t_F) = [f^{(0)}(t_F^0) - \mu^*\epsilon(t_F^0)\Delta\gamma^{(0)}]e^{-\beta(\zeta^{(n)}\Delta\gamma^{(n)} + \zeta^{(0)}\Delta\gamma^{(0)})}.$$

(d) Calculation of the Magnitude of the Inelastic Strain Increment $\Delta\gamma^{(n)}$

For a single slip system, $S^{(n)}$, the increment of inelastic strain is calculated by imposing the yield condition, i.e.,

$$Y^{(n)} = \mu f^{(n)}(t_F) + \mu f^{(0)}(t_F) = 0. \quad (7.36)$$

Substituting from (7.34), into (7.36) and solving for $\Delta\gamma^{(n)}$, we find that

$$\Delta\gamma^{(n)} = \frac{\mu f^{(n)}(t_F^0) + \mu f^{(0)}(t_F^0)}{\epsilon(t_F^0)[\mu^*|\mu| + \mu\zeta^{(n)}(\lambda^* + 2\mu^*)]}. \quad (7.37)$$

For the double slip system, $DS^{(n,0)}$, substituting from (7.35) into the yield conditions,

$$Y^{(n)} = \mu f^{(n)}(t_F) + \mu f^{(0)}(t_F) = 0, \quad (7.38)$$

$$Y^{(0)} = \mu f^{(0)}(t_F) = 0,$$

and solving for the magnitudes of the inelastic strain increments, we obtain

$$\Delta\gamma^{(0)} = \frac{f^{(n)}(t_F^0) - \mu(\lambda^*/\mu^* + 2)\zeta^{(n)}f^{(n)}(t_F^0)}{\epsilon(t_F^0)\zeta^{(0)}(\lambda^* + 2\mu^*)}, \quad (7.39)$$

and

$$\Delta\gamma^{(n)} = \frac{\mu f^{(n)}(t_F^0)}{\epsilon(t_F^0)\mu^*}. \quad (7.40)$$

8. INITIAL AND BOUNDARY CONDITIONS

In the numerical calculations, it is often necessary to obtain the initial distribution of contact forces, given the initial confining stress and the initial fabric. An expression relating the contact forces to the macroscopic stress and fabric is developed in Section 8.1. Boundary conditions are described in Section 8.2.

8.1 Initial Contact Forces

An expression for the average (initial) contact force in each class could be obtained by assuming that this quantity is related to the contact normal which identifies that particular class, by means of a polynomial expression; the coefficients of the polynomial are macroscopic quantities, i.e., they are class-independent. For simplicity, following Mehrabadi, Nemat-Nasser, and Oda (1982), we assume that

$$M_0 \epsilon^0 f_i^0 = A_{ij} m_j^0, \quad (8.1)$$

where A_{ij} are global quantities independent of class. The distribution of contact forces given by (8.1) must be compatible with a symmetric Cauchy stress, Σ_{ij}^0 , defined by (2.19) and (2.22). Thus, substituting from (8.1) into (2.19), using (2.22), we must have

$$\Sigma_{ij}^0 = \langle m_i^0 m_j^0 \rangle A_{jk}. \quad (8.2)$$

Introducing the traceless second-rank fabric tensor, J_{ij} , defined by the relation

$$J_{ij} = 4(\langle m_i m_j \rangle - \frac{1}{2} \delta_{ij}), \quad (8.3)$$

into (8.2), the initial macroscopic Cauchy stress is found to be

$$\Sigma_{ij}^0 = \frac{1}{2} A_{ij} + \frac{1}{4} J_{jk} A_{ik}. \quad (8.4)$$

To calculate the contact force from (8.1), one has to solve (8.4) for A_{ij} in terms of the given initial values of the stress and fabric and then substitute the result in (8.1). To this end, define the symmetric and skew parts of A_{ij} by

$$A_{ij}^+ = \frac{1}{2}(A_{ij} + A_{ji}) \quad , \quad A_{ij}^- = \frac{1}{2}(A_{ij} - A_{ji}) \quad , \quad (8.5)$$

so that

$$A_{ij} = A_{ij}^+ + A_{ij}^- \quad . \quad (8.6)$$

Using the identities

$$A^+ J + J A^+ = (\text{tr} A^+) J + (\text{tr} J A^+) \delta \quad , \quad \text{tr} J A^- = 0 \quad , \quad (8.7)$$

where δ is the unit tensor, in (8.4), one can show that

$$A^- = \frac{1}{4}(J A^+ - A^+ J) \quad . \quad (8.8)$$

Now employing (8.3) and the identities

$$J A^+ J = \frac{1}{2} [2(\text{tr} J A^+) J - (\text{tr} J^2) A^+ + (\text{tr} A^+) (\text{tr} J^2) \delta] \quad , \quad J^2 = \frac{1}{2} (\text{tr} J^2) \delta \quad , \quad (8.9)$$

in (8.4), we obtain the following relation

$$16 \Sigma^0 = (8 - \text{tr} J^2) A^+ + [2(\text{tr} A^+) + (\text{tr} J A^+)] J + \frac{1}{2} [4(\text{tr} J A^+) + (\text{tr} A^+) (\text{tr} J^2)] \delta \quad . \quad (8.10)$$

Note that the identities (8.7) and (8.9) are limited to two dimensions. Solving (8.10) for A^+ , one obtains

$$A^+ = \frac{4}{8 - \text{tr} J^2} [4 \Sigma^0 - (\text{tr} \Sigma^0) J - (\text{tr} \Sigma^0 J) 1] \quad . \quad (8.11)$$

Substituting from (8.11) into (8.8) yields

$$A^- = \frac{4}{8 - \text{tr} J^2} (J \Sigma^0 - \Sigma^0 J) \quad . \quad (8.12)$$

Finally, the expression for A_{ij} is obtained by adding (8.11) and (8.12) according to (8.6).

Note that for an initially isotropic sample,

$$J = 0 \quad , \quad A = 2 \Sigma^{\circ} \quad , \quad (8.13)$$

where (8.3), (2.17), (8.11), (8.12), and (8.6) have been used. Employing (8.13)₂ in (8.1), it then follows that

$$M_0 \ell^{\circ} f_i^{\circ} = 2 \Sigma_{ij}^{\circ} m_j^{\circ} \quad . \quad (8.14)$$

Hence, when the initial confining stress is also isotropic, there is no shear force present at any contact point.

8.2 Boundary Conditions

To assess the predictive capability of the model, the incremental procedure described in the previous section is employed to calculate the response of the model to shearing deformation (Fig.2). In the initial configuration, the sample which is in the shape of the unit square shown, is assumed to be in equilibrium under constant confining loads P_1 and P_2 . Keeping the vertical force (P_2) constant, an increment of shear strain ΔL_{12} is then applied to the sample. Requiring that the side A'B' remains parallel to the horizontal side AB and that A'B' = AB = OC at all times, the volume change of the sample is calculated from

$$\Delta N_{22} = 0 \quad , \quad L_{11} = 0 \quad . \quad (8.15)$$

9. NUMERICAL RESULTS AND DISCUSSIONS

Numerical calculations corresponding to the two-dimensional behavior of the model under monotonic and cyclic shear are presented in this section. In these calculations 48 discrete orientations are used between 0° and 360° to define 48 classes of contacts. The initial conditions and material constants for the monotonic loading (Section 9.1) are chosen so that the behavior of the model corresponds to that of densely packed granular materials; while for the cyclic loading (Section 9.2), the initial conditions and constants are chosen so that the model behavior corresponds to a loosely packed sample. The material constants and initial conditions used in the two cases are summarized in Table I.

Table I Material constants and initial conditions

	Monotonic Shear	Cyclic Shear
λ^0/p_R	200.0	200.0
μ^0/p_R	200.0	200.0
μ	0.40	0.40
ζ	0.36	0.36
b	-100.0	-1.0
β	0.01	0.1
n	-10.0	-10.0
α_0/a_R^2	0.048	0.048
$M_0 t^0 a_R$	10.0	10.0
Σ^0/p_R	$\begin{bmatrix} -2.0 & 0.0 \\ 0.0 & -4.0 \end{bmatrix}$	$\begin{bmatrix} -1.0 & 0.0 \\ 0.0 & -1.0 \end{bmatrix}$
ΔL_{12}	0.0010 (50 Increments)	± 0.0015 (100 Increments)

In this Table, p_R and a_R are reference stress and area, respectively, and α_0 is the initial value of α defined by (4.40)₂. The initial orientational distribution of contact normals is assumed to be isotropic for both cases. As shown in Table I, except for the constants b and β , the remaining constants have been chosen to be identical for both cases. Examination of (7.11) and (7.12) reveals that the constant b which was first introduced in (4.5), governs the value of the parameter ϵ and the volumetric behavior of the material. On the other hand, it can be verified from (4.40) that the parameter ϵ and the

constant β strongly affect the orientational distribution of contact normals. Notice that the chosen values of b and β , in the two cases, differ by two and one orders of magnitude, respectively. We shall find out that the model behaves like densely packed materials for a large absolute value of b , while it behaves similarly to a loosely packed material for a relatively large value of β . A thorough study of the interrelationship among the various constants has been left for future investigation.

9.1 Behavior of the Model Under Monotonic Shearing

(a) Stress-Strain-Volumetric Behavior

The stress-strain behavior of the model under monotonic loading is depicted in Fig.3, where the ratio of shearing stress to the mean normal stress is plotted versus the magnitude of shear strain. The volumetric strain versus shear strain is plotted in Fig.4. The data points indicate the beginning of an increment of loading. The numbers 5, 20, 30, 40, and 50 appearing on the plots identify the increments for which the orientational distribution of contact normals and other microstructural quantities are presented here for discussion. At increment 5, the behavior is still elastic (with no slip taking place at any contact) and no significant change in volume occurs anywhere. This linear elastic behavior continues until about increment 14, when slip occurs at certain contacts and when a change in volume starts to take place. Failure occurs at about increment 30 at which time the material starts to soften up until increment 50 when large deformations can take place under a constant stress ratio. The volumetric and stress-strain behavior of the model with the constants and initial conditions given in Table I, clearly correspond to the observed behavior of dense granular materials.

(b) Evolution of Contact Normal Distribution

When the sample is isotropic, there are an equal number of contacts in all classes. Hence, it follows from (2.16) that

$$E(m) = \frac{1}{2\pi} , \quad (9.1)$$

so that the distribution of the number of contacts in various classes, represented by the quantity $2\pi E(m)$ in polar coordinates is a unit circle. The distribution of the quantity $2\pi E(m)$ at increments 0, 5, 20, 30, 40, and 50 is compared to this unit circle in Fig.5. There are 48 data points in each plot of Fig.5

corresponding to the 48 classes.

No significant change in the number of contacts occurs in the elastic regime up until increment 14 when a few contacts become active. As a class of contacts becomes active, the magnitude of the average contact force corresponding to that class *increases* (see the next section for details). The increase in this contact force then leads to an increase in the number of contacts in the active classes (see Fig.5, increment 20). Since the total number of contacts in the sample changes only slightly, the increase in the total number of contacts for active classes is accompanied by a decrease in the number of contacts in all the inactive classes including the class of contacts whose normal is in the maximum compressive stress direction. As more classes of contacts become active, the number of contacts in the class whose normal is in the direction of maximum compressive stress decreases to a critical value at the peak strength (increment 30; see Fig.3) when further shearing of the sample causes a collapse of the load-bearing columns formed by the contacts belonging to this class. The collapse of these columns leads to the loss in strength and the softening of the sample. This point is further discussed in the next section in connection with the evolution of the contact force magnitudes and active contacts.

(c) Evolution of the Contact Force Magnitudes and the Critical Contacts

The distribution of the contact force magnitudes and the status of various classes of contacts in terms of whether they are critical or not, is considered in Figs. 6a and 6b. The 48 data points in each plot of these figures correspond to the 48 classes of contacts. The magnitudes of the contact forces are represented by the non-dimensional quantity $M \ell f/p$, where $p = -(1/2) \text{tr } \Sigma$; while the status of the contacts is represented by the non-dimensional quantity $-f_i/\mu f_m$. This latter quantity varies between -1 and +1. It equals -1 or +1 for active contacts undergoing negative or positive slip, respectively. The intermediate values correspond to non-critical contacts where there is no slip.

Since the initial confining pressure on the horizontal plane is -4 and on the vertical plane is -2, the distribution of the magnitudes of the contact forces (see Fig.6a, Increment 00) is such that the maximum and minimum contact forces are carried by the classes of contacts whose normals are, respectively, along the vertical and horizontal axis. The initial directional distribution of $-f_i/\mu f_m$ (Fig.6a, Increment 00), indicates that there are no critical classes of contacts and the sample is indeed initially at equilibrium. As might be expected, however, this distribution is biased so that several classes whose

normals are making angles of about 40° or 220° are close to becoming active with a positive slip. Similarly, those classes whose contact normals are making an angle of about 135° or 325° with the horizontal axis, have the potential to become active and undergo a negative slip.

As the sample is sheared to the right, the maximum compressive stress rotates in a clockwise direction causing the contact force distribution to rotate accordingly (see Fig.6a, and 6b). In the elastic regime, no significant change in the shape of the distribution of the magnitudes of the contact forces occurs (see Fig.6a, Increment 05). As the distribution of the magnitudes of the contact forces rotates, however, the normal components of the contact forces, f_n , (which have a distribution very similar to the magnitudes of the contact forces, f) decrease for nearly critical contacts. This decrease in f_n leads to an increase in the absolute value of $-f_t/\mu f_n$. Eventually this value increases to unity and the nearly critical contacts become active (see Fig.6a, Increment 20).

The initiation of slip at critical contacts, causes mostly a change in the shape (and little or no rotation) of the distribution of the contact force magnitudes, as can be verified by comparing the plots of increments 20, 30, 40, and 50, in Figs.6a and 6b. As a class of contacts becomes active, the local slip-induced dilatancy causes an increase in the magnitude of the contact force. This can be verified by inspecting Eqs. (7.34), noting that the final values of the components of the contact forces are exponential functions of the slip-induced dilatancy and that the constant b is negative. At the peak strength, i.e., at about increment 30, the magnitudes of the contact forces of an active class becomes comparable with the magnitudes of the contact forces corresponding to the class whose normal is along the maximum compressive stress direction. This causes an instability, as mentioned earlier, in the form of buckling or collapse of the load-bearing columns, as can be seen by comparing the plots of increments 20 and 30. This behavior is consistent with the experimental results of Oda (1972). After the peak strength and buckling of the load-carrying columns, the sample gradually softens until a critical stress state is reached.

9.2 Behavior of the Model Under Cyclic Shearing

(a) Stress-Strain-Volumetric Behavior

The stress-strain and volumetric behavior of the model under cyclic shear is shown in Figures 7 and 8, respectively. Once again, the data points indicate the beginning of an increment of loading. The transition from linear elastic behavior to inelastic behavior begins just after increment 5, when the

sample volume begins to increase. Unlike the previous example, there is no loss in strength or softening of the material in this case so that the behavior resembles that of a loosely packed granular material.

At increment 25 and 75 the strain-rate direction is reversed. The stress-strain behavior of the model is in good qualitative agreement with the observed behavior of loosely packed granular materials. However, the volumetric behavior is not in good agreement with the observed behavior because the model predicts a net dilatancy rather than a net densification at the end of the cycle.

(b) Evolution of Contact Normal Distribution

The distribution of the quantity $2\pi E(m)$ at increments 0, 5, 25, 39, 50, and 75 is represented in Fig.9. Again, there are 48 data points in each plot of Fig.9 corresponding to the 48 classes. Since the sample is assumed to be initially isotropic the distribution of normals is a unit circle at increment 0.

In this example, there is a slight change in the number of contacts within a class in the elastic regime (see, Fig.9, Increment 05). As the sample is sheared, even at the very beginning of the loading in the course of elastic behavior, the fabric adapts itself to the rotation of the principal stress axes so that there are more contacts along the maximum compressive stress (Fig.9, Increments 5, etc.). This should be contrasted with the evolution of contacts in the previous example where a reduction of contacts led to the buckling and collapse of the load-carrying columns along the maximum compressive stress direction which in turn led to a loss of strength or softening of the material. Another interesting point is that the distribution of contact normals at increments 39 and 92 (not shown), when the stress ratio is zero, is nearly isotropic and hence it is similar to the initial distribution of contact normals.

(c) Evolution of the Contact Force Magnitudes and the Critical Contacts

The distribution of the contact force magnitudes and the history of active and inactive classes of contacts are considered in Figs. 10a and 10b. Again, the magnitudes of the contact forces are represented by the non-dimensional quantity $M \ell f/p$, while the status of contacts is represented by the non-dimensional quantity $-f_r/\mu f_m$.

Since the initial confining pressure is isotropic, the distribution of the magnitudes of the contact forces (see Fig. 10a, Increment 00) is the same for all classes of contacts. As mentioned earlier in section 8.1 (see, Eq. 8.14), since the initial confining stress and the initial fabric are both isotropic, the

component of the shear force vanishes for all the classes of contacts and hence, the quantity $-f/\mu f_m$ is initially zero; see, the initial directional distribution of $-f/\mu f_m$ (Fig.10a, Increment 00).

As mentioned earlier, during shearing, the rotation of the maximum compressive stress causes the contact force distribution to rotate accordingly (see Figs.10a, and 10b). After the initial rotation and a significant redistribution of contact forces in the very beginning of loading during the elastic regime (Fig.10a, Increment 05), no significant rotation occurs up until increment 39 when a stress reversal occurs. At about increment 39, the distribution of contact forces is only slightly anisotropic, and hence approximately similar to the initial distribution of contact forces. Note, however, that there are several active classes of contacts at increment 39, while the sample is initially in a state of equilibrium.

10. SUMMARY AND CONCLUSIONS

A micromechanically-based model for the two-dimensional behavior of granular materials is presented in this paper. The model is systematically formulated as follows:

1. The relationship between the overall stress and the microscopic quantities is examined. These microscopic quantities include the interparticle forces and the number and orientation of contacts, and the average size of the particles.

2. The relationship between the overall velocity gradient and the microscopic deformation measures characterizing the relative frictional sliding and rotation of the granules is considered.

3. Local constitutive equations are introduced for the rate of change of the contact forces, the evolution of contact normals, the mechanism of local failure, and for the number of contacts in a particular orientation. The local constitutive relations are simple enough to permit an analytical integration over a small time interval. This is an important feature of the present model because the overall nominal stress can be computed directly by employing the relationship for the overall stress, mentioned in (1) above.

4. Macroscopic rate constitutive relations are developed for the stress rate by adopting a Taylor-averaging method and by writing explicit relations between the number of contacts per unit volume and the incremental change in volume. The analytical integration of the local constitutive relations mentioned in the previous step are used to obtain the overall stiffness from (5.13).

5. Due to the nonlinearity of the local constitutive relations, the material response is computed

by an incremental procedure. By employing this procedure, the nominal stress can also be computed by incrementally integrating the expression for the overall nominal stress rate.

6. The predictions of the model in the case of shearing deformation were obtained by means of two numerical examples. In addition to the overall stress and strain diagrams, explicit and detailed results are presented for the evolution of fabric, contact force, and the history of active and inactive classes of contacts. By examining these results it has become possible to clearly explain the mechanism of failure and softening of densely packed materials as well as the mechanism of the inelastic deformation of loosely packed materials. In so far as the shearing deformation is concerned, the stress-strain behavior of the model is in excellent qualitative agreement with the observed behavior of granular materials. However, the volumetric response of the model in cyclic shear is not realistic because it predicts a net dilatancy rather than a net densification at the conclusion of cyclic deformation.

ACKNOWLEDGEMENT

The work of MMM was initially supported by the National Science Foundation under grant MEA 8318967 to Tulane University and later by a grant from the Solid Mechanics Laboratory, Ecole Polytechnique, Palaiseau, France, the Tulane School of Engineering, as well as by the Grant No. AFOSR-87-0079 to University of California, San Diego (UCSD), by Air Force Office of Scientific Research (AFSOR). The work of BL was supported by a post-doctoral fellowship from NATO. The work of SNN was supported by AFOSR Grant No. AFOSR-87-0079 to UCSD.

The authors thank B. Balendran for his comments on an earlier draft of this paper, and David Mouton and Ramesh Vangal for their help in programming.

REFERENCES

- Anand, L. 1983 *J. Mech. Phys. Solids* 31, 105-122.
- Christoffersen, J., Mehrabadi, M. M., & Nemat-Nasser, S. 1981 *J. Appl. Mech.* 48, 339-344.
- Cowin, S.C. & Satake, M., eds. 1978 *Proc. U.S.-Japan Seminar on Continuum Mechanical and Statistical Approaches in the Mechanics of Granular Materials* Tokyo: Gakujutsu Bunken Fukyukai.
- Havner, K.S. & Shalaby, A.H. 1977 *Proc. R. Soc. Lond. A* 358, 47-70.
- Hill, R. 1965 *J. Mech. Phys. Solids* 13, 89-101.
- Hill, R. 1972 *Proc. R. Soc. Lond. A* 326 131-147.
- Hill, R. 1984 *Math. Proc. Can. Phil. Soc.* 95, 481-494.
- Hill, R. & Rice, J. R. 1972 *J. Mech. Phys. Solids* 20, 401-413.
- Iwakuma, T., & Nemat-Nasser, S. 1984 *Proc. R. Soc. Lond. A* 394, 87-119.
- Jagota, A., Dawson, P. R., & Jenkins, J. T. 1988 *Mechanics of Materials* 7, 255-269.
- Jenkins, J.T. & Satake, M., eds. 1983 *Mechanics of Granular Materials: New Models and Constitutive Relations* Amsterdam: Elsevier Science Publishers.
- Kanatani, K. 1984 *Int. J. Eng. Sci.* 22, 149-164.
- Love, A. E. H. 1927 *A Treatise On the Mathematical Theory of Elasticity*. Dover.
- Mehrabadi, M. M. & Cowin, S. C. 1978 *J. Mech. Phys. Solids* 26, 269-284.
- Mehrabadi, M. M. & Cowin, S. C. 1980 *J. Engng. Mech. Div. Am. Soc. Civil Engrs.* 106, 991-1003.
- Mehrabadi, M. M., Nemat-Nasser, S. & Oda, M. 1982 *Int. J. for Numerical and Anal. Methods in Geomech.* 6, 95-108.
- Mehrabadi, M. M., Nemat-Nasser, S., Shodja, H. M. & Subhash, G. 1988 In *Micromechanics of Granular Materials* (eds. M. Satake & J. T. Jenkins), pp. 253-262. Amsterdam: Elsevier.
- Nemat-Nasser, S. 1983 *J. Appl. Mech.* 50, 1114-1126.
- Nemat-Nasser, S. & Mehrabadi, M. M. 1983 In *Mechanics of Granular Materials: New Models and Constitutive Relations* (eds. J. T. Jenkins & M. Satake), pp. 1-8. Amsterdam: Elsevier.
- Nemat-Nasser, S. & Mehrabadi, M. M. 1984 In *Mechanics of Engineering Materials* (eds. C. S. Desai & R. H. Gallagher), pp. 451-463. John Wiley & Sons.
- Nemat-Nasser, S., Mehrabadi, M. M. & Iwakuma, T. 1981 In *Three-Dimensional Constitutive Relations and Ductile Fracture* (ed. S. Nemat-Nasser), pp. 157-172. Amsterdam: North-Holland.
- Nemat-Nasser, S. & Obata, M. 1986 *Proc. R. Soc. Lond. A* 407, 343-375.
- Oda, M. 1972 *Soils and Foundations* 12, 17-36.
- Petrakis, E. & Dobry, R. 1989 *Micromechanical Behavior and Modelling of Granular Soil*. Report prepared under Grant No. AFSOR-86-0135, Dept. of Civil Engineering, Rensselaer Polytechnic Institute. Troy: New York 12180.
- Satake, M. & Jenkins, J.T., eds. 1988 *Micromechanics of Granular Materials* Amsterdam: Elsevier.
- Spencer, A. J. M. 1964 *J. Mech. Phys. Solids* 12, 337-351.
- Spencer, A. J. M. 1982 In *Mechanics of Solids* (eds. H. G. Hopkins & M. J. Sewell), pp. 607-652. Oxford: Pergamon Press.

APPENDIX A. DERIVATION OF RELATIONS (7.17) AND (7.18)

Writing (7.16) in the form

$$\theta(t) = \bar{\theta}_0 - w_{12}t, \quad (\text{A } 1)$$

where $\bar{\theta}_0 = \theta_0 + w_{12}t_0$ is a constant, we note that when $w_{12} = 0$,

$$\begin{aligned} \int_{t_0}^t \cos 2\theta \, dt &= \cos 2\theta_0(t-t_0) \\ &= [m_1^2(t_0) - m_2^2(t_0)](t-t_0). \end{aligned} \quad (\text{A } 2)$$

Similarly,

$$\begin{aligned} \int_{t_0}^t \sin 2\theta \, dt &= \sin 2\theta_0(t-t_0) \\ &= 2m_1(t_0)m_2(t_0)(t-t_0). \end{aligned} \quad (\text{A } 3)$$

Integrating (7.15), using (A 2) and (A 3), substituting the result into (7.14), and solving for the normal and tangential components of the contact force, Eqs. (7.17) will be obtained.

When $w_{12} \neq 0$, we have

$$\begin{aligned} \int_{t_0}^t \cos 2\theta \, dt &= \int_{t_0}^t \cos 2(\bar{\theta}_0 - w_{12}t) \, dt \\ &= \frac{1}{w_{12}} [\sin \theta_0 \cos \theta_0 - \sin \theta \cos \theta] \\ &= \frac{1}{w_{12}} [m_1(t_0)m_2(t_0) - m_1(t)m_2(t)]. \end{aligned} \quad (\text{A } 4)$$

Similarly,

$$\int_{t_0}^t \sin 2\theta \, dt = \frac{1}{w_{12}} [m_1^2(t) - m_1^2(t_0)]. \quad (\text{A } 5)$$

Again, integrating (7.15), using (A 4) and (A 5), substituting the result into (7.14), and solving for the normal and tangential components of the contact force, Eqs. (7.18) will be obtained.

FIGURE CAPTIONS

- Figure 1: Schematic representation of the local yield condition, Eqs. (4.14).
- Figure 2: Dilatant shearing deformation of a sample of granular materials.
- Figure 3: Predicted stress-strain response of the material under monotonic shear.
- Figure 4: Predicted volumetric behavior of the material under monotonic shear.
- Figure 5: Distribution of contact normals at increments indicated on the stress-strain curve of Fig. 1.
- Figure 6: Distribution of magnitudes of contact forces and the directional distribution of the ratio of shear to normal forces at various increments marked on the stress-strain curve of Fig. 1.
- Figure 7: Stress-strain response of the model under cyclic shear.
- Figure 8: Volumetric behavior of the model under cyclic shear.
- Figure 9: Distribution of contact normals at increments indicated on the stress-strain curve of Fig. 7.
- Figure 10: Distribution of magnitudes of contact forces and the directional distribution of the ratio of shear to normal forces at various increments marked on the stress-strain curve of Fig. 7.

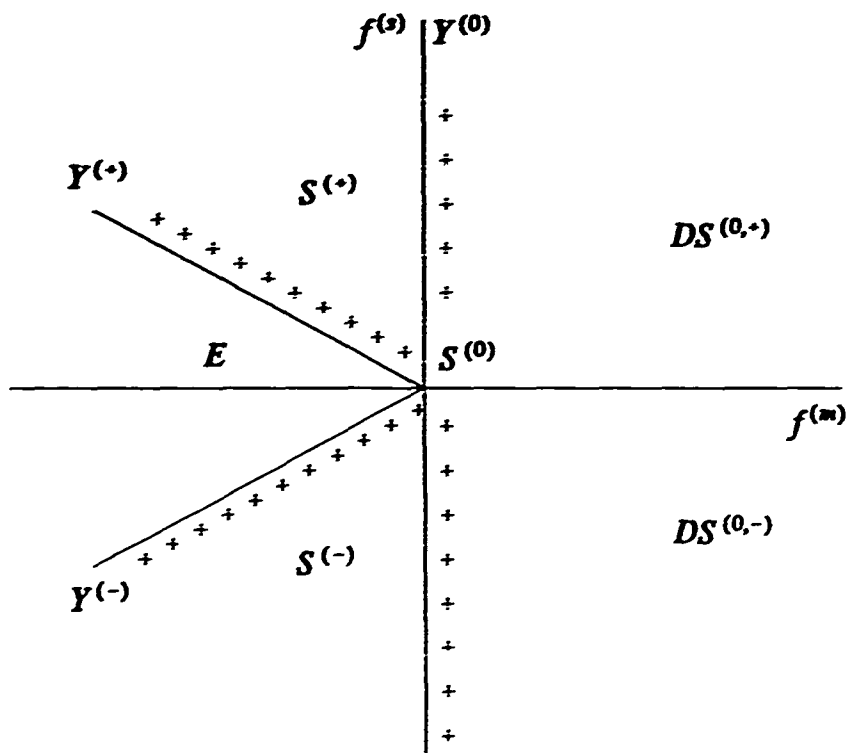


Fig. 1

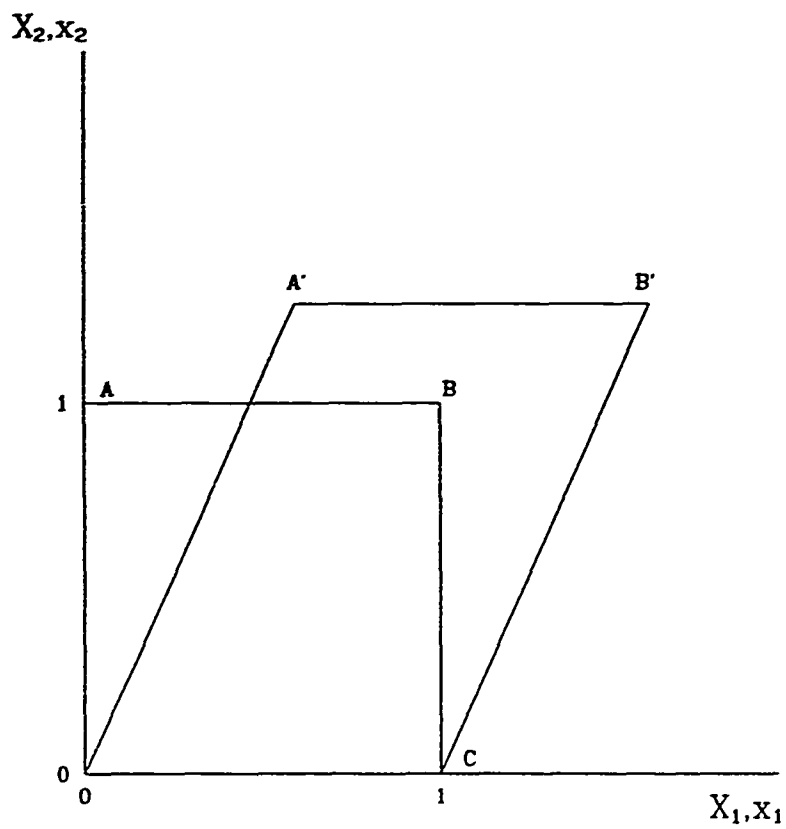


Fig. 2

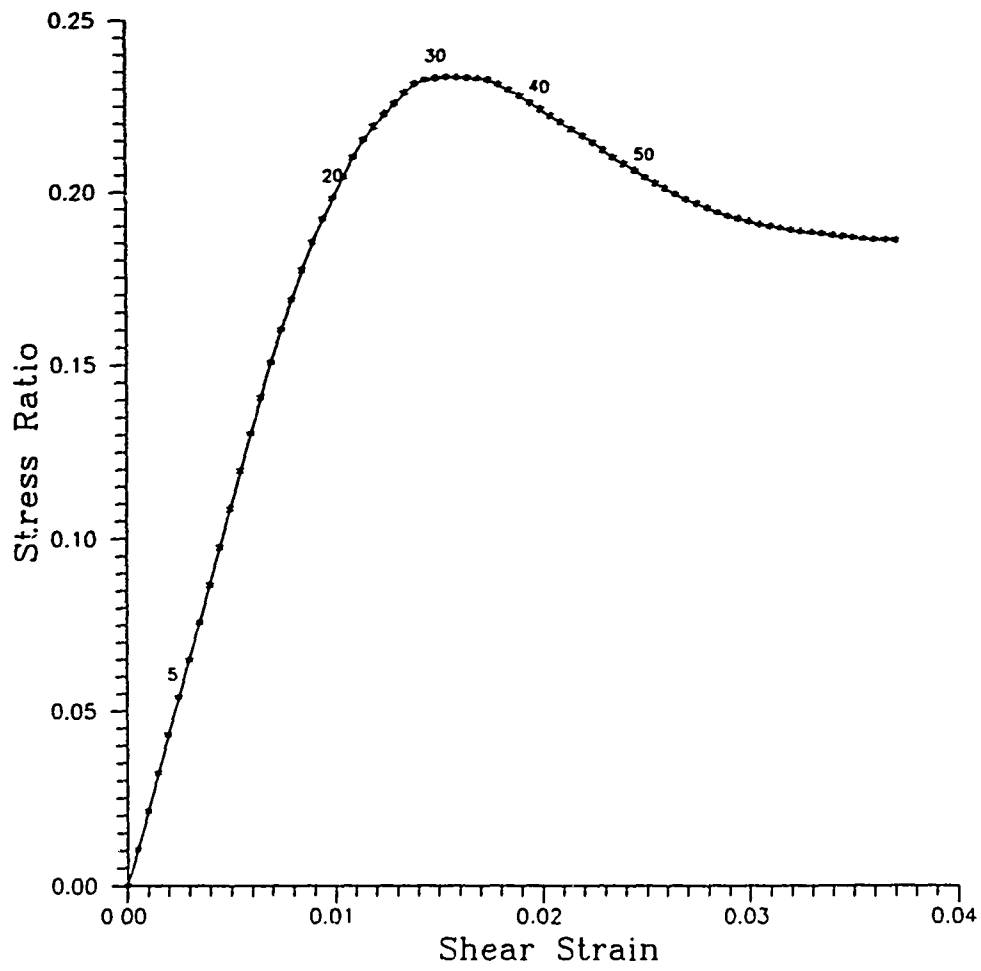


Fig. 3

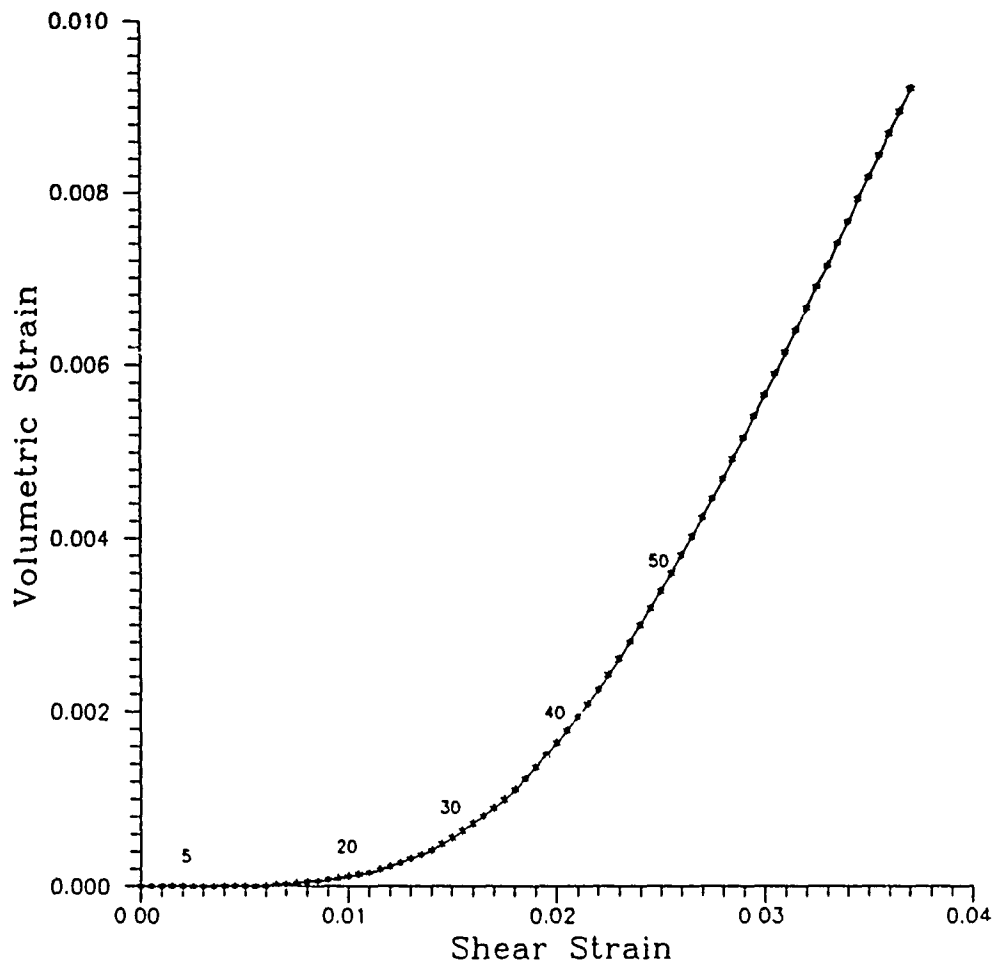


Fig. 4

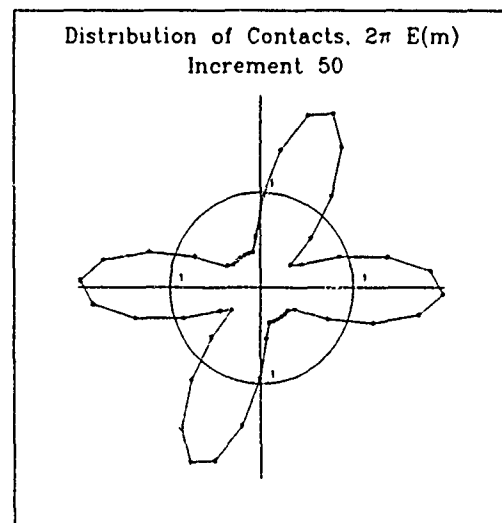
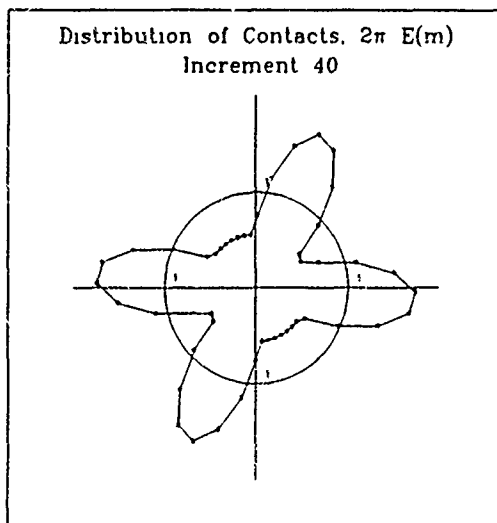
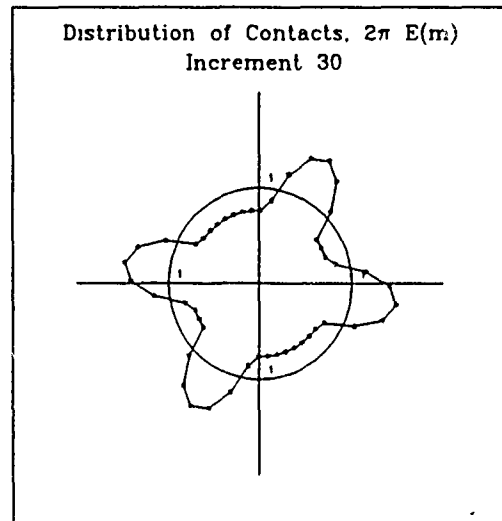
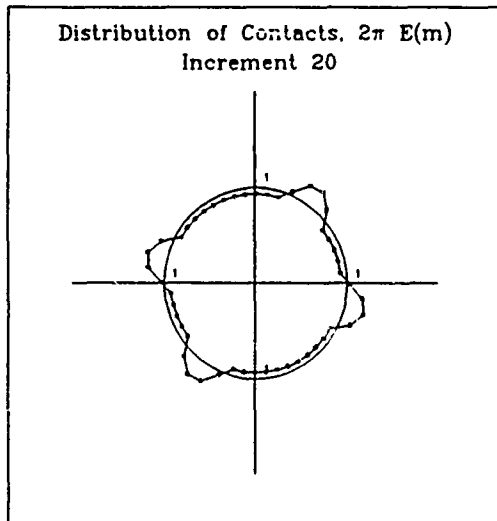
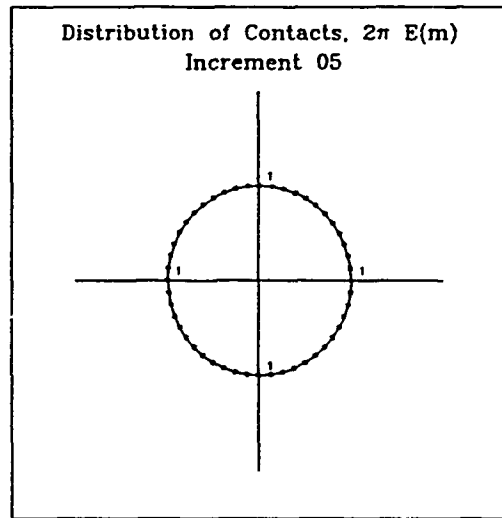
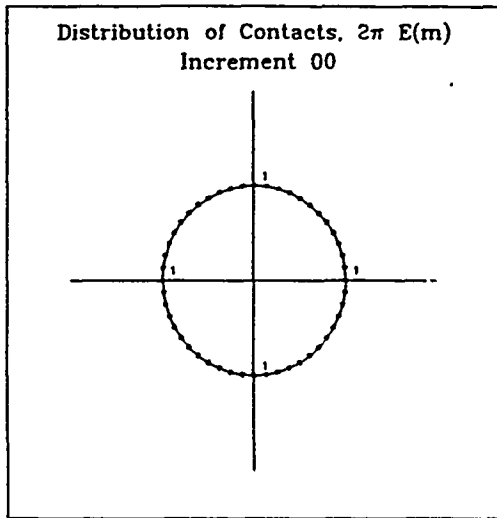
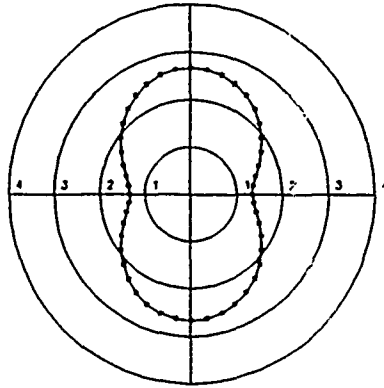
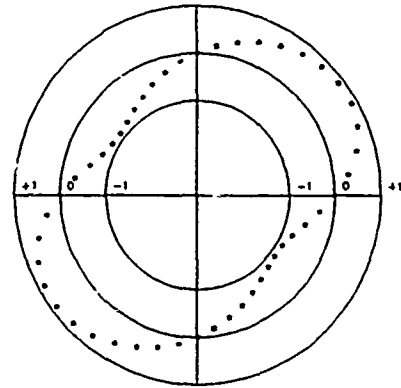


Fig 5

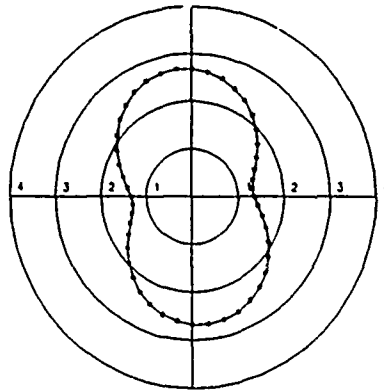
Distribution of Contact Force Magnitudes, Mlf/p
Increment 00



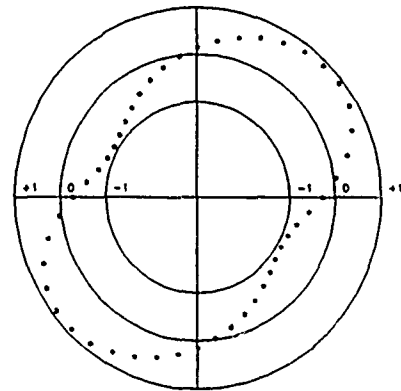
Directional Distribution of $-f^{(n)}/\mu f^{(m)}$
Increment 00



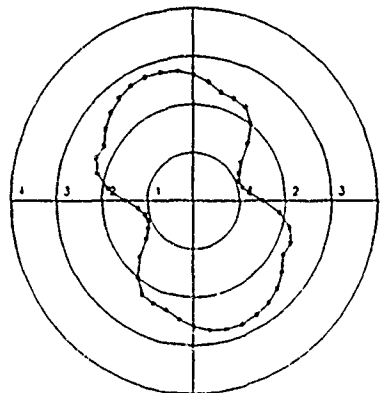
Distribution of Contact Force Magnitudes, Mlf/p
Increment 05



Directional Distribution of $-f^{(n)}/\mu f^{(m)}$
Increment 05



Distribution of Contact Force Magnitudes, Mlf/p
Increment 20



Directional Distribution of $-f^{(n)}/\mu f^{(m)}$
Increment 20

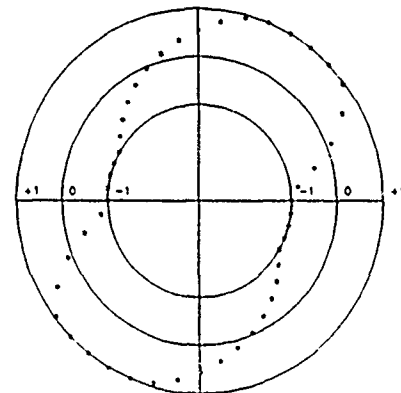
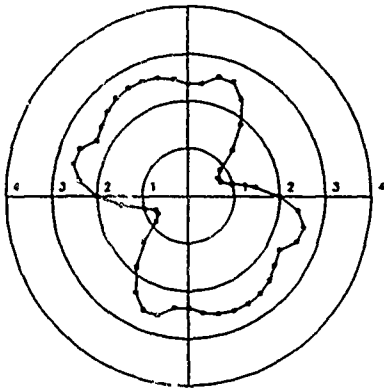
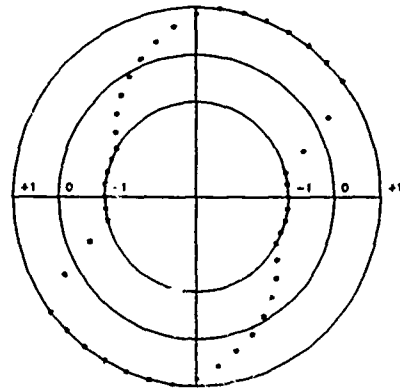


Fig. 6a

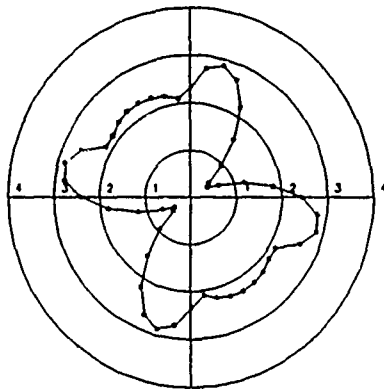
Distribution of Contact Force Magnitudes, Mf/p
Increment 30



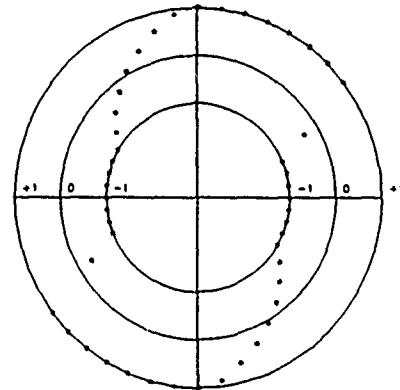
Directional Distribution of $-f^{(a)}/\mu f^{(m)}$
Increment 30



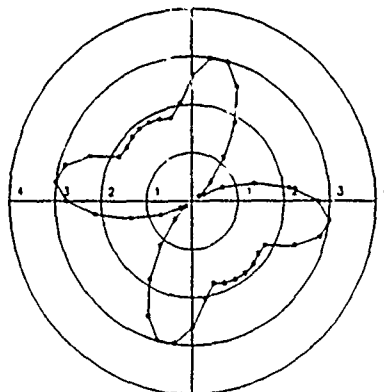
Distribution of Contact Force Magnitudes, Mf/p
Increment 40



Directional Distribution of $-f^{(a)}/\mu f^{(m)}$
Increment 40



Distribution of Contact Force Magnitudes, Mf/p
Increment 50



Directional Distribution of $-f^{(a)}/\mu f^{(m)}$
Increment 50

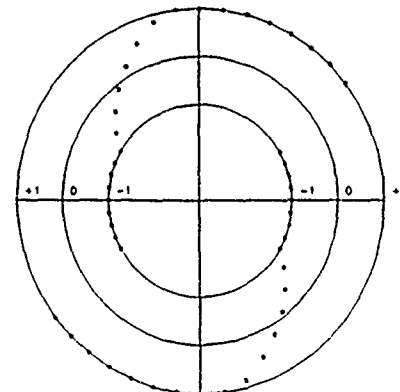


Fig. 6b

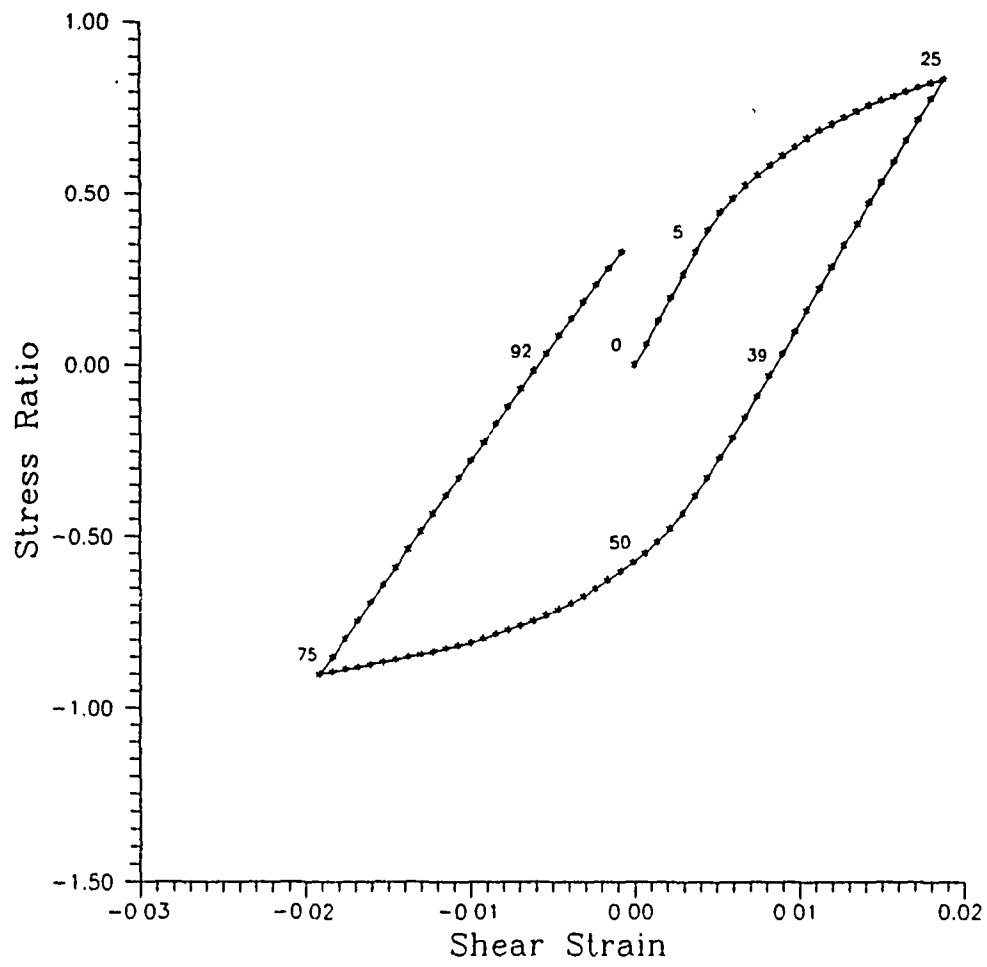


Fig. 7

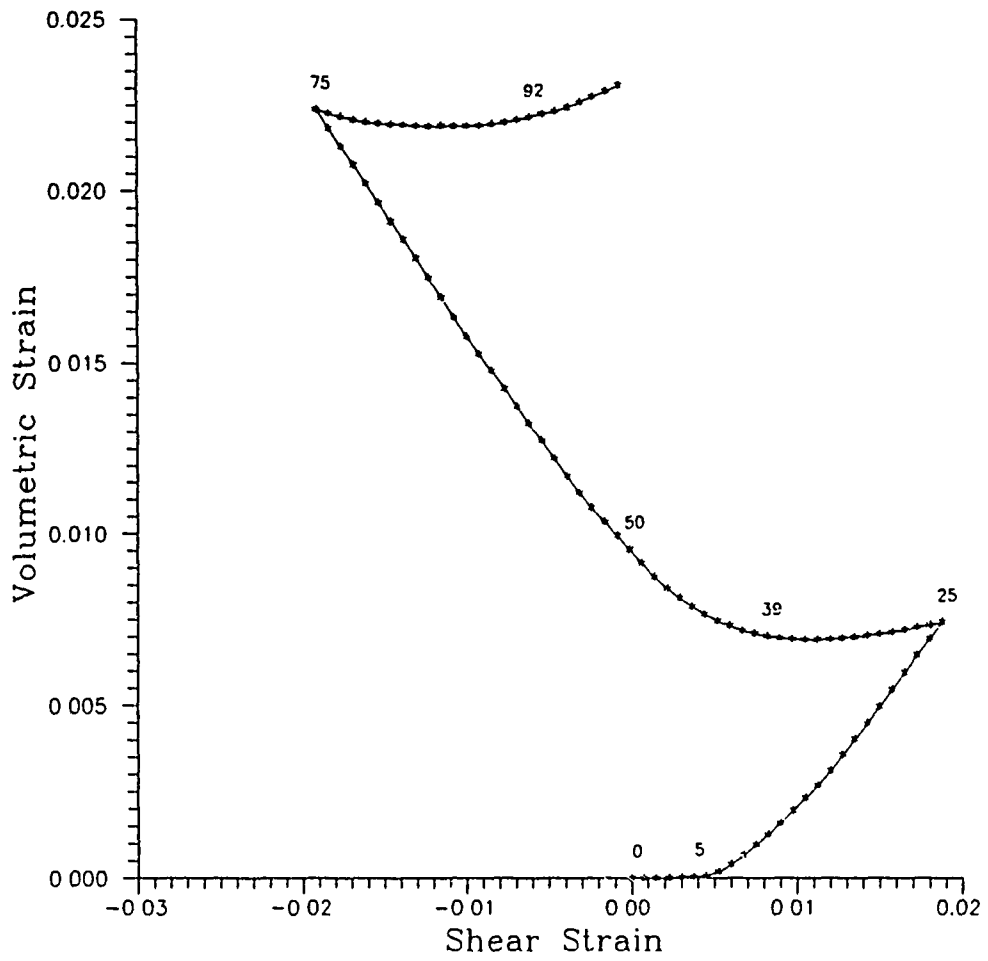


Fig. 8

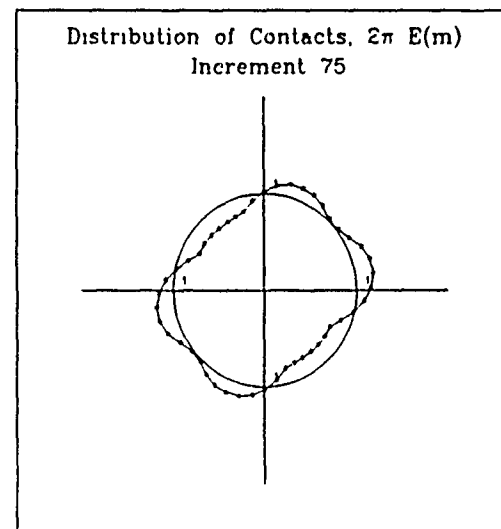
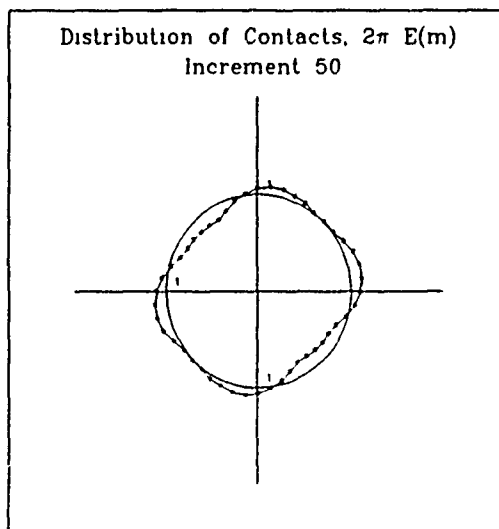
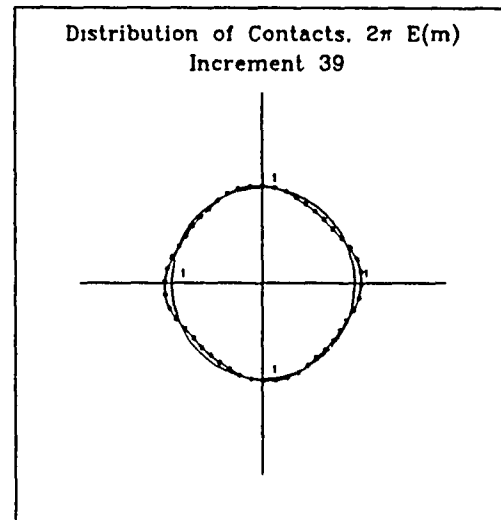
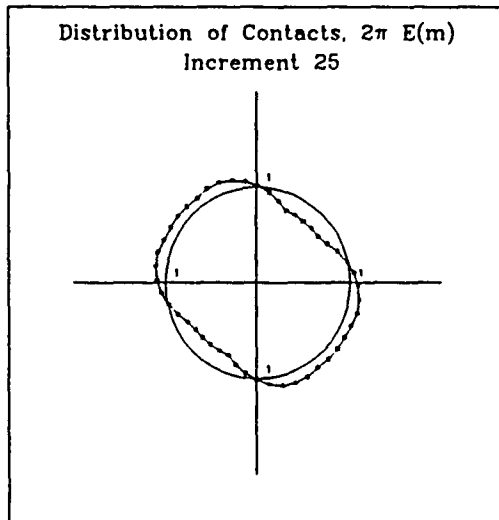
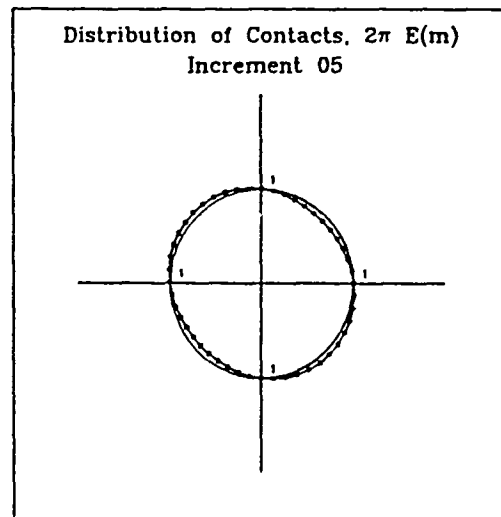
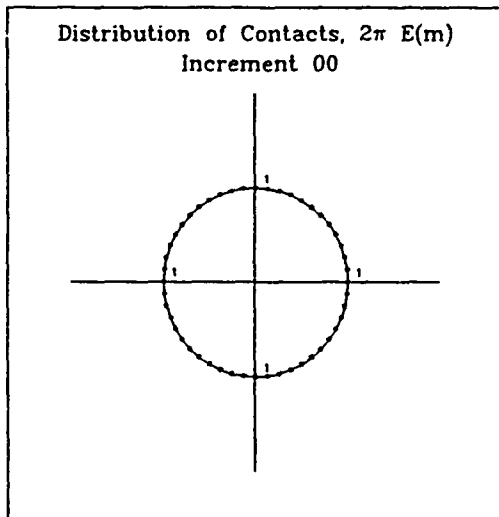
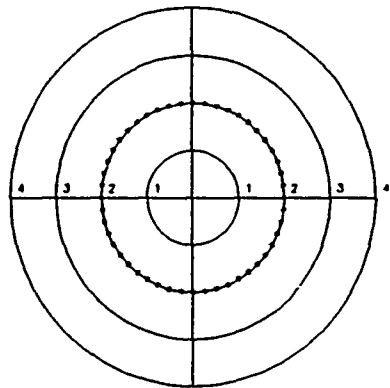
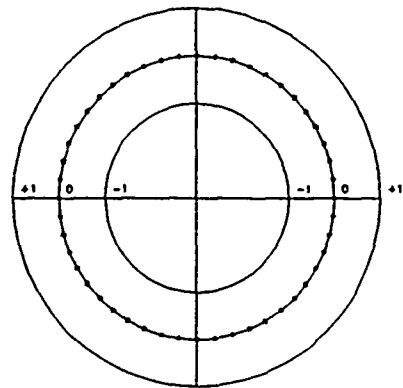


Fig 9

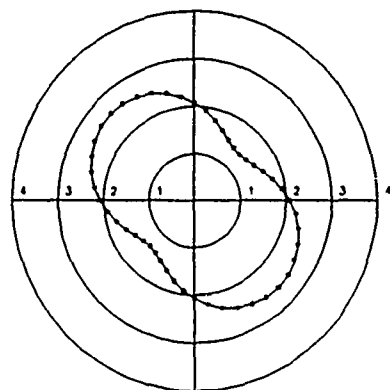
Distribution of Contact Force Magnitudes, Mf/p
Increment 00



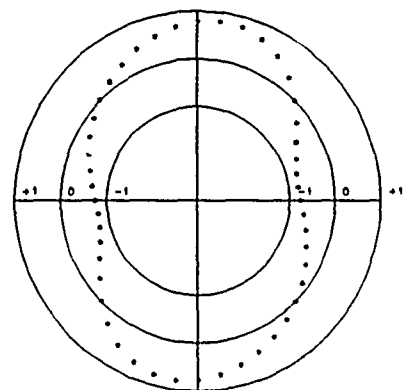
Directional Distribution of $-f_x/\mu f_m$
Increment 00



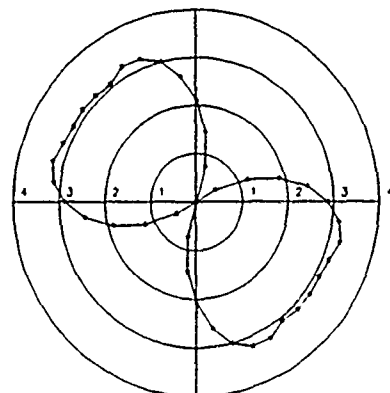
Distribution of Contact Force Magnitudes, Mf/p
Increment 05



Directional Distribution of $-f_x/\mu f_m$
Increment 05



Distribution of Contact Force Magnitudes, Mf/p
Increment 25



Directional Distribution of $-f_x/\mu f_m$
Increment 25

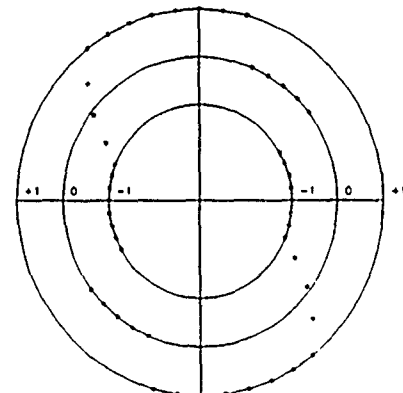
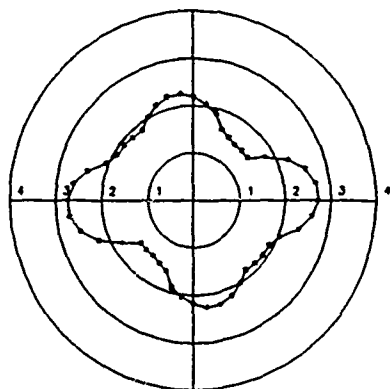
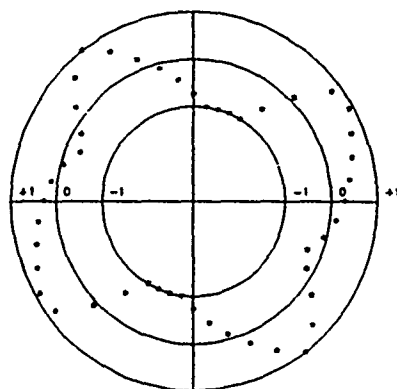


Fig. 10a

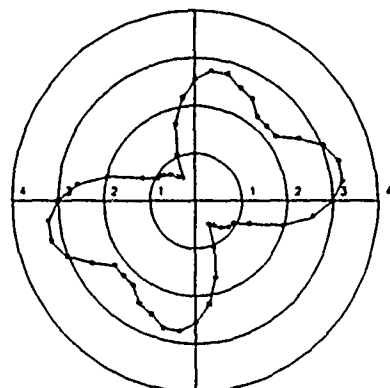
Distribution of Contact Force Magnitudes, Mf/p
Increment 39



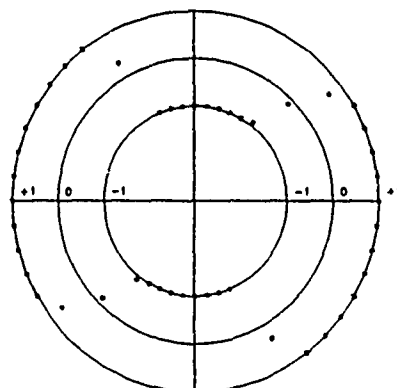
Directional Distribution of $-f_x/\mu f_m$
Increment 39



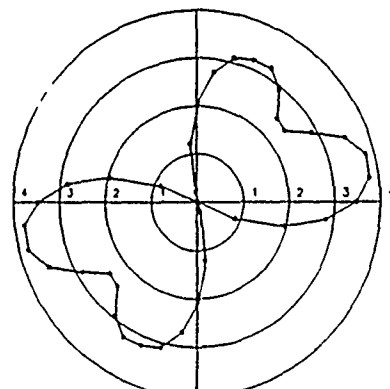
Distribution of Contact Force Magnitudes, Mf/p
Increment 50



Directional Distribution of $-f_x/\mu f_m$
Increment 50



Distribution of Contact Force Magnitudes, Mf/p
Increment 75



Directional Distribution of $-f_x/\mu f_m$
Increment 75

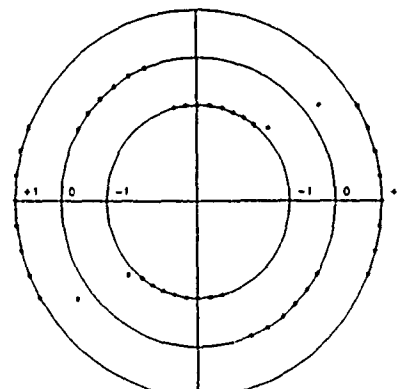


Fig. 10b

A constitutive model for granular materials based on micromechanics

M. M. Mehrabadi^a, B. Loret^b and S. Nemat-Nasser^c

^aDepartment of Mechanical Engineering, Tulane University, New Orleans, Louisiana 70118, U.S.A.

^bNational Polytechnic Institute of Grenoble, Institute of Mechanics, BP 53X 38041 Grenoble Cédex, FRANCE

^cCenter of Excellence for Advanced Materials, Department of Applied Mechanics and Engineering Sciences, University of California, San Diego, La Jolla, CA 92093, U.S.A.

Abstract

A recently proposed constitutive model for two-dimensional flow of granular materials is briefly reviewed and some numerical results are presented in this paper. First, the concept of fabric and the relations between the overall stresses and the relevant microscopic quantities are reviewed. Then, the kinematics is briefly examined. A significant concept underlying all these developments is the notion of the *class* of contact unit normals with a continuously evolving distribution function, even though individual members of various classes may change discontinuously, as contacts are lost and new contacts are developed in the course of granular flow. Next, local and macroscopic constitutive relations are discussed and the evolution of the density of contacts in a particular class is considered. As an illustration, the overall response of a two-dimensional assembly of disks subjected to an overall shearing deformation is determined. The stress-strain relations and the evolution of fabric are in excellent qualitative agreement with the observed behavior of granular materials. In light of these results, the micromechanisms of failure and inelastic deformation of dense as well as loose granular materials are discussed.

1. INTRODUCTION

Development of overall macroscopic constitutive relations for granular materials on the basis of simple and reasonable micromechanical assumptions is of great interest. A systematic approach to this problem inevitably would include considerations of: 1) a description of the overall macroscopic stresses in terms of contact forces, their distribution, and some relevant geometric measures of the microstructure; 2) a description of the overall measures of incremental deformation in terms of quantities that characterize micromechanisms of relative sliding or sliding and rolling of granules; 3) a description of the time rate of change of the overall stress in terms of the overall deformation-rate and the overall moduli. A procedure for achieving all of these goals is described in [1]. A brief

review of this procedure and some numerical results are presented in this paper.

Since, in the course of deformation, new contacts are constantly being generated as some of the existing contacts are being lost, the analytic identification of the history of individual contacts is extremely difficult unless one approaches the problem numerically, using a large-scale computer program (see, e.g., [2]). On the other hand, in the course of continuous deformation of a granular mass, one expects that suitable measures of the distribution of contacts can be employed which characterize a certain class of contacts and, therefore, undergo continuous change. Adopting this viewpoint in [1], the authors introduce simple constitutive models at the microlevel, which relate the change (or the rate of change) in the contact force associated with a given class of contacts to the corresponding micro-deformation increment (or rate) produced by the corresponding changes in the microstructure. Such an approach (which deals with classes of contacts rather than with individual contacts) bypasses the difficult issue of continuous loss of contacts and formation of new ones.

After a brief review of the concept of stress and fabric in granular materials in Section 2, kinematics is reviewed in Section 3. At the local level, the description of kinematics corresponds to the double shearing model [3-4] and its extension to dilatant materials [5-6]. The local constitutive assumptions, the evolution of the probability density function of contact normals, and the macroscopic constitutive relations are summarized in Section 4.

As an illustration, the response of a two-dimensional assembly of rigid cylindrical disks of circular cross section subjected to shearing deformation is described in Section 5. Two numerical examples are presented, one of which simulates the response of loose and the other corresponds to the behavior of dense granular materials. The mechanism of strain hardening and failure followed by strain softening which is a characteristic response of densely packed samples of granular materials, and the inelastic deformation mechanism corresponding to the loosely packed samples are discussed in light of the model predictions of the evolution of fabric. The resulting stress-strain relations and the evolution of fabric and the evolution of contact forces are in excellent qualitative agreement with the observed behavior of granular materials.

2. DESCRIPTION OF FABRIC AND STRESS

We consider an ideal granular material composed of rigid, dry particles. For simplicity, particles are assumed to be spherical or cylindrical with circular cross-section. Following Oda [7], the fabric is represented by the distribution of the unit contact normals. Each orientation corresponds to a large number of contacts which, while individually may undergo abrupt changes, collectively evolve in a continuous manner during the course of the continuous flow of the representative granular sample. In this manner, one can, for example, identify an initial and a current orientation for a given class of contacts, while clearly the same identification may not, in general, be possible for an individual and specific contact.

The group of M contacts per unit volume of a representative sample of granular material is divided into, say Q classes, each with a common contact plane defined by the corresponding unit contact normal. Let M_a , ($a = 1, 2, \dots, Q$), be the number of contacts which belong to class a with common unit contact normal m^a . Then

$$\sum_{a=1}^Q \frac{M_a}{M} = 1. \quad (1)$$

When the number of classes, Q , is very large, we can introduce the distribution density function $E(m)$ to describe the angular distribution of unit branches. In this case (1) becomes

$$\int_0 E(m) d\Omega = 1, \quad (2)$$

where $E(m) = E(-m)$, and where $d\Omega$ is an elemental angle of the unit circle Ω . With (2), the average of any quantity $\varphi(m)$ is given by

$$\langle \varphi \rangle \equiv \sum_{a=1}^Q \frac{M_a}{M} \varphi(m^a) = \int_0 E(m) \varphi(m) d\Omega. \quad (3)$$

The primary microscopic quantities associated with a typical contact α_a in class a are shown in Fig. 1. In this figure, f_i^a is the interparticle contact force and l^a is the branch length. Denoting the average of these quantities by f_i^a and l^a , respectively, the Cauchy stress is given by

$$\Sigma_{ij} \equiv \langle \sigma_{ij} \rangle \equiv \sum_{a=1}^Q \frac{M_a}{M} \sigma_{ij}^a, \quad \sigma_{ij}^a = M l^a m_i^a f_j^a. \quad (4)$$

The nominal stress-rate is described by (see, [1] for details)

$$\dot{N}_{ij} = M \langle l m_i \dot{f}_j \rangle. \quad (5)$$

3. KINEMATICS

Under the action of an overall applied load, the flow of a granular mass consisting of rigid granules occurs through sliding and rolling of grains over each other. As the sample deforms, the distribution of unit normals changes and this change characterizes a corresponding change of the fabric or microstructure. The overall deformation is viewed as a suitable average of the local deformations associated with each class of contacts. Hence, denoting by l_{ij}^a , ($a=1, \dots, Q$), the components of the velocity gradient associated with a typical class of contacts, a , the overall velocity gradient is written as

$$L_{ij} = \langle l_{ij} \rangle. \quad (6)$$

The local velocity gradient is resolved into two parts as follows:

$$l_{ij}^a = l_{ij}^{*a} + l_{ij}^{**a}, \quad (a=1, \dots, Q), \quad (7)$$

where l^{*a} is the velocity gradient corresponding to the fabric change, and l^{**a} is the velocity gradient stemming from the relative sliding motion of the grains, which leaves the fabric unchanged. The part l^{**a} in (7) is the counterpart of the slip-induced velocity gradient in single crystals, and the part l^{*a} is the counterpart of that associated with the elastic lattice distortion. Note that since, in a granular material which is modeled by rigid granules, no elastic deformation can be involved, it is the change in fabric that produces the change in the overall stress.

4. CONSTITUTIVE RELATIONS

Constitutive assumptions are made at the local level for the time rate of change of the average contact force for each class, and for the evolution of the distribution density function of contact normals. These relations are then used in conjunction with a local yield criterion to arrive at the time rate of change of local nominal stress; see [1] for details. Using this local nominal stress-rate and (5), the overall constitutive relation is obtained in the form

$$\dot{N}_{ij} = \langle \kappa_{ijk} l_k \rangle, \quad (8)$$

where the local moduli κ_{ijk}^a , i.e., those associated with a typical class a , explicitly depend on the fabric, the local contact force, and the material constants [1].

Next, we have to make assumptions concerning the dependence of the local velocity gradient l_{ij}^a on the microstructure. In self-consistent theories for polycrystalline materials [8] and in our earlier work on granular materials [9], a fourth-rank (concentration) tensor, A_{ijkl} , is introduced which depends on microstructure and which relates the local velocity gradient in a typical micro-element, e.g. a single crystal, to the macroscopic uniform velocity gradient (see, [9-10] for more details). This concentration tensor must then be calculated using an appropriate model. Iwakuma and Nemat-Nasser [10] use a fully nonlinear self-consistent model proposed by Hill [8,11], and actually calculate the corresponding concentration tensor for plane problems. It can, however, be shown that this type of self-consistent calculation breaks down when the density of voids or cracks is suitably large. For the granular materials, voids are connected through contact zones which may be viewed as cracks. Hence, the application of the self-consistent method is problematic, leading to unrealistic estimates of the overall instantaneous moduli. In order to develop the simplest micromechanical model that exhibits the basic features of granular material behavior, a Taylor-averaging method is adopted in [1], i.e., it is assumed as a first approximation that the concentration tensor is the identity tensor, leading to

$$l_{ij}^a = L_{ij}. \quad (9)$$

With assumption (9), (8) now reduces to

$$\dot{N}_{ij} = \langle \kappa_{ijk} \rangle L_{ik} \equiv \mathcal{F}_{ijk} L_{ik}, \quad (10)$$

where \mathcal{F}_{ijk} are the overall moduli defined by

$$\mathcal{F}_{ijk} = \langle \kappa_{ijk} \rangle = \sum_{a=1}^Q \frac{M_a}{M} \kappa_{ijk}^a. \quad (11)$$

Denoting the spin tensor by W , the Jaumann rate of macroscopic Cauchy stress, i.e.,

$$\dot{\Sigma}_{ij} = \dot{\Sigma}_{ij} - W_{ik} \Sigma_{kj} + \Sigma_{ik} W_{kj}, \quad (12)$$

and the rate of deformation, D_{ij} , are related as follows [1]:

$$\dot{\Sigma}_{ij} + D_{ik} \Sigma_{kj} = \frac{1}{2} (\mathcal{F}_{ijk} + \mathcal{F}_{jik} + \delta_{ij} \Sigma_{kk} + \delta_{ik} \Sigma_{jj}) D_{kl}. \quad (13)$$

Equations (13), subject to the stress symmetry constraint and with the overall moduli defined by (11), are the macroscopic constitutive relations of the model.

In order to calculate an overall quantity from the corresponding local quantity (e.g., the overall moduli from (11)), an expression for the distribution density function of the contact normals is needed. Since the number of contacts in each class is strongly influenced by the magnitude of the contact force for that particular class as well as by the local volumetric change, the density of contacts in each class is related to the magnitude of the corresponding contact force and the associated volumetric strain rate by the relation [1]

$$\frac{M_a}{M} = \frac{1}{\alpha} \varepsilon^2 e^{\beta \hat{f}}, \quad \alpha = \sum_{a=1}^Q \varepsilon^2 e^{\beta \hat{f}}, \quad (14)$$

where β is a macroscopic constant, ε is a local quantity with the dimension of area, and \hat{f} is a nondimensional quantity related to the magnitude of the contact force for class a , i.e., f^a , as follows

$$\hat{f} = \frac{M_0 \ell^0 f}{-(1/2) \text{tr} \Sigma}. \quad (15)$$

Note that, for ease in writing, the superscript a is omitted in (14) and (15). Employing (14), the average of any local quantity can be found in the manner of (3). In quantitative crystallography, it is customary to expand the density function of the orientational data in a series of generalized spherical harmonics. In works on granular materials, it has also become customary in recent years to describe the distribution density in terms of "fabric tensors" of various ranks [12-14]. Note that here and in [1], to characterize the fabric, we have made a constitutive assumption for the density distribution function itself, rather than for various approximations of it in the form of macroscopic "fabric tensors".

Finally, an expression for the evolution of the coefficient $M\ell$ is assumed in [1]. This is required for calculating the stress and stress-rate from (4) and (5), respectively. Recalling that M is the number of contacts per unit volume and that ℓ is the branch length, the quantity $M\ell$ with the dimension of (area)⁻¹, is intimately related to the volumetric strain and strain rate represented by the jacobian $\det G$ and by $\text{tr} D$, respectively. Hence, it is assumed that

$$M\ell = M_0 \ell^0 e^{n(\det G)\eta}, \quad (16)$$

where n is a negative constant, and where

$$\eta = \int_{t_0}^t \text{tr} D \, dt = (t - t_0) \text{tr} D(t^*); \quad (17)$$

here $t_0 \leq t^* \leq t$, and for the numerical illustration given at the end of this paper, we have used $t^* = (1/2)(t + t_0)$. An equation resembling (16) has been introduced by Jagota, *et al.* [5], for the evolution of the coordination number, in connection with the sintering and compaction of powder packings. The relation (16) follows from the assumption that the rate of change of $(M\ell)$ per its own unit is proportional to $(\det G)(\text{tr} D)$, i.e.,

$(M\ell)/(M\ell) = n(\det G)(tr D)$. Upon integration over the time increment and using the value of $\det G$ at the start of time step (i.e., retaining only linear terms in $(t-t_0)$), we obtain (16) and (17).

Due to the nonlinearity of the rate constitutive equations, the response must be computed by an incremental procedure. This procedure is described in detail in [1], where local and overall constitutive equations are cast into an incremental form by using a first-order approximation of the local yield function.

Owing to the simplicity of the local rate constitutive equations, an analytical integration is possible and is carried out in [1], whereby explicit relations are derived, including those for the contact forces and contact normals. Hence, using these relations, the overall nominal stress can be computed in two alternative ways, either using the analytical integration procedure or the incremental procedure described in the previous paragraph.

5. NUMERICAL RESULTS AND DISCUSSIONS

Numerical calculations corresponding to the two-dimensional behavior of the model under simple dilating shear are presented in this section. In these calculations 48 discrete orientations are used between 0° and 360° to define 48 classes of contacts. Two cases are considered. In case (1), the initial conditions and material constants are chosen so that the behavior of the model corresponds to that of loosely packed granular materials; while for case (2), the initial conditions and constants are chosen so that the model behavior corresponds to a densely packed sample. The material constants and initial conditions used in the two cases are summarized in Table 1. In this Table, λ^* , μ^* are Lamé-type constants governing the rate of change of local stress (due to the fabric distortion); p_R and a_R are reference stress and area, respectively; μ is the interparticle friction coefficient; ζ is the dilatancy coefficient; b is a constant that governs the value of the parameter ε and the volumetric behavior of the material [1, Eq. (4.5)]; β and n which appeared first in (14) and (16), respectively, strongly affect the orientational distribution of contact normals as well as the total number of contacts; α_0 is the initial value of α defined by (14)₂; Σ^0 is the initial confining overall stress on the sample. The initial orientational distribution of contact normals is assumed to be isotropic for both cases. As shown in Table I, except for the constants b and β , the remaining constants have been chosen to be identical for both cases. Notice that the chosen values of b and β , in the two cases, differ by two and one orders of magnitude, respectively. The model behaves like densely packed materials for a large absolute value of b , while it behaves similarly to a loosely packed material for a relatively large value of β .

The stress-strain behavior of the model in the two cases are depicted in Fig.2 and 4, where the ratio of shearing stress to the mean normal stress is plotted versus the magnitude of the shear strain. The volumetric strain versus shear strain is plotted in Fig.3 and 5. The data points indicate the beginning of an increment of loading in shear equal to 0.001. The stress-strain and volumetric behavior of the model are in good qualitative agreement with the observed behavior of granular materials.

The orientational distribution of contact normals at increments identified on the plots of Fig.2-5 are presented in Fig.6. Since the samples are assumed to be initially isotropic the initial distribution of normals is a unit circle at increment 0. For the loose sample, as the sample is sheared (to the right), the fabric immediately adapts itself to the rotation of the

principal stress axes so that there are more contacts along the maximum compressive stress (Fig.6, Increments 5). This is in contrast with the evolution of contacts in the dense sample where a gradual reduction of contacts leads to the buckling and collapse of the load-carrying columns along the maximum compressive stress direction which in turn leads to a loss of strength or softening of the material.

Table 1
Material constants and initial conditions

	Dense	Loose
λ^*/p_R	200.0	200.0
μ^*/p_R	200.0	200.0
μ	0.40	0.40
ζ	0.36	0.36
b	-100.0	-1.0
β	0.01	0.1
n	-10.0	-10.0
α_0/a_R^2	0.048	0.048
$M_0 \ell^0 a_R$	10.0	10.0
Σ^0/p_R	$\begin{bmatrix} -2.0 & 0.0 \\ 0.0 & -4.0 \end{bmatrix}$	$\begin{bmatrix} -1.0 & 0.0 \\ 0.0 & -1.0 \end{bmatrix}$

ACKNOWLEDGEMENT

This work was partially supported by AFOSR Grant No. AFOSR-870079 to UCSD.

REFERENCES

1. M. M. Mehrabadi, B. Loret, S. Nemat-Nasser, submitted for publication.
2. E. Petrakis & R. Dobry, 1989 *Micromechanical Behavior and Modelling of Granular Soil*. Report prepared under Grant No. AFOSR-86-0135, Dept. of Civil Engineering, Rensselaer Polytechnic Institute. Troy: New York 12180.
3. A. J. M. Spencer, 1964 *J. Mech. Phys. Solids* 12, 337-351.
4. A. J. M. Spencer, 1982, In *Mechanics of Solids* (eds. H. G. Hopkins & M. J. Sewell), pp. 607-652. Oxford: Pergamon Press.

5. M. M. Mehrabadi & S. C. Cowin, 1978 *J. Mech. Phys. Solids* **26**, 269-284.
6. M. M. Mehrabadi & S. C. Cowin, 1980 *J. Engng. Mech. Div. Am. Soc. Civil Engrs.* **106**, 991-1003.
7. M. Oda, 1972 *Soils and Foundations* **12**, 17-36.
8. R. Hill, 1965 *J. Mech. Phys. Solids* **13**, 89-101.
9. S. Nemat-Nasser & M. M. Mehrabadi, 1984 In *Mechanics of Engineering Materials* (eds. C. S. Desai & R. H. Gallagher), pp. 451-463. John Wiley & Sons.
10. T. Iwakuma & S. Nemat-Nasser, 1984 *Proc. R. Soc. Lond. A* **394**, 87-119.
11. R. Hill, 1972 *Proc. R. Soc. Lond. A* **326** 131-147.
12. M. M. Mehrabadi, S. Nemat-Nasser & M. Oda, 1982 *Int. J. for Numerical and Anal. Methods in Geomech.* **6**, 95-108.
13. S. Nemat-Nasser & M. M. Mehrabadi, 1983 In *Mechanics of Granular Materials: New Models and Constitutive Relations* (eds. J. T. Jenkins & M. Satake), pp. 1-8. Amsterdam: Elsevier.
14. K. Kanatani, 1984 *Int. J. Eng. Sci.* **22**, 149-164.
15. A. Jagota, P. R. Dawson & J. T. Jenkins, 1988 *Mechanics of Materials* **7**, 255-269.

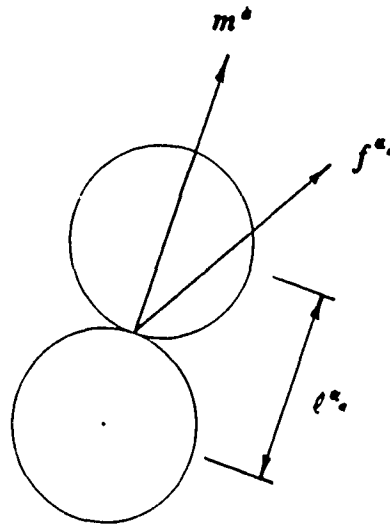


Figure 1. A typical contact α in class a ; m^α is the common unit normal for all contacts in class a ; f_i^α is the interparticle contact force; l^α is the branch length.

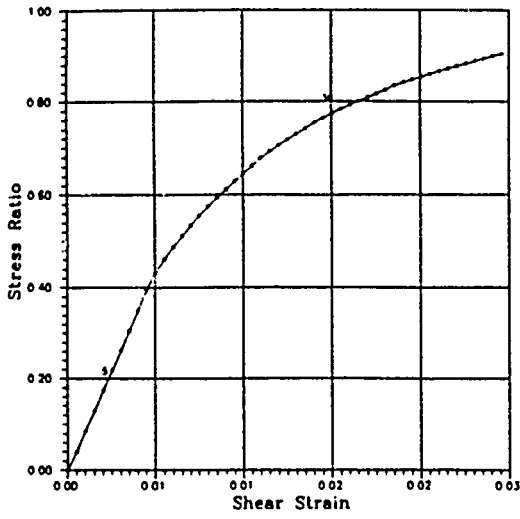


Figure 2. Predicted stress-strain response for a loosely packed sample.

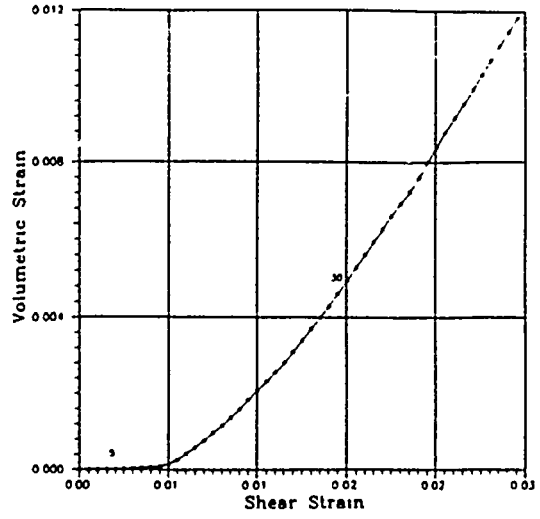


Figure 3. Predicted volumetric behavior for a loosely packed sample.

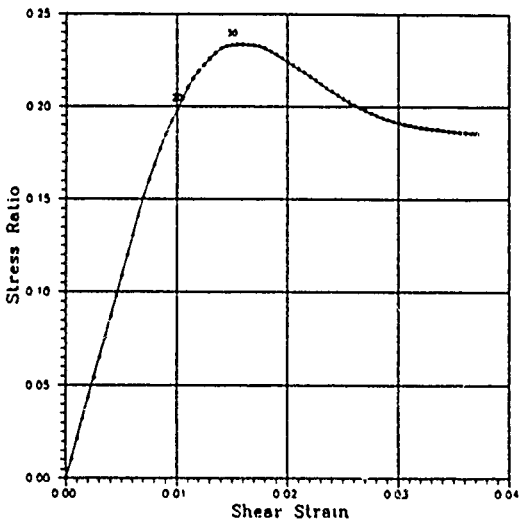


Figure 4. Predicted stress-strain response for a densely packed sample.

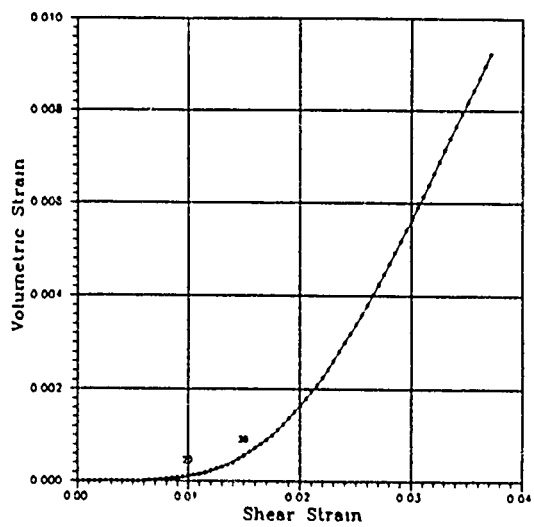


Figure 5. Predicted volumetric behavior for a densely packed sample.

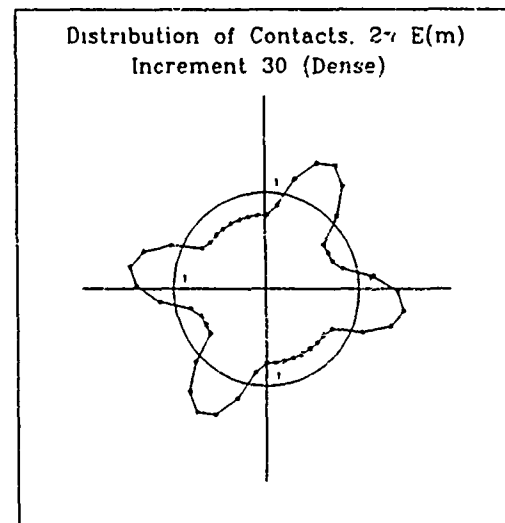
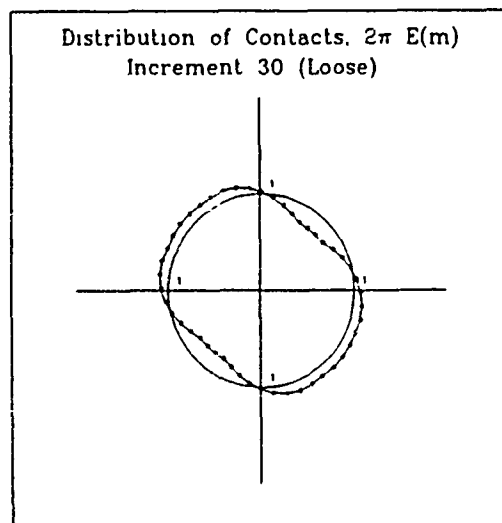
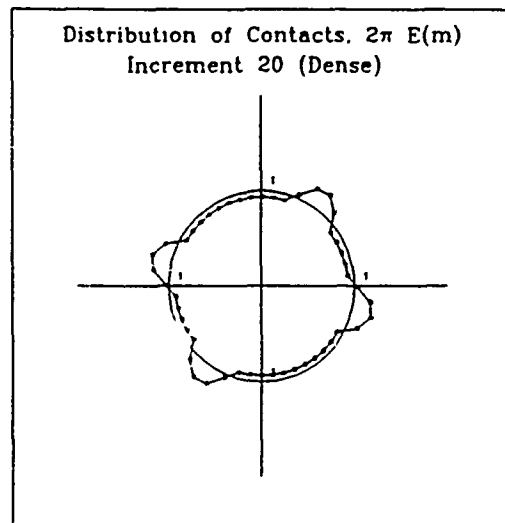
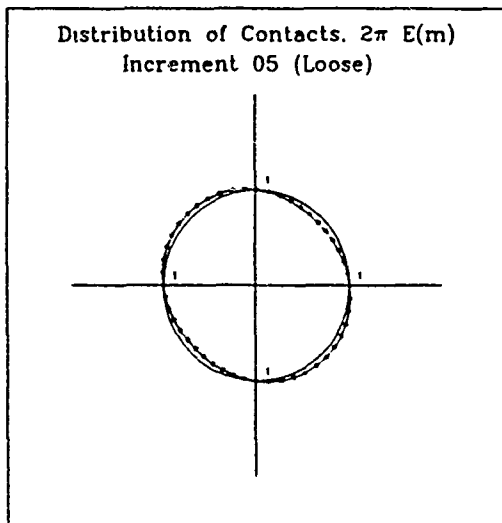
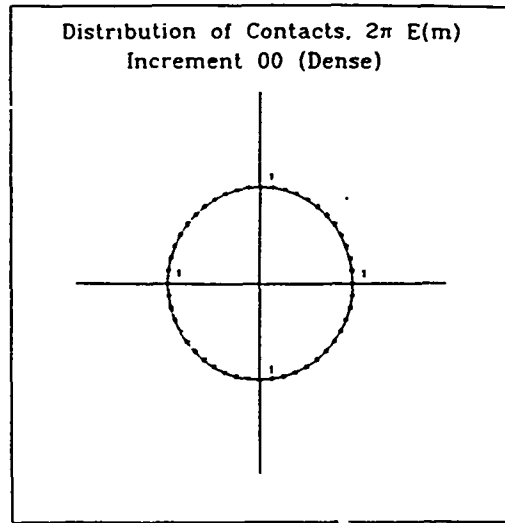
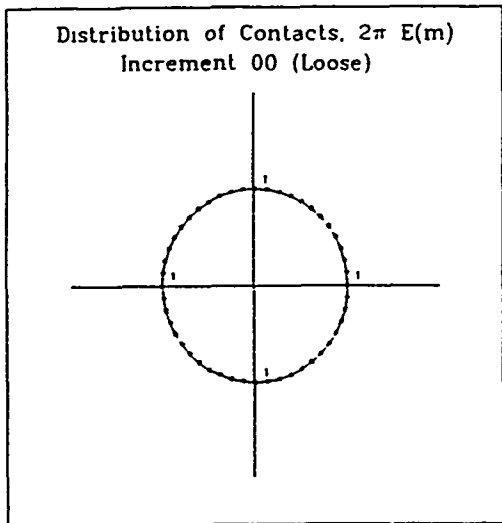


Figure 6

Micromechanics of flow and failure modes of particulate media over a wide range of strain rates

Sia Nemat-Nasser and B. Balendran

Center of Excellence for Advanced Materials, Department of Applied Mechanics and Engineering Sciences, University of California, San Diego, La Jolla, CA 92093

Abstract

A basic framework is proposed for the systematic micromechanically-based constitutive modeling of the flow of granular materials, over a broad range of strain rates, from quasi-static to high strain rates. Frictional effects, pressure sensitivity, and coupling between shearing and volumetric strain are included. Stress-induced anisotropy in elastic and inelastic instantaneous material response is incorporated. The model is flexible enough to account for both rate-independent and rate-dependent frictional sliding and rolling of the grains. For illustration, typical results for biaxial and simple shearing of granular materials with various void ratios are calculated in monotonic, as well as cyclic loading, and they are shown to accurately correspond to actual observations.

1. INTRODUCTION

The resistance of a granular mass to plastic flow is strongly influenced by the corresponding interparticle friction and the void ratio. In addition, existing experimental results suggest that the fabric structure and its changes play an important role in the mechanical behavior of granular materials. As an implicit measure of the granular fabric, the statistical distribution of contact normals is widely used. In a virgin sample, the distribution may be isotropic. However, during a course of shearing, the distribution of contact normals may develop a strong bias, leading to a strong anisotropy.

A number of experiments has been conducted using photoelastic cylindrical granules to study the variation of the distribution of the contact normals, in a course of deformation; see Konishi *et al.* (1982), Oda *et al.* (1985), and Subhash *et al.* (1991). In these experiments, it has been observed that the distribution of the contact normals changes in such a manner as to produce a greater concentration of contact normals along an orientation which parallels the direction of the maximum principal compressive stress.

During the course of granular flow, on a microscale, grains override each other, resulting in sliding on planes which pass through active contact points. We denote by ν the angle that the microscopic plane of motion at a typical contact point makes with the macroscopic shearing direction. If the angle ν is positive as in Fig. 1a, then the normal force transmitted to the

granules tends to hinder their sliding and rolling motion, resulting in an increase in the effective resistance to the macroscopic shearing. On the other hand, if the angle v is negative as in Fig. 1b, the motion of the granules is assisted by the normal force, and hence, the effective resistance to macroscopic shearing is reduced. When sliding occurs, the motion of the granules with positive angles of dilatancy tends to contribute to the overall dilatancy, whereas the granules with negative angles of dilatancy tend to produce densification.

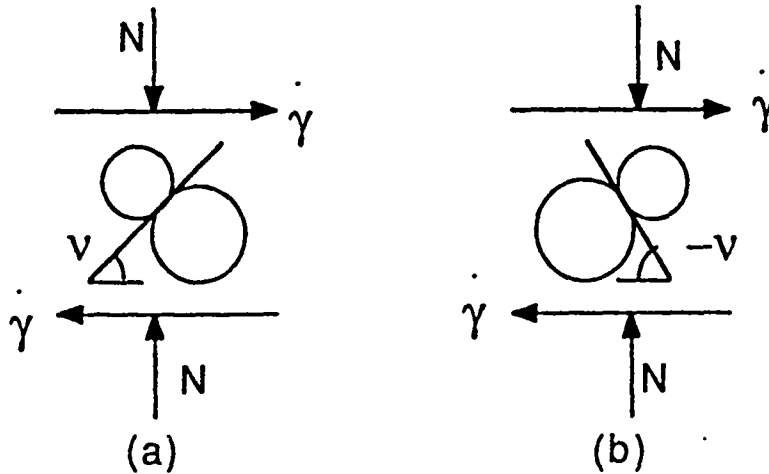


Figure 1. Active contacts with (a) positive angle of dilatancy (b) negative angle of dilatancy.

During the course of deformation, more and more contacts with positive dilatancy angles, v , are formed, while contacts with negative v are continually lost. This process tends to increase the resistance to continued loading and decrease the material resistance in unloading and reverse loading. In this manner, the potential for dilatancy in continued loading, and for densification in unloading and reverse loading, is increased.

In addition to the resistance due to interparticle friction and the fabric, the confining pressure affects the material resistance to flow. This is an isotropic effect, depending on the density of the granular mass. This resistance increases with the density of the granular mass.

We consider the planar deformation† of granular materials in the x_1, x_2 -plane. Based on the above observation, we write the sliding criterion, a variant of Coulomb's criterion, for granular flow in a direction s , in a plane with unit normal m , as follows:

$$\begin{aligned} f_1 &\equiv \tau_n + \sigma_n \tan\phi_1^L - p \tan\phi_2 \leq 0, & \text{for loading,} \\ f_2 &\equiv -\tau_n + \sigma_n \tan\phi_1^U - p \tan\phi_2 \leq 0, & \text{for unloading,} \end{aligned} \quad (1)$$

where τ_n and σ_n are the shear and normal stresses on the sliding planes, given by

$$\tau_n = \sigma : (m \otimes s), \quad \sigma_n = \sigma : (m \otimes m), \quad p = -tr(\sigma)/2, \quad (2)$$

with the usual sign convention of continuum mechanics in which tensile stress components are positive. Here dyadic notation is used and $:$ denotes a double contraction, e.g., $\sigma : (m \otimes s) \equiv \sigma_{ij} m_i s_j$, with σ denoting the Cauchy stress with rectangular Cartesian

† Planar deformation corresponds to two-dimensional flow of cylindrical granules.

components, σ_{ij} , and repeated indices are summed.

In the sliding criterion (1), the angles, ϕ_1^L and ϕ_1^U , represent the effective frictional resistance to sliding by the interparticle friction as well as the fabric structure, while the angle ϕ_2 represents the resistance due to the isotropic interaction of particles. The angle ϕ_1^L is for continued loading, whereas ϕ_1^U corresponds to unloading and reverse loading. Based on comments made at the beginning of this section, the angle ϕ_1^L is *always positive and greater than the angle ϕ_1^U which may be either positive or negative, depending on the local granular fabric, where a negative value corresponds to the collapse of voids upon unloading and load reversal. This has been observed in photoelastic experiments as well as in numerical modeling, and is an important ingredient of the present theory. The energy equation then ensures that the process is in fact dissipative.*

The resistance to flow due to the interaction of particles, increases as the material densifies and decreases when the material dilates. Hence, the angle ϕ_2 varies with the void ratio.

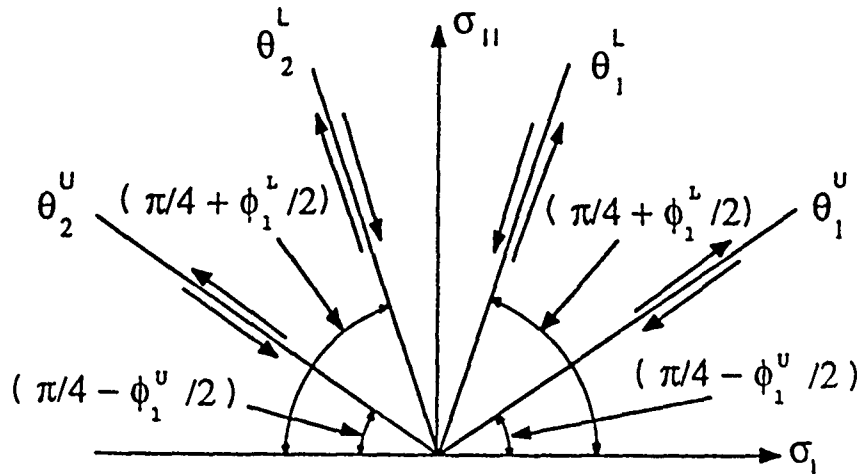


Figure 2. Sliding planes in loading and unloading.

Sliding takes place on planes where f , given by (1), is maximum and non-negative. There are two planes on which f attains maximum values. These planes are symmetrical about, and make angles of $\pi/4 + \phi_1^L/2$ (θ_1^L, θ_2^L -planes for loading) and $\pi/4 - \phi_1^U/2$ (θ_1^U, θ_2^U -planes for unloading), with the direction of the greater principal stress, σ_1 ; see Fig. 2. Therefore, the sliding criterion, (1), can be expressed in terms of pressure, p , and the effective shear stress, q , in the form,

$$-M^U p \leq q \leq M^L p, \quad q = (1/2 \sigma' : \sigma')^{1/2}, \quad (3)$$

$$M^L = \sin(\phi_1^L + \phi_2)/\cos\phi_2, \quad M^U = \sin(\phi_1^U + \phi_2)/\cos\phi_2. \quad (4)$$

Denote by δ the angle that the effective microscopic plane of motion makes with the corresponding sliding plane. From the energy equation for the frictional loss on the effective microscopic plane of motion, the angle of dilatancy, δ , is related to the microscopic, ϕ_μ , and macroscopic (ϕ_1^L, ϕ_1^U , and ϕ_2), angles of friction by (see Nemat-Nasser, 1980),

$$\begin{aligned} \delta &= \phi_1^L + \phi_2 - \phi_\mu \quad \text{for loading,} \\ \delta &= \phi_1^U + \phi_2 - \phi_\mu \quad \text{for unloading.} \end{aligned} \tag{5}$$

2. CONSTITUTIVE EQUATIONS

We seek to obtain the phenomenological constitutive relations implied by the double-sliding theory, in line with the flow mechanism discussed in Section 1. To this end, we assume that the kinematics of the instantaneous granular flow is expressed by the velocity gradient $L = \partial v / \partial x$, consisting of a symmetric part D , the deformation rate tensor, and an antisymmetric part W , the spin tensor. Each of these rates are separated into elastic and plastic parts as follows:

$$D = D^* + D^p, \quad W = W^* + W^p, \tag{6}$$

where superscript p denotes the plastic part which is due to the shearing along the sliding directions, and the superscript $*$ denotes the elastic part; note that W^* also includes the rigid spin.

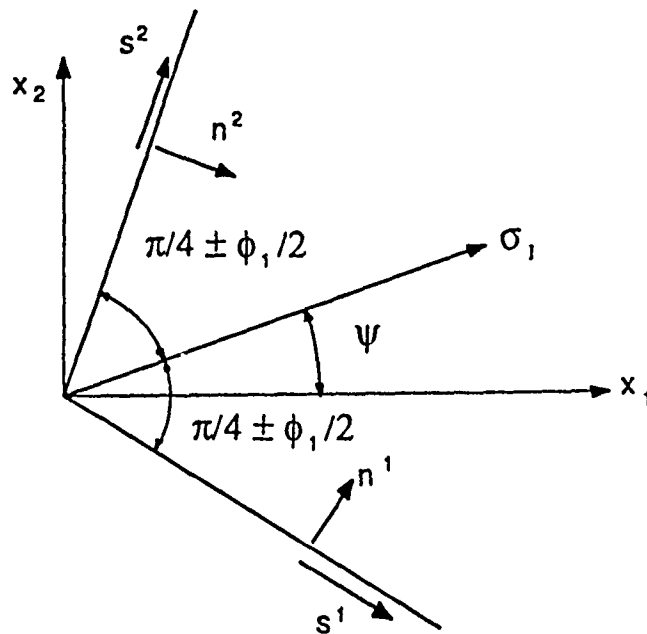


Figure 3. The unit vectors in the direction and normal to the direction of sliding

In plane flow, there are two preferred sliding lines, symmetrically situated about the principal stress directions. The first, the θ_1 -line, makes an angle $\theta_1 = \psi - \pi/4 \mp \phi_1/2$, and the second, the θ_2 -line, makes an angle $\theta_2 = \psi + \pi/4 \pm \phi_1/2$, with the positive x_1 -axis. *Here and in the sequel, both loading and unloading are considered together, superscripts L and U are omitted, and the symbols \pm and \mp are used where necessary, with the upper and lower signs corresponding to the loading and unloading, respectively.* Assuming that the plastic deformation is due to the shearing on the sliding lines, and denoting the rate of shearing on the θ_α -sliding system by $\dot{\gamma}^\alpha$ ($\alpha = 1, 2$), we write the plastic part of the velocity gradient as

$$D^p = \pm \dot{\gamma}^{\alpha} p^{\alpha}, \quad W^p = \pm \dot{\gamma}^{\alpha} r^{\alpha} \quad (\alpha \text{ summed}), \quad (7)$$

$$p^{\alpha} = \frac{1}{2}(s^{\alpha} \otimes m^{\alpha} + m^{\alpha} \otimes s^{\alpha}) \pm m^{\alpha} \otimes m^{\alpha} \tan \delta,$$

$$r^{\alpha} = \frac{1}{2}(s^{\alpha} \otimes m^{\alpha} - m^{\alpha} \otimes s^{\alpha}). \quad (8)$$

Here, s^{α} and m^{α} are unit vectors in the direction and normal to the direction of sliding of the α -sliding system, and the angle ψ is the orientation of the smallest (compressive) principal stress direction with the x_1 -axis (see Fig. 3).

In the present model, it is assumed that the fabric is not affected by the plastic shearing deformation along the active sliding planes, and that only the elastic part of the velocity gradient, $L^* = D^* + W^*$, is responsible for the change in fabric, giving rise to stress changes. To describe the local elastic response, we consider the objective Jaumann rate of stress,

$$\delta = \dot{\sigma} - W\sigma + \sigma W,$$

and relate it to the elastic deformation rate by

$$\delta = C:D^* = C:(D - D^p), \quad (9)$$

where C is the instantaneous elasticity tensor. Further, based on the experimental observations that the fabric (defined by the distribution of contact normals) rotates with the principal stress directions, we assume,

$$W_{12}^* = -\dot{\psi} = (\sigma'_{11}\dot{\sigma}'_{12} - \sigma'_{12}\dot{\sigma}'_{11})/2q^2. \quad (10)$$

Denoting the unit deviatoric stress tensor by μ , and in view of (10), the plastic part of the velocity gradient, D^p , can be rewritten in the form,

$$D_{kk}^p = \pm \dot{\gamma} B, \quad W_{12}^p = \pm (\dot{\gamma}^1 - \dot{\gamma}^2),$$

$$D^p = \mp \alpha \frac{\dot{\mu}}{\sqrt{2}} \pm \dot{\gamma} \frac{\mu}{\sqrt{2}}, \quad \mu = \frac{\sigma'}{\sqrt{2}q}, \quad \alpha = \frac{\sin(\phi_1 - \delta)}{\cos \delta},$$

$$\dot{\gamma} = (\dot{\gamma}^1 + \dot{\gamma}^2) \frac{\cos(\phi_1 - \delta)}{\cos \delta}, \quad B = \pm \frac{\sin \delta}{\cos(\phi_1 - \delta)}, \quad (11)$$

where α is the noncoaxiality coefficient, characterizing the deviation of the plastic strain rate orientation from the orientation of the stress deviator, B is the dilatancy parameter, and $\dot{\gamma}$ is the effective inelastic strain rate.

The elastic response of a granular mass, in general, is anisotropic when the stress state is anisotropic. Many authors, however, have used isotropy to simplify the corresponding results. If the elasticity is assumed to be isotropic, (see Balendran and Nemat-Nasser (1991) for a discussion of the general case), with bulk modulus, K , and shear modulus, G , then the constitutive equations reduce to

$$\delta_{kk} = 2K(D_{kk} \mp \dot{\gamma} B),$$

$$\delta' = 2G \left[D' \pm \beta(1 - \mu \otimes \mu):D' \mp \dot{\gamma} \frac{\mu}{\sqrt{2}} \right], \quad \beta = \frac{G\alpha}{q \mp G\alpha}. \quad (12)$$

For rate-independent sliding, the average slip rate, $\dot{\gamma}$, is related to the deformation rate through the rate form of the sliding criterion as,

$$\dot{\gamma} = H (\pm \sqrt{2G} \mu \cdot D' + M K D_{\mu}).$$

$$H = (kp + G \pm MKB)^{-1}, \quad h = \frac{\partial M}{\partial \gamma}. \quad (13)$$

The framework is flexible enough to account for rate-dependent sliding which will be discussed elsewhere; Balendran and Nemat-Nasser (1991).

Equations (12) correspond to the usual J_2 -plasticity, except for two very important differences. First, there is a shearing-induced dilatancy or densification embedded in (12) by the dilatancy parameter B , and second, the term associated with β in (12) renders the plastic strain rate noncoaxial with the stress deviator. As has been pointed out by many authors (Spencer, 1964, 1982; Rudnicki and Rice, 1975; Mehrabadi and Cowin, 1978; Nemat-Nasser *et al.*, 1981; and Nemat-Nasser, 1983), this is due to the presence of friction and is removed only if $\phi_1 = \delta$, *i.e.*, when the friction coefficient is equal to the dilatancy angle. This, however, cannot, in general, be true.

3. HARDENING AND SOFTENING

Consider now the evolution of the effective frictional resistance in loading and in unloading. It is convenient to write the evolution equations in terms of the frictional coefficients defined by,

$$\mu_1^{L,U} \equiv \tan \phi_1^{L,U}, \quad \mu_2 \equiv \tan \phi_2. \quad (14)$$

We consider a very simple model where the rate of change of the effective frictional resistance due to fabric, with respect to the rate of shearing, is linearly related to its deviation from the maximum saturation value, $\mu_s = \tan \phi_s$. We also assume that the resistance to inelastic shearing due to pressure becomes very large as the void ratio reaches its smallest value; Nemat-Nasser and Shokoh (1979). In this manner, we write the evolution equations for the frictional resistances as follows:

$$\mu_2 = \tan(\phi_\mu - \phi_s) + a \left[\frac{1}{(e - e_m)^n} - \frac{1}{(e_c - e_m)^n} \right]. \quad (15)$$

$$\frac{\partial \mu_1^L}{\partial \gamma} = b (\mu_s - \mu_1^L), \quad \text{for continued loading, } i.e., \dot{q} - M^L \dot{p} > 0,$$

$$\frac{\partial \mu_1^U}{\partial \gamma} = b (\mu_s - \mu_1^U), \quad \text{for reverse loading, } i.e., \dot{q} + M^U \dot{p} < 0, \quad (16)$$

where e is the void ratio, e_c is the critical void ratio, and e_m is the minimum void ratio. We further assume that both sliding conditions are always met, both in loading and in unloading. This results in,

$$q = M^L p = -M^U p, \quad \phi_1^L + \phi_1^U = -2\phi_2. \quad (17)$$

This assumption also implies that when a granular mass (in present illustration) is subjected to only hydrostatic stress, the microstructure is isotropic and the macroscopic angles of friction are related to the void ratio by,

$$\phi_1^L = \phi_1^U = -\phi_2 = \tan^{-1}(\mu_2(e)). \quad (18)$$

4. EXAMPLES

We now consider several illustrative examples in order to bring out the features embedded in our general constitutive relations. We start with a hydrostatic state of stress and set the initial values of the angles of friction from (18) for the given void ratio of the sample. In all examples, we use $G = 100p_0$, $K = 200p_0$, $a = 5$, $b = 20$, $n = 5$, $\phi_s = 40^\circ$, $\phi_\mu = 15^\circ$, $e_m = 0.2$, and $e_c = 0.6$, where p_0 is the initial pressure.

We consider the application of the proposed model to simple shearing of a granular material at constant confining pressure, ($\dot{\sigma}_{11} = \dot{\sigma}_{22} = 0$, $L_{11} = L_{21} = 0$), and biaxial shearing of a granular material at constant lateral stress, ($\dot{\sigma}_{11} = 0$, $L_{12} = L_{21} = 0$). The results of these simulations are given in the form of relations between the stress ratio, (σ_{12}/p in simple shear and σ'_{11}/p in biaxial compression), void ratio, e , and shear strain ($F_{12}/2$ in simple shear and $(F_{11} - F_{22})/2$, in biaxial compression) where F is the deformation gradient. In Fig.4, the results from the simulation of monotonic shearing are given. They correlate very well with the following experimentally observed phenomena:

- (1) There is always an initial densification, the magnitude of which decreases as the initial void ratio approaches its minimum value.
- (2) If the sample is dense, then the initial densification is followed by dilatancy which continues until a critical void ratio is attained asymptotically. The stress ratio increases monotonically in densification and reaches its peak value during dilatancy and then asymptotically drops to a critical value as the critical void ratio is reached.
- (3) If the sample is loose, it densifies continually until the critical void ratio is reached asymptotically. The stress ratio increases monotonically and asymptotically reaches a critical value.

The results from the simulation for five cycles of shearing deformation are given in Fig.5. They show:

- (1) When the shearing is reversed, the material tends to densify, resulting in a net densification at the completion reversed shearing.
- (2) If the shearing is continued in the opposite direction, the sample tends to dilate.
- (3) Upon completion of each cycle of deformation, there is a net densification.
- (4) The amount of net densification per cycle decreases with the number of cycles.

5. CONCLUSION

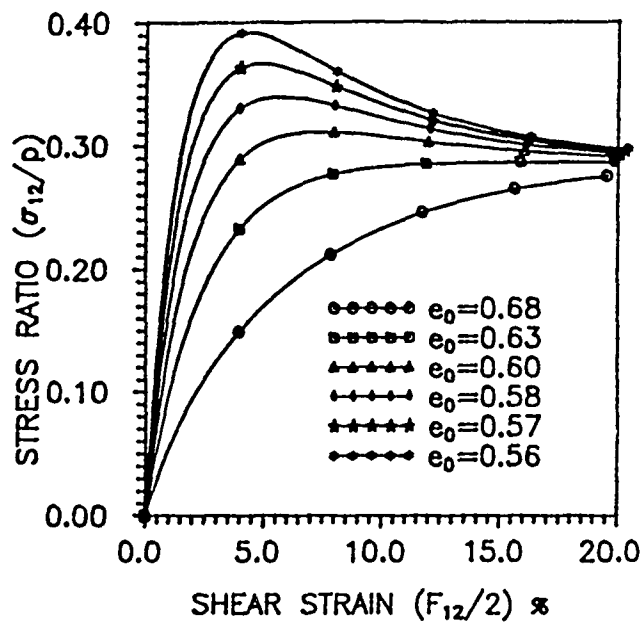
A physically-based elastoplastic constitutive model is presented for dilatant, pressure-sensitive, workhardening materials. The model is applied to simple shearing and biaxial deformation of granular materials, both in monotonic and in cyclic deformation, and it has been shown to predict all the basic features of the shear deformation of granular materials.

6. ACKNOWLEDGEMENTS

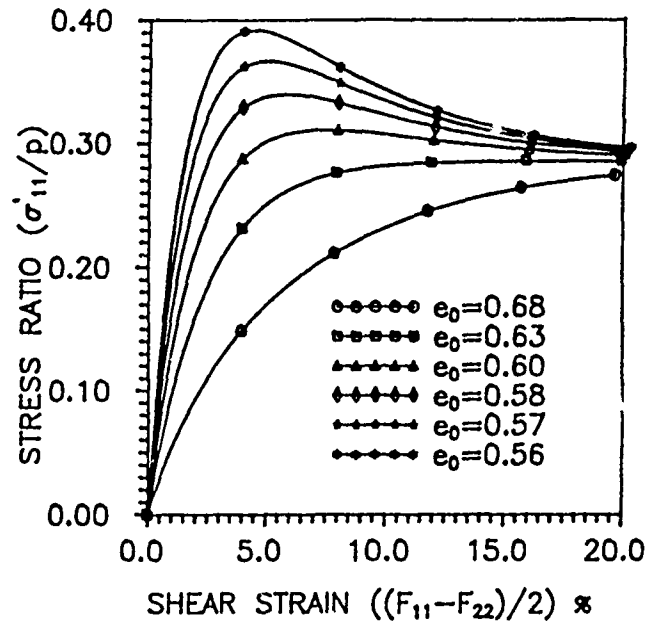
This work has been supported by the Air Force Office of Scientific Research under Grant No. AFOSR-87-0079 to the University of California, San Diego.

7. REFERENCES

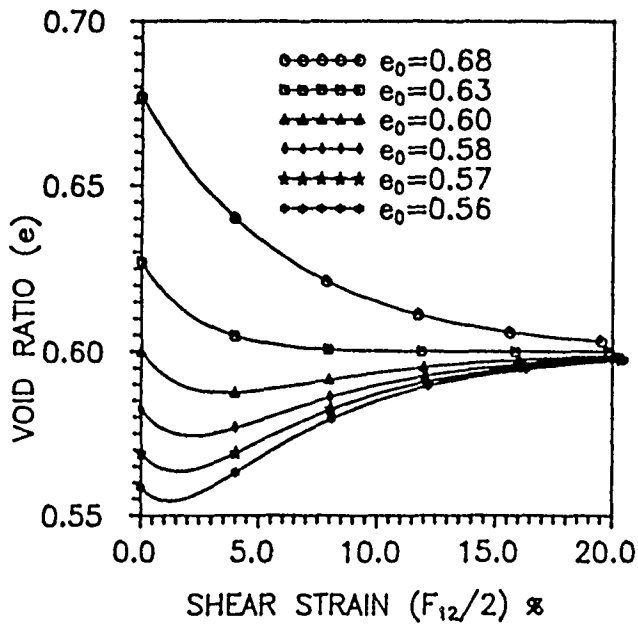
- 1 Konishi, J., Oda, M., Nemat-Nasser, S., 1982, Inherent Anisotropy and Shear Strength of Assembly of Oval Cross-Sectional Rods, *Deformation and Failure of Granular Materials*, Vermeer, P.A., Luger, H.J., eds., A.A. Balkema Publishers, 403-412.
- 2 Oda, M., Nemat-Nasser, S., Konishi, J., 1985, Stress-Induced Anisotropy in Granular Masses, *Soils and Foundations*, 25, No.3, 85-97.
- 3 Subhash, G., Nemat-Nasser, S., Mehrabadi, M.M., Shodja, H.M., 1991, Experimental Investigation of Fabric-Stress Relations in Granular Materials, *Mechanics of Materials*, 11, 87-106.
- 4 Nemat-Nasser, S., 1980, On Behavior of Granular Materials in Simple Shear, *Soils and Foundation*, JSSMFE, 20, No.3, 59-73.
- 5 Balendran, B., Nemat-Nasser, S., 1991, Double Sliding Model for Cyclic Deformation of Granular Materials, Including Dilatancy Effects, In Preparation.
- 6 Spencer, A.J.M, 1964, A Theory of the Kinematics of Ideal Soils Under Plane Strain Conditions, *J. Mech. Phys. Solids*, 12, 337-351.
- 7 Spencer, A.J.M, 1982, Deformation of Ideal Granular Materials, *Mechanics of Solids, The Rodney Hill 60th Anniversary Volume*, , Hopkins, H.G, and Sewell, M.J, eds., Pergamon Press, Oxford, 607-652.
- 8 Rudnicki, J.W., Rice, J.R., 1975, Conditions for the Localization of Deformation in Pressure-Sensitive Dilatant Materials, *J. Mech. Phys. Solids*, 23, 371-394.
- 9 Mehrabadi, M.M, Cowin, S.C, 1978, Initial Planar Deformation of Dilatant Granular Materials, *J. Mech. Phys. Solids*, 26, 269-284.
- 10 Nemat-Nasser, S., Mehrabadi, M.M, Iwakuma, T., 1981, On Certain Macroscopic and Microscopic Aspects of Plastic Flow of Ductile Materials, in *Three-Dimensional Constitutive Relations and Ductile Fracture*, Proc. IUTAM Symp., Nemat-Nasser, S., ed., North-Holland Publishers, 157-172.
- 11 Nemat-Nasser, S., 1983, On finite plastic flow of crystalline solids and geomaterials, *ASME J. Appl. Mech.*, 50, 1114-1126.



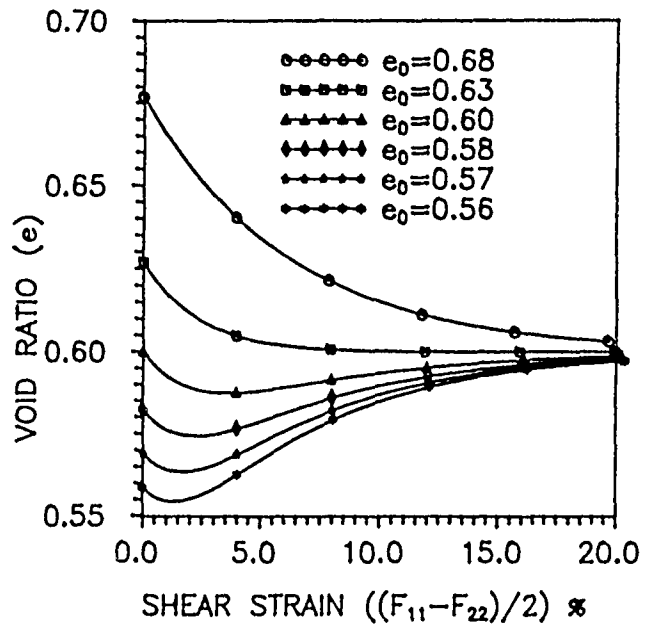
(a)



(b)



(c)



(d)

Fig. 4. Relation between stress ratio, volumetric strain and shear strain in monotonic shearing; (a), (c) in simple shearing; (b), (d) in biaxial deformation.

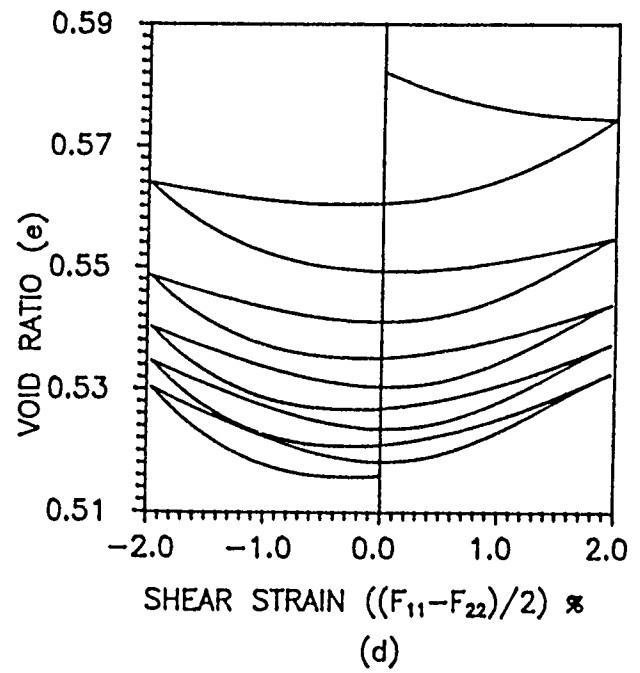
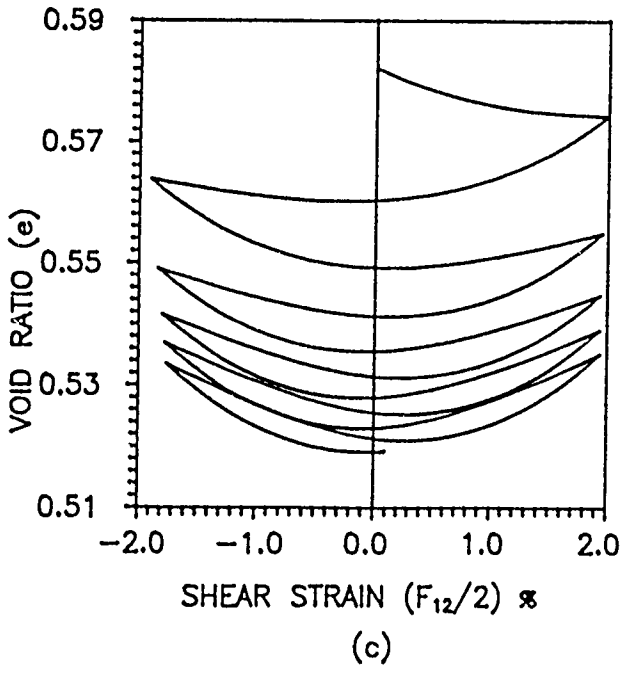
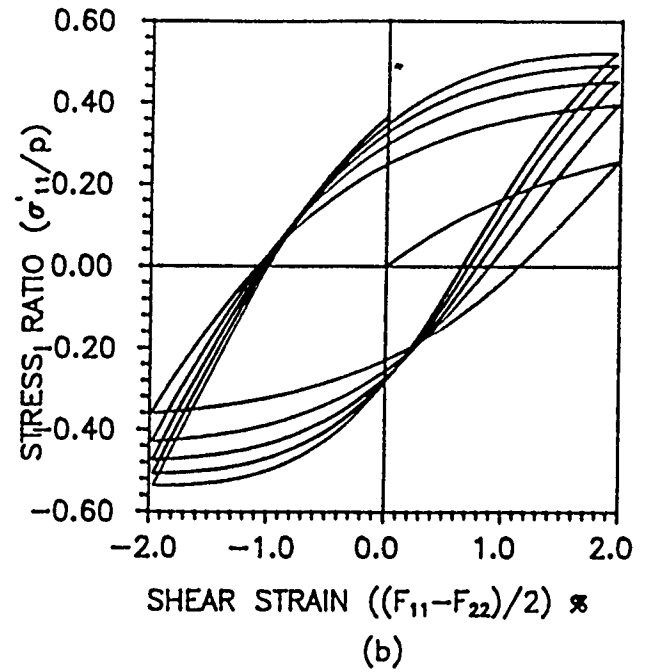
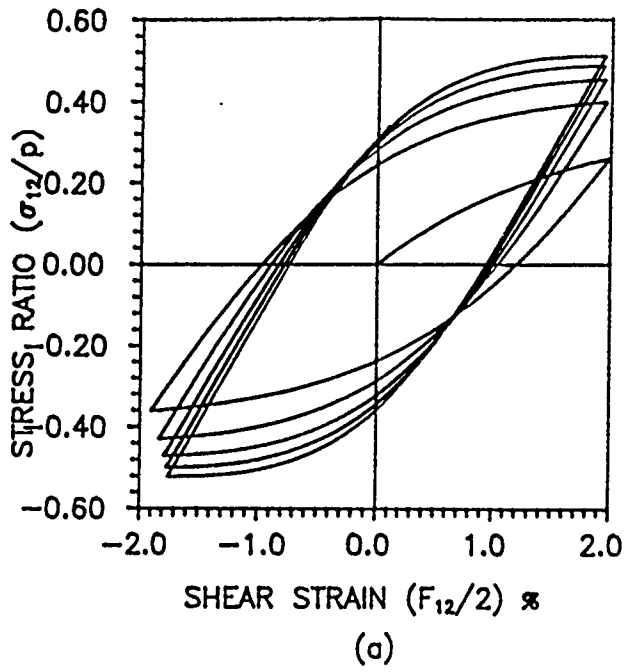


Fig. 5. Relation between stress ratio, volumetric strain and shear strain in cyclic shearing; (a), (c) in simple shearing; (b), (d) in biaxial deformation.

ENERGY DISSIPATION IN INELASTIC FLOW
OF COHESIONLESS GRANULAR MEDIA

N. Okada
and
S. Nemat-Nasser

Center of Excellence for Advanced Materials
Department of Applied Mechanics and Engineering Sciences, R-011
University of California at San Diego
La Jolla, CA 92093

July 26, 1991

ABSTRACT

The results of a systematic study of energy dissipation in cohesionless granular media are presented. First, the relation between the excess pore water pressure, accumulated in a water-saturated granular mass, and the corresponding external work in cyclic loading is studied experimentally. Second, a micromechanical model of internal energy dissipation due to slip between contacting granules is introduced, and the results are compared with experimental measurements.

A series of undrained experiments is carried out using water-saturated large hollow cylindrical specimens. Most experiments are performed under displacement-controlled conditions. The imposed cyclic angular displacement which produces the applied shear strain, has a triangular time variation with constant strain rate over each quarter cycle. The specimens are subjected to two sequences of loading in order to simulate the reliquefaction phenomenon. External work per unit volume is calculated from the experimental results, and its correlation with the excess pore water pressure is examined. In the first loading, a unique nonlinear relation is observed to exist between the excess pore water pressure and the external work per unit volume. This relation is found to be independent of the shear strain amplitude. In the second loading, however, this relation is a function of strain amplitude. The cyclic shear strength is seen to have increased in the second loading, because of the strain history of the first loading.

External work supplied to cohesionless granular media is mainly consumed by the frictional slip between contacting granules. A micromechanical model is developed and validated by the experimental results. It is shown that the internal dissipation per unit volume in cohesionless granular media, can be expressed in terms of the time-history of the applied effective pressure and a single scalar parameter which depends on the density and strain amplitude. The model is further validated by torsion tests with random variation in the applied strain amplitude. The theoretical predictions are in excellent agreement with the experimental results.

Table of Contents

ABSTRACT	ii
Table of Contents	iii
List of Figures	iv
1. INTRODUCTION	1
2. EXPERIMENTAL SETUP	3
2.1 Motivation and Background	3
2.2 Specimen Preparation and Installation	3
2.3 Experimental Procedure and Data Acquisition	7
3. EXPERIMENTAL RESULTS	17
3.1 First Loading	17
3.2 Second Loading	19
4. THEORETICAL MODELING	37
4.1 Energy Dissipation in Granular Media	37
4.2 Formulation of Frictional Energy Loss	39
4.3 Cyclic Torsional Loading	41
4.4 Random Torsional Loading	43
5. DISCUSSION	57
ACKNOWLEDGEMENT	58
REFERENCES	59

List of Figures

Figure 1. Triaxial load frame	10
Figure 2. Particle size distribution curve	11
Figure 3. Inner membrane and pedestal	12
Figure 4. Overall figure of built up molds	13
Figure 5. Specimen under applied vacuum with torque load cell and potentiometer	13
Figure 6. Overall assembly of MTS and triaxial load frame	14
Figure 7. Universal joint	15
Figure 8. Air clamp	15
Figure 9. Schematic diagram of air pressure and water supply system	16
Figure 10. Relation between shear strain and effective pressure in first loading of loose specimens; strain amplitudes are 0.2% and 1.0%	22
Figure 11. Relation between shear stress and effective pressure in first loading of loose specimens; strain amplitudes are 0.2% and 1.0%	23
Figure 12. Relation between shear stress and shear strain in first loading of loose specimens; strain amplitudes are 0.2% and 1.0%	24
Figure 13. Relation between external work per unit volume and excess pore water pressure in first loading of loose specimens	25
Figure 14. Relation between external work per unit volume and excess pore water pressure in first loading of dense specimens	26
Figure 15. Relation between shear stress and effective pressure in first loading of dense specimen subjected to random torsional loading	27
Figure 16. Relation between external work per unit volume and excess pore water pressure in first loading of both loose and dense specimens	28
Figure 17. Relation between shear strain and effective pressure in first and second loading of dense specimen whose strain amplitude is 0.5%	29

Figure 18. Relation between number of cycles and excess pore water pressure in first and second loading of both loose and dense specimens whose strain amplitude is 0.5%	30
Figure 19. Relation between external work per unit volume and excess pore water pressure in second loading of loose specimens where strain amplitude used in second loading is the same as in first loading	31
Figure 20. Relation between external work per unit volume and excess pore water pressure in second loading of dense specimens where strain amplitude used in second loading is the same as in first loading	32
Figure 21. Contours of external work per unit volume in relation between excess pore water pressure and shear strain amplitude in second loading of loose specimens	33
Figure 22. Contours of external work per unit volume in relation between excess pore water pressure and shear strain amplitude in second loading of dense specimens	34
Figure 23. Relation between external work and excess pore water pressure in second loading of loose specimens where strain amplitude used in second loading is different from that used in first loading	35
Figure 24. Relation between external work and excess pore water pressure in second loading of dense specimens where strain amplitude used in second loading is different from that used in first loading	36
Figure 25. Contour S and slips s^α in the considered region D	45
Figure 26. Changes of C_k against number of cycles in first and second loading of loose specimens	46
Figure 27. Changes of C_k against number of cycles in first and second loading of dense specimens	47
Figure 28. Changes of C_k against excess pore water pressure in first and second loading of loose specimens	48
Figure 29. Changes of C_k against excess pore water pressure in first and second loading of dense specimens	49
Figure 30. The C -values obtained experimentally	50
Figure 31. Relation between external work and calculated internal work in first loading of loose specimens	51
Figure 32. Relation between external work and calculated internal work in second loading of loose specimens	52

Figure 33. Relation between external work and calculated internal work in first loading of dense specimens	53
Figure 34. Relation between external work and calculated internal work in second loading of dense specimens	54
Figure 35. Relation between shear stress and effective pressure in second loading of dense specimen subjected to random torsional loading	55
Figure 36. Relation between external work and calculated internal work in first and second loading of dense specimen subjected to random torsional loading	56

1. INTRODUCTION

Liquefaction is a complex phenomenon in which fluid-saturated granular media may momentarily behave like fluids. It is an important aspect of earthquake-resistant foundation design of many structures, especially those located in coastal areas, which are often built on sand with high underground water levels. As liquefaction takes place under seismic loading, saturated sand behaves more like a fluid, and therefore fails to support the applied loads of the building. Severe damage to the structure is often the result. Damage resulting from liquefaction has been observed in the aftermath of many earthquakes; the Loma Prieta earthquake (1989), the Niigata earthquake (1964), and the Alaska earthquake (1964) are a few examples.

The mechanism of liquefaction is closely related to the dilatancy of granular media. Dilatancy was first studied by Reynolds (1885). It is defined as the rate of volume expansion in granular media per unit rate of shearing. The granules are rearranged during shear deformation, and this results in a change in the total volume. If the granular medium (*e.g.* sand) is water saturated, a tendency toward densification (negative dilatancy) results in an increase in pore water pressure and hence a decrease in the corresponding frictional resistance of the contacting granules. Consider a sample of sand which is saturated with water while contained in a flexible rubber membrane, and is subjected to a hydrostatic pressure denoted by P_o . Static equilibrium requires that the total internal pressure be P_o . The internal pressure may be divided into two separate parts: pore water pressure P_i which is carried by the water, and the effective pressure P which is carried by the sand as contact stresses at granule/granule and granule/boundary interfaces. Upon externally applied cyclic shearing, the granules are rearranged, resulting in a tendency towards a decrease in the water volume. This results in an increase in the pore water pressure, P_i , and a corresponding decrease in the effective pressure, P . In continued cyclic shearing, the pore water pressure at the termination of each cycle increases until it reaches a value close to the applied hydros-

tatic pressure, P_o . When this occurs, the contact resistance of the granules is essentially negligible, leading to loss of load-bearing capacity of the sand mass. The sample then ceases to behave like a solid body. This is what is meant by liquefaction, in the present paper; see Casagrande (1975) and Seed (1979).

Liquefaction has been experimentally treated extensively by a number of researchers; see, for example, Silver and Seed (1971), Castro (1975), and Ishihara and Yasuda (1975). Parameters influencing the onset of liquefaction of the sand within a control volume are identified and measured. These parameters typically include overall density, initial packing conditions, and granule size distribution; see Seed (1979), Miura and Toki (1982), and Tatsuoka *et al.* (1982). In addition to these internal characteristics, the applied loading also affects the onset and nature of liquefaction; see Ishihara and Towhata (1983, 1985), and Symes *et al.* (1984).

Previous work has, in general, studied liquefaction from the experimental point of view. Theoretical work has focused more on phenomenological considerations of this topic rather than a micromechanical approach. A unified energy model for densification and liquefaction of cohesionless sand was proposed by Nemat-Nasser and Shokooh (1979) who compared its prediction with experimental results of Peacock and Seed (1968), Youd (1970, 1972), and DeAlba *et al.* (1976), and obtained excellent agreements.

The present work correlates the results of an experimental program with a theoretical model based on micromechanics and energy principles. Models of this kind seek to relate the overall response of granular materials to the response of their microconstituents. Examples of micromechanical analyses of densification and liquefaction phenomena, which are also coordinated with experiments, are Nemat-Nasser (1980), Nemat-Nasser and Tobita (1982), and Nemat-Nasser and Takahashi (1984).

2. EXPERIMENTAL SETUP

2.1 Motivation and Background

Cohesionless granular materials support general external loads through contact friction. An experimental program must include compression and shearing of reproducible samples in a fully controlled manner with reliable data. The study of granular material behavior requires complex experimental facilities, with a closed-loop feedback system to control the experiment and to monitor the specimen deformation. The specimen geometry used for the present investigation is a large hollow cylinder, 25cm high, with inner and outer diameters of 20cm and 25cm, respectively. This geometry is such that in torsion, the shear stress remains (approximately) homogeneous throughout the thickness of the specimen; see Hight *et al.* (1983) for a detailed examination of this and related issues. The specimen is supported by a triaxial load frame; see Figure 1. The axial and torsional deformations are controlled through an MTS servohydraulic loading system. In addition, the specimen is subjected to lateral hydrostatic pressure, on both its inside and outside cylindrical surface. In this manner, triaxial states of stress can be imposed on the material under controlled conditions with complete data acquisition capability. This load frame to our knowledge is one of four that have been constructed to date. Our load frame is fully computer-controlled, where either the stress- or the strain-path can be preprogramed with mode switching capabilities.

2.2 Specimen Preparation and Installation

The granular material chosen for this study is Silica 60 manufactured by U.S. Silica. This sand is chosen for its fine particle size. This is necessary in order to avoid membrane penetration phenomena that would otherwise invalidate the test results. The particle size distribution is shown in Figure 2. The mean particle diameter is $220\mu\text{m}$

and the specific gravity of the sand is 2.645. Depending on the packing conditions, different void ratios are obtained; void ratio is defined as the ratio of the void volume and the sand volume. For Silica 60, the minimum and maximum void ratios are 0.631 and 1.095, respectively, these are measured by the JSSMFE method; Committee of JSSMFE on the Test Method of Relative Density of Sand (1979).

Special fixtures are used to prepare hollow cylindrical sand specimens. These fixtures include inner and outer molds to which rubber membranes are attached. The sand is initially supported on the bottom by a ring of porous metal with six evenly spaced fins, called the pedestal, that in combination with a mating top ring, called the cap, applies the torsional load to the specimen. The inner mold with attached rubber membrane is shown in Figure 3. The pedestal (with associated fins) is attached to the bottom support plate. The outer membrane is then slid over the inner membrane and fixed to the pedestal with o-rings. The outer mold is bolted in place and the top of the outer membrane is draped over the outer mold and held in place by o-rings. A separate fixture is installed on top of the outer mold (Figure 4) to prevent sand spillage on the rest of the triaxial load frame. This fixture also allows for an overflow amount of sand so that a desired packing condition can be obtained. The excess sand is removed later. The tube extending from the outer mold in Figure 4 is used to create a vacuum between the outer mold and outer membrane, thereby holding it securely in place.

It is well known that the initial packing condition of the sand has a noticeable effect upon the material response of the specimen; see Arthur and Menzies (1972), Oda (1972), and Miura and Toki (1982). The specimen preparation method must therefore achieve a consistent initial packing condition so that experiments are repeatable. To this end, a technique has been adopted in the soils community that is known as the rodding method. This method consists of pouring an approximately 2cm deep layer of sand into the mold and then inserting a rod into the latest layer approximately 1-1.5cm deep. The rod is moved around the circumference of the sand in an up-and-

down motion for 2-3 revolutions. This procedure is continued until the mold is filled. We have used 10 layers to obtain loose packing conditions and 14 layers for dense packing conditions. Experiments performed with loose conditions use the sand in a wet form. Here the sand has been air dried and then mixed with 8 weight percent water before pouring in the mold. The water is needed to prevent non-homogeneous initial packing conditions in the loose form. The void ratio for this condition varies between 0.865 and 0.874 . Experiments performed with dense conditions use only air-dried sand with the void ratio varying between 0.708 and 0.725 .

The fixture that was attached to the top of the outer mold is then removed and the amount of overfilled sand is 'cut' away. The cap is installed next; it consists of the same porous metal as the pedestal and also has six fins. A second vacuum system is connected to the cap and pedestal. The purpose of this vacuum system is to make the specimen rigid under atmospheric pressure. The vacuum level is maintained at 29.4 kN/m^2 . The first vacuum system that keeps the outer membrane affixed to the outer mold is then released. The outer mold is then removed, followed by the inner mold. A torque load cell unit is first bolted onto the ram of the triaxial load frame (Figure 1), and then bolted onto the cap. Next, a potentiometer is attached to the load frame (Figure 5). The potentiometer measures the twist angle during the experiment. A plexiglass chamber with steel bands is installed over the entire specimen, and a top plate is installed. The top plate is affixed to the bottom plate via stainless steel tie bars. The bars hold the chamber firmly in place. The purpose of the chamber is manifold. First, it provides confinement of the experiment if the sand mold loses integrity. Second, it holds the water that is used to apply hydrostatic pressure to the specimen. Finally, it is used as a viewport to observe the progress of the experiment.

The entire specimen assembly is now complete. The assembly is then raised to the level of the MTS load frame via a forklift. A special work frame has been built onto the MTS load frame. This work frame allows attachment of all connections to the

specimen assembly as well as providing a railway for installation and removal of the specimen into and from the MTS load frame. The overall assembly is shown in Figure 6.

The MTS load frame used for this experiment has an axial capability of 89 kN (20,000 lb), and a torsional capability of 565 N-m (5,000 lb-in) which can be used independently. This system uses a Digital Equipment Corporation PDP-11 computer to control the servohydraulic actuators. The system is closed-loop so that feedback from any selected transducer can be used to control the test.

Once the triaxial load frame has been rolled into place over the ram of the MTS load frame, it is secured in place by both vertical and horizontal clamps (Figure 1). The hydraulics for the MTS system are turned on and the MTS ram is raised to the level of the universal joint (Figure 7), using displacement control. An air clamp (Figure 8) that is fixed to the top of the MTS ram is then actuated and grips the universal joint on the bottom of the ram of the triaxial load frame. The universal joint is required to accommodate any misalignment between the ram of the MTS load frame and the ram of the triaxial load frame.

The first step in the experimental procedure is to fill the plexiglass chamber with water until the specimen is completely submerged. The remaining space above the specimen is pressurized with air to 29.4 kN/m^2 , which is the same value as the vacuum inside the specimen. During this operation the vacuum in the specimen is released and water pressurized in such a manner as to keep the effective pressure in the specimen constant, 29.4 kN/m^2 .

The specimen is then water saturated in the following manner. To attain full saturation, first the specimen is saturated with CO_2 gas through the porous metal in the pedestal and cap. The flow of gas is continued until all air is removed from the specimen. CO_2 gas is used because of its high solubility in water. A fixed amount, 4 liters, of de-aired water is used to saturate the specimen. The small amounts of air and CO_2

gas remaining in the specimen must then be removed as much as possible. The pore water pressure is then increased to 196kN/m^2 as back pressure, using a buret system, while at the same time the external hydrostatic pressure is increased to 225.4kN/m^2 so as to keep the effective pressure constant (29.4kN/m^2) during this procedure. This procedure reduces the volume of the excess gas in the specimen due to the relatively high pore water pressure.

To perform experiments of this type, it is required that the specimen be highly saturated. The degree of saturation is measured by the B-value. To measure the B-value the specimen must be in the undrained condition. This condition is met by closing the valve to the buret, ensuring that the specimen remains at a fixed volume. The specimen is said to be perfectly saturated ($B=1$) if an incremental increase in external hydrostatic pressure has the effect of increasing the pore water pressure in the specimen by an identical amount. The B-value is defined as the ratio of the incremental increase of pore water pressure to the incremental increase of hydrostatic pressure. The values for all of our experiments are in excess of 0.99.

The last step of specimen preparation is to increase the effective pressure to 196kN/m^2 . To do this, the valve to the buret is reopened, allowing water to drain from the specimen. The external hydrostatic pressure is thereby increased to 392kN/m^2 , where pore water pressure is 196kN/m^2 . A schematic diagram of the pressurization system is shown in Figure 9. Finally, the specimen is left undisturbed in this condition to isotropically consolidate for a period of 3 hours.

2.3 Experimental Procedure and Data Acquisition

The MTS load frame has a computer-operated controller system. The computer operates three independent controllers. Each controller has three independent feedback channels. Controller number one is associated with the vertical movement of the

MTS/triaxial load frame ram assembly; channel one is used to monitor the load from the torque load cell, whereas channel two is used to monitor the vertical displacement of the specimen. Channel three is not used with any controller. Controller number two is associated with the pressure; channel one is used to monitor the chamber pressure, P_o , and channel two is used to monitor the pore water pressure, P_i . Controller number three is associated with the twist of the ram assembly; channel one monitors the torque from the torque load cell and channel two monitors the angle of twist from the potentiometer.

The experiment is conducted by using two closed-loop feedback systems. System one uses channel one of controller one in load control to keep the specimen in a state of hydrostatic compression in accord with the external pressure, P_o . The second feedback system uses channel two of controller number three in displacement control to cyclically twist the specimen to desired shear strain amplitudes and at desired shear strain rates. The imposed cyclic angular displacement which produces the applied shear strain, has a triangular time variation with constant strain rate, $2/3$ %/minute over each quarter cycle. Shear strain amplitudes are 0.2%, 0.5%, and 1.0% for both loose and dense specimens. Tests at 0.4% and 2.0% shear strain amplitudes are performed on dense specimens. All tests are continued until the excess pore water pressure reaches 95% of the initial effective pressure, *i.e.*, 186.2kN/m^2 . In actuality, the tests are stopped at the end of the cycle after which transducer two of controller two (pore pressure transducer) reaches a value of 382.2kN/m^2 . This entire process is defined as the *first loading*.

The valve to the buret is then opened and the pore water pressure, P_i , is reduced to its initial value of 196kN/m^2 . The specimen is not disturbed for three hours for reconsolidation purposes. The valve to the buret is closed and then the exact procedure for the first loading is repeated. This is then called the *second loading*. After the second loading, the experiment is disassembled. Care is taken to remove the sand

from the specimen and place it in an oven for drying. The sand is dried for 24 hours and then weighed.

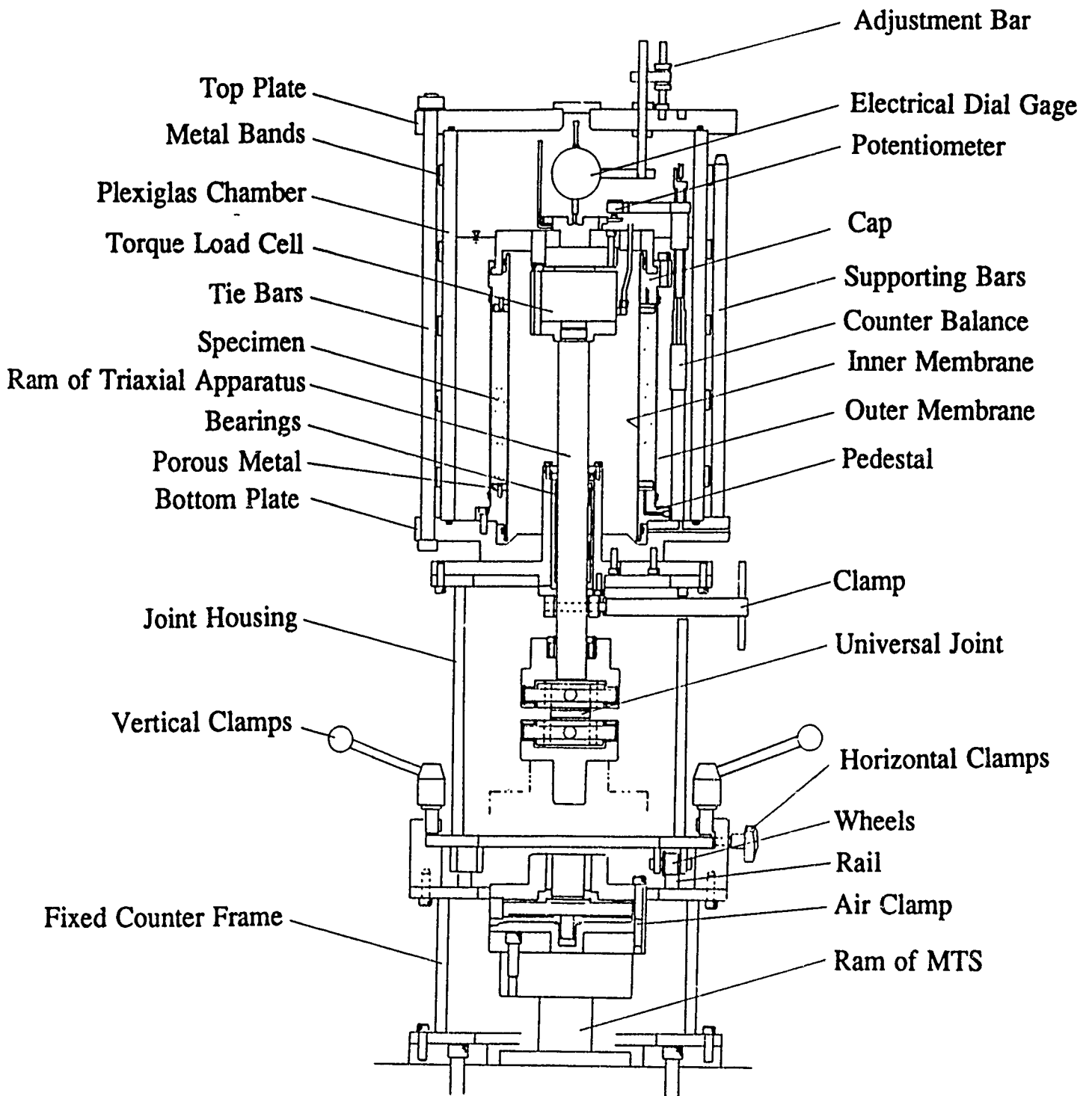


Figure 1. Triaxial load frame

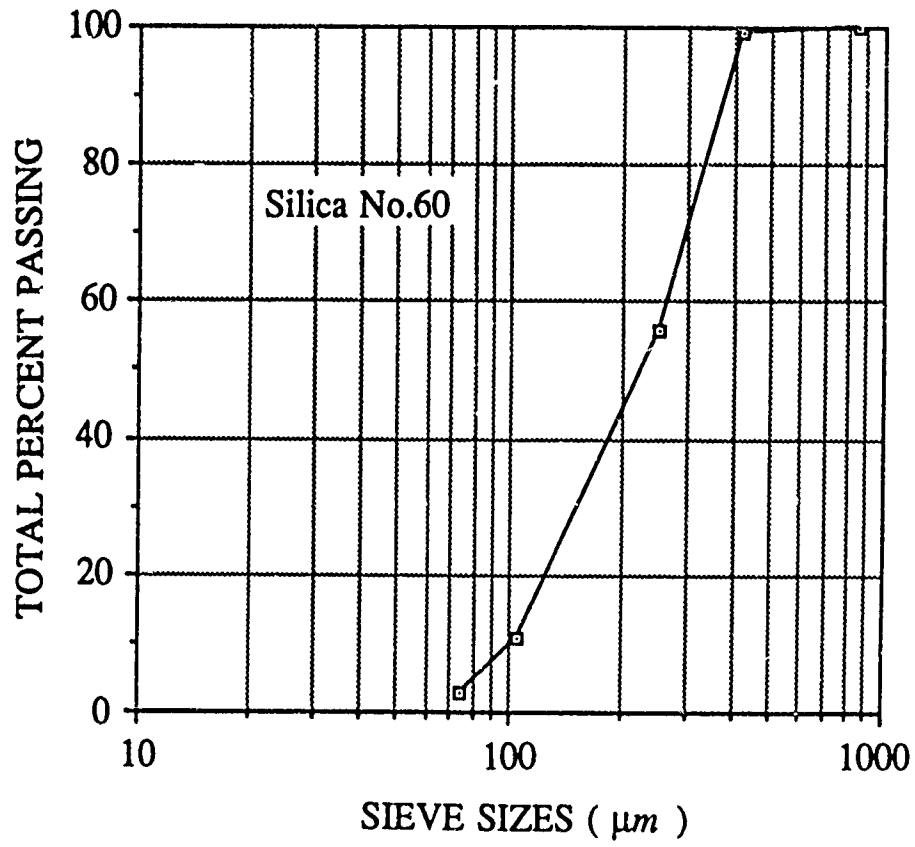


Figure 2. Particle size distribution curve

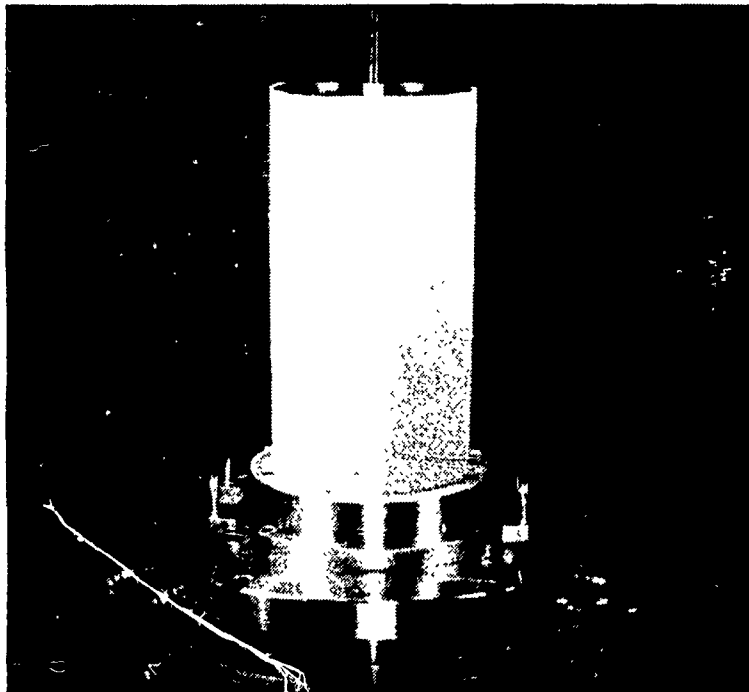


Figure 3. Inner membrane and pedestal

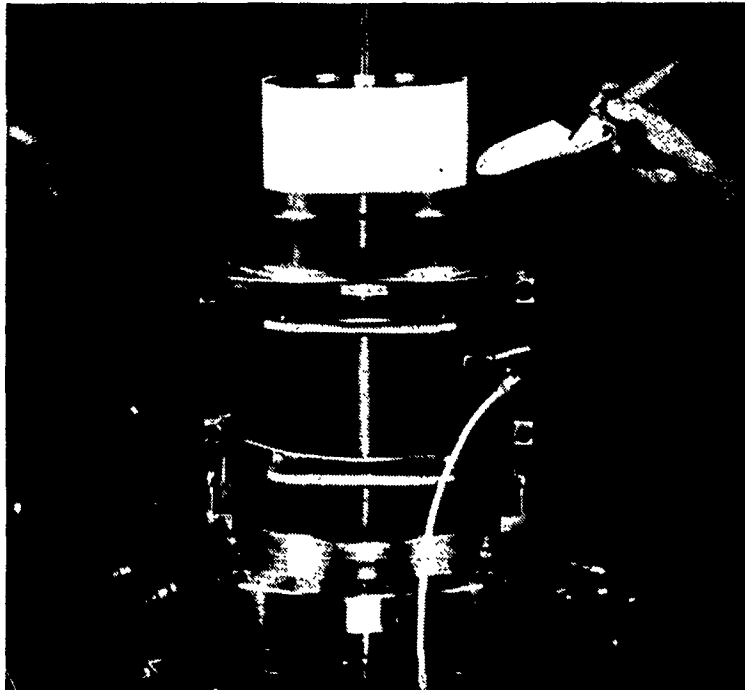


Figure 4. Overall figure of built-up molds

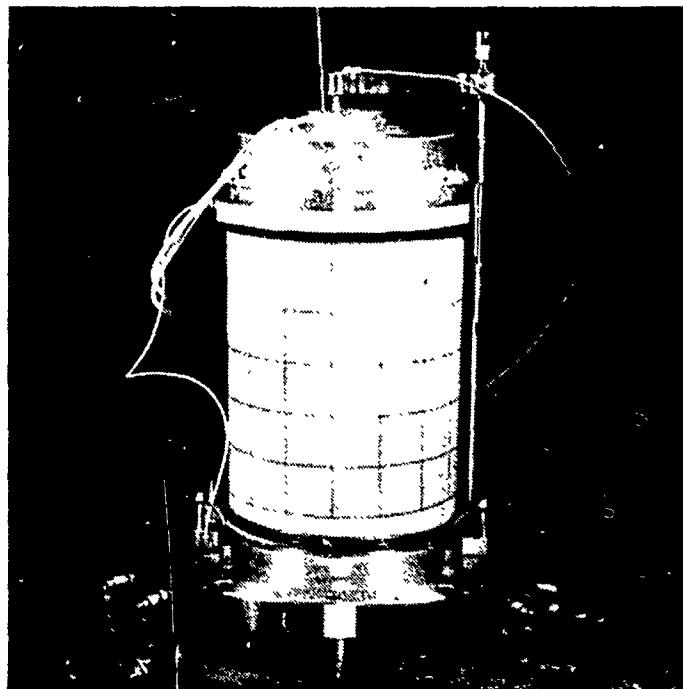


Figure 5. Specimen under applied vacuum with torque load cell and potentiometer

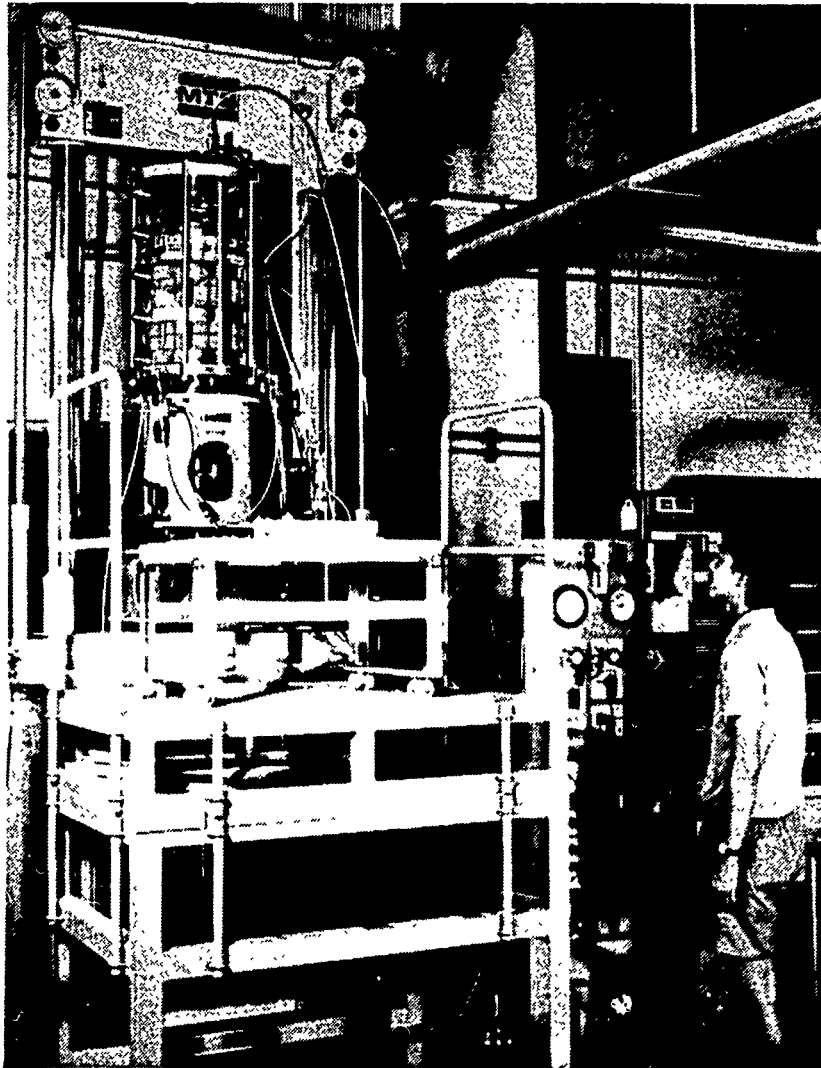


Figure 6. Overall assembly of MTS and triaxial load frame

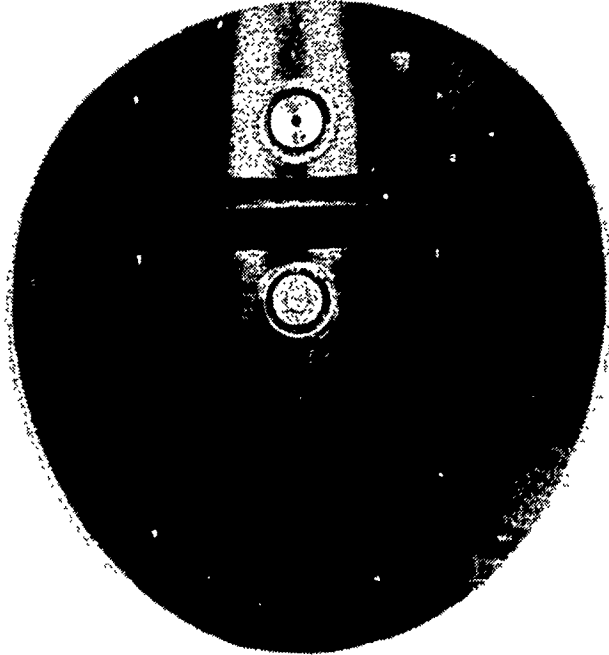


Figure 7. Universal joint

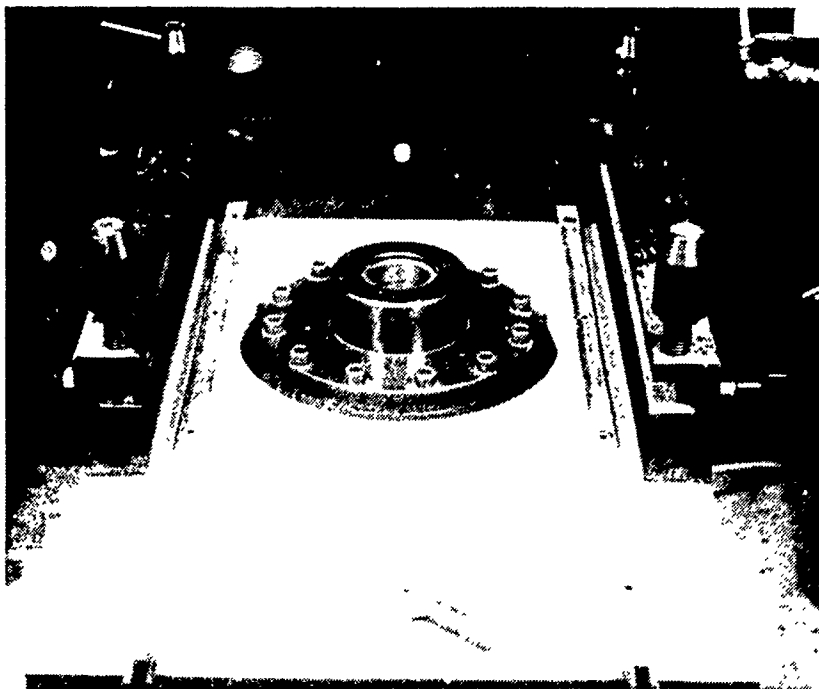


Figure 8. Air clamp

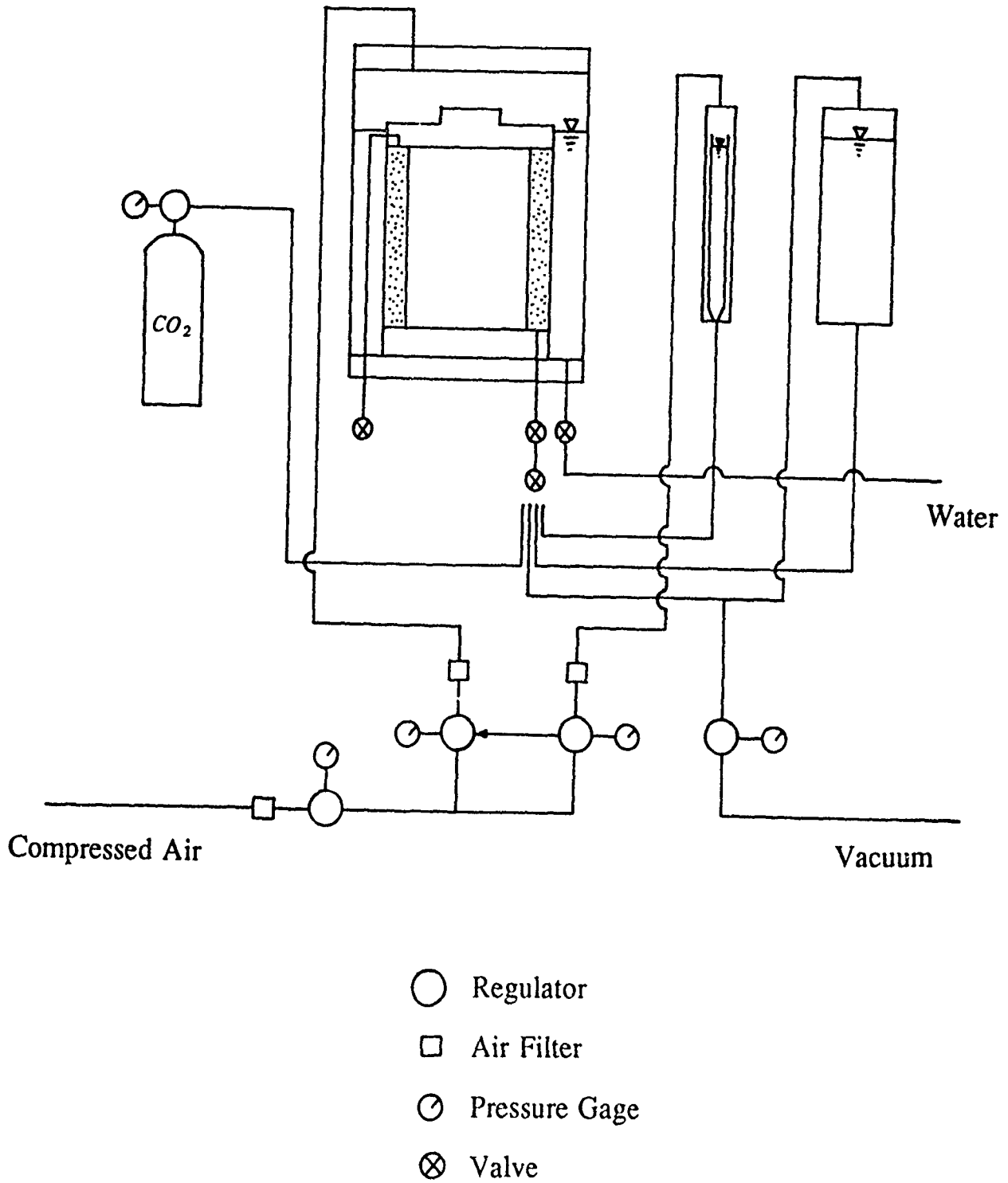


Figure 9. Schematic diagram of air pressure and water supply system

3 EXPERIMENTAL RESULTS

3.1 First Loading

The results of the first loading for both loose and dense samples are presented in this section. First, we discuss the cyclic shear deformation characteristics of water saturated specimens in strain-controlled conditions. Second, we examine the relation between the external work, measured per unit volume, and the corresponding excess pore water pressure.

All our experiments are under a strain-controlled condition. This is in contrast to most other researchers who have conducted the undrained cyclic shear tests under stress-controlled conditions; see, for example, Ishihara and Yasuda (1975), Seed (1979), and Tatsuoka *et al.* (1982). Figure 10 shows the relation between the shear strain and the effective pressure for loose samples, for two strain amplitudes, 0.2% and 1.0%. It is seen that the effective pressure decreases during each cycle. The reduction after the first cycle is especially large. It is also seen that the number of cycles required for the excess pore pressure to attain 95% of the initial effective pressure, depends on the employed strain amplitude: 27 cycles are needed for 0.2%, and only 2 cycles for 1.0% strain amplitude. Figure 11 shows the relation between the shear stress and the effective pressure, while Figure 12 is for the corresponding shear stress vs. the shear strain. It is seen that the peak shear stress (and the secant modulus) decreases after each cycle.

The energy supplied through the external work is mainly consumed by the frictional loss at contacting granules, resulting in a change of the microstructure in the granular mass. Therefore, the external work may be used to measure the history of fabric change in a granular mass.

The rate of external work per unit volume, $\langle \dot{w}_E \rangle$, can be evaluated in terms of the applied boundary tractions, τ , and the boundary velocity field, \dot{u} ,

$$\langle \dot{w}_E \rangle = \frac{1}{V} \int_{\partial D} \tau \cdot \dot{\mathbf{n}} \, dS, \quad (3.1)$$

where dot denotes the inner-product, and ∂D is the boundary of the sample domain D .

If we assume that the boundary tractions are *uniform*, then (3.1) can be expressed in terms of the overall stresses and strain rates as (Hill, 1963, 1967)

$$\langle \dot{w}_E \rangle = \langle \sigma_{xx} \rangle \langle \dot{\epsilon}_{xx} \rangle + \langle \sigma_{yy} \rangle \langle \dot{\epsilon}_{yy} \rangle + \langle \sigma_{zz} \rangle \langle \dot{\epsilon}_{zz} \rangle + \langle \sigma_{xy} \rangle \langle \dot{\gamma}_{xy} \rangle. \quad (3.2)$$

Since the specimen is isotropically pressurized by the external pressure, P_o , throughout the experiment, all the three normal stresses equal P_o . Denoting the average volumetric strain rate by $\frac{\dot{V}}{V}$, (3.2) can be rewritten as

$$\begin{aligned} \langle \dot{w}_E \rangle &= P_o (\langle \dot{\epsilon}_{xx} \rangle + \langle \dot{\epsilon}_{yy} \rangle + \langle \dot{\epsilon}_{zz} \rangle) + \langle \sigma_{xy} \rangle \langle \dot{\gamma}_{xy} \rangle. \\ &= P_o \frac{\dot{V}}{V} + \langle \sigma_{xy} \rangle \langle \dot{\gamma}_{xy} \rangle. \end{aligned} \quad (3.3)$$

Since, for the pressure levels used here, sand particles and water can be assumed to be incompressible, $\frac{\dot{V}}{V}$ is zero during the undrained experiment if the sample is completely saturated. The rate of external work per unit volume then becomes

$$\langle \dot{w}_E \rangle = \langle \sigma_{xy} \rangle \langle \dot{\gamma}_{xy} \rangle. \quad (3.4)$$

The pressure term does not contribute to the rate of external work for incompressible materials, as is evident at the outset. The external work per unit volume, $\langle w_E \rangle$, up to time t can then be evaluated by the time-integration of (3.4),

$$\langle w_E \rangle = \int_{t_0}^t \langle \sigma_{xy} \rangle \langle \dot{\gamma}_{xy} \rangle \, dt, \quad (3.5)$$

where t_0 denotes the time at which the experiment is started.

The external work is calculated from the experimental results, and correlated with the accumulated pore water pressure for both loose and dense specimens. The relation between the external work per unit volume and the excess pore water pressure for the loose specimens is shown in Figure 13. Three strain amplitudes, 0.2%, 0.5% and 1.0%, are used here. The data at the end of each cycle in each experiment are plotted in Figure 13. It is clearly seen that there exists a unique nonlinear relation between

the external work and the accumulated pore water pressure; this relation is independent of the employed shear-strain amplitude, but the number of cycles to the 95% initial effective pressure does depend on the strain amplitude.

The relation between external work per unit volume and the excess pore water pressure for dense specimens is shown in Figure 14. Five different strain amplitudes, 0.2%, 0.4%, 0.5%, 1.0% and 2.0%, are employed. It is clearly seen that here again a unique nonlinear relation exists between the external work and the accumulated pore water pressure.

To further explore this interesting phenomenon, randomly varying shear-strain amplitudes up to 1.0% are applied to a specimen. The relation between the shear strain and the effective pressure is shown in Figure 15. *The relation between the external work and the excess pore water pressure for this random loading is also included in Figure 14, where the accumulated pore pressure at zero shear strain is plotted against the corresponding external work.* It is seen that the randomness in loading does not affect the unique nonlinear relation between these two quantities.

The effect of specimen density on the above-studied relation is now considered. It is seen that both the loose and dense specimens in first loading display a unique relation between the external work and the corresponding excess pore water pressure. The two curves are compared in Figure 16. They essentially coincide up to 130 kN/m^2 pore water pressure, i.e., 65% of the initial effective pressure. A significant difference appears thereafter, with the loose samples developing higher pore pressure, as should be expected.

3.2 Second Loading

The experimental results for the second loading for both loose and dense specimens are presented in this section. After the first loading discussed in the previous

subsection, specimens are reconsolidated under the same initial effective pressure, 196 kN/m^2 , as in the first loading. The second loading is then applied to the specimens. First, we discuss the results where the strain amplitude in the second loading is the same as that in the first loading. Then, we examine the results where the strain amplitude in the second loading is different from the one in the first loading.

The shear deformation characteristics in the second loading are compared with the results of the first loading. Figure 17 shows the first two cycles of the relation between the shear strain and the effective pressure in both the first (solid curve) and second (dotted curve) loading for a dense specimen deformed at a strain amplitude of 0.5%. It is seen that the excess pore water pressure accumulated during the second loading is much less than that in the first loading, and the number of cycles required to reach 95% of the initial effective pressure in the second loading is much greater than that in the first loading.

Figure 18 is a direct comparison of the pore water pressure variation in loose and dense specimens, deformed at a strain amplitude of 0.5%. It is clearly seen that it takes a greater number of cycles for the pore water pressure to reach a specified level in the second loading than it does in the first loading, for both cases. This is due to the ordered arrangement of the granules, attained upon the completion of the first loading. Specifically, the contact normals tend to be oriented after the first loading such that the specimen is better able to resist a similar shearing. *Another trend to notice is that the pore water pressure builds up faster during the first loading of the dense specimen than it does in the second loading of the loose specimen. This is also explained by the oriented contact normals, despite the large difference in densities.* These trends are seen in all our results when we compare the behavior of loose and dense specimens deformed at a constant strain amplitude. It should be noted, however, that, in a strain-controlled test, the deformation of the specimen is limited by the prescribed strain amplitude. This prevents extensive particle rearrangement which often occurs in

stress-controlled tests, once sufficiently high pore pressures are attained; see Nemat-Nasser and Tobita (1982).

The relation between the external work per unit volume and the excess pore water pressure in the second loading will now be presented. Figures 19 and 20 show this for loose and dense specimens, respectively. There are no significant differences up to half the initial effective pressure. However, after that, the relation in the second loading seems to depend on the employed strain amplitude, although this same relation in the first loading does not. Figures 21 and 22 show the relation between the excess pore water pressure and the employed strain amplitude for loose and dense specimens, respectively.

To understand why the relation between the pore water pressure and the supplied work per unit volume is independent of the strain amplitude in the first loading but not in the second loading of the same sample, we observe that for the same density, the sample packing is the same for all samples at the start of the first loading, whereas at the start of the second loading each sample has experienced a different stress and strain history during its first loading with a strain amplitude different from the other samples. It is still not clear whether the strain amplitude used in the first loading affects the relation between external work and the excess pore water pressure in the second loading. In order to investigate the true effect of the strain amplitude during the second loading, the specimens are subjected to cyclic loading at several different strain amplitudes, and then the second loading is performed for each specimen *at the same common strain amplitude*. The results are shown in Figures 23 and 24. It is clearly seen that *the stress and strain history in the first loading does not affect the relation between the external work and the excess pore water pressure in the second loading, i.e., this relation in the second loading depends on the strain amplitude employed during the second loading, and not that during the first loading.*

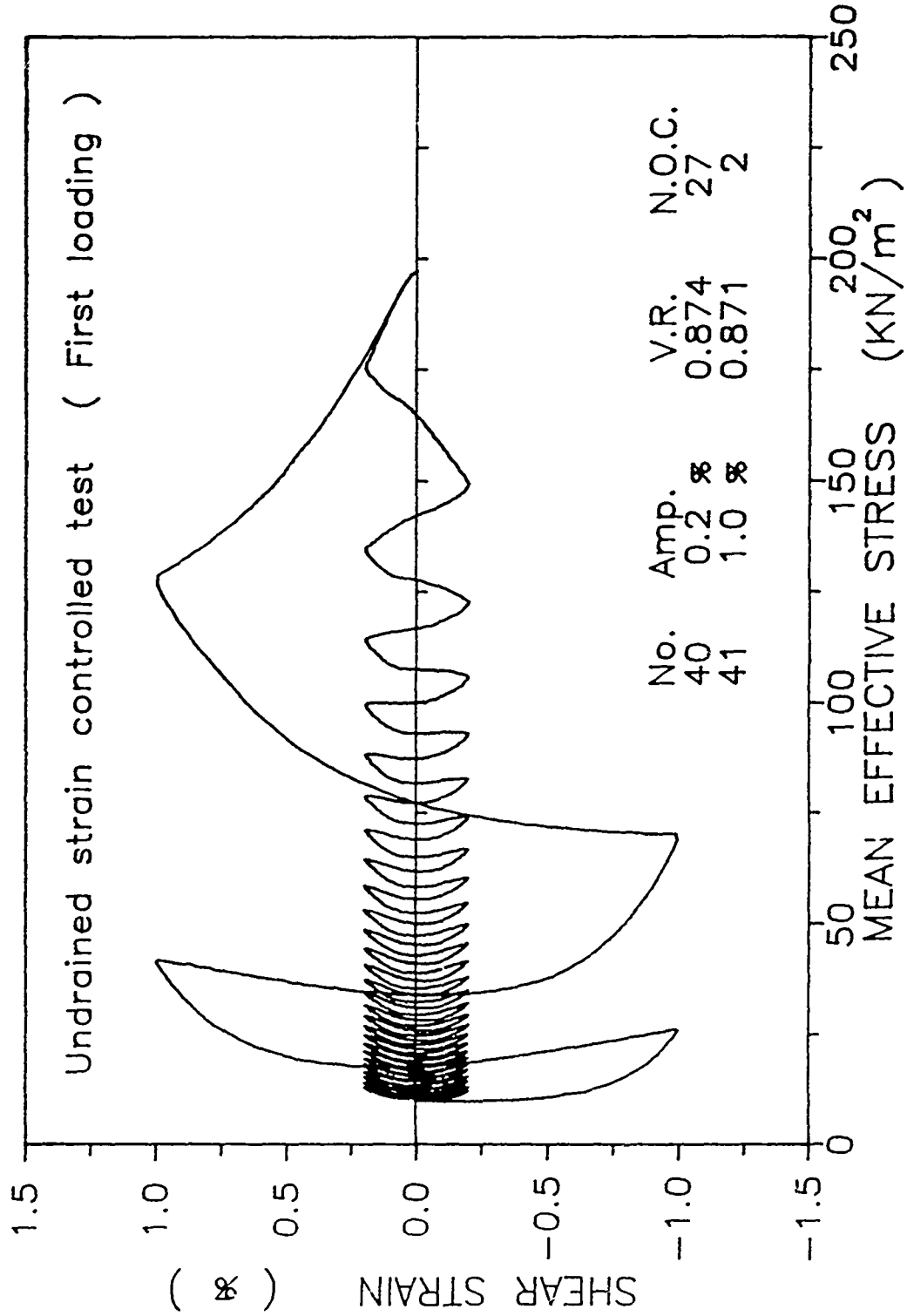


Figure 10. Relation between shear strain and effective pressure in first loading of loose specimens; strain amplitudes are 0.2% and 1.0%

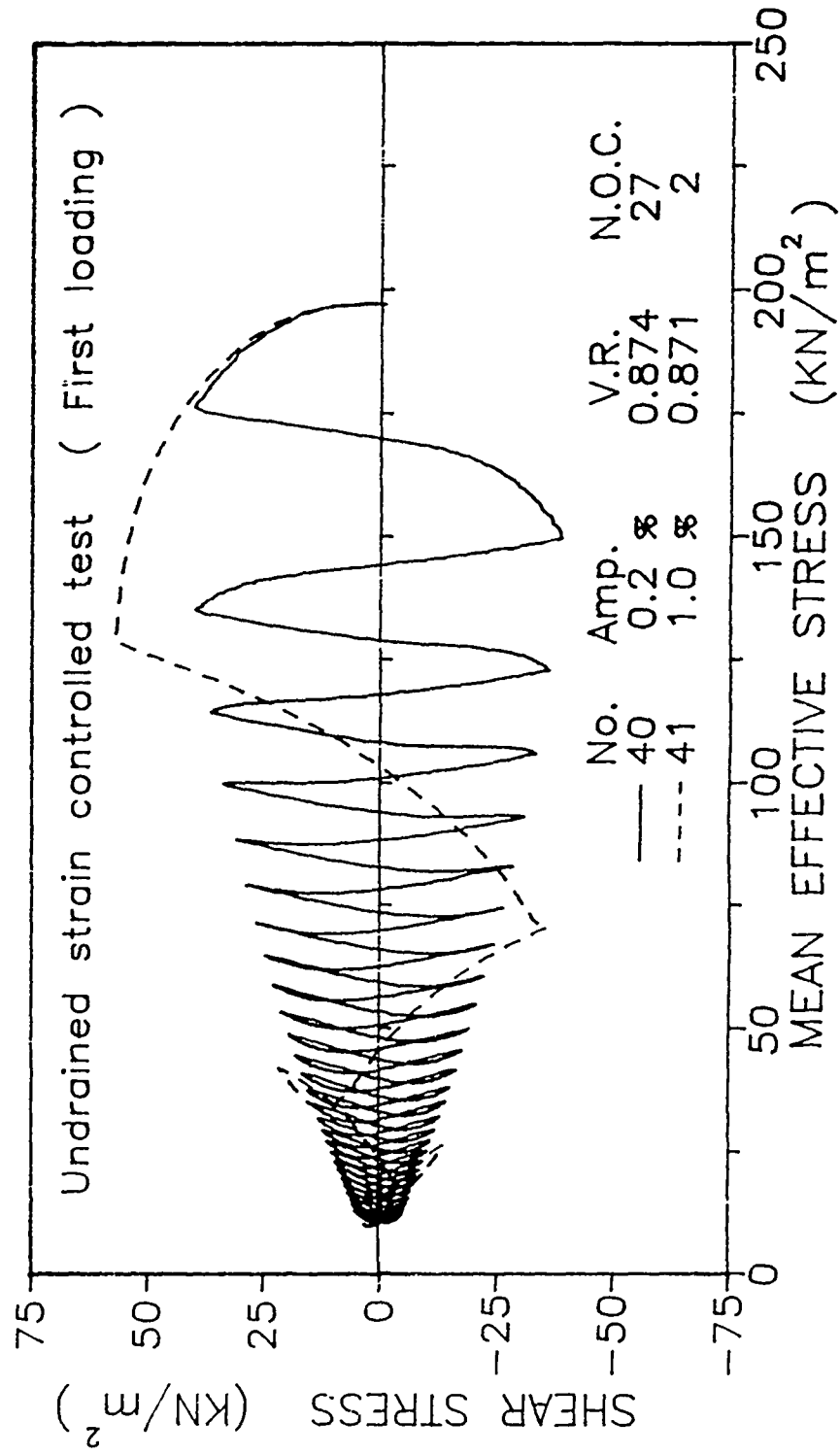


Figure 11. Relation between shear stress and effective pressure in first loading of loose specimens; strain amplitudes are 0.2% and 1.0%

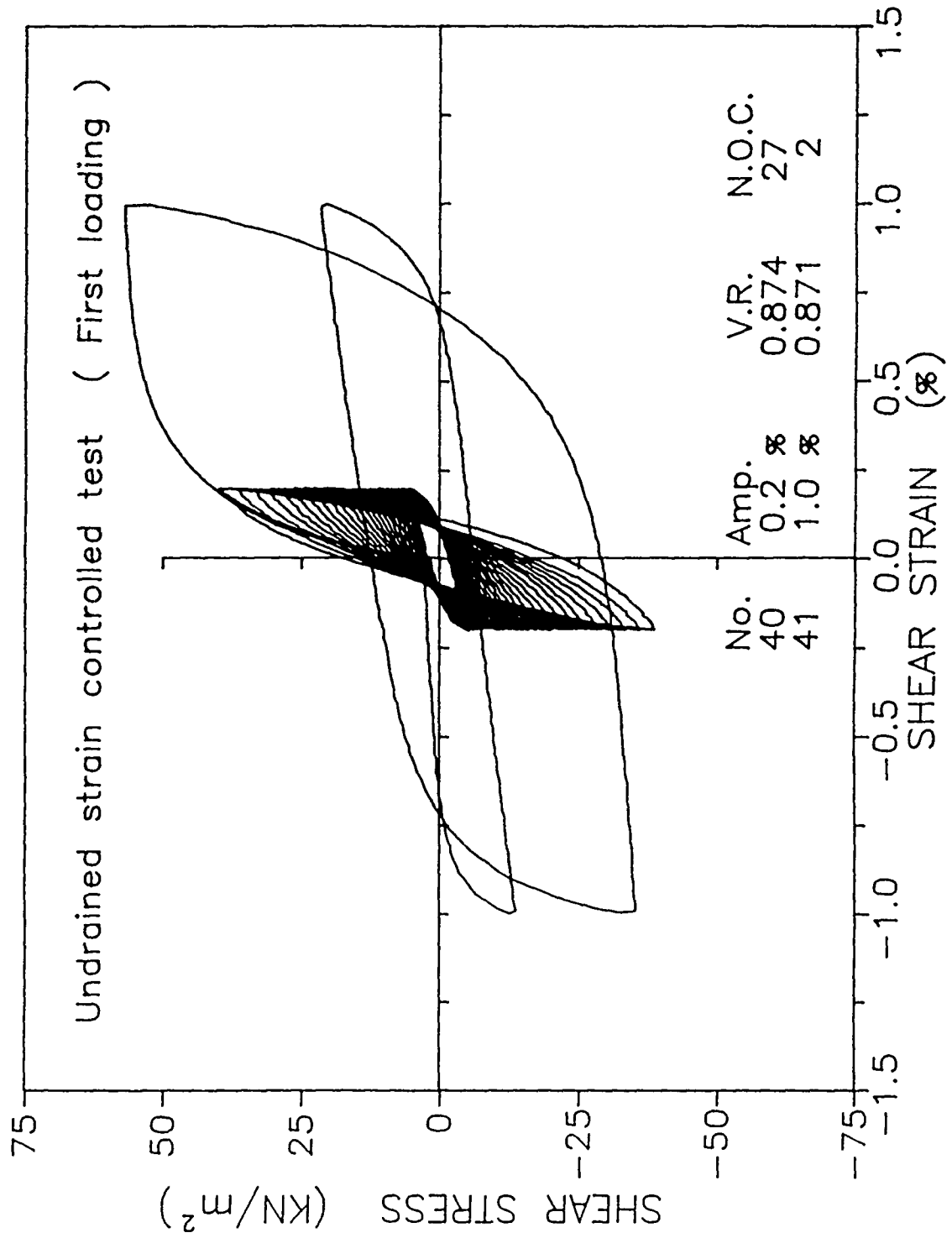


Figure 12. Relation between shear stress and shear strain in first loading of loose specimens; strain amplitudes are 0.2% and 1.0%

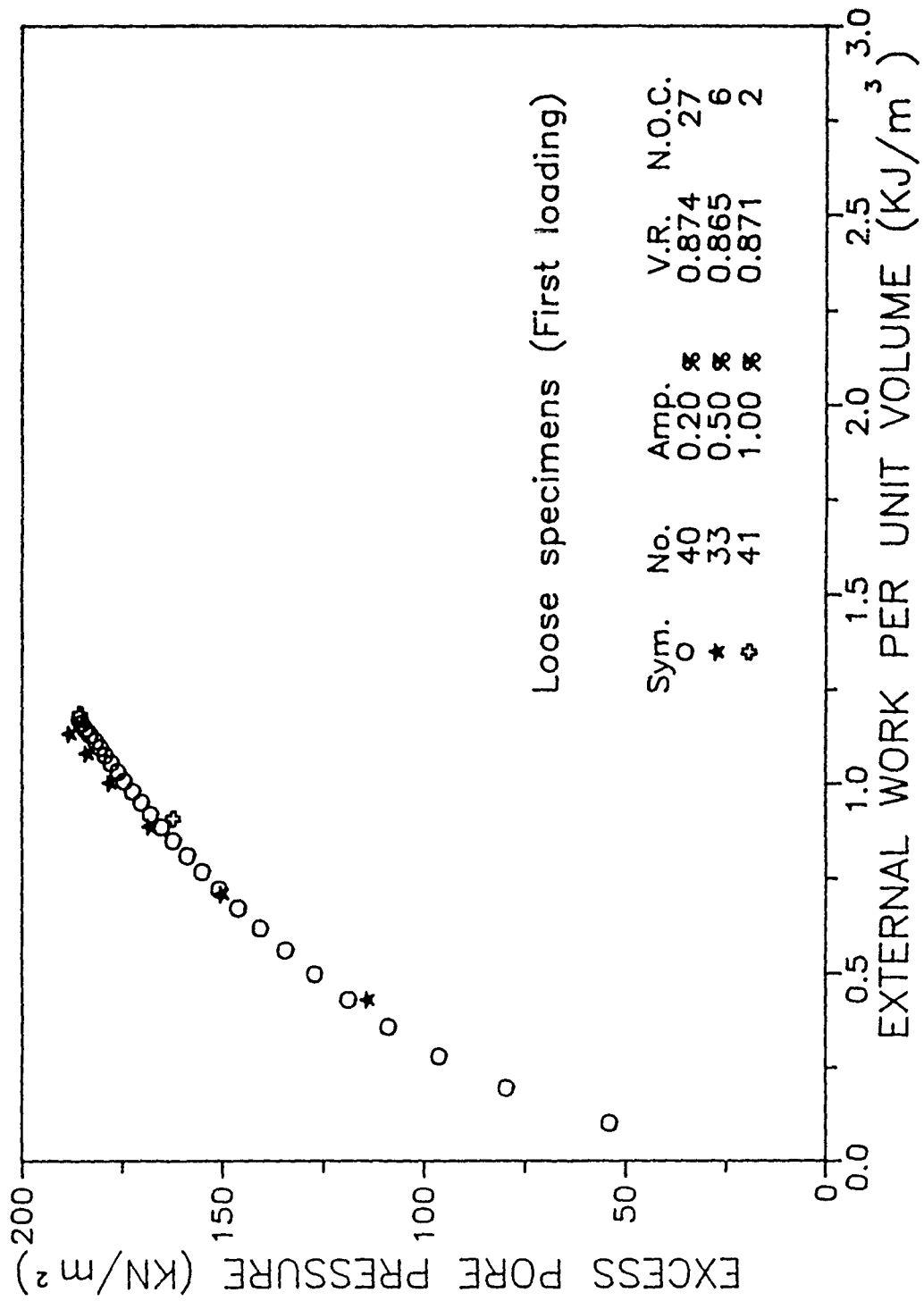


Figure 13. Relation between external work per unit volume and excess pore water pressure in first loading of loose specimens

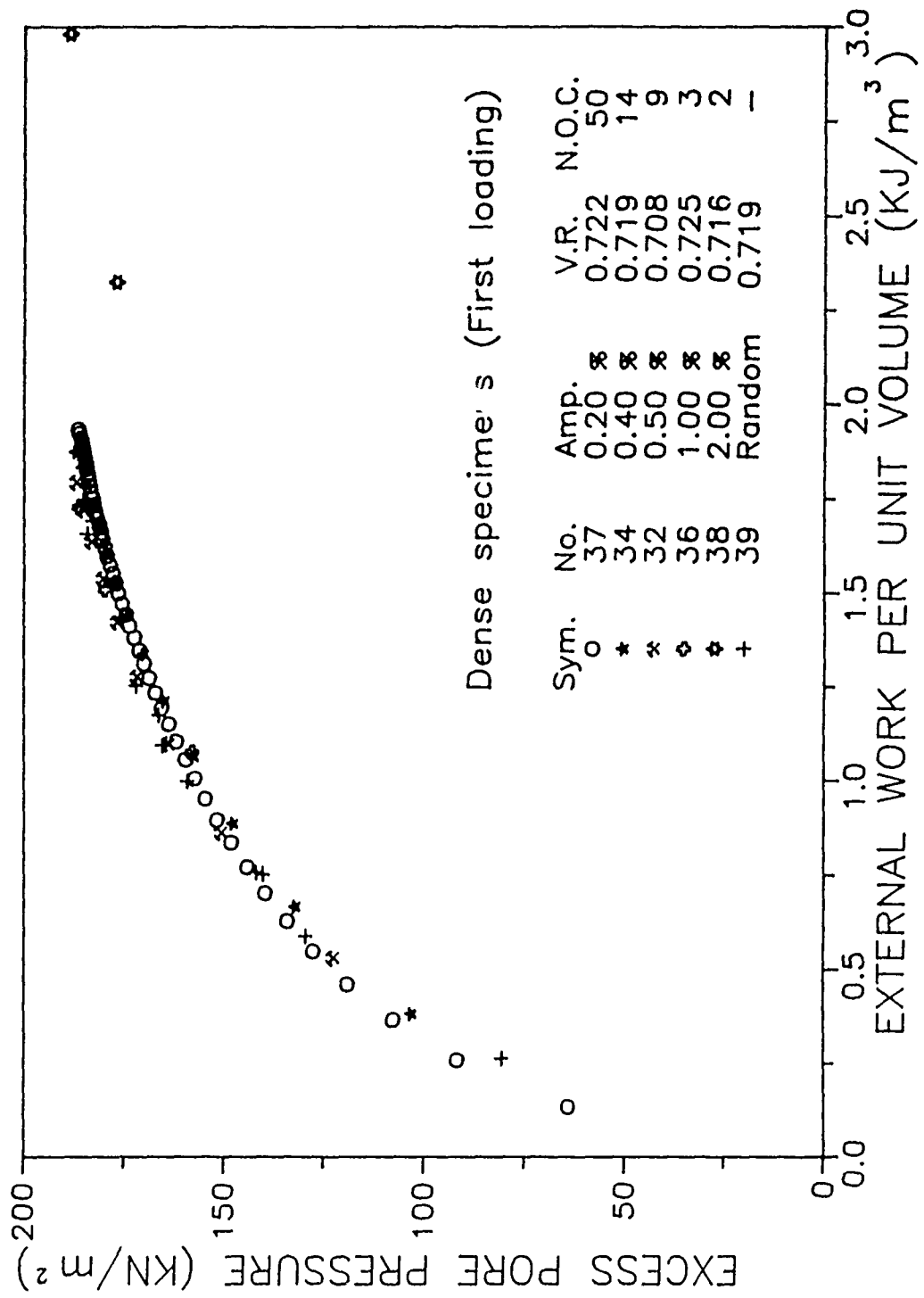


Figure 14. Relation between external work per unit volume and excess pore water pressure in first loading of dense specimens

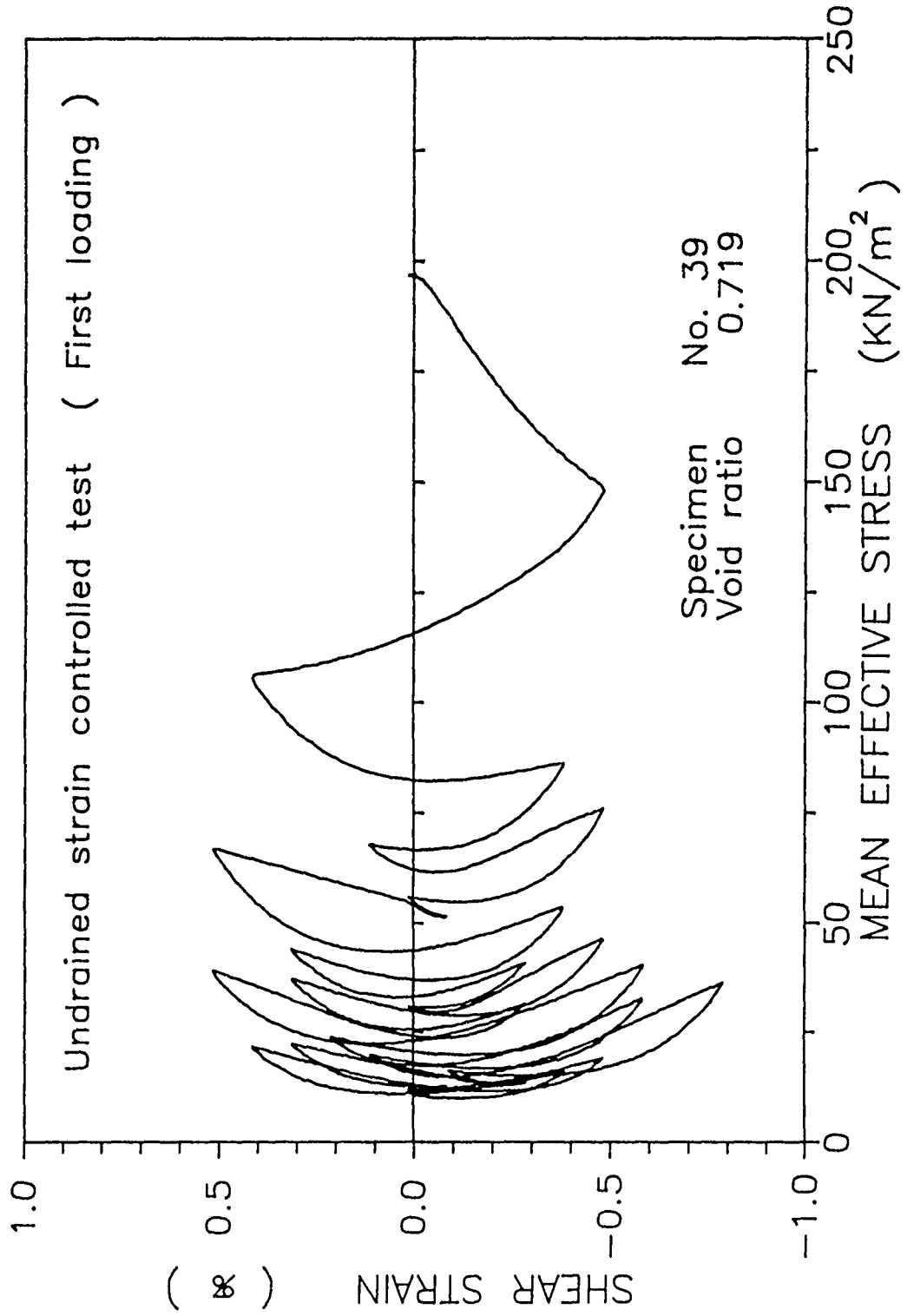


Figure 15. Relation between shear stress and effective pressure in first loading of dense specimen subjected to random torsional loading

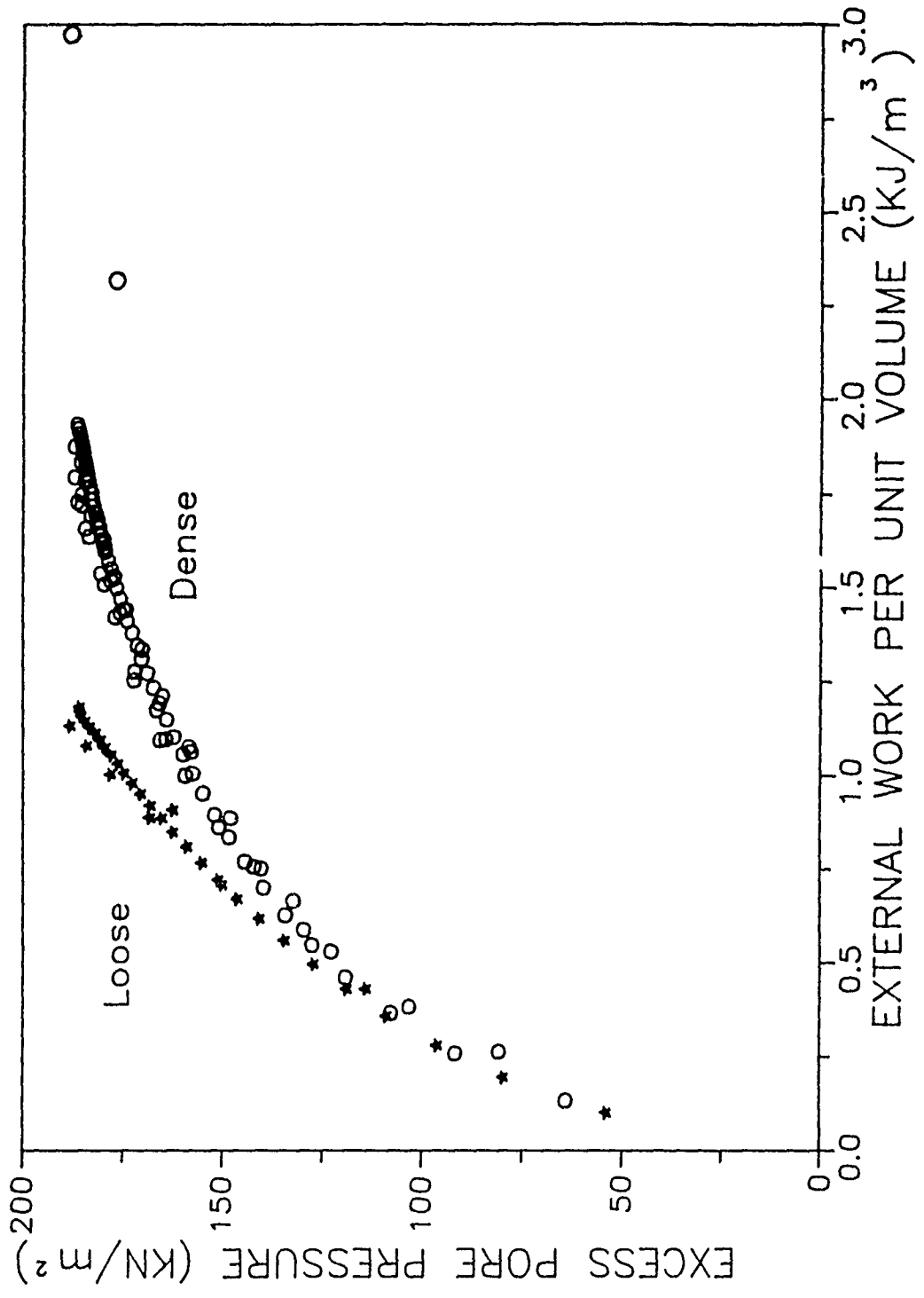


Figure 16. Relation between external work per unit volume and excess pore water pressure in first loading of both loose and dense specimens

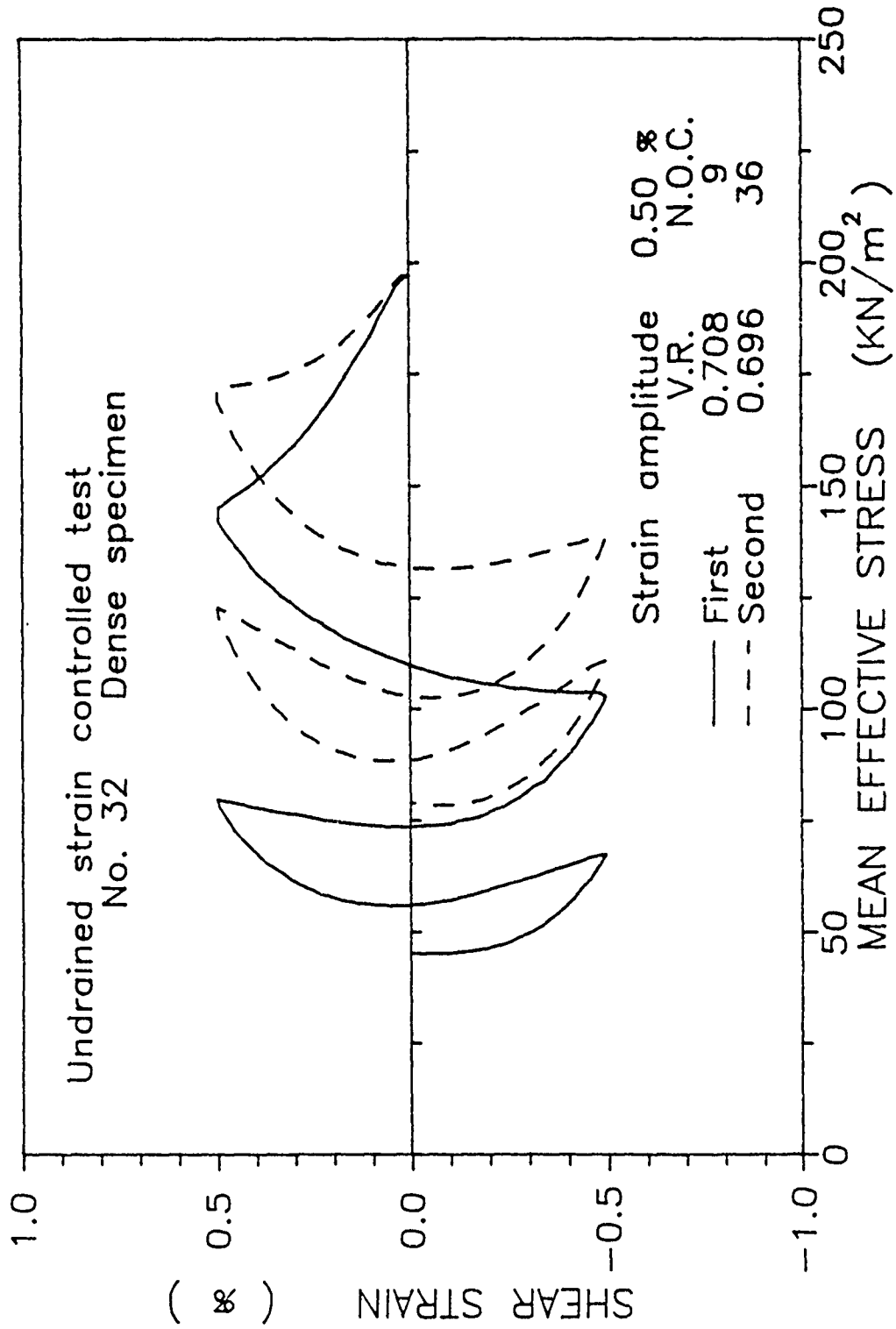


Figure 17. Relation between shear strain and effective pressure in first and second loading of dense specimen whose strain amplitude is 0.5%

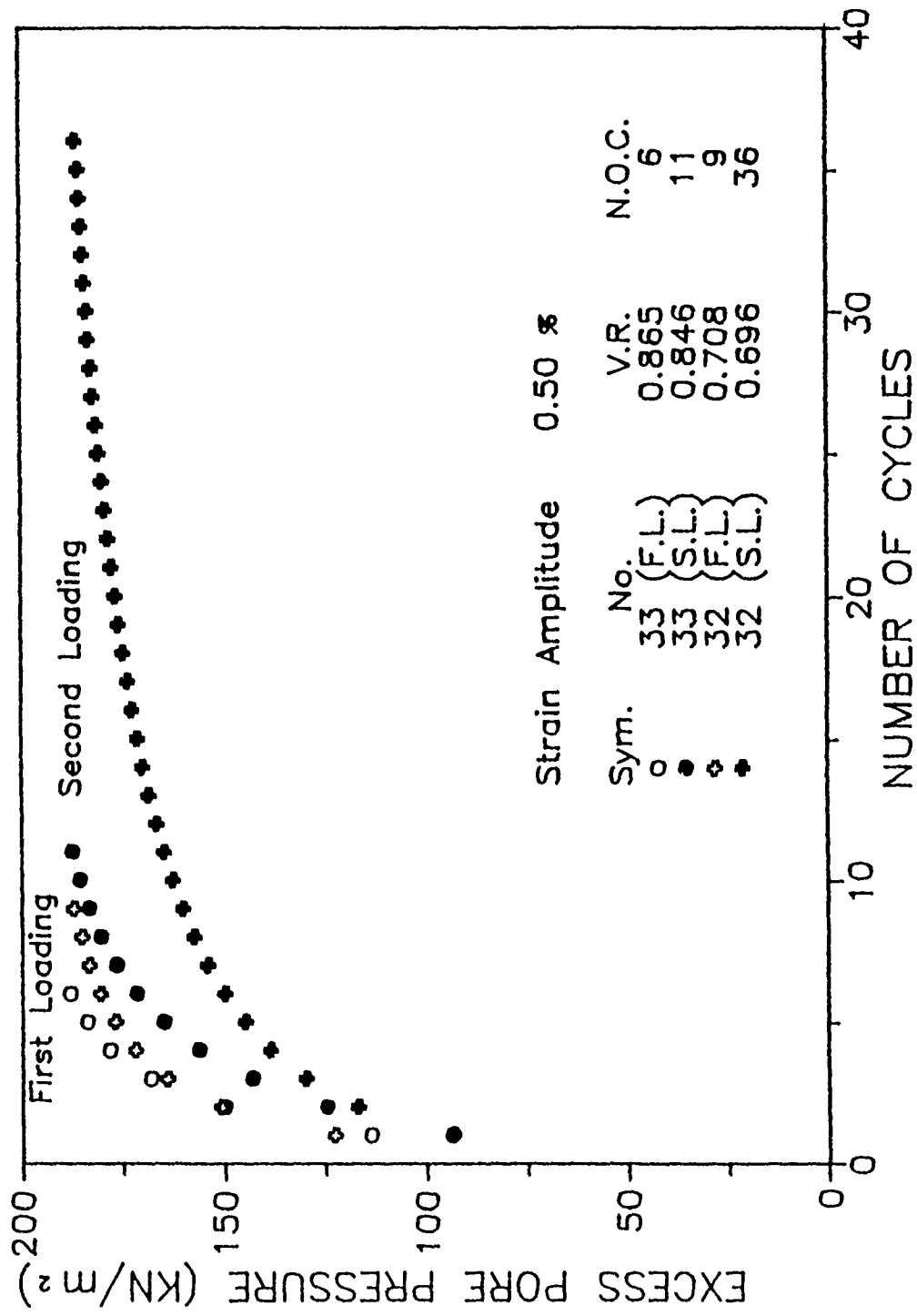


Figure 18. Relation between number of cycles and excess pore water pressure in first and second loading of both loose and dense specimens whose strain amplitude is 0.5%

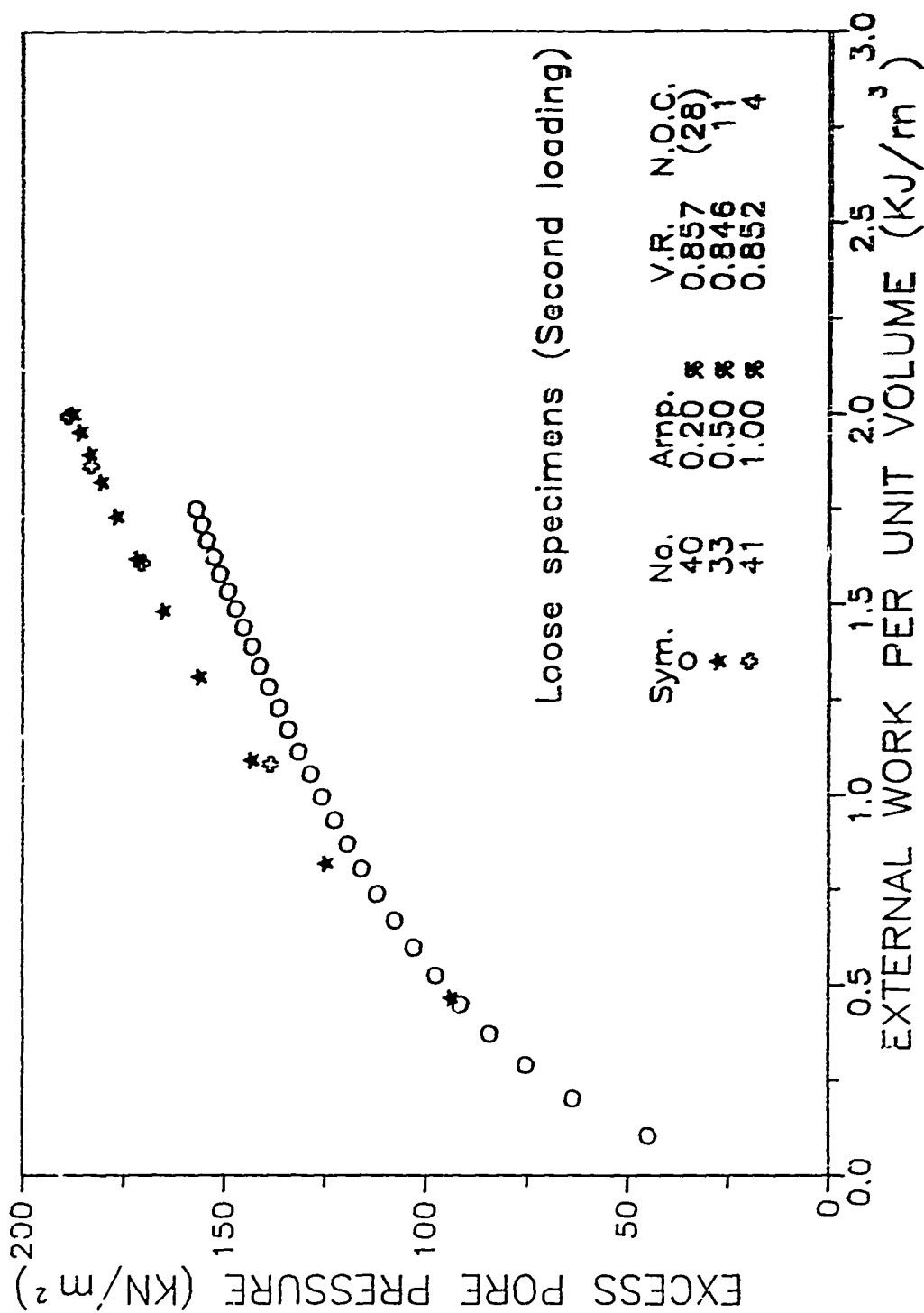


Figure 19. Relation between external work per unit volume and excess pore water pressure in second loading of loose specimens where strain amplitude used in second loading is the same as in first loading

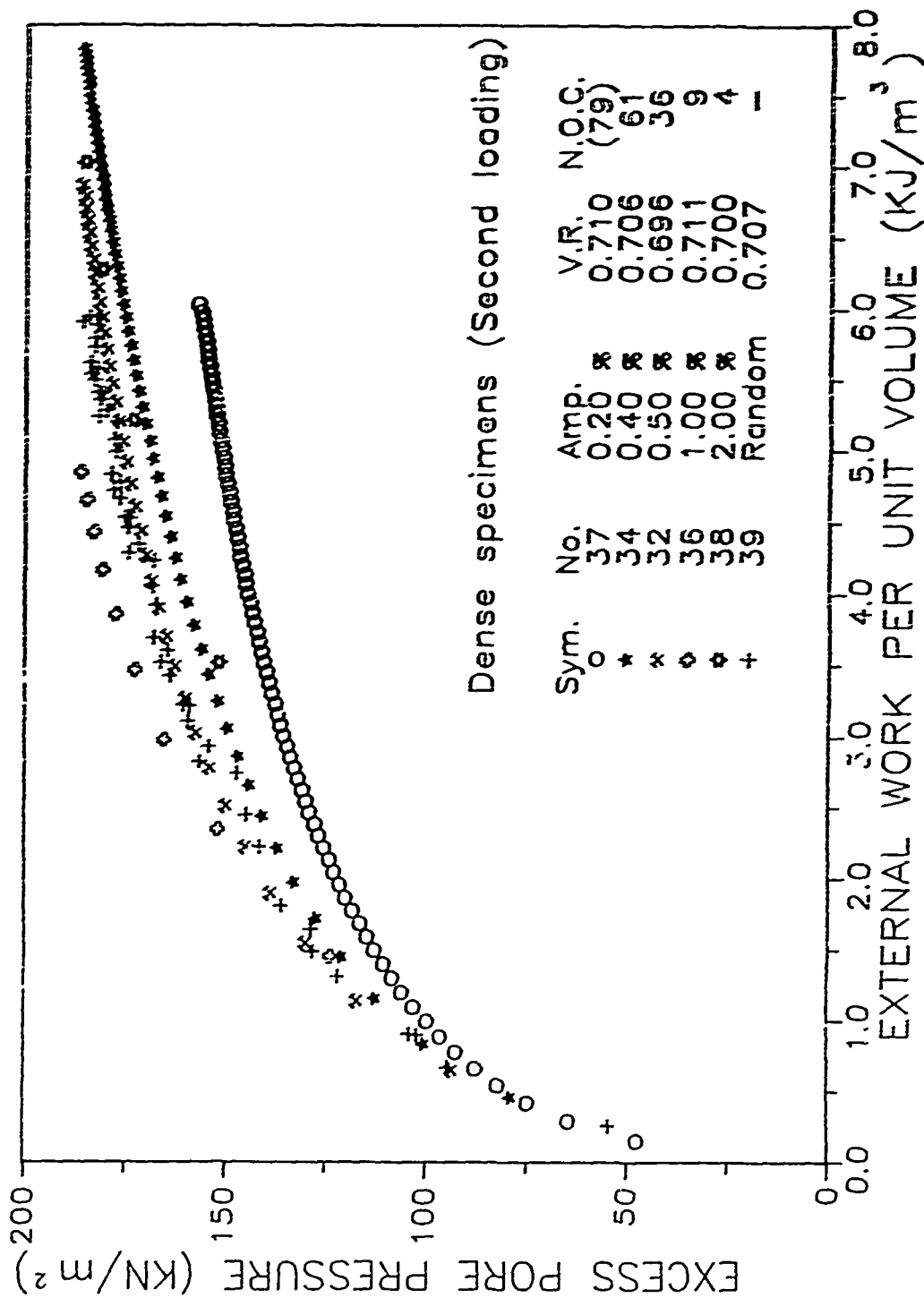


Figure 20. Relation between external work per unit volume and excess pore water pressure in second loading of dense specimens where strain amplitude used in second loading is the same as in first loading

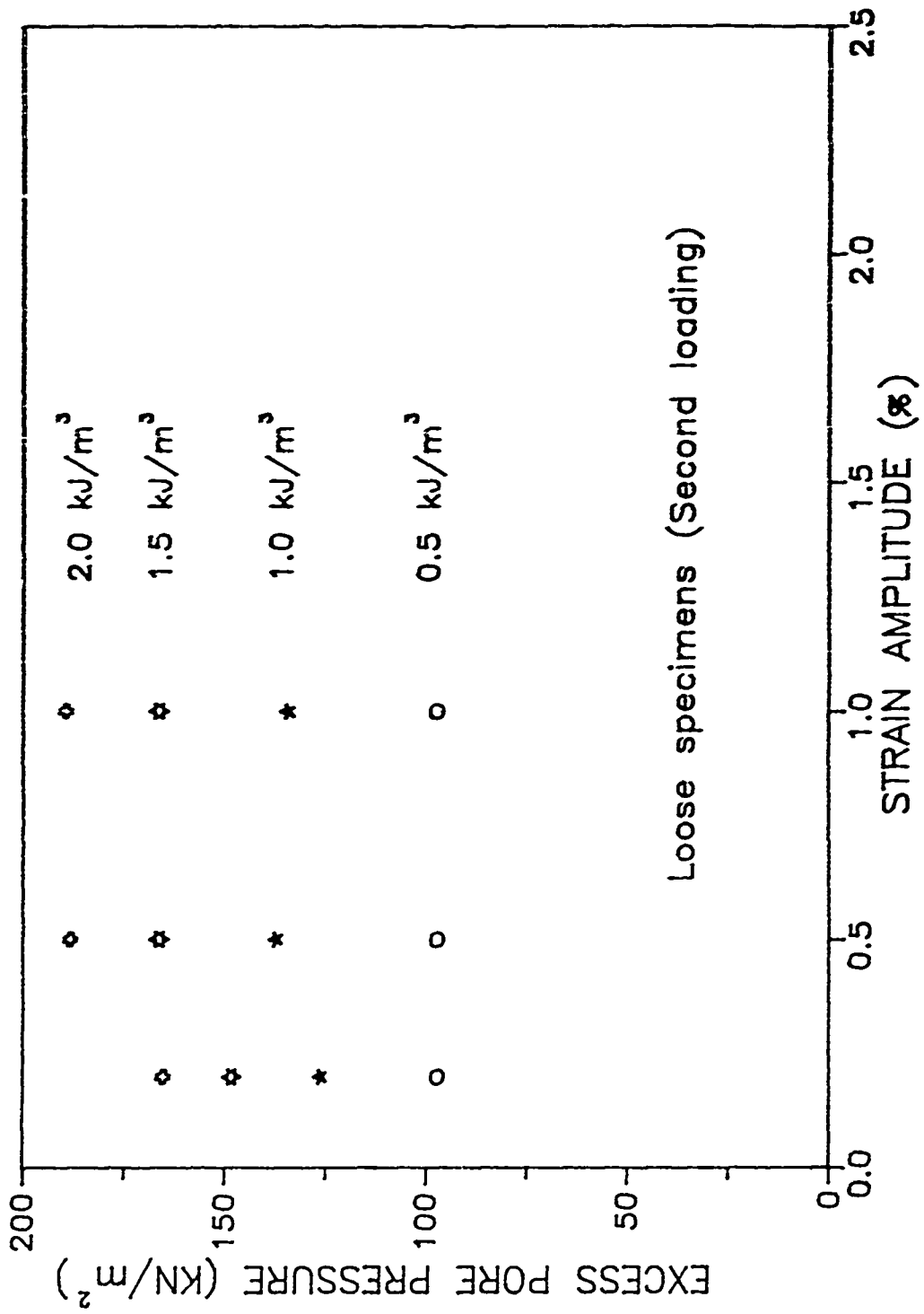


Figure 21. Contours of external work per unit volume in relation between excess pore water pressure and shear strain amplitude in second loading of loose specimens

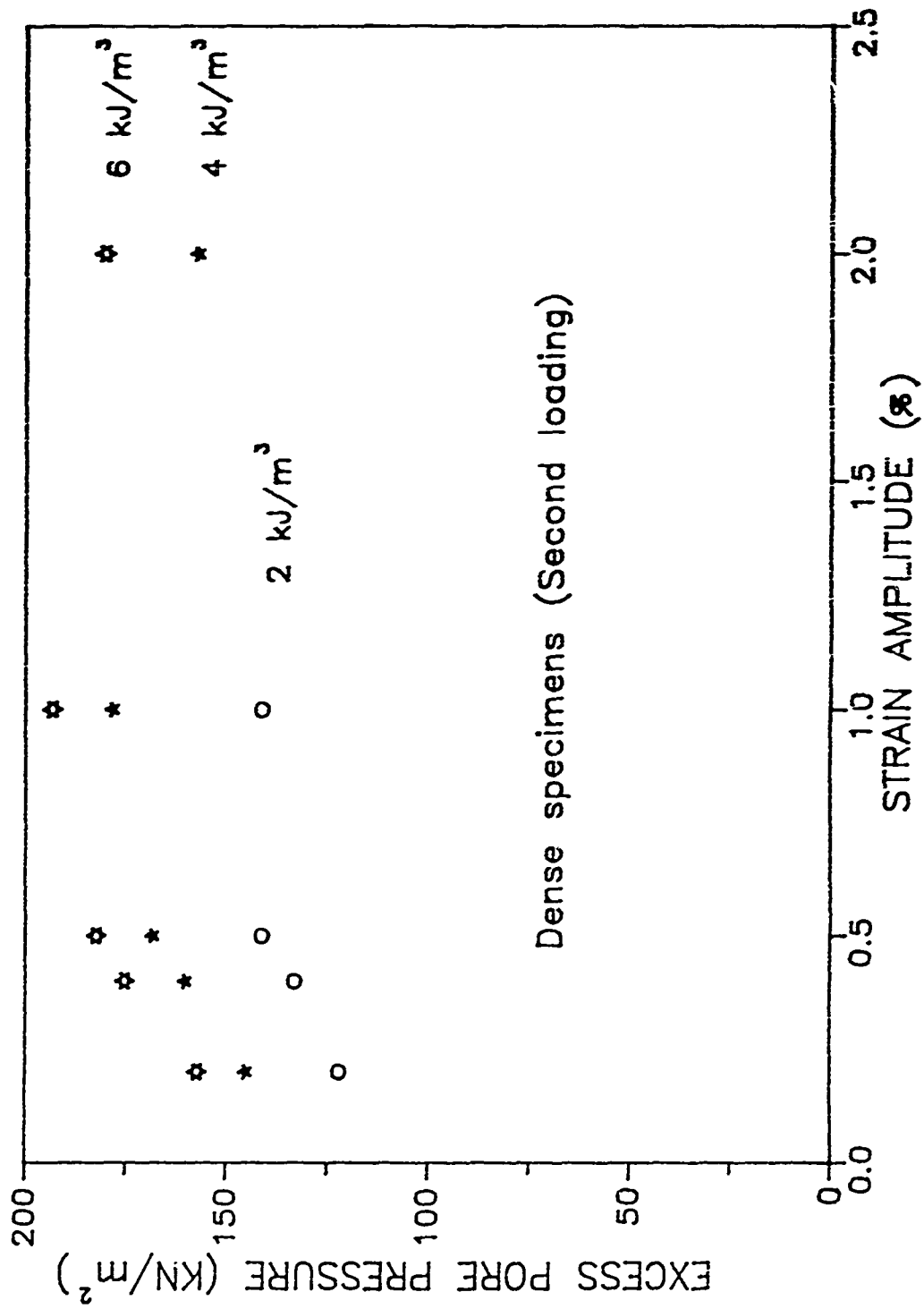


Figure 22. Contours of external work per unit volume in relation between excess pore water pressure and shear strain amplitude in second loading of dense specimens

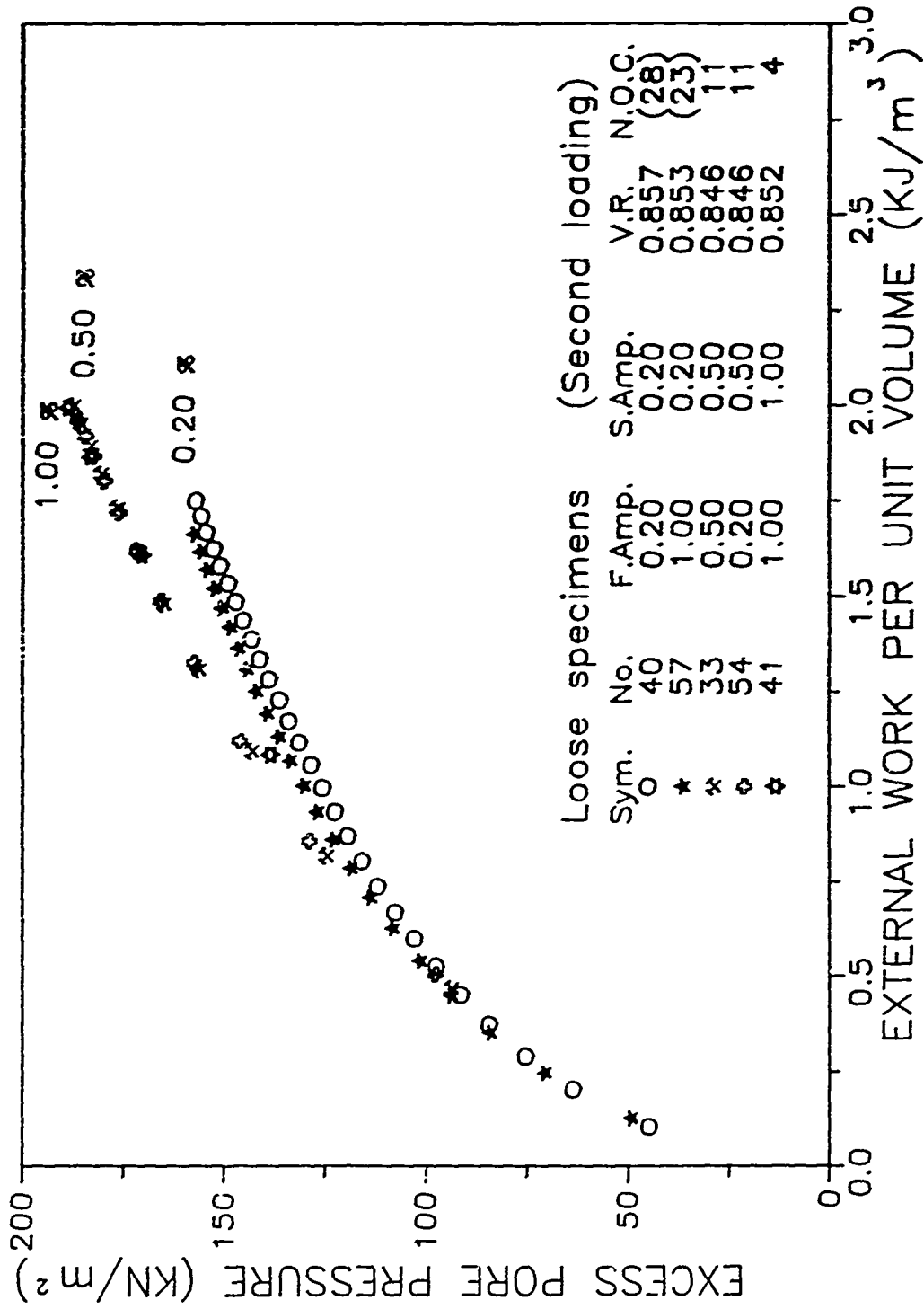


Figure 23. Relation between external work and excess pore water pressure in second loading of loose specimens where strain amplitude used in second loading is different from that used in first loading

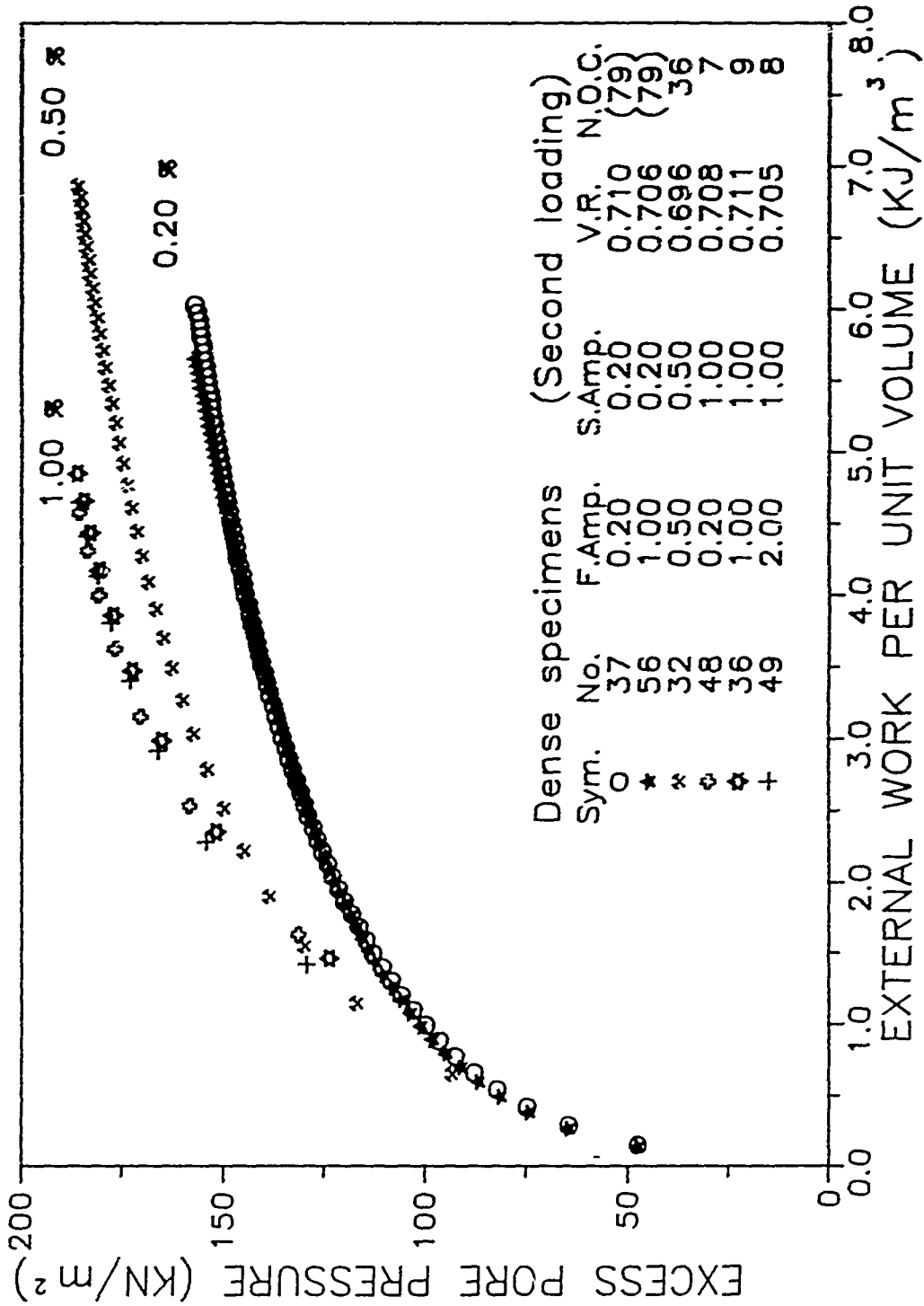


Figure 24. Relation between external work and excess pore water pressure in second loading of dense specimens where strain amplitude used in second loading is different from that used in first loading

4. THEORETICAL MODELING

4.1 Energy Dissipation in Granular Media

In the present context, the external work that is supplied at constant temperature to a material sample is either dissipated through friction or is stored in the material as strain energy. The relation between the external work and the internal dissipation provides a basic constitutive constraint for the flow of granular media; Rowe (1962). For stress levels considered in our experiments, essentially the entire external work is dissipated by slip between contacting granules, and, hence, very little is stored in the granules and the fluid as strain energy; Schofield and Wroth (1968). In this section, energy dissipation in granular media is micromechanically modeled, and is related to the pore pressure built up in cyclic shearing of saturated undrained samples.

We consider the low-strain-rate shear loading of a granular mass that occupies spatial region D of volume V . The region Ω within D is occupied by the granules, whereas $D - \Omega$ is occupied by water (the specimen is saturated). The rate of external work per unit volume is expressed in terms of the boundary tractions $\boldsymbol{\tau}$, and the boundary velocity field $\dot{\mathbf{u}}$, by

$$\langle \dot{w}_E(t) \rangle = \frac{1}{V} \int_{\partial D} \boldsymbol{\tau}(\mathbf{x}, \mathbf{v}, t) \cdot \dot{\mathbf{u}}(\mathbf{x}, t) dS(\mathbf{x}). \quad (4.1)$$

The tractions $\boldsymbol{\tau}$ relate to the exterior unit normal \mathbf{v} on ∂D by

$$\boldsymbol{\tau}(\mathbf{x}, \mathbf{v}, t) = \boldsymbol{\sigma}(\mathbf{x}, t) \cdot \mathbf{v}(\mathbf{x}, t), \quad (4.2)$$

where $\boldsymbol{\sigma}$ is some stress field in equilibrium with the applied tractions; Hill (1967).

Using (4.2) in (4.1), we have

$$\langle \dot{w}_E(t) \rangle = \frac{1}{V} \int_{\partial D} (\boldsymbol{\sigma}(\mathbf{x}, t) \cdot \mathbf{v}(\mathbf{x}, t)) \cdot \dot{\mathbf{u}}(\mathbf{x}, t) dS(\mathbf{x}). \quad (4.3)$$

To apply the Gauss theorem, we note that for granular materials, slip at contacting granules renders the velocity field discontinuous there. Therefore, the Gauss theorem cannot be directly applied to (4.3). The velocity jumps at contacting granules must be

included. Suppose that there are N slip surfaces in D at contacting granules at time t . Let s^α be the area on which the α 'th slip occurs. Then, the velocity field is discontinuous on $\sum_{\alpha=1}^N s^\alpha$ where velocity jumps $[\dot{\mathbf{u}}]$ take place; here we define the jump by,

$$[\dot{\mathbf{u}}(\xi, t)] = \lim_{\mathbf{x}^+ \rightarrow \xi} \dot{\mathbf{u}}(\mathbf{x}^+, t) - \lim_{\mathbf{x}^- \rightarrow \xi} \dot{\mathbf{u}}(\mathbf{x}^-, t). \quad (4.4)$$

The velocity field is therefore differentiable everywhere except on $\sum_{\alpha=1}^N s^\alpha$. Now, we consider a surface S shown in Figure 25, which included the slip surface $\sum_{\alpha=1}^N s^\alpha$ in D at time t , *i.e.*, we let $\sum_{\alpha=1}^N s^\alpha \subset S$, and which divides region D into M subregions $\sum_{\beta=1}^M D^\beta = D$.

We apply the Gauss theorem to each subregion to arrive at

$$\frac{1}{V} \sum_{\beta=1}^M \int_{\partial D^\beta} \boldsymbol{\tau} \cdot \dot{\mathbf{u}} dS = \frac{1}{V} \sum_{\beta=1}^M \int_{D^\beta} ((\nabla \cdot \boldsymbol{\sigma}) \cdot \dot{\mathbf{u}} + \boldsymbol{\sigma} : \nabla \dot{\mathbf{u}}) dV, \quad (4.5)$$

where ∂D^β denotes the boundary of subregion D^β . Using the equilibrium equation with no body and inertia forces, we have

$$\nabla \cdot \boldsymbol{\sigma} = 0. \quad (4.6)$$

The symmetry of the stress tensor gives

$$\boldsymbol{\sigma} = \boldsymbol{\sigma}^T. \quad (4.7)$$

Then (4.5) yields

$$\frac{1}{V} \sum_{\beta=1}^M \int_{\partial D^\beta} \boldsymbol{\tau} \cdot \dot{\mathbf{u}} dS = \frac{1}{V} \sum_{\beta=1}^M \int_{D^\beta} \boldsymbol{\sigma} : \dot{\boldsymbol{\epsilon}} dV, \quad (4.8)$$

where

$$\dot{\boldsymbol{\epsilon}} = \frac{1}{2} (\nabla \dot{\mathbf{u}} + (\nabla \dot{\mathbf{u}})^T) \quad (4.9)$$

is the strain-rate tensor.

We consider the left-hand side of (4.8), and note that

$$\sum_{\beta=1}^M \partial D^\beta(\mathbf{x}, \mathbf{v}, t) = \partial D(\mathbf{x}, \mathbf{v}, t) + S^+(\mathbf{x}, \mathbf{v}, t) + S^-(\mathbf{x}, \mathbf{v}, t), \quad (4.10)$$

where S^+ and S^- are opposite faces of the same surface S , i.e.,

$$S^+(\mathbf{x}, \mathbf{v}, t) = S^-(\mathbf{x}, -\mathbf{v}, t). \quad (4.11)$$

Using (4.10), the left-hand side of (4.8) becomes

$$\frac{1}{V} \sum_{\beta=1}^M \int_{\partial D^\beta} \boldsymbol{\tau} \cdot \dot{\mathbf{u}} \, dS = \frac{1}{V} \left(\int_{\partial D} \boldsymbol{\tau} \cdot \dot{\mathbf{u}} \, dS + \int_{S^+} \boldsymbol{\tau} \cdot \dot{\mathbf{u}} \, dS + \int_{S^-} \boldsymbol{\tau} \cdot \dot{\mathbf{u}} \, dS \right). \quad (4.12)$$

Since the surface tractions $\boldsymbol{\tau}$ satisfy

$$\boldsymbol{\tau}(\mathbf{x}, \mathbf{v}, t) = -\boldsymbol{\tau}(\mathbf{x}, -\mathbf{v}, t), \quad (4.13)$$

the second and the third terms in (4.12) cancel out for any $\mathbf{x} \in (S - \sum_{\alpha=1}^N s^\alpha)$, where the

velocity field is continuous. Equation (4.12) then becomes

$$\frac{1}{V} \sum_{\beta=1}^M \int_{\partial D^\beta} \boldsymbol{\tau} \cdot \dot{\mathbf{u}} \, dS = \frac{1}{V} \left(\int_{\partial D} \boldsymbol{\tau} \cdot \dot{\mathbf{u}} \, dS - \sum_{\alpha=1}^N \int_{s^\alpha} \boldsymbol{\tau} \cdot [\dot{\mathbf{u}}] \, dS \right), \quad (4.14)$$

and (4.8) reduces to

$$\frac{1}{V} \int_{\partial D} \boldsymbol{\tau} \cdot \dot{\mathbf{u}} \, dS = \frac{1}{V} \left(\int_D \boldsymbol{\sigma} : \dot{\boldsymbol{\varepsilon}} \, dV + \sum_{\alpha=1}^N \int_{s^\alpha} \boldsymbol{\tau} \cdot [\dot{\mathbf{u}}] \, dS \right). \quad (4.15)$$

The first and second terms in the right-hand side of (4.15) are the strain energy and the frictional energy terms, respectively. The strain energy in (4.15) can be decomposed to the strain energy for granules and for water, leading to

$$\frac{1}{V} \int_{\partial D} \boldsymbol{\tau} \cdot \dot{\mathbf{u}} \, dS = \frac{1}{V} \left(\int_{\Omega} \boldsymbol{\sigma} : \dot{\boldsymbol{\varepsilon}} \, dV + \int_{D-\Omega} \boldsymbol{\sigma} : \dot{\boldsymbol{\varepsilon}} \, dV + \sum_{\alpha=1}^N \int_{s^\alpha} \boldsymbol{\tau} \cdot [\dot{\mathbf{u}}] \, dS \right), \quad (4.16)$$

which is the energy dissipation equation for saturated granular media.

4.2 Formulation of Frictional Energy Loss

In this section, we formulate the frictional energy term in (4.16) as a linear function of the effective pressure P . The unit contact normal to a slip plane and the unit vector in the slip direction are denoted by \mathbf{n} and \mathbf{s} , respectively. The traction $\boldsymbol{\tau}$ on the slip surface $\sum_{\alpha=1}^N s^\alpha$ in D , is decomposed as

$$\boldsymbol{\tau}(\mathbf{x}, \mathbf{n}, t) = \tau^n(\mathbf{x}, t) \mathbf{s}(\mathbf{x}, t) + \tau^s(\mathbf{x}, t) \mathbf{n}(\mathbf{x}, t), \quad (4.17)$$

where τ^n and τ^s are the normal and shear components of the tractions, respectively.

Now, we assume that the velocity jump has only a shear component,

$$[\dot{\mathbf{u}}](\mathbf{x}, t) = [\dot{u}](\mathbf{x}, t) \mathbf{s}(\mathbf{x}, t). \quad (4.18)$$

Using (4.17) and (4.18), the frictional energy term in (4.16) becomes

$$\frac{1}{V} \sum_{\alpha=1}^N \int_{s^\alpha(\mathbf{x}, \mathbf{n}, t)} \boldsymbol{\tau}(\mathbf{x}, t) \cdot [\dot{\mathbf{u}}](\mathbf{x}, t) dS(\mathbf{x}) = \frac{1}{V} \sum_{\alpha=1}^N \int_{s^\alpha(\mathbf{x}, \mathbf{n}, t)} \tau^s(\mathbf{x}, t) [\dot{u}](\mathbf{x}, t) dS(\mathbf{x}). \quad (4.19)$$

Denote the effective frictional coefficient on $\sum_{\alpha=1}^N s^\alpha$ by $\mu(\mathbf{x}, t)$. Then the shear component τ^s is expressed in terms of the normal component τ^n and the effective frictional coefficient as

$$\tau^s(\mathbf{x}, t) = \mu(\mathbf{x}, t) \tau^n(\mathbf{x}, t). \quad (4.20)$$

Substitution from (4.20) into (4.19) yields

$$\begin{aligned} \frac{1}{V} \sum_{\alpha=1}^N \int_{s^\alpha(\mathbf{x}, \mathbf{n}, t)} \boldsymbol{\tau}(\mathbf{x}, t) \cdot [\dot{\mathbf{u}}](\mathbf{x}, t) dS(\mathbf{x}) \\ = \frac{1}{V} \sum_{\alpha=1}^N \int_{s^\alpha(\mathbf{x}, \mathbf{n}, t)} \mu(\mathbf{x}, t) \tau^n(\mathbf{x}, t) [\dot{u}](\mathbf{x}, t) dS(\mathbf{x}). \end{aligned} \quad (4.21)$$

Since the granules carry the effective pressure through intergranular frictional contacts,

it is reasonable to assume that the normal tractions τ^n at a slipping contact in $\sum_{\alpha=1}^N s^\alpha$, are

linearly dependent on the effective pressure P ,

$$\tau^n(\mathbf{x}, t) = \Psi(\mathbf{x}, t) P(t), \quad (4.22)$$

where Ψ is a scalar-valued function defined at points where slip occurs. In general, Ψ

depends on the size of the granules, the packing, the loading condition, and other

relevant factors. Then (4.21) yields

$$\begin{aligned} \frac{1}{V} \sum_{\alpha=1}^N \int_{s^\alpha(\mathbf{x}, \mathbf{n}, t)} \boldsymbol{\tau}(\mathbf{x}, t) \cdot [\dot{\mathbf{u}}](\mathbf{x}, t) dS(\mathbf{x}) \\ = \frac{1}{V} \sum_{\alpha=1}^N \int_{s^\alpha(\mathbf{x}, \mathbf{n}, t)} \mu(\mathbf{x}, t) \Psi(\mathbf{x}, t) P(t) [\dot{u}](\mathbf{x}, t) dS(\mathbf{x}). \end{aligned} \quad (4.23)$$

Since the effective pressure $P(t)$ is not a function of \mathbf{x} , we obtain

$$\begin{aligned} \frac{1}{V} \sum_{\alpha=1}^N \int_{s^{\alpha}(\mathbf{x}, t)} \boldsymbol{\tau}(\mathbf{x}, t) \cdot [\dot{\mathbf{u}}](\mathbf{x}, t) dS(\mathbf{x}) \\ = \left(\frac{1}{V} \sum_{\alpha=1}^N \int_{s^{\alpha}(\mathbf{x}, t)} \mu(\mathbf{x}, t) \Psi(\mathbf{x}, t) [\dot{\mathbf{u}}](\mathbf{x}, t) dS(\mathbf{x}) \right) P(t) \end{aligned} \quad (4.24)$$

$$\equiv \langle \dot{c}(t) \rangle P(t), \quad (4.25)$$

where

$$\langle \dot{c}(t) \rangle = \frac{1}{V} \sum_{\alpha=1}^N \int_{s^{\alpha}(\mathbf{x}, t)} \mu(\mathbf{x}, t) \Psi(\mathbf{x}, t) [\dot{\mathbf{u}}](\mathbf{x}, t) dS(\mathbf{x}). \quad (4.26)$$

Since a negligibly small part of the rate of external work is stored in the granules and water at stress levels considered in our experiments, the strain energy terms for granules and water in (4.16) is negligibly small compared with the friction term. We, therefore, set

$$\langle \dot{e} \rangle = \frac{1}{V} \left(\int_{\Omega} \boldsymbol{\sigma} : \dot{\boldsymbol{\epsilon}} dV + \int_{D-\Omega} \boldsymbol{\sigma} : \dot{\boldsymbol{\epsilon}} dV \right). \quad (4.27)$$

Then, the energy dissipation in granular media becomes

$$\frac{1}{V} \int_{\partial D} \boldsymbol{\tau} \cdot \dot{\mathbf{u}} dS = \langle \dot{c} \rangle P + \langle \dot{e} \rangle. \quad (4.28)$$

4.3 Cyclic Torsional Loading

The energy dissipation for a cyclic torsion test performed on a hollow cylindrical specimen is now considered. Experiments are performed under undrained conditions. The shear strain is cyclically applied to the isotropically consolidated specimen, as described in Section 3. The rate of external work per unit volume under these condition is expressed in terms of the average stresses and strains as

$$\frac{1}{V} \int_{\partial D} \boldsymbol{\tau}(\mathbf{x}, \mathbf{v}, t) \cdot \dot{\mathbf{u}}(\mathbf{x}, t) dS = \langle \sigma_{z\theta}(t) \rangle \langle \dot{\gamma}_{z\theta}(t) \rangle. \quad (4.29)$$

Equation (4.28) yields

$$\langle \sigma_{z\theta}(t) \rangle \langle \dot{\gamma}_{z\theta}(t) \rangle = \langle \dot{c}(t) \rangle P(t) + \langle \dot{e}(t) \rangle. \quad (4.30)$$

Consider the energy per cycle. Integrating (4.30) over the n'th cycle, we have

$$\int_{t_{n-1}}^{t_n} \langle \sigma_{z\theta}(t) \rangle \langle \dot{\gamma}_{z\theta}(t) \rangle dt = \int_{t_{n-1}}^{t_n} \langle \dot{c}(t) \rangle P(t) dt + \int_{t_{n-1}}^{t_n} \langle \dot{e}(t) \rangle dt, \quad (4.31)$$

where t_n denotes the time at which the n'th cycle is completed. Decomposing (4.31) by pulling P outside of the integral and accounting for the resulting error by the addition of a term denoted by ϵ_n , we arrive at

$$\int_{t_{n-1}}^{t_n} \langle \sigma_{z\theta}(t) \rangle \langle \dot{\gamma}_{z\theta}(t) \rangle dt = \bar{P}_n \int_{t_{n-1}}^{t_n} \langle \dot{c}(t) \rangle dt + \epsilon_n + \int_{t_{n-1}}^{t_n} \langle \dot{e}(t) \rangle dt, \quad (4.32)$$

where \bar{P}_n is the average effective pressure in the n'th cycle given by

$$\bar{P}_n = \frac{1}{t_n - t_{n-1}} \int_{t_{n-1}}^{t_n} P(t) dt. \quad (4.33)$$

If the effective pressure changes only slightly in the n'th cycle, the error ϵ_n , is small.

Summing (4.32) over all cycles up to the k'th cycle, we now have

$$\sum_{n=1}^k \int_{t_{n-1}}^{t_n} \langle \sigma_{z\theta}(t) \rangle \langle \dot{\gamma}_{z\theta}(t) \rangle dt = \sum_{n=1}^k \left(\bar{P}_n \int_{t_{n-1}}^{t_n} \langle \dot{c}(t) \rangle dt + \epsilon_n + \int_{t_{n-1}}^{t_n} \langle \dot{e}(t) \rangle dt \right). \quad (4.34)$$

Finally, (4.34) is written as

$$\begin{aligned} \int_{t_0}^{t_k} \langle \sigma_{z\theta}(t) \rangle \langle \dot{\gamma}_{z\theta}(t) \rangle dt &= \frac{1}{t_k - t_0} \int_{t_0}^{t_k} \langle \dot{c}(t) \rangle dt \int_{t_0}^{t_k} P(t) dt + \sum_{n=1}^k \epsilon_n + \int_{t_0}^{t_k} \langle \dot{e}(t) \rangle dt, \quad (4.35) \\ &= C_k \int_{t_0}^{t_k} P(t) dt, \quad (4.36) \end{aligned}$$

where

$$C_k = \frac{1}{t_k - t_0} \int_{t_0}^{t_k} \langle \dot{c} \rangle dt + \left(\sum_{n=1}^k \epsilon_n + \int_{t_0}^{t_k} \langle \dot{e} \rangle dt \right) / \int_{t_0}^{t_k} P dt. \quad (4.37)$$

Equation (4.36) represents the energy dissipation up to the k'th cycle. C_k will be called the energy dissipation coefficient. It is regarded as representing the microstructural arrangement of the granular mass at each instant.

The coefficient C_k in (4.36) can be estimated experimentally. Its variation is plotted against the number of cycles in Figures 26 and 27 for loose and dense specimens,

respectively, and against the excess pore water pressure in Figures 28 and 29. These results show that C_k is nearly constant throughout the experiment when a constant strain amplitude is cyclically applied to the specimen. There is only a small difference in the C_k -value between the first and second loading, even though there exists a large difference in the corresponding number of cycles. These results suggest that C_k does not depend on the strain history, but does depend on the strain amplitude. The relation between C_k and the strain amplitude for both loose and dense specimens is given in Figure 30. It is seen that C_k depends on the strain amplitude and density, but not on the strain history.

From these results, it seems reasonable to assume that, at constant density and strain amplitude, C_k is a constant, say, C , related to the internal work per unit volume of a given granular mass. It can be evaluated experimentally, as long as the same strain amplitude is cyclically applied to the specimen. The C -values shown in Figure 30 are used to calculate the internal work per unit volume at the end of each cycle, and these results are plotted in Figures 31 - 34 along with the corresponding external work. Clearly, the data points match closely in each case.

These results show that energy dissipation in granular media for cyclic torsional loading can be expressed in terms of the time history of the effective pressure, along with a constant C -value which depends on the strain amplitude and density only.

4.4 Random Torsional Loading

Energy dissipation for a torsional loading test in which the shear strain is applied randomly (rather than cyclically), is studied as an application of the above results. The experiments are performed using dense specimens. Shear strains are applied to a specimen at randomly varying strain amplitudes, but at a constant shear strain rate over each quarter cycle. The relation between the shear strain and the effective pressure in the first loading is shown in Figure 15 and examined in Section 3.2. The same

relation in the second loading is shown in Figure 35.

Since C -values are essentially independent of the strain history, as discussed in Section 4.3, the energy balance for a random torsional loading gives, upon modifying (4.36),

$$\int_{t_0}^{t_m} \langle \sigma_{s\theta}(t) \rangle \langle \dot{\gamma}_{s\theta}(t) \rangle dt = \sum_{i=1}^m C_i \int_{t_{i-1}}^{t_i} P dt , \quad (4.38)$$

where t_i is the time of the i 'th zero shear strain, and C_i is the i 'th C -value. The value of C_i is determined as follows. First, the maximum shear strain between t_{i-1} and t_i is found. Then, the C -value corresponding to the shear strain is obtained from Figure 30 which shows the relation between the C -value and the shear strain amplitude (dashed line).

The internal work per unit volume is calculated from the right-hand side of (4.38), using experimental results. It is displayed in Figure 36 along with the external work per unit volume. These two quantities are in excellent agreement, which tends to support the validity of (4.38).

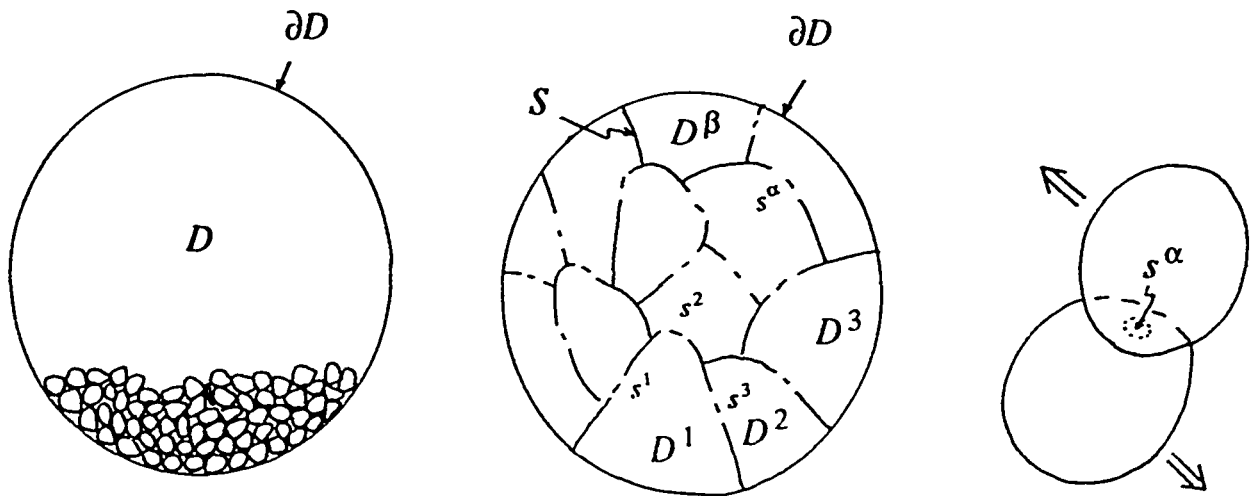


Figure 25. Contour S and slips s^α in the considered region D

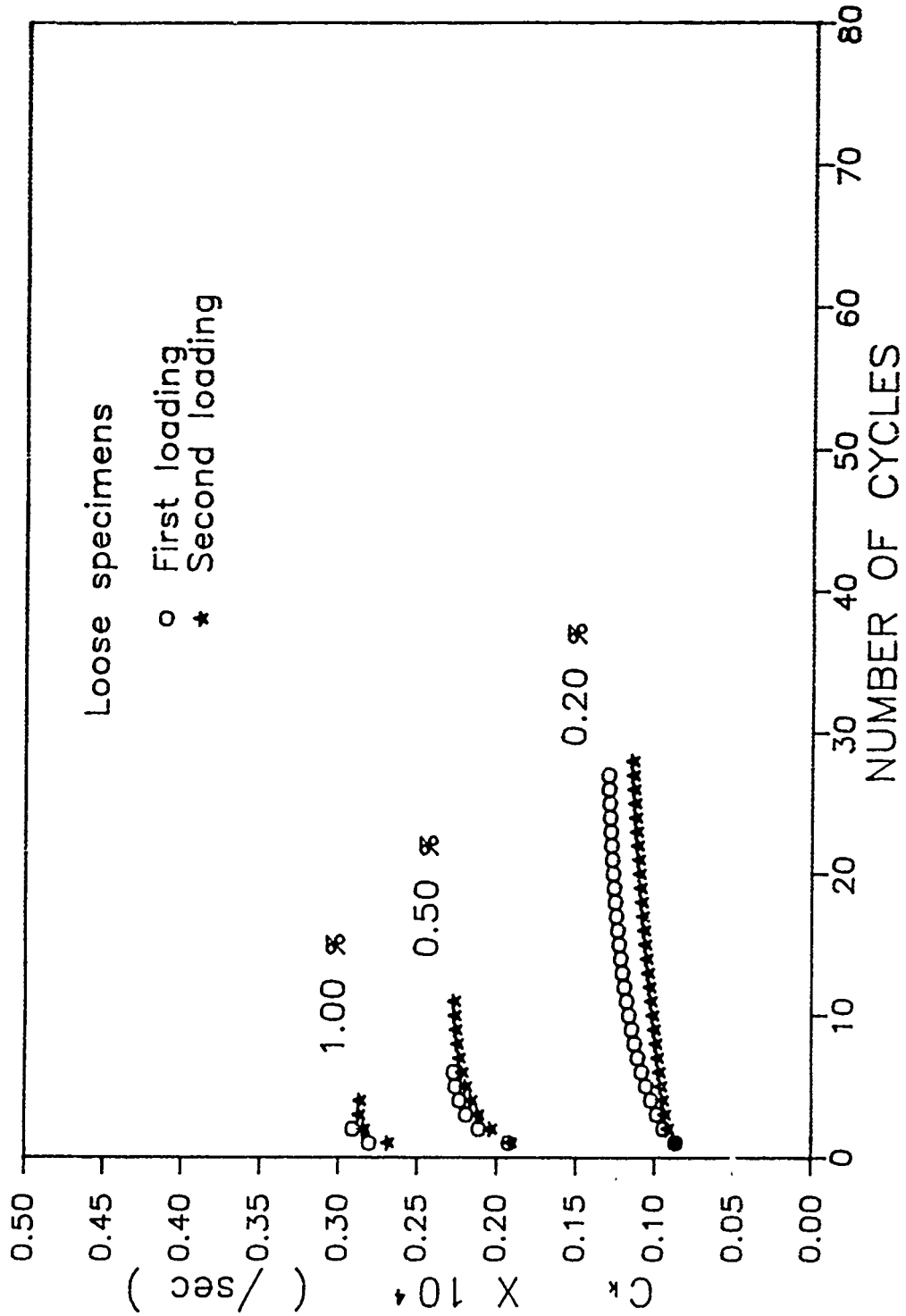


Figure 26. Changes of C_t against number of cycles in first and second loading of loose specimens

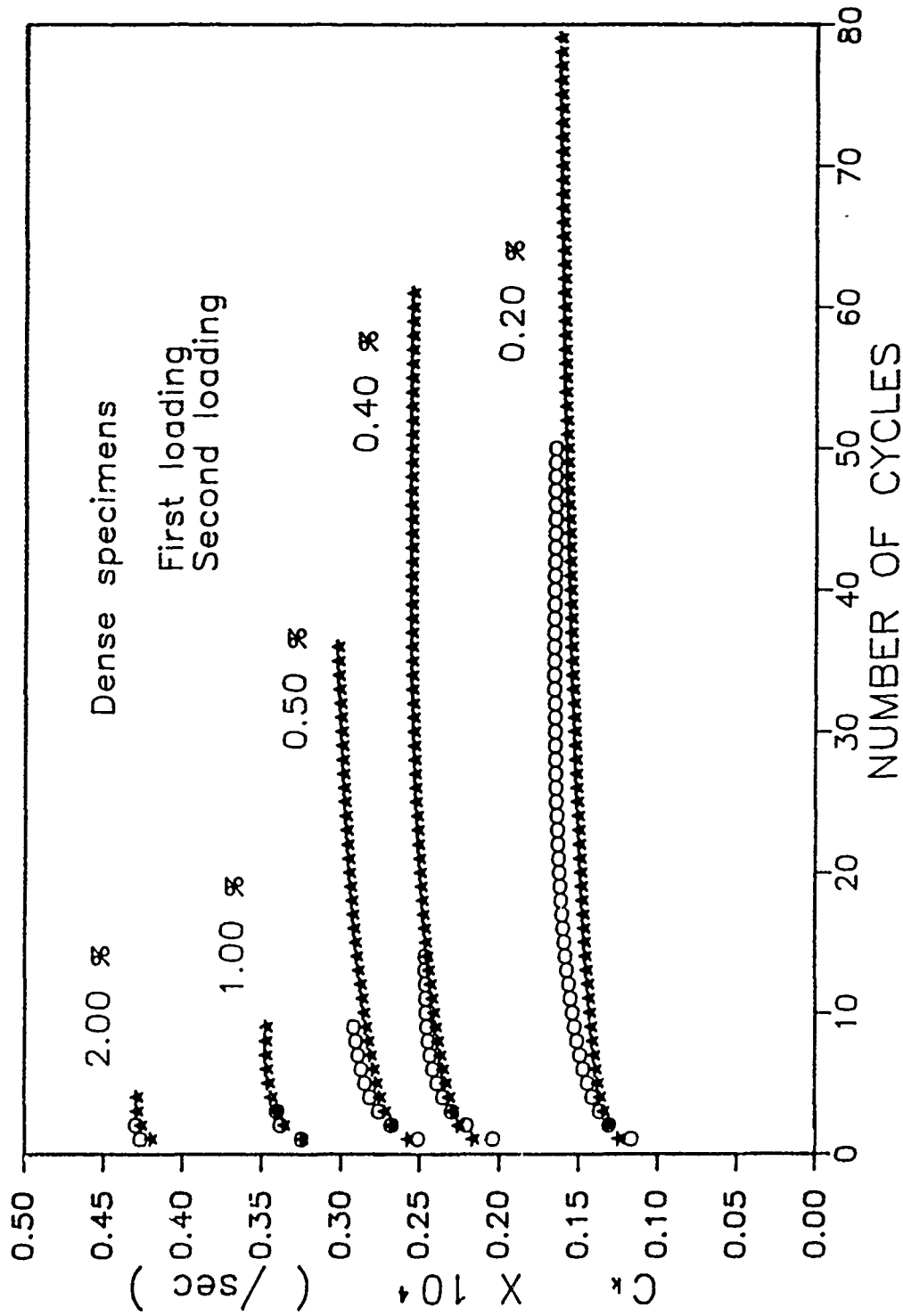


Figure 27. Changes of C_t against number of cycles in first and second loading of dense specimens

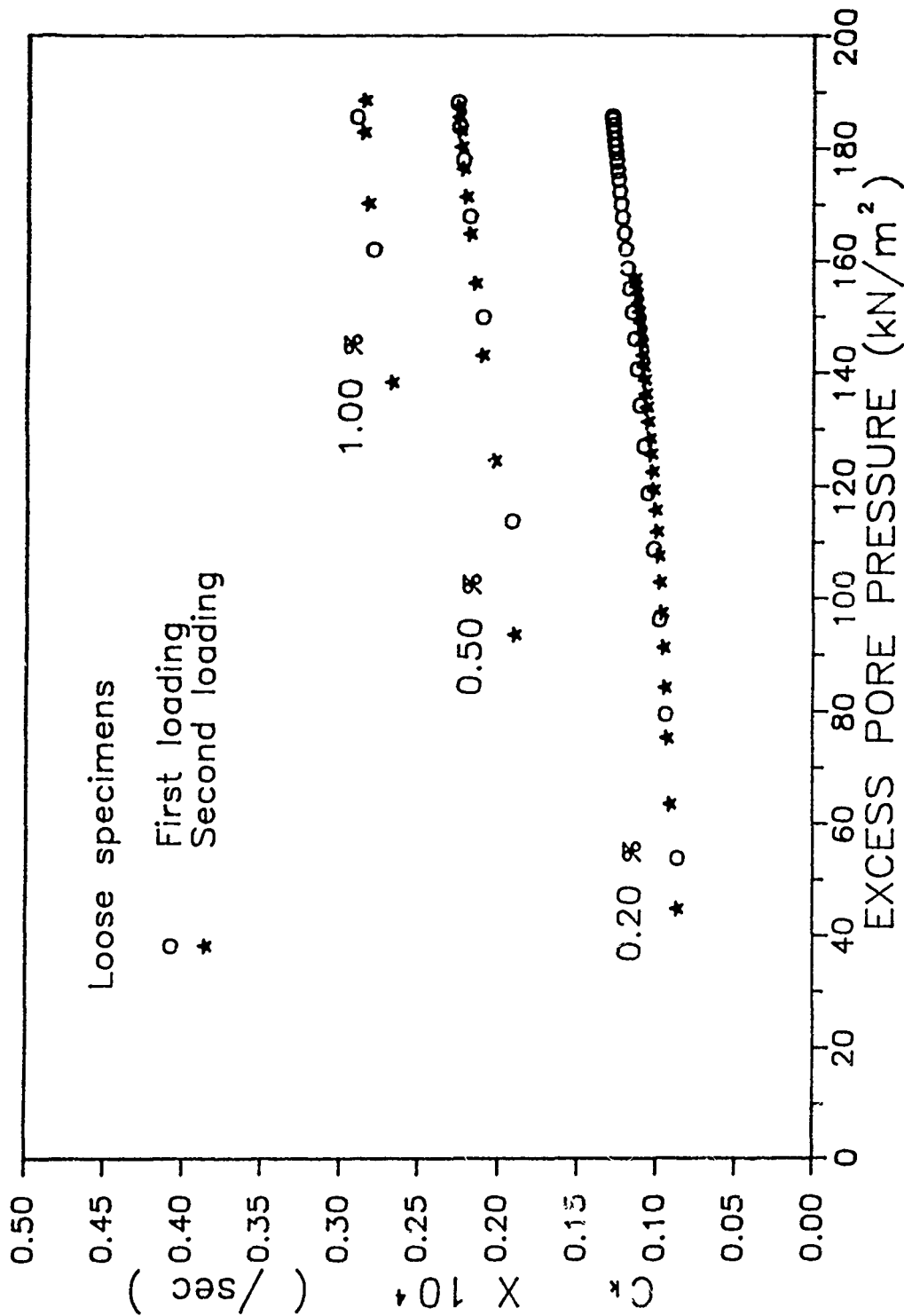


Figure 28. Changes of C_v against excess pore water pressure in first and second loading of loose specimens

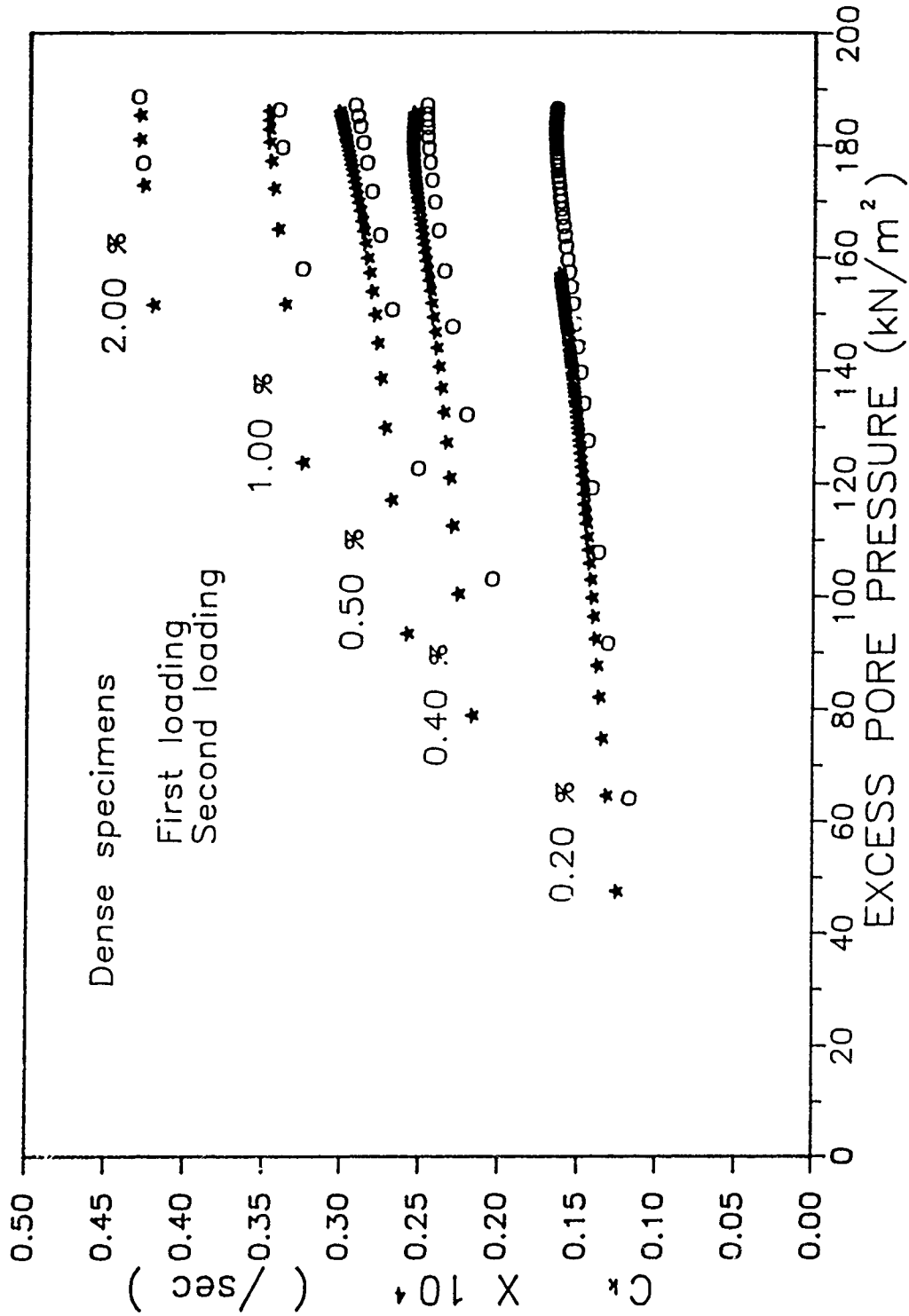


Figure 29. Changes of C_t against excess pore water pressure in first and second loading of dense specimens

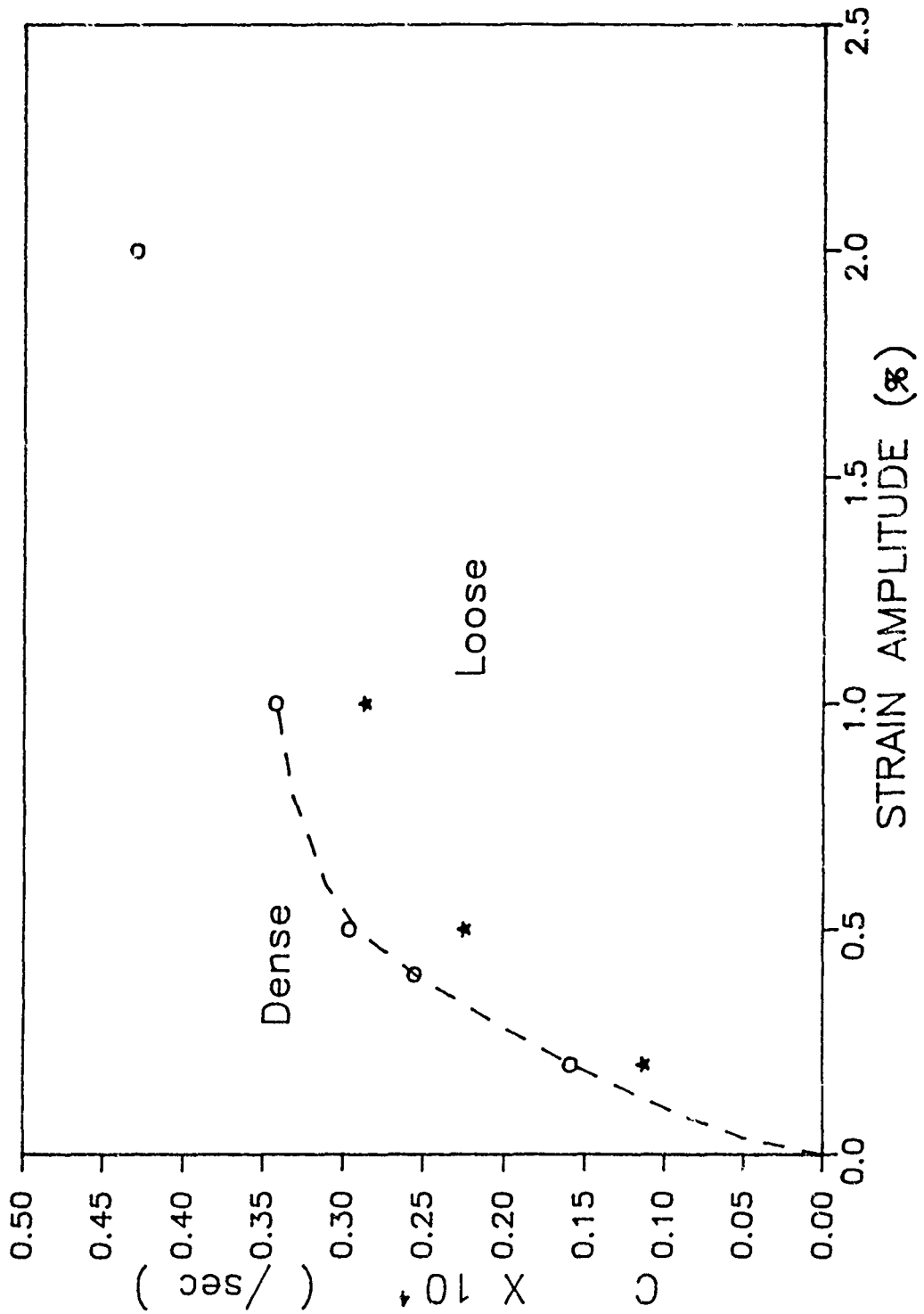


Figure 30. The C-values obtained experimentally

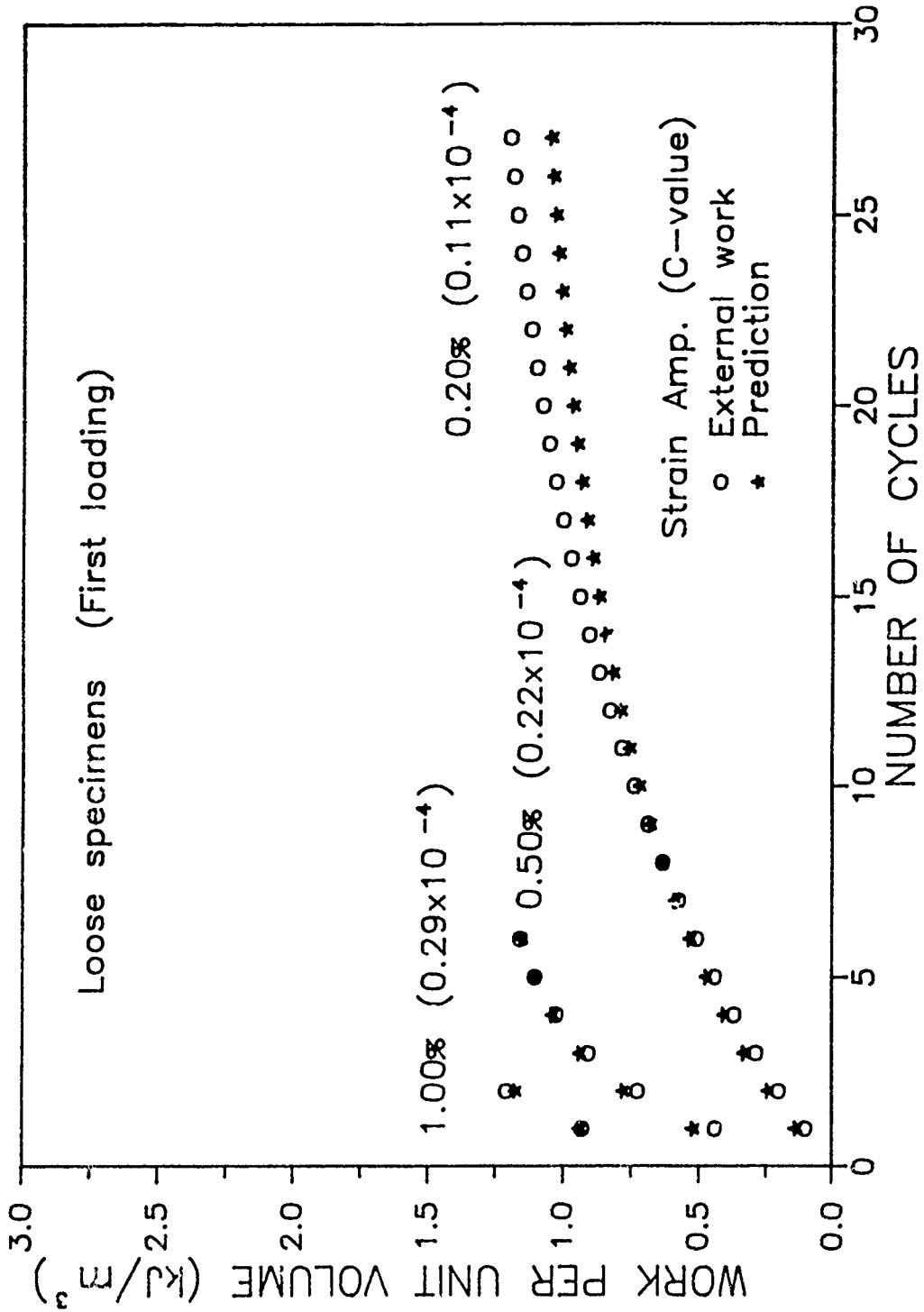


Figure 31. Relation between external work and calculated internal work in first loading of loose specimens

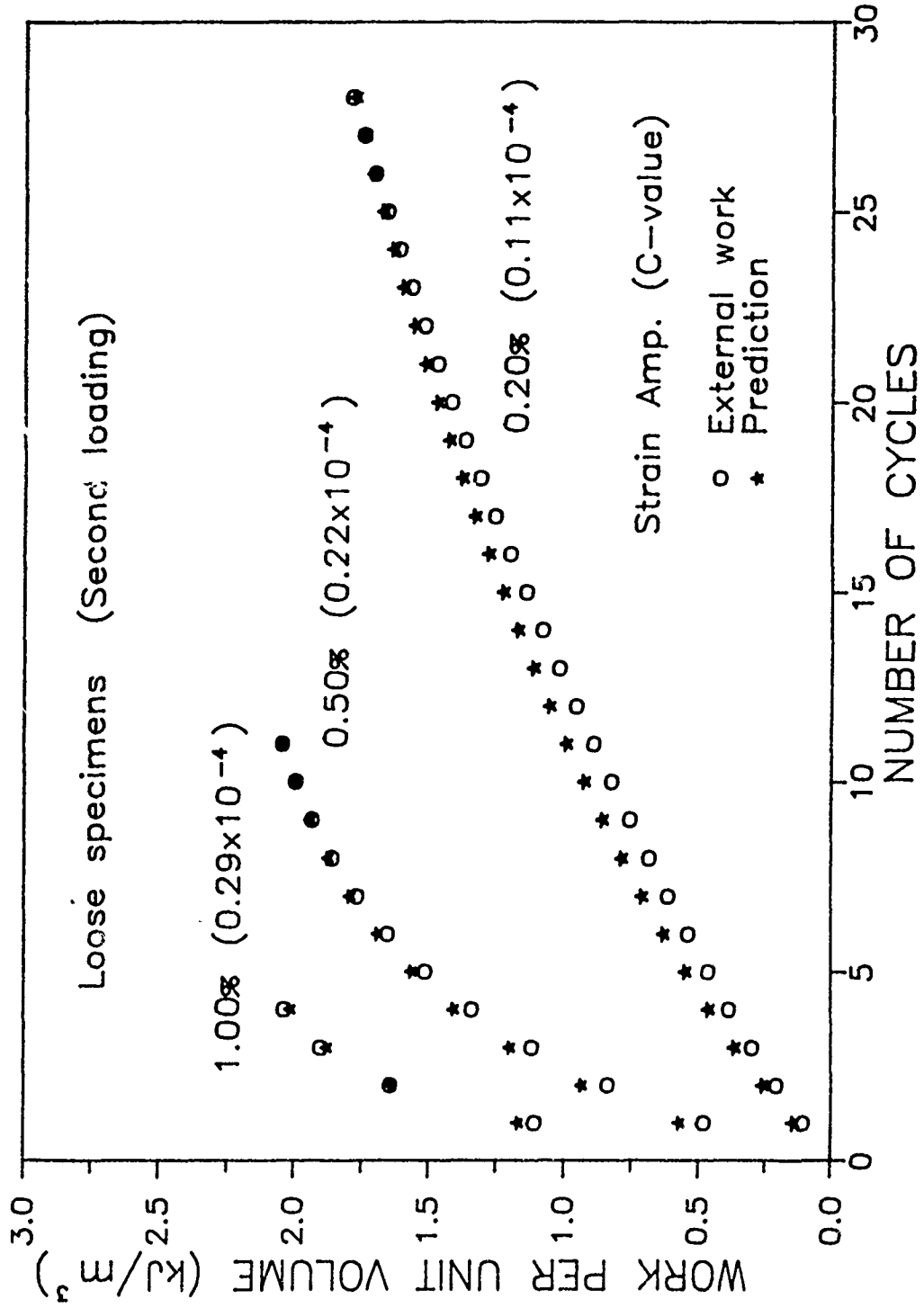


Figure 32. Relation between external work and calculated internal work in second loading of loose specimens

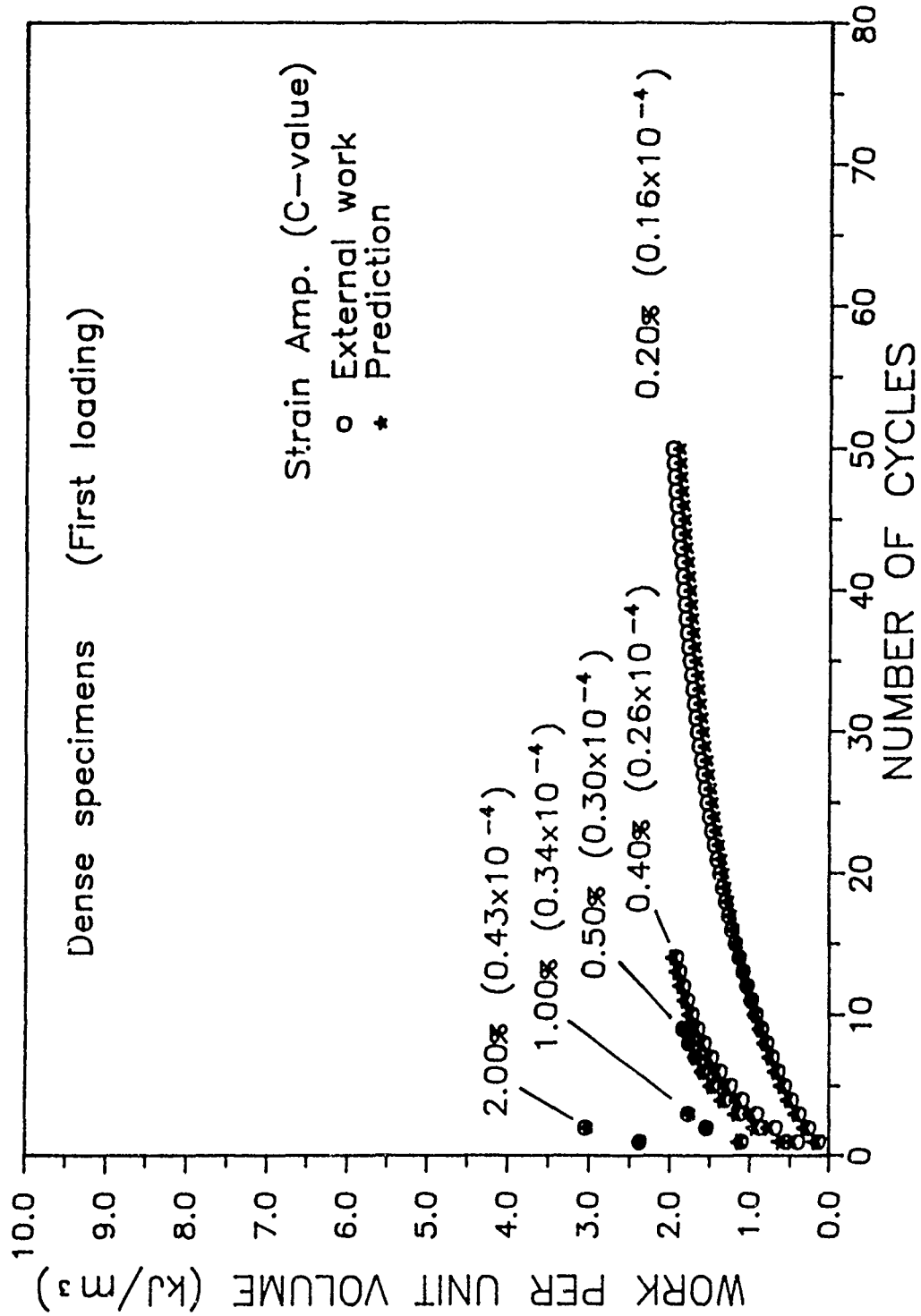


Figure 33. Relation between external work and calculated internal work in first loading of dense specimens

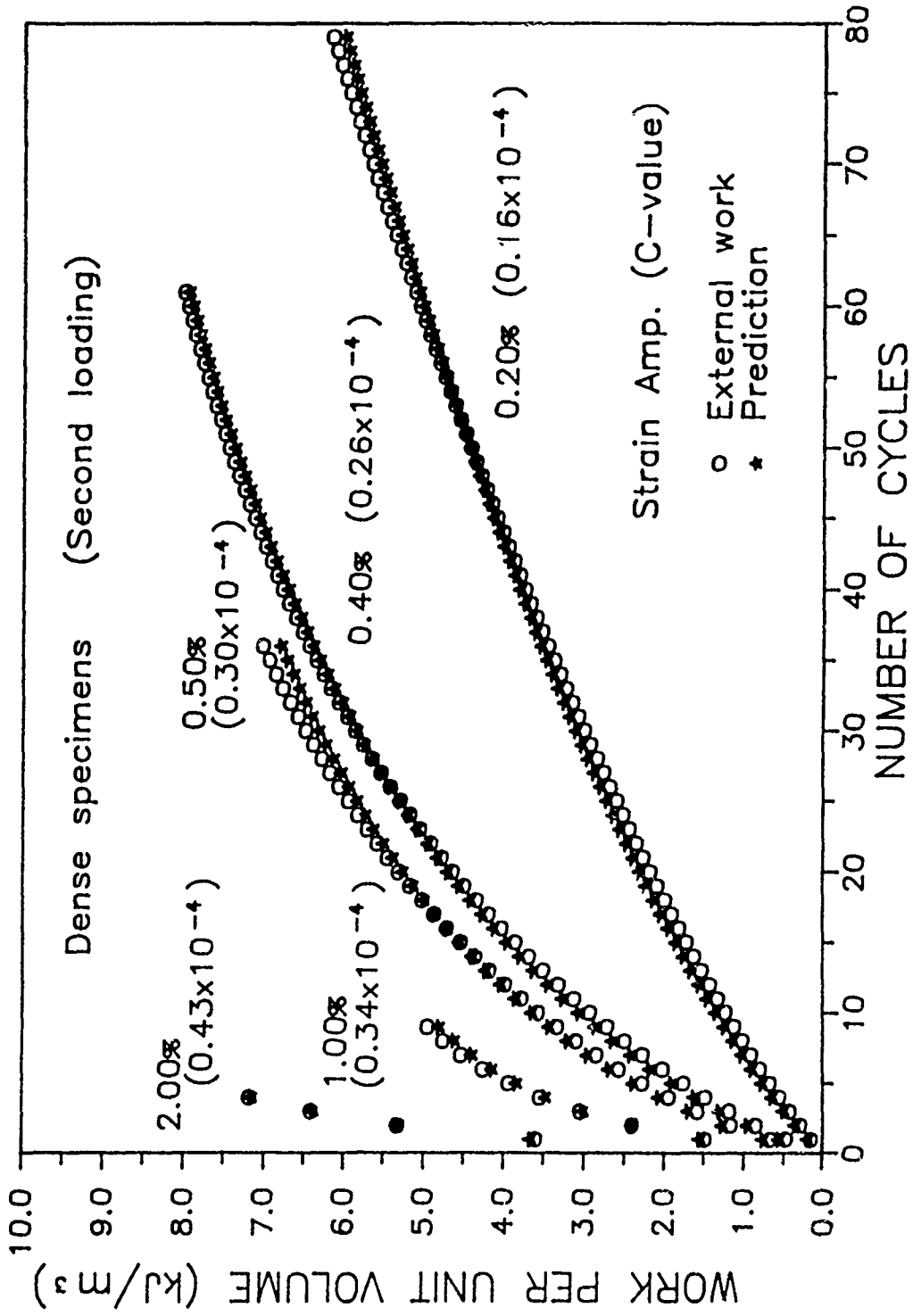


Figure 34. Relation between external work and calculated internal work in second loading of dense specimens

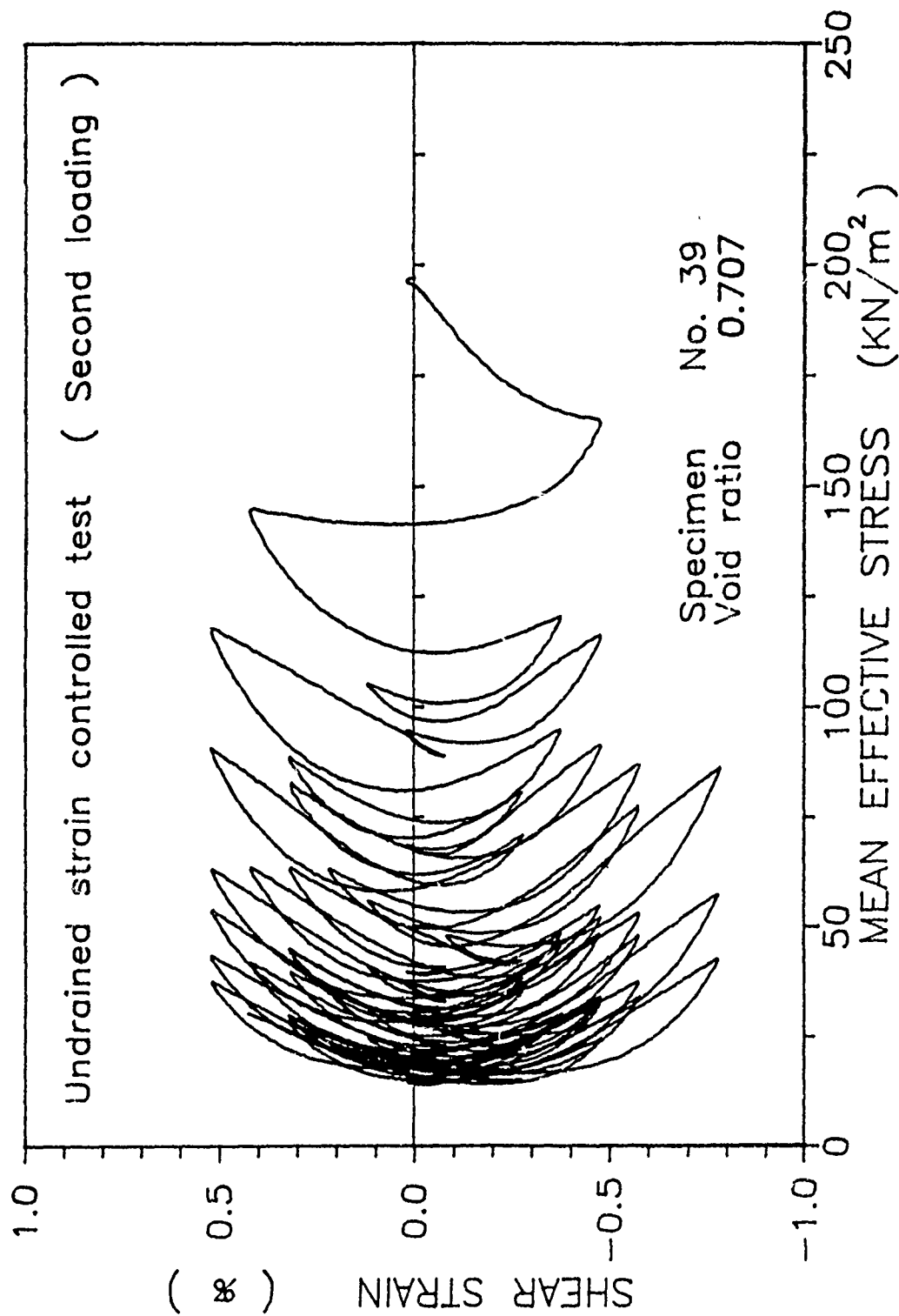


Figure 35. Relation between shear stress and effective pressure in second loading of dense specimen subjected to random torsional loading

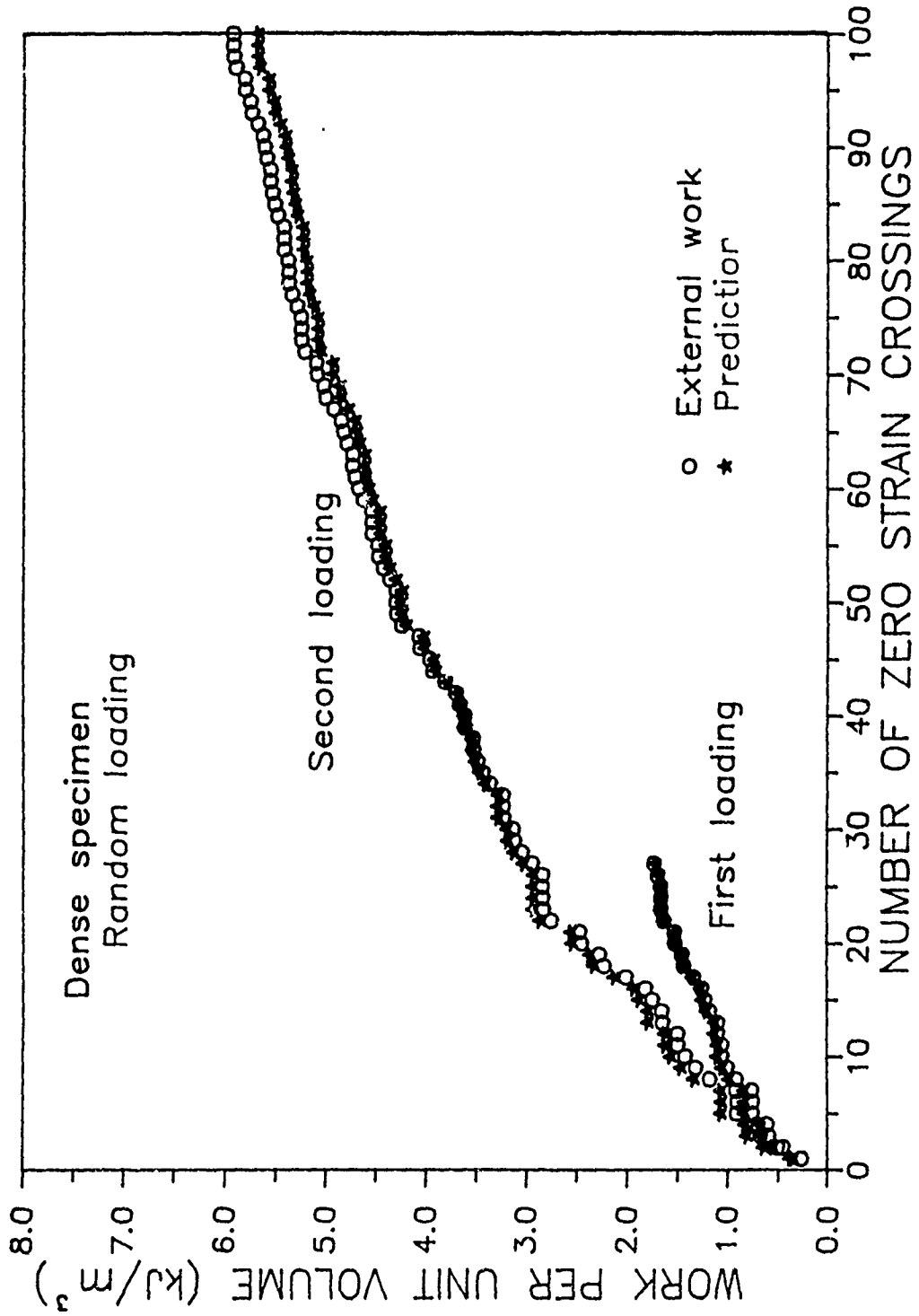


Figure 36. Relation between external work and calculated internal work in first and second loading of dense specimen subjected to random torsional loading

5. DISCUSSION

Energy dissipation in the flow of cohesionless granular media is considered in this report. A theoretical formulation is proposed in Section 4 based on a simple micromechanical model. The internal work for cyclic torsional loading is shown to depend on the time history of the effective pressure and an experimentally obtainable parameter C . The results of a series of experiments show that C depends on the strain amplitude and density, but is essentially independent of the stress or strain history. On the other hand, the effective pressure clearly depends on the strain history, as shown by the large difference in the number of cycles between the first and second loading required to attain the same pore water pressure. Therefore, the right-hand side of (4.36) consists of a strain-history-dependent part, $\int_{t_0}^{t_k} P dt$, and a strain-history-independent part, C .

ACKNOWLEDGMENT

The authors wish to express their appreciation to Dr. Muneo Hori for his critical suggestions and to Mr. Ryuichi Sugimae for his assistance in carrying out the experiments. This work has been supported by the U.S. Air Force Office of Scientific Research Grant No. AFOSR 87-0079 to the University of California, San Diego.

REFERENCES

- Arthur, J.R.F. and Menzies, B.K. (1972), "Inherent anisotropy in a sand," *Geotechnique*, Vol. 22, No. 1, pp. 115-128.
- Casagrande, A. (1975), "Liquefaction and cyclic deformation of sands - a critical review," *Fifth Pan American Conference on Soil Mechanics and Foundation Engineering*, held at Buenos Aires, Argentina.
- Castro, G. (1975), "Liquefaction and cyclic mobility of saturated sands," *Journal of the Geotechnical Engineering Division, ASCE*, Vol. 101, No. GT6, pp. 551-569.
- Committee of JSSMFE on the Test Method of Relative Density of Sand (1979), "Maximum-minimum density test method of sand," *Procedure for Testing Soils, Second Revised Edition, JSSMFE, Part 2*, pp. 172-188 (in Japanese).
- DeAlba, P., Seed, H.B. and Chan, C.K. (1976), "Sand liquefaction in large-scale simple shear tests," *Journal of the Geotechnical Engineering Division, ASCE*, Vol. 102, GT9, pp. 909-927.
- Hight, D.W., Gens, A. and Symes, M.J. (1983), "The development of a new hollow cylinder apparatus for investigating the effects of principal stress rotation in soil," *Geotechnique*, Vol. 33, No. 4, pp. 355-383.
- Hill, R. (1963), "Elastic properties of reinforced solids: some theoretical principles," *J. Mech. Phys. Solids*, Vol. 11, pp. 357-372.
- Hill, R. (1967), "The essential structure of constitutive laws for metal composites and polycrystals," *J. Mech. Phys. Solids*, Vol. 15, pp. 79-95.
- Ishihara, K. and Yasuda, S. (1975), "Sand liquefaction in hollow cylinder torsion under irregular excitation." *Soils and Foundations*, Vol. 15, No. 1, pp. 45-59.
- Ishihara, K. and Towhata, I. (1983), "Sand response to cyclic rotation of principal stress directions as induced by wave loads," *Soils and Foundations*, Vol. 23, No. 4, pp. 11-26.
- Ishihara, K. and Towhata, I. (1985), "Sand response to cyclic rotation of principal stress directions as induced by wave loads (closure)," *Soils and Foundations*, Vol. 25, No. 1, pp. 117-120.
- Miura, S. and Toki, S. (1982), "A sample preparation method and its effect on static and cyclic deformation-strength properties of sand," *Soils and Foundations*, Vol. 22, No. 1, pp. 61-77.
- Moroto, N. (1976) : "A new parameter to measure degree of shear deformation of granular material in triaxial compression tests," *Soils and Foundations*, Vol. 16, No. 4, pp. 1-9.

Nemat-Nasser, S. (1980), "On behavior of granular materials in simple shear," *Soils and Foundations*, Vol. 20, No. 3, pp. 59-73.

Nemat-Nasser, S. and Shokooh, A. (1979), "A unified approach to densification and liquefaction of cohesionless sand in cyclic shearing," *Can. Geotech. J.*, No. 16, pp. 659-678.

Nemat-Nasser, S. and Takahashi, K. (1984), "Liquefaction and fabric of sand," *Journal of Geotechnical Engineering, ASCE*, Vol. 110, No. 9, pp. 1291-1306.

Nemat-Nasser, S. and Tobita, Y. (1982), "Influence of fabric on liquefaction and densification potential of cohesionless sand," *Mechanics of Materials*, Vol. 1, No. 1, pp. 43-62.

Oda, M. (1972), "Initial fabric and their relations to mechanical properties of granular materials," *Soils and Foundations*, Vol. 12, No. 1, pp. 17-36.

Peacock, W.H. and Seed, H.B. (1968), "Sand liquefaction under cyclic loading simple shear conditions," *Journal of the Soil Mechanics and Foundations Division, ASCE*, Vol. 94, SM3, pp. 689-708.

Reynolds, O. (1885), "The dilatancy of media composed of rigid particles in contact," *Phi. Mag. S. 5*, Vol. 20, pp. 469-481.

Rowe, P. W. (1962), "The stress-dilatancy relation for static equilibrium of an assembly of particles in contact," *Proc. Roy. Soc. London, Ser. A*, Vol. 269, pp. 500-527.

Schofield, A.N. and Wroth, C.P. (1968) "Critical state soil mechanics," McGraw-Hill, London.

Seed, H.B. (1979), "Soil liquefaction and cyclic mobility evaluation for level ground during earthquakes," *Journal of the Geotechnical Engineering Division, ASCE*, Vol. 105, No. GT2, pp. 201-255.

Silver, M.L. and Seed, H.B. (1971), "Deformation characteristics of sands under cyclic loading," *Journal of Soil Mechanics and Foundation Division, ASCE*, Vol. 97, No. SM8, pp. 1081-1098.

Symes, M.J.P.R., Gens, A. and Hight, D.W. (1984), "Undrained anisotropy and principal stress rotation in saturated sand," *Geotechnique*, Vol. 34, No. 1, pp. 11-27.

Tatsuoka, F. Muramatsu, M. and Sasaki, T. (1982), "Cyclic undrained stress-strain behavior of dense sands by torsional simple shear test," *Soils and Foundations*, Vol. 22, No. 2, pp. 55-70.

Towhata, I. and Ishihara, K. (1985), "Shear work and pore water pressure in undrained shear," *Soils and Foundations*, Vol. 25, No. 3, pp. 73-84.

Youd, T.L. (1970), "Densification and shear of sand during vibration," *Journal of Soil Mechanics and Foundations Division, ASCE*, Vol. 96, No. SM3, pp. 863-880.

Youd, T.L. (1972), "Compaction of sands by repeated shear straining," Journal of Soil Mechanics and Foundations Division, ASCE, Vol. 98, No. SM7, pp. 709-725.